Clinical Implications of Cancer Stem Cell Properties in Oral Squamous Cell Carcinoma.

Emich, Helena

Barts and The London
School of Medicine and Dentistry

Clinical Implications of Cancer Stem Cell Properties in Oral Squamous Cell Carcinoma

A thesis submitted in accordance with regulations for the degree of Doctor of Philosophy by

Helena Emich

Supervisors:
Prof. Ian Mackenzie
Mr. Iain Hutchison

January 2014

Centre for Cutaneous Research
Barts and the London School of Medicine and Dentistry
Queen Mary, University of London

STATEMENT OF ORIGINALITY

I, Helena Emich, confirm that the research included within this thesis is my own work or that where it has been carried out in collaboration with, or supported by others, that this is duly acknowledged below and my contribution indicated. Previously published material is also acknowledged below.

I attest that I have exercised reasonable care to ensure that the work is original, and does not to the best of my knowledge break any UK law, infringe any third party's copyright or other Intellectual Property Right, or contain any confidential material.

I accept that the College has the right to use plagiarism detection software to check the electronic version of the thesis.

I confirm that this thesis has not been previously submitted for the award of a degree by this or any other university.

Signature: Helena Emich
Date: 20/01/2014

ACKNOWLEDGEMENTS

Foremost, I would like to express my sincere gratitude to my PhD supervisor Prof Ian Mackenzie for his invaluable scientific and technical advice and his continuous support throughout the time of my PhD. I would also like to thank Mr Iain Hutchison for his immense clinical expertise and Prof Kim Piper for acquisition of tissue samples and her help with interpreting the clinical reports.

I would like to acknowledge the financial support provided by The Facial Surgery Research Foundation Saving Faces and Barts and the London Charity, without which this work would not have been possible.

I am most grateful to my colleagues Dr Adrian Biddle, Dr Luke Gammon and Dr Emilios Gemenetzidis for their kind help and constant encouragement. It has been a great pleasure working with them and I could not have imagined having more reliable and helpful lab colleagues. My sincere thanks also go to David Chapireau for his help with the statistical analysis of my data.

Lastly, I would like to thank my family and friends for their deep love and their strong belief in me. I am particularly indebted to my parents Wilhelm and Valentina Emich who raised me with a love of science and who continue to support me in all my pursuits.

ABBREVIATIONS

5-FU	5-Fluorouracil
ALDH	aldehyde dehydrogenase
AML	acute myeloid leukaemia
APC	allophycocyanin
C (°C)	Celsius (degree Celsius)
CD	cluster of differentiation
CD44s	standard CD44 isoform
CO_2	carbon dioxide
CSCs	cancer stem cells
DAB	3,3'-diaminobenzidine
DAPI	4',6-diamidino-2-phenylindole
DMSO	dimethyl sulfoxide
DNA	deoxyribonucleic acid
ECM	extracellular matrix
ECS	extracapsular spread
EDTA	ethylenediaminetetraacetic acid
e.g.	lat: exempli gratia (engl: for example)
EGFR	epidermal growth factor receptor
EMT	epithelial to mesenchymal transition
ESA	epithelial specific antigen
FACS	flowcytometry activated cell sorting
FCS	fetal calf serum
FITC	fluorescein isothiocyanate
g	standard gravity
GTP	guanosine triphosphate
Gy	Gray
h	hour
HA	hyaluronan
H&E	hematoxylin and eosin
HNSCC	head and neck squamous cell carcinoma
HPV	human papilloma virus

HRP	horseradish peroxidase
i.e.	lat: id est (engl: that is)
IHC	immunohistochemistry
kDa	kilo Dalton
mA	milliampere
MET	mesenchymal to epithelial transition
MFI	median fluorescence intensity
min	minute(s)
miR	microRNA
mm	millimeter
mM	millimolar
MMP	matrix metallopeptidase
mRNA	messeger-RNA
nm	nanometer
NOD/SCID	non obese-diabetic mice with severe combined immunodeficiency disease
OR	odds ratio
OSCC	oral squamous cell carcinoma
OTSCC	squamous cell carcinoma of the mobile tongue
PBS	phosphate buffered saline
PE	phycoerythrin
P-EGFR	phosphorylated epithelial growth factor receptor
PFA	paraformaldehyde
RNA	ribonucleic acid
RND	radical neck dissection
SCC	squamous cell carcinoma
SDS	sodium dodecyl sulfate
sec	second(s)
SND	selective neck dissection
SSE	stratified squamous epithelium
TBS	tris buffered saline
TBS-T	tris buffered saline with 0.01% Tween-20
TGFβ	transforming growth factor β
TNFα	tumour necrosis factor α

TNM	tumour-node-metastasis
U	unit
VEGF	vascular endothelial growth factor

CONTENTS

1. Abstract

CD44 has been described as a marker of cancer stem cells in oral squamous cell carcinoma (OSCC). The main objective of this study was to characterise expression of CD44 in both fresh samples of human OSCC and in cell lines generated from them, and to examine its correlation with selected clinico-pathological parameters of the tumours of origin.

The epithelial fraction in 20 fresh OSCC samples was identified by the standard method using the negative selection technique with antibodies against non-tumour cells. A novel method of identifying the epithelial fraction, termed positive selection, was also developed and used for analysis of 14 additional OSCC samples. This new method, using epithelial-specific antibodies, led to a considerable improvement in the efficiency and the accuracy of the procedure.

The frequency of $CD44^+$ cells in the epithelial fraction of the tumour specimens was assessed by FACS and varied widely (3-97%). High frequency of $CD44^+$ cells in tumour samples was found to be associated with high tumour grade, discohesive invasion front and presence of lymph node metastases ($p<0.01$, as calculated with Spearman's ranked test and Fisher's exact test).

It was also observed, that the percentage of $CD44^+$ cells changes when cells isolated from tumour samples are propagated in culture. Nearly all cells in cell lines generated from OSCC samples showed CD44 expression when analysed by FACS. However, a markedly higher level of CD44 expression (as assessed by median fluorescence intensity for cell surface CD44) was found for early passage cell lines generated from metastatic OSCC and lymph node metastases as compared to cell lines generated from non-metastatic OSCC.

These findings show that a high frequency of $CD44^+$ cells in fresh OSCC tissue and a high level of CD44 expression in cultured OSCC cells correlate

with more aggressive tumour behaviour. These results might provide important information of prognostic and therapeutic value.

2. Aims and Objectives

The aims and objectives of this study were:

- to characterise cancer stem cells (CSCs) in oral squamous cell carcinoma (OSCC), assessing the proportion of these cells in individual tumours by flow cytometry;
- to collect clinical and histopathological data and relate the size of the CSC fraction to the properties of the tumour *in vivo* and the clinical outcome;
- to investigate malignant cell lines derived from tumours as suitable models for analysis of CSCs.

Analysis of CSCs relies on their accurate identification and isolation from tumour tissue. While a lot of research focuses on the properties of these cells, the methods of their identification and isolation have not been studied in great detail. For epithelial tumours like OSCC, one of the challenges lies in distinguishing the tumour cells from the stromal cells present in cell suspensions isolated from the tumour specimen. In the present study, I tested the standard technique and also tried to develop a new method of identifying and isolating epithelial cells from cell suspensions produced from tumour samples (section 5.1). I then used both methods to analyse 34 primary OSCC specimens for CD44 expressing cells and examined the data for a statistical correlation with clinical and pathological parameters of the tumours of origin (section 5.2). Finally, I examined cell lines that I have generated from the tumour specimens and compared these data to the data obtained from analysis of cells from fresh tumour samples (section 5.3).

3. Introduction

3.1 Organisation of the human oral mucosa

The oral mucosa is a mucous tissue that forms the lining of the oral cavity. The main functions of the oral mucosa are protection, sensation and secretion. It acts as a barrier preventing pathogens and toxic substances from entering the body. It also protects the underlying structures from mechanical damage during chewing. The oral mucosa has an extensive innervation allowing the mouth to sense hot and cold temperatures and contains taste buds on the surface of the tongue that are necessary for the recognition of taste. Production of saliva by minor salivary glands embedded in the oral mucosa is another important function. Saliva contains enzymes essential for digestion of food starches. It also facilitates swallowing by lubricating the food particles.

The oral mucosa consists of epithelial tissue, the basement membrane, and connective tissue, formed by lamina propria and submucosa (Figure 3.1). Human oral mucosa can be divided into three structurally and functionally different subtypes: lining mucosa, masticatory mucosa and specialised mucosa. Lining mucosa is non-keratinized epithelium found in the cheeks (also known as buccal mucosa), the floor of the mouth, the soft tissue at the back of the roof of the mouth (soft palate) and the ventral surface of the tongue. Masticatory mucosa is a partially or fully keratinized (para- or ortho-keratinized) epithelium found at the front of the roof of the mouth (hard palate) and the gums (gingiva). Specialised mucosae include the dorsal surface of the tongue which contains specialised structures such as taste buds and papillae. Figure 3.2 shows the distribution of the different mucosal subtypes in the oral cavity (Figure 3.2).

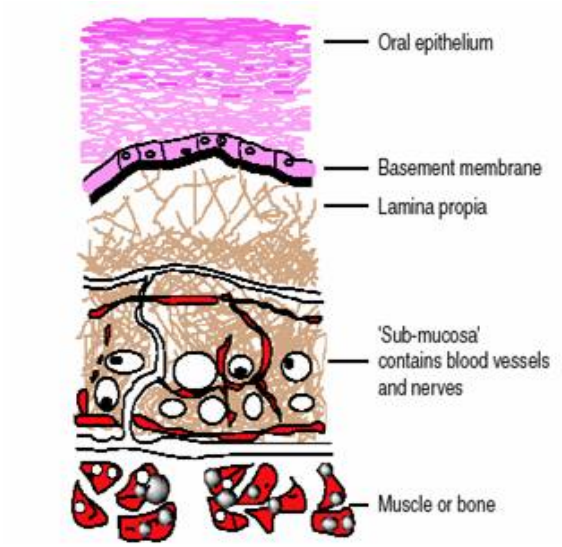

Figure 3.1*: Schematic representation of the oral mucosa. Human oral mucosa is comprised of the following structures: oral epithelium, basement membrane, lamina propria and submucosa that joins the underlying bony and muscular tissue. *Adapted from [1]

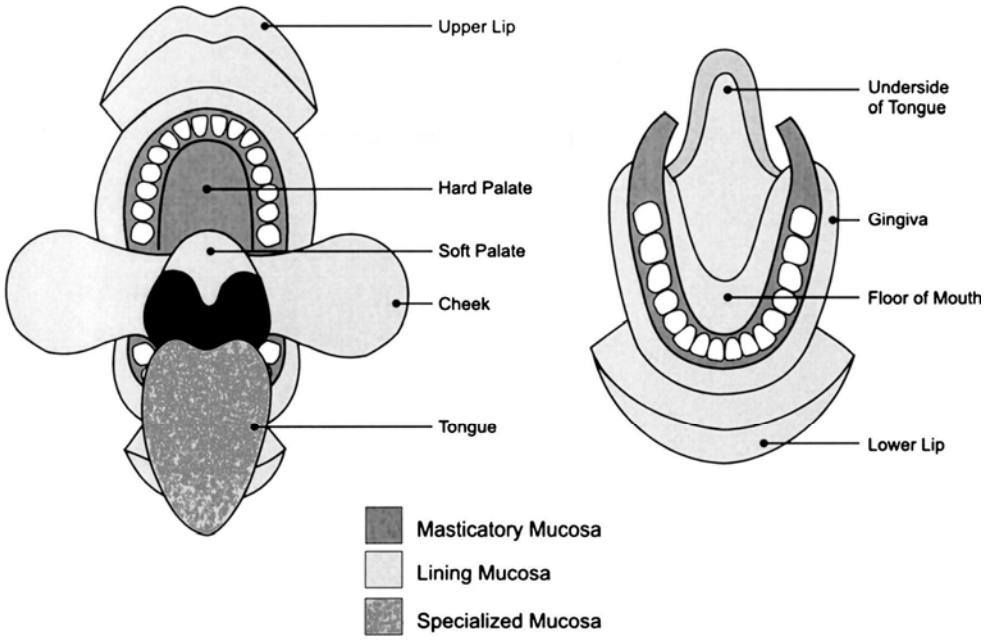

Figure 3.2*: Distribution of the different subtypes of the oral mucosa in the oral cavity. Lining mucosa (light grey) covers the largest area of the oral cavity, including the inner lining of lips and cheeks, soft palate, the ventral area of the tongue and the floor of mouth. Masticatory mucosa (dark grey) forms the lining of the hard palate and the gums (gingiva). Specialised mucosa (spotty grey) is found on the dorsal surface of the tongue. *Modified from [2]

The oral mucosal epithelium is composed of squamous (flattened and thin) cells that are arranged in multiple layers and is therefore classified as stratified squamous epithelium (SSE). The outermost layer of the skin (epidermis), the inner lining of the oesophagus, the anal canal and vagina belong to the same type of epithelia. Human stratified squamous epithelia usually contain four distinct cell layers. The innermost layer is the basal layer (stratum basale, SB); it is followed by the spinous layer (stratum spinosum, SS), the granular layer (stratum granulosum, SG) and the outermost cornified layer (stratum corneum, SC) (Figure 3.3 A).

3.1.1 Proliferation and differentiation patterns

The stratification of these types of epithelia is a result of finely balanced cell proliferation and differentiation. During normal homeostasis the production of cells that takes place in the deeper layers of the epithelium is strictly balanced by the loss of cells from the surface. The proliferating and the differentiating cells are spatially separated, being located in different layers of the SSE. The proliferating cells are only present in the inner layers of the epithelium and form two distinct populations: stem cells and amplifying cells. The stem cells are slow-cycling cells that reside in the basal layer. They divide giving rise to amplifying cells, which migrate laterally and upwards towards the surface of the epithelium. The function of the amplifying cells is to enhance the production of new cells. Proliferation of the amplifying cells takes place in the basal layer and, in some epithelia, in a few cell layers above the basal layer (termed epi- or para-basal layers) [3] [4] [5]. As these cells migrate upwards they gradually lose the ability to proliferate and finally undergo terminal differentiation to form the protective dead squames that are shed from the surface of the epithelium (process known as desquamation). Terminal differentiation is accompanied by degradation of the nucleus, autolysis of cell organelles and formation of a cell envelope, which is a rigid protein structure that replaces the plasma membrane in terminally differentiated keratinocytes of the cornified layer [6] [7]. Depending on the type of epithelium, cells in the outermost layer of the stratified squamous

epithelia can be fully keratinized (ortho-keratinized), partially keratinized (para-keratinized) or non-keratized.

3.1.2 Site-specific variability

Although most types of SSE comprise four distinct cell layers (Figure 3.3 A), there is some site-related variability. For example, the cornified layer and the granular layer are missing in the non-keratinized oral epithelium. Instead, the epithelium contains stratum distendum (SD) and stratum filamentosum (SF) (Figure 3.3 B). The upper cell layers of para- and non-keratinised epithelia show a partial disintegration of the nucleus and the organelles. The cell envelope of para- and non-keratinized epithelia is considerably thinner as compared to that of the keratinized epithelium and the whole epithelial cell assembly is a lot more flexible.

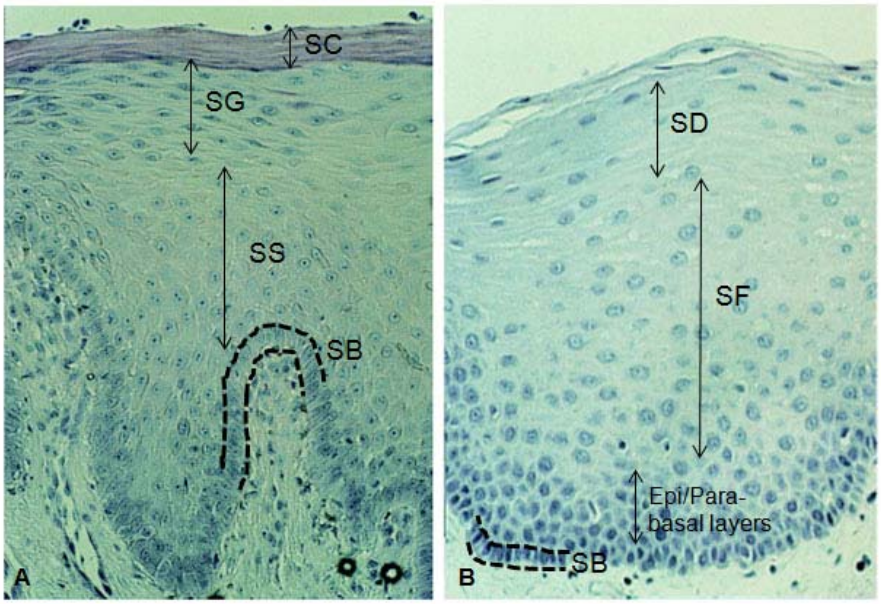

Figure 3.3*: Site-specific differences in the organisation of the oral mucosal epithelia. Tissue sections from two different sites of the oral cavity: hard palate (A) and buccal mucosa (B) are shown. The mucosa of the hard palate (A) contains the four typical layers of the stratified squamous epithelium: stratum basale (SB), stratum spinosum (SS), stratum granulosum (SG) and stratum corneum (SC). The cornified epithelial layer and the granular layer are absent from the buccal mucosa (B). Instead, the buccal mucosa contains three layers: stratum basale (SB), stratum filamentosum (SF) and stratum distendum (SD). *Modified from [4]

3.1.3 Malignant transformation

Altered patterns of cell growth and disturbances in the balance between cell proliferation and differentiation lead to tumour development. During normal homeostasis each stem cell divides, giving rise to one stem cell and one amplifying cell. In malignancy there is a shift from asymmetric to symmetric cell division, in which both daughter cells remain stem cells. This leads to an increase in the proportion of stem cells and the total number of cells produced, resulting in formation of a tumour.

The malignant transformation process involves multiple stages: initiation, clonal expansion and growth autonomy. During the initiation stage cells acquire mutations caused by physical, chemical, viral or genetic factors. These initiation events typically involve genes controlling cell proliferation and apoptosis. One of the genes involved in malignant cell transformation of oral mucosal cells is the tumour suppressor gene *TP53*. The product of the gene (protein 53, known as p53) is involved in cell cycle control at the G1/S as well as G2/M stage regulation point [8]. It activates DNA repair proteins and can initiate apoptosis if DNA damage cannot be repaired. p53 is mutated in the majority of OSCC [9] [10]. Loss of functional p53 results in genetic instability and often leads to aneuploidy [11] and generation of cells with abnormal DNA. Mutations in genes encoding ErbB family receptor tyrosine kinases and Ras family proteins may also be involved in malignant transformation of oral epithelial cells. Epidermal growth factor receptor (*EGFR*), a member of ErbB family, is frequently overexpressed in OSCC [12] [13]. This proto-oncogene encodes a membrane tyrosine kinase that can be activated by ligands such as epidermal growth factor (EGF) and transforming growth factor α (TGFα). Its activation triggers signalling pathways that stimulate cellular proliferation and migration and inhibit apoptosis [14]. Some members of the *Ras* oncogene family have been found overexpressed in oral cancer [15] [16]. In addition, the *Ras* proto-oncogenes frequently get activated via acquired point mutations that result in conformational changes which prevent hydrolysis of GTP. Mutated Ras proteins are then locked in a “turned-on” state and lead to

a constitutively active mitogenic signalling cascade and uncontrolled cell growth [17].

Initiated cells usually have a prolonged life span, increased proliferative capacity and are more resistant to apoptotic stimuli. These selective growth advantages lead to hyperplasia, clonal expansion and eventually to growth autonomy resulting in the formation of malignant tumours. Multiple genetic alterations are acquired during this transformation process and it has been estimated that at least five are required to transform a normal cell into a cancer cell [18].

Cancer can develop many years after exposure to a carcinogen. Existence of this “latent period” implies that initiated cells remain in the tissue for long periods of time during which they are able to acquire further genetic alterations that eventually lead to transformation and development of a tumour. The long-lived stem cells are able to accumulate mutations whereas differentiating cells are soon lost from the tissue. Clinical and experimental data also support the notion that mutations in the stem cells rather than the differentiating progeny are responsible for cancer development [19].

3.2 Oral Squamous Cell Carcinoma (OSCC)

Squamous cell carcinoma is a form of cancer that arises from the uncontrolled growth of malignant cells in squamous epithelium. Squamous cell carcinoma (SCC) can develop in many organs including skin, oral mucosa, lung, prostate, gut, vagina and cervix. The diversity of its origin makes SCC one of the most common types of cancer.

Oral squamous cell carcinoma (OSCC) is a cancer that originates in the oral mucosa and belongs to the group of head and neck cancers (also referred to as head and neck squamous cell carcinoma, HNSCC). 90% of cancers in the head and neck area are SCC with the majority being SCC of the oral cavity. The oral cavity includes a number of anatomic structures shown in figure 3.4 (Figure 3.4).

It is not entirely clear whether tumours developing at different sites of the oral cavity differ biologically, but it has been suggested that some types of OSCC are more aggressive than others. For example, SCC of the oral mobile tongue (OTSCC) is increasingly regarded as a biologically different entity compared to other types of OSCC as it is more aggressive and generally associated with higher rates of metastasis [20].

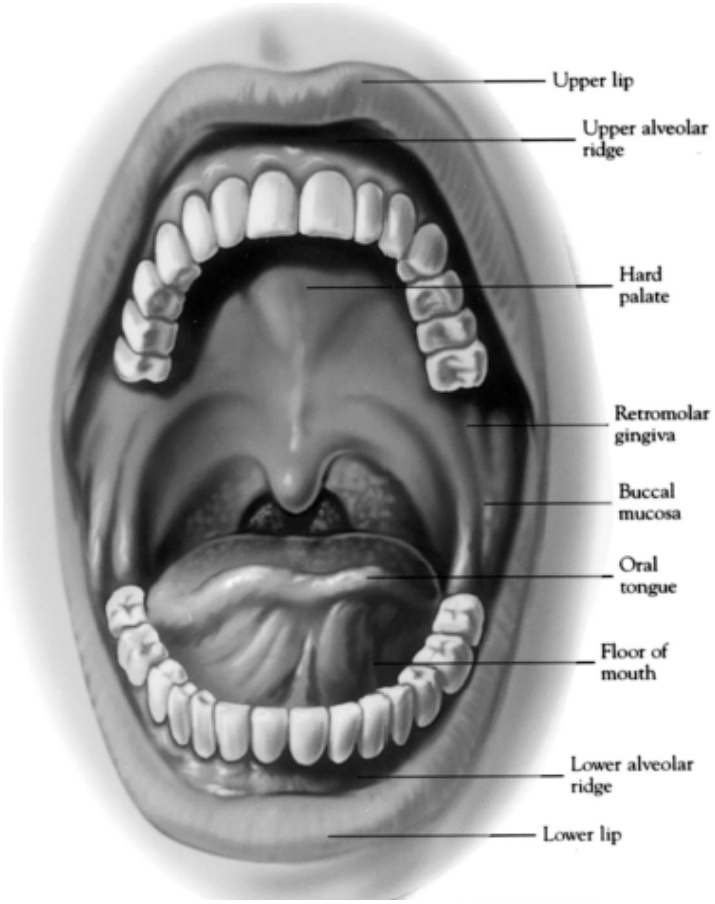

Figure 3.4*: Anatomic subsites of the oral cavity. Mouth anatomy showing anatomical subsites where cancer can develop. These include lips, lining of the lips (including upper and lower alveolar ridge) and cheeks (buccal mucosa), the roof of the mouth (hard palate and soft palate), the floor of the mouth, gums (gingiva), gum area behind the wisdom teeth (retromolar gingiva or retromolar trigone) and the tongue. *Adapted from [21]

OSCC is the 6th most common cancer worldwide and is second to lung cancer as the most common smoking-related malignancy [22] [23]. It is mostly seen in older men. Tobacco and alcohol are the major risk factors, but many other factors related to lifestyle, environment and genetics may play a role (Figure 3.5). Lifestyle factors include chewing of betel quid (particularly in Asia) as well as low intake of fruit and vegetables [24]. Exposure to other chemical and physical mutagenic stimuli also drives development of oral cancer, especially in individuals with compromised immunity and weakened DNA repair ability [25]. In addition, poor oral hygiene and infections of the oral cavity are regarded as possible risk factors [26] [27]. A link to infections with human papilloma virus (HPV) has been suggested in recent years,

although HPV infections have been primarily linked to cancers of the oropharynx, tonsils and base of tongue areas, which do not fall into the group of oral cancers. Some non-malignant oral lesions tend to undergo malignant transformation and lead to the development of OSCC. Leukoplakia, lichenoid lesions and erythroplakia are regarded as disorders with the highest risk of malignant transformation [23] [25].

OSCC is an aggressive malignancy, frequently associated with a poor clinical outcome. Most commonly, loco-regional metastases from OSCC affect lymph nodes in the neck. Distant metastases are rare, but if present, affect bone, brain or lungs.

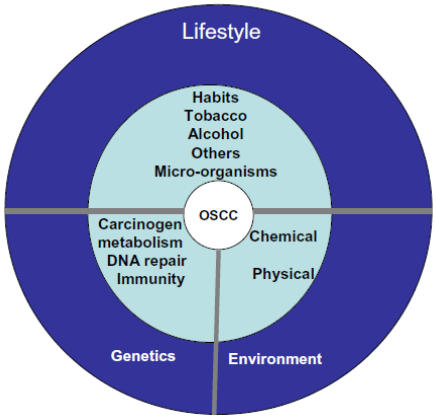

Figure 3.5*: Schematic summary of main OSCC risk factors. Numerous factors associated with lifestyle, genetics and environment can increase the risk of developing OSCC. *Adapted from [25]

3.2.1 Treatment of OSCC

For all types of oral cancer surgical removal of the tumour is the preferred method of treatment. Sometimes surgery is preceded by other treatments such as radio- and chemo-therapy which reduce the size of the tumour. When surgical removal of the tumour is not feasible, radio- or chemo-therapy can be administered as palliative treatment with the aim to alleviate symptoms and to provide the best possible quality of life for patients.

Despite recent advances in treatment of OSCC, the mortality amongst OSCC patients remains high. The 5 year survival rate is less than 55% [28] [29]. The low survival rate is partly due to advanced disease stage at the time of diagnosis as less advanced tumours have higher survival rates. Because early stages of oral cancer may not cause any symptoms or pain, cancerous lesions in the mouth may not be noticed and over 50% of OSCC are diagnosed when they have already metastasised to lymph nodes in the neck [30], when prognosis is significantly worse than when cancers are localised to an intraoral area.

In many cases, surgical removal of OSCC tumours is a major surgical intervention that severely impairs the quality of life for patients. The surgery usually includes the removal of the primary tumour in the mouth and, if present, removal of clinically diagnosed metastatic lymph nodes in the neck. The original type of neck dissection (radical neck dissection, RND) involves the removal of all lymph nodes in the dissected side of the neck along with non-lymphatic structures including sternocleidomastoid muscle and spinal accessory nerve. RND is associated with significant postoperative morbidity with the typical permanent shoulder dysfunction. The selective neck dissection (SND) is a type of surgery where only selected nodal groups at risk for metastatic disease, predictable on the bases of primary tumour location and size, are removed. SND guarantees conservation of non-lymphatic structures leading to improved functional results, while having equivalent oncologic outcomes as the RND [31].

After surgery, patients considered at high risk of tumour recurrence are usually administered radio- and/or chemo-therapy, which remain the most common adjuvant therapy options in the UK.

In recent years, alternative molecularly targeted therapies have been explored. Their development was permitted by identification of typical molecular alterations such as overexpression/constitutive activation of epidermal growth factor receptor (EGFR), reported for 80-100% of OSCC [32]. EGFR is a 170–180 kDa transmembrane glycoprotein tyrosine kinase

receptor that is expressed in the basal cell layer of the normal oral mucosa and is ubiquitously expressed in cells of HNSCC [33]. EGFR binds several ligands including EGF and TGFα. Ligand-binding triggers:

- receptor dimerization,
- activation of the intrinsic kinase domain,
- autophosphorylation of tyrosine residues within the cytoplasmic tail.

These events result in activation of the receptor and trigger a complex signaling cascade that leads to a strong mitogenic activity [34].

The potential value of EGFR as a therapeutic target is supported by the correlation between increased EGFR protein expression or *EGFR* gene copy number amplification and poor outcomes for HNSCC patients [35]. Cetuximab (trade name Erbitux) is an EGFR inhibitor that has been shown to improve overall survival, progression free survival and tumour response rates in patients with advanced HNSCC [36]. Cetuximab is the only molecularly targeted therapy that has been approved for use in HNSCC treatment to date.

Another molecular target is vascular endothelial growth factor (VEGF) for which monoclonal antibodies including bevacizumab (trade name Avastin) are being investigated for treatment of HNSCC [37]. Similar to EGFR, increased levels of VEGF appear to induce tumour growth, metastatic spread and therapy resistance [38] [39] [40]. A direct correlation between high levels of VEGF and worse prognosis for OSCC patients has also been reported [41].

Several other drugs are currently being studied in phase III clinical trials. These include tyrosine kinase inhibitors, such as erlotinib and gefinitib (already approved for treatment of lung cancer, pancreatic cancer, breast cancer and other cancers). In addition, the use of COX-2 inhibitors, farnesyl inhibitors, and proteasome inhibitors in treatment of head and neck cancers is also being investigated [42].

The high mortality amongst OSCC patients is also partly due to the lack of patient-tailored treatment options. The therapy (surgery, sometimes followed by radio- and chemo-therapy) is highly standardised and often doesn't take into account distinct characteristics of a given tumour and patient. More research needs to be done focusing on the properties of individual OSCC tumours and on the differences between tumours from different patients. Studies performing a more in-depth analysis of individual OSCC tumours (investigating cellular and molecular aspects) and examining their correlation to the clinical parameters of the respective tumours may lead to a better understanding of OSCC and act as guides to development of new therapeutic interventions.

3.2.2 Clinicopathological parameters in diagnostics and treatment of OSCC

As with other cancers, tumour tissue is examined by a pathologist after its surgical removal from the patient. The aim of this examination is to confirm the clinical diagnosis, i.e. diagnosis that has been made prior to surgery based on physical and radiological examination of the patient, and usually a tumour biopsy. The biopsy (a tissue probe taken from the tumour) or the resected tumour itself is examined for the presence of unusual nuclei, aberrant motises and presence of invasion, all of which are typical characteristics of cancer. In addition, various pathological characteristics of the tumour are examined, which are regarded as prognostic factors and play a role in determining the choice of the post-surgical treatment. Pathological parameters of a particular relevance to prognosis are listed in table 3.1 and are discussed in the following sections.

Table 3.1: Pathological and histological parameters of OSCC with prognostic value.

Parameter	Possible classifications
TNM stage	see below*
Extracapsular spread	Yes/No
Grade	undifferentiated (G4, high grade) poorly differentiated (G3, high grade) moderately differentiated (G2, intermediate grade) well differentiated (G1, low grade)
Invasion pattern	cohesive/discohesive
Tumour depth	[mm]
Perineural Invasion	Yes/No
Lymphovascular invasion	Yes/No
Excision (surgical margin)	complete (clear) (>5 mm) close (close) (1-5 mm) incomplete (involved) (<1 mm)

*****For a detailed description of the TNM staging system see below

3.2.2.1 TNM staging system for oral cancer

The tumour-node-metastasis (TNM) staging system was first described in the 1940s [43]. Some 20 years later the TNM system was adapted by the International Union Against Cancer for staging of tumours in 23 body sites. With regular revision and constant improvement, the system is still in wide use today as an important prognostic tool characterising the severity of the disease for many types of cancers including HNSCC.

TNM primarily describes the tumour size and spread. The T stage refers to the size of the primary tumour and ranges from 1 to 4 for most cancers. In addition, there is "carcinoma *in situ*" (T*is*), which is defined as an early stage tumour that is not yet invading adjacent tissue and has not penetrated the basement membrane. T1-T4 characterise invasive tumours of a varying size (Table 3.2). The N stage refers to regional lymph node metastases and characterises location and number of the involved lymph nodes in the neck. The M stage describes metastases at distant body sides. TNM staging system for OSCC is outlined in the table below (Table 3.2).

Table 3.2 TNM staging system for oral squamous cell carcinoma.

Stage	Description
Tx	Primary tumour cannot be assessed
T0	No evidence of primary tumour
T*is*	Carcinoma in situ
T1	The tumour is not larger than 2 cm in its greatest dimension
T2	The tumour is between 2 cm and 4 cm large in its greatest dimension
T3	The tumour is larger than 4 cm in its greatest dimension
T4	The tumour is larger than 4 cm and invades adjacent structures
Nx	Regional lymph nodes cannot be assessed
N0	No lymphatic nodes are affected
N1	Metastasis in a single ipsilateral lymphatic node, not larger than 3 cm
N2a	Metastasis in a single ipsilateral lymphatic node, between 3 cm and 6 cm
N2b	Metastasis in multiple ipsilateral lymphatic nodes, not larger than 6 cm
N2c	Metastasis in bilateral/contralateral lymphatic nodes, not larger than 6 cm
N3	Metastasis larger than 6cm
Mx	Distant metastases cannot be assessed
M0	No distant metastasis are present
M1	The cancer has spread to distant organs

3.2.2.2 Other prognostic factors

Together with advanced TNM staging, other parameters such as high grade, discohesive invasion pattern and perineural or/and lymphovascular invasion (Table 3.1) characterise aggressive tumours. Patients with tumours displaying a combination of these characteristics, as well as patients, whose tumours have been incompletely excised, have poorer prognosis and are considered at high risk of developing recurrent disease.

High grade tumours are cancers that mostly consist of immature undifferentiated cells with a great proliferative potential. They are classified as poorly differentiated tumours. In contrast, intermediate and low grade tumours (classified as moderately and well differentiated, respectively) are regarded as less able to proliferate and to drive tumour growth.

The invasion pattern, a property of the invasion front of the tumour, can either be cohesive or discohesive. It is cohesive when the entire body of the tumour expands and is being pushed into the adjacent tissue as the tumour grows,

or discohesive when single cells or groups of cells detach from the main body of the tumour and are found at some distance from it in the neighbouring non-malignant tissue.

Perineural invasion is present when tumour cells are seen in spaces surrounding the nerves. The spread of tumour cells into the blood vessels or lympatic vessels is termed lymphovascular invasion. Vascular invasion is the spread to the blood vessels only, but the term lymphovascular invasion is preferred as it is difficult to distinguish small lymphatic spaces from small vascular spaces when assessing the tumour tissue under the microscope.

The depth of tumour is another prognostic indicator, although its significance is controversial. In general, deep tumour growth is associated with aggressive tumours and poor outcome. A study by O-charoenrat and co-workers reported that a tumour thickness above 5 mm is a strong predictor of metastases in the neck lymph nodes [44]. However, the depth of the tumour can be limited by anatomy as tumours are much less likely to invade bony tissue than soft tissue. Consequently, tumours, which due to their location in the oral cavity are surrounded by bony tissue, are unlikely to reach a large depth, regardless of their aggressiveness.

Following surgery, the margin of the resected tissue is examined for the presence of tumour cells. The tumour has been “completely excised” if no tumour cells are found within a distance of 5 mm from the resection edge. The tumour has been “closely excised” or “incompletely excised”, if it is present within 1-5 mm or <1 mm from the edge of the resected tissue, respectively. Incomplete excisions are also referred to as “involved tumour margins”. With close, and especially with incomplete excisions, there is a higher risk of post-operative tumour recurrence and spread.

The presence of lymph node metastases in the neck is widely accepted as one of the most significant prognostic factors [45] [46] [47] and extension of the metastatic deposits beyond the nodal capsule (extracapsular spread, ECS) is associated with even higher rates of locoregional recurrence and

distant metastases and lower rates of survival [47] [48]. Greenberg and co-workers found that the 5 year survival rate is considerably lower in patients with multiple ECS^+ lymph nodes as compared to patients without ECS [47]. In general, patients with involved lymph nodes at the time of diagnosis are much more likely to relapse and develop local recurrences or new metastases. To reduce the risk of recurrences patients with an advanced N stage are usually given adjuvant therapy.

3.2.3 Adjuvant therapy: Mechanisms of action and side effects

Adjuvant therapy is defined as treatment administered in addition to the initial main treatment. In the great majority of cases, surgery is the main treatment for OSCC with adjuvant therapy being radiotherapy and/or chemotherapy [49] [50]. The aim of the adjuvant therapy is to eliminate cancer cells that have remained in the patient's body after the surgery. This can occur either due to incomplete removal of the tumour or because cancer cells had disseminated to distant body sites prior to the removal of the tumour.

The decision about whether or not an OSCC patient should be treated with adjuvant therapy is made by a team of clinicians from different disciplinary backgrounds. This multidisciplinary team usually includes surgeons, radiologists and pathologists [49] [51]. The main indications for adjuvant therapy include positive resection margin and lymph node involvement (in particular, lymph node metastases with ECS) [50] [52]. Other indications for adjuvant therapy are close resection margin, poorly or moderately differentiated tumour, lymphovascular and/or perineural invasion, high T stage and uncertainty of histology [52].

3.2.3.1 Radiotherapy

The type of radiotherapy used in treatment of head and neck cancers is photon radiotherapy [52]. Photon radiotherapy is ionising radiation that causes DNA damage including an array of lesions such as single-strand breaks, base alterations, oxidative damage and double-strand breaks [53].

Radiation can ionize molecules that make up DNA and water molecules producing hydroxyl radicals which damage the DNA.

The total dose of radiation administered to OSCC patients is usually 60 Gy (Gray). The total dose is fractionated such that the patient is exposed to 2-3 Gy every day for 5 days a week [52] [50]. This fractionation implies that tumour cells in a radiation resistant phase of the cell cycle are allowed to progress to a radiation sensitive phase of the cell cycle before the next fraction is administered. Consequently, fractionated radiation maximises the number of tumour cells damaged by radiation and increases the tumour cell death rate.

3.2.3.2 Chemotherapy

The main chemotherapy agents currently used for treatment of OSCC are cisplatin and 5-FU (5-Fluorouracil) [52]. Cisplatin is usually administered orally in form of tablets, but both Cisplatin and 5-FU can be administered intravenously.

Cisplatin belongs to the group of platinum-containing anti-cancer drugs and its main mechanism of action relies on binding to DNA and causing DNA crosslinking that results in replication stop and ultimately leads to cell death. In addition to the DNA there are other cellular targets. Cisplatin can bind to phospholipids and phosphatidylserine in the cell membrane when entering the cell. In the cytoplasm, cisplatin can bind to RNA, sulphur-containing molecules and other platinum-binding sites [54]. Binding to these non-DNA target biomolecules enhances the cytotoxic effects of cisplatin.

5-FU is a pyrimidine analogue which is transformed in specific metabolites inside the cell that can then be incorporated into DNA and RNA and ultimately cause cell cycle arrest and apoptosis [55]. 5-FU also exerts toxicity through irreversible inhibition of thymidylate synthase, an enzyme involved in the synthesis of thymidine, without which DNA replication comes to a halt [56].

3.2.3.3 Side effects

Locally applied radiation severely affects the oral mucosal epithelium that becomes thin and/or ulcerated. Ulceration, and sometimes atrophy, can develop into a serious, dose-limiting complication of treatment [57]. Over 80% of OSCC patients receiving radiotherapy suffer from this condition, called mucositis, which is defined as a painful inflammation and ulceration of mucous membranes [58]. Mucositis lesions primarily appear on the soft palate, tongue, and cheeks causing severe pain and dysphagia (swallowing difficulty) [59].

Radiation may also cause damage to salivary glands resulting in reduced saliva production and an increased risk of infection by oral microorganisms.[60] Increased vascular permeability leading to tissue oedema and infiltration of inflammatory cells is another radiotherapy-associated side effect [61]. Severe blood vessel damage can lead to hypovascularity and ischemia of the oral mucosal tissue, which slows down the healing process [61].

Despite the local administration of the radiotherapy to only the head and neck area, radiotherapy-related systemic side effects can also occur. These include fatigue, nausea, vomiting, loss of appetite, temporary or permanent hair loss, changes in skin (blistering and leaking fluid) and blood [62]. Such side effects are due to direct damage to fast proliferating stem and progenitor cells in various tissues including the gastrointestinal tract, skin, hair follicles and bone marrow and can also be caused by chemotherapy.

Pain, dehydration, compromised nutritional status due to painful chewing and swallowing and infections are debilitating side effects caused by radiotherapy (and chemotherapy) [61]. Compromised function of the oral mucosa may persist for a long time after therapy completion [61]. Because of the severity, and sometimes long-term persistence of the side effects chemo- and radio-therapy are only prescribed when benefits clearly outweigh the risks.

3.3 Cancer stem cell hypothesis

Adult (somatic) stem cells are defined as immature cells that possess the ability to self-renew as well as the ability to produce different types of mature cells of a particular tissue. Based on this definition cancer stem cells (CSCs) are characterised by:

- indefinite ability to self-renew,
- ability to initiate formation of a new tumour,
- ability to reconstitute the phenotypic heterogeneity associated with differentiation of the parental tumour.

It is now recognised that tumours comprise heterogeneous populations of cancer cells. There are two different models of heterogeneity in solid cancers that aim to explain the mechanisms of tumour growth, recurrence and spread. In the stochastic model, every proliferative cell of the tumour is regarded as capable of indefinite proliferation and of giving rise to new tumours (Figure 3.6 A). In the cancer stem cell model only a subpopulation of proliferative cells of the tumour have the ability to proliferate indefinitely and to initiate new tumour growth (Figure 3.6 B).

The proof for the existence of CSCs (also referred to as tumour-initiating or tumourigenic cells) in a particular type of cancer is the ability of some proliferative cancer cells, but not others, to initiate the human disease when transplanted into immunocompromised mice. Apart from proliferating and forming a new tumour in mice, CSCs should also be capable of reconstituting the heterogeneity of the parental human tumour, i.e. within the new tumour their progeny should be able to differentiate into all the different phenotypes found in the human tumour, including the non-tumourigenic cells.

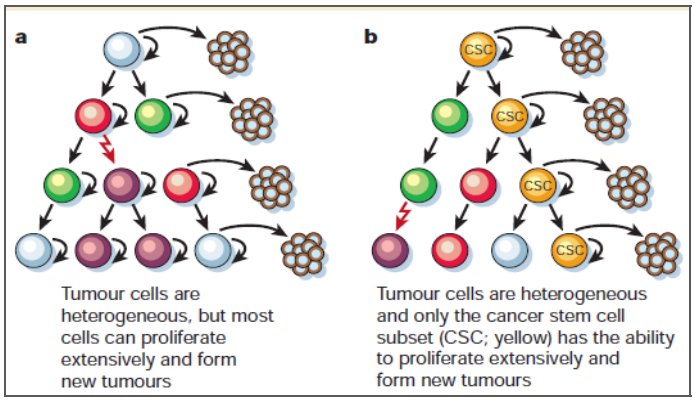

Figure 3.6*: Two general models of heterogeneity in solid cancers. Tumours are seen as heterogeneous populations of cancer cells with different phenotypic and physiological characteristics. Different cell phenotypes are shown in different colours. In the stochastic model, every proliferative cell of the tumour is able to self-renew (curved arrow) and to give rise to new tumours (horizontal arrow) (a). In the cancer stem cell model only a subpopulation of tumour cells (named cancer stem cells, CSCs, shown in yellow) is able to self-renew and initiate new tumour growth (b). *Adapted from [19]

The idea that stem cells could be at the origin of cancer was first proposed more than a century ago, when Virchow suggested that tumours arise from embryonic-like cells [63]. The cancer stem cell hypothesis re-emerged in 1997 when Bonnet and Dick found that in acute myeloid leukaemia (AML) only cells with the $CD34^{+}CD38^{-}$ phenotype were capable of initiating the human AML in non-obese-diabetic mice with severe combined immunodeficiency disease (NOD/SCID mice). The frequency of these cells in patients' blood samples was low, ranging from as little as 0.2 to 100 cells per 10^{6} mononuclear cells [64].

More recently, CSCs have been described in solid cancers including cancers of breast, central nervous system (CNS), colon and head and neck. Attempts to identify cancer stem cells (i.e. to distinguish them from their more differentiated progeny and from stromal cells) have explored different approaches based on distinctive properties of these cells. One of these properties is the ability to actively efflux dyes like Hoechst 33342 via the multidrug transporters. In HNSCC, cells with this ability (also known as the side-population) were shown to have greater clonogenicity and a high tumourigenic potential [65]. Certain enzymatic functions (e.g. aldehyde

dehydrogenase activity) have also been described as specific features of CSCs. Aldehyde dehydrogenase (ALDH) is an intracellular enzyme that catalyses the conversion of retinol to retinoic acid [66]. ALDH expressing cells have been identified in many cancers, including cancers of breast [67] brain [68], prostate [69] and head and neck [70]. In these cancers $ALDH^+$ cells were found to be able to self-renew and to initiate tumours in immunocompromised mice. Anchorage-independent growth is another well-established attribute of CSCs. It was first described as a distinctive characteristic of normal mammary stem cells, when a small fraction of normal breast cells was found to survive in non-adherent conditions and formed floating spherical colonies, termed mammospheres [71]. These cells were able to give rise to all three mammary epithelial progenitors and expressed genes associated with stem and progenitor cells [71]. This method of non-adherent culture was adapted for enrichment of CSCs and has been successfully applied in various cancer models such as breast [72], prostate [73] and head and neck cancers [74].

With advances in the development of the fluorescent activated cell sorting (FACS), identification and isolation of CSCs based on expression of distinct cell surface markers has become particularly attractive. Many studies have reported the isolation of CSCs on the basis of their surface phenotype (Table 3.3).

Table 3.3*: Cell surface phenotype of CSCs in different types of cancers

Malignancy	Molecular phenotype	Reference
AML	$CD34^{+}CD38^{-}$	[64]
Bladder	$Lin^{-}CD44^{+}CK5^{+}CK20^{-}$	[75]
Breast	$CD44^{+}CD24^{-/lo}Lin^{-}EPCAM^{+}$	[76]
CNS	$CD133^{+}$	[77]
Colon	$CD133^{+}$	[78]
Colon	$CD133^{+}$	[79]
Colon	$EPCAM^{hi}CD44^{+}Lin^{-}(CD166^{+})$	[80]
Ewing	$CD133^{+}$	[81]
Head and neck	$CD44^{+}Lin^{-}$	[82]
Liver	$CD90^{+}$	[83]
Melanoma	$ABCB5^{+}$	[84]
Ovarian	$CD44^{+}CD117^{+}$	[85]
Pancreatic	$CD44^{+}CD24^{+}EPCAM^{+}$	[86]
Pancreatic	$CD133^{+}$	[87]

* Adapted from [88]

3.3.1 Cancer stem cell hypothesis. Clinical implications

One of the reasons for therapeutic failure in cancer treatment is the intrinsic or acquired resistance of cancer cells to chemo- and/or radiotherapy. Very often there is initial tumour shrinkage at the start of the therapy, but this is followed by tumour recurrence at a later stage. Such clinical observations suggest that the majority of the tumour cells respond to therapy and die, but a small fraction of cells is resistant to therapy and survives the treatment. Therapy resistance has been attributed to CSCs rather than the bulk of tumour cells [89] [90]. Upon completion of chemo- or radiotherapy surviving CSCs are able to drive tumour growth and produce a recurrent tumour (Figure 3.7 A). CSCs have also been associated with tumour invasion and cancer metastasis [91] [87].

Cellular and molecular mechanisms that may contribute to the therapeutic resistance of CSCs include increased recognition and repair of DNA damage, alterations of cell cycle checkpoints, impairment of apoptotic pathways and reduced accumulation of cytotoxic chemotherapeutic agents through enhanced energy-dependent drug efflux [92].

The presence of therapy-resistant CSCs has been reported in various cancers. In glioma $CD133^+$ stem cells were found to be resistant to radiation due to enhanced activation of DNA damage response [93]. In breast cancer $CD44^+$ stem cells selectively survived radiation [94] and in HNSCC $CD44^+$ stem cells have been shown to be resistant to a wide range of apoptotic stimuli including UV, TNFα, cisplatin, etoposide and neocarzinostatin [95]. In melanoma the $ABCB5^+$ stem cell fraction was shown to possess increased resistance to the chemotherapeutic agent doxorubicin as a result of reduced intracellular drug accumulation [96].

These findings imply that conventional chemo- and radio-therapies, while effective on the bulk of tumour cells, fail to eliminate the stem cell fraction in many cancers allowing tumour recurrence after initial decrease of the tumour mass (Figure 3.7 A). Elucidating the molecular properties of these resistant CSCs may lead to development of CSCs-targeted therapies and contribute to development of more successful cancer treatments (Figure 3.7 B).

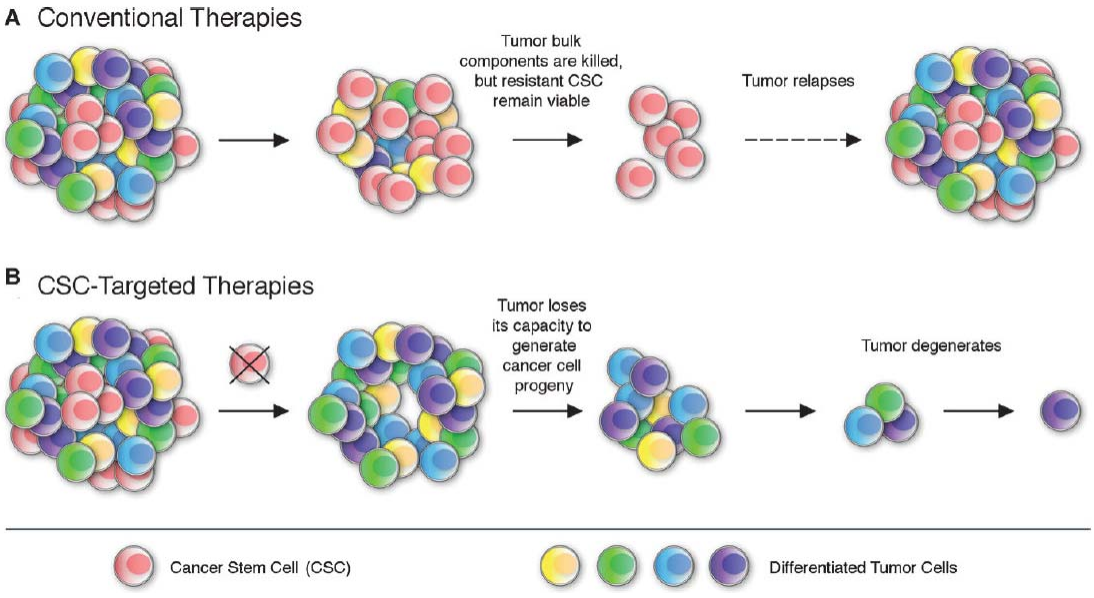

Figure 3.7*: Conventional therapies vs. CSCs-targeted therapies. Conventional therapies target the bulk of tumour cells, but may fail to kill the cancer stem cells leading to treatment failure and tumour relapse (A). Novel therapies specifically target cancer stem cells leading to a complete elimination of the tumour (B). *Adapted from [92]

3.3.2 CD44 - a marker of cancer stem cells in HNSCC

CD44 was first identified as a marker of CSCs in breast cancer [76]. Cells with the $CD44^{+}CD24^{-/low}lineage^{-}$ phenotype were isolated from patients and xenograft transplantations of as few as 100 of these cells led to initiation of tumour growth in immunocompromised mice, whereas tens of thousands of cells with alternative phenotypes did not give rise to tumours. A few years later similar results were reported for $CD44^{+}$ cells in SCC of the head and neck. Prince and co-workers performed a series of xenograft transplantations to compare the tumourigenic potential of $CD44^{+}$ and $CD44^{-}$ cells isolated from samples of human head and neck squamous cell carcinoma. They found that 5000 transplanted $CD44^{+}lineage^{-}$ cells were able to initiate tumours in mice, whereas $CD44^{-}lineage^{-}$ cells did not have this ability, even when cell numbers as large as 500,000 were introduced [82]. Analysis of the resulting tumour transplants revealed that transplanted $CD44^{+}$ cells generated both $CD44^{+}$ and $CD44^{-}$ cells. These findings demonstrated that implanted $CD44^{+}$ human tumour cells are able to produce tumours in mice that phenotypically mirror their parental human tumours. Moreover, $CD44^{+}$ cells in human tumours were found to express the transcription factor BMI1 that is associated with self-renewal functions in embryonic stem cells [97], somatic stem cells [98] and was also linked with tumourigenesis [99]. The role of CD44 (either alone or in combination with other markers) as a marker of cancer stem cells has since been confirmed by several independent studies [100] [101]. Krishnamurthy and co-workers reported that introducing 1000 $CD44^{+}ALDH^{+}$ cells isolated from human HNSCC resulted in a successful xenograft in 13 of 15 implantations, whereas 10,000 $CD44^{-}ALDH^{-}$ cells generated tumours only in 2 of 15 implantations [102]. Tumours generated by $CD44^{+}ALDH^{+}$ cells could be serially passaged, whereas tumours from the double negative cells could not, indicating self-renewal properties of the double positive but not the double negative cells.

Present evidence suggests that CD44 is one of the most frequent markers of CSCs in several solid tumours (Table 3.4) and many studies have linked

CD44 to tumour progression and poor clinical outcome in numerous types of cancers.

Table 3.4*: CD44 expression by CSCs in different cancers

Tumour type	Marker profile	References
AML	**CD44$^+$**CD34$^+$CD38$^-$Thy-1$^-$c-kit-IL3Rα$^+$	[103] [104]
CML	**CD44$^+$**	[105]
Stomach	**CD44$^+$**	[106]
Colon	**CD44$^+$**EPCAM$^+$CD166$^+$ (CD133$^+$)	[80] [79] [78]
Liver	**CD44$^+$**CD90$^+$CD45$^+$ or **CD44$^+$**CD133$^+$	[107] [108]
Gall bladder	**CD44$^+$**CD133$^+$	[109]
Pancreas	**CD44$^+$**CD24$^+$EPCAM$^+$	[86]
Breast	**CD44$^+$**EPCAM$^+$CD24$^{+/-}$ or ALDH$^+$**CD44$^+$**CD24$^-$	[76] [110] [111] [72]
Cervix uteri	**CD44$^+$**CK17$^+$	[112]
Ovary	**CD44$^+$**CD117$^+$CD133$^+$	[85]
Prostate	**CD44$^+$** or **CD44$^+$**CD24$^+$ or **CD44$^+$**CD133$^+$	[113] [114] [115]
Bladder	**CD44$^+$**lineage$^-$CK5$^+$CK20$^-$ or CD44v6$^+$EPCAM	[75] [116]
Head and neck	**CD44$^+$**lineage$^-$Bmi-1$^+$ or CD44v3$^+$ or CD44v6$^+$	[82] [117] [118] [119]
Parathyroid gland	**CD44$^+$**CD24$^-$	[120]
Lung	**CD44$^+$** (SCC) **CD44$^+$**CD133$^+$ (adenocarcinoma)	[121] [122]
Bone (sarcoma)	**CD44$^+$**Stro-1$^+$CD105$^+$	[123]
CNS	**CD44$^+$** (glioblastoma) **CD44$^+$**CD166$^+$ (meningoma)	[124] [125]

* Modified from [126]

3.3.2.1 Structure of CD44

CD44 is a transmembrane glycoprotein receptor, encoded by the *CD44* gene, typically located in glycolipid-enriched microdomains in the plasma membrane. The numerous products of the *CD44* gene vary in size due to post-translational modifications (N-glycosylation and O-glycosylation) as well as alternative splicing [127]. The receptor has 7 extracellular domains, a transmembrane domain and a cytoplasmic domain [128]. The human *CD44*

gene contains 20 exons [126]. Exons 1 to 5 and 16 to 20 are used in every CD44 isoform (standard exons), whereas exons 6 to 15 (variant exons) are inserted by alternative splicing into specific CD44 variant isoforms (Figure 3.8). The smallest CD44 isoform (known as the standard isoform, CD44s) contains only the standard exons and is abundantly expressed by many types of vertebrate cells [129]. Variant CD44 isoforms are expressed in specific tissues, during embryogenesis, lymphocyte maturation and activation and some types of carcinoma [130].

Products of the five amino-terminal exons build a globular structure, which harbours binding sites for CD44 ligands. Hyaluronan (HA), a major glycosaminoglycan component of the extracellular matrix (ECM) [131] is regarded as the main ligand of the receptor [132] [133]. Additionally, binding sites for collagen, laminin [134], and fibronectin [135] have been described. Two binding sites for other glycosaminoglucans are also known [136]. CD44 interaction with HA has been reported to activate signalling pathways linked to tumour invasion and metastasis [137] [138]. The 46 amino acids long region between the transmembrane domain and the globular ligand binding N-terminal domain [139] is heavily glycosylated and contains potential proteolytic cleavage sites [140].

The cytoplasmic domain of CD44 can interact with the cytoskeletal proteins ankyrin and the ERM protein family members ezrin, radixin and meosin [141]. Ankyrin and the ERM proteins link CD44 to the actin cytoskeleton. Through this interaction CD44 is implicated in cell adhesion and cell migration [142] [143] [144] and is involved in signal transduction, mediated through transmembrane and cytosolic kinases and linker proteins [129] [145] [146].

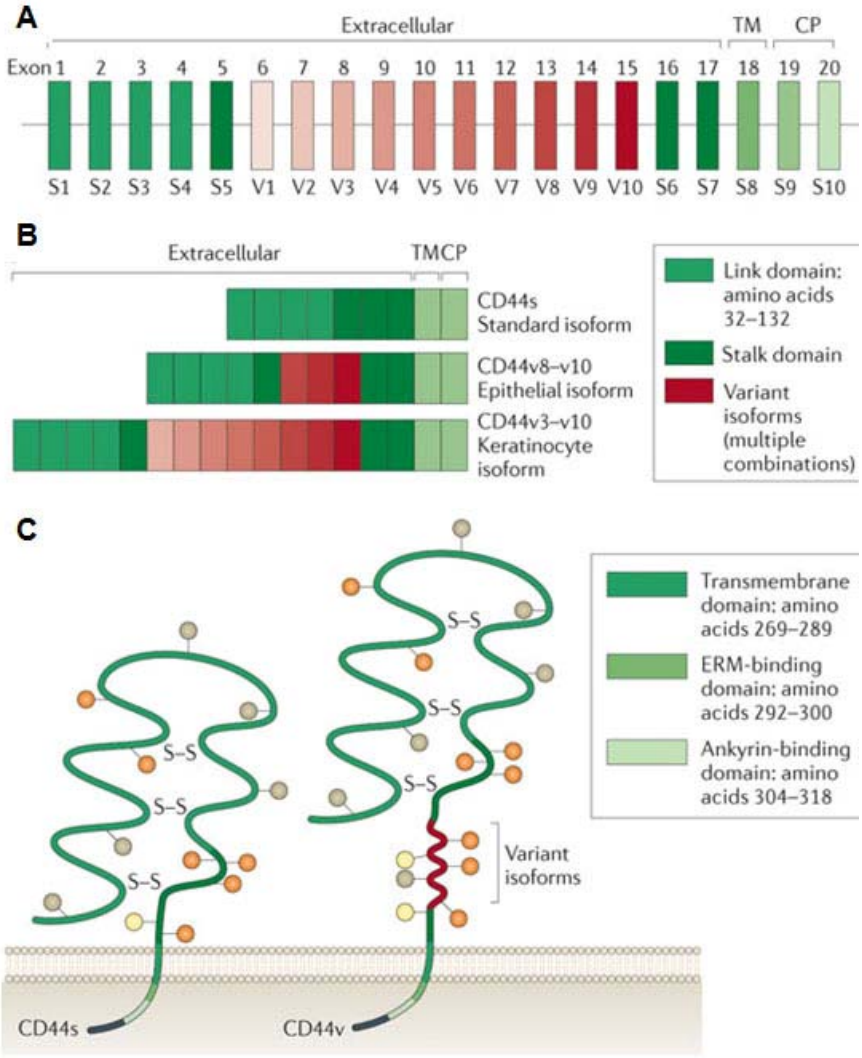

Figure 3.8*: Structure and assembly of the CD44 standard and variant isoforms. (A) The human *CD44* gene consists of 20 exons. Exons 1 to 5 and 16 to 20 are used in every CD44 isoform (standard exons, green bars). Exons 6 to 15 are inserted by alternative splicing into certain CD44 isoforms only (variant exons, red bars). (B) Exon composition of some CD44 isoforms is shown. (C) Shematic representation of the sterical confirmation of the standard (left) and variant (right) CD44 isoforms, showing sites for N-glycosylation (grey circles), O-glycosylation (orange circles) and two glucosaminoglycan binding sites (white circles). *Modified from [126]

Direct involvement of CD44 in the maintenance of stem cell-related properties has been demonstrated by many researchers. Our own laboratory found that down-regulation of CD44 leads to a reduced rate of population expansion and changes in colony morphology indicative of stem cell loss and to decreased levels of Oct4A [147]. In a different study examining CD44-regulated GSK3β signalling pathway, we reported decrease in holoclone and

tumour sphere formation and reduced expression of stem cell markers Sox2, Oct4 and Nanog upon inactivation of CD44 [148]. This also resulted in up-regulation of differentiation markers calgranulin B and involucrin. Recently, CD44v3 was discovered to mediate the Oct4-Sox2-Nanog pathway to stimulate transcription of microRNA-302 leading to self-renewal, clonal formation and cisplatin resistance [149].

3.3.3 Epithelial to mesenchymal transition in cancer metastasis

Epithelial to mesenchymal transition (EMT) is a process, in which epithelial cells undergo physiological changes that lead to a partial or a complete loss of the epithelial phenotype and to the acquisition of mesenchymal traits. Three subtypes of EMT occurring in the three distinct biological settings of embryogenesis, wound healing and cancer have been described [150].

EMT is a complex process that involves many molecular events including activation of transcription factors, expression of specific cell surface proteins, cytoskeleton remodelling, production of ECM degrading enzymes and changes in microRNAs expression [151]. Based on such cellular changes a wide range of markers has been used to identify EMT occurring *in vivo* and *in vitro* (Table 3.5).

Table 3.5*: Markers of EMT[1)]

Markers of EMT

Acquired markers		Attenuated markers	
Name	**EMT type**	**Name**	**EMT type**
Cell-surface proteins			
N-cadherin	1, 2	E-cadherin	1, 2, 3
OB-cadherin	3	ZO-1	1, 2, 3
α5β1 integrin	1, 3		
αVβ6 integrin	1, 3		
Syndecan-1	1, 3		
Cytoskeletal markers			
FSP1	1, 2, 3	Cytokeratin	1, 2, 3
α-SMA	2, 3		
Vimentin	1, 2		
β-Catenin	1, 2, 3		
ECM proteins			
α1(I) collagen	1, 3	α1(IV) collagen	1, 2, 3
α1(III) collagen	1, 3	Laminin 1	1, 2, 3
Fibronectin	1, 2		
Laminin 5	1, 2		
Transcription factors			
Snail1 (Snail)	1, 2, 3		
Snail2 (Slug)	1, 2, 3		
ZEB1	1, 2, 3		
CBF-A/KAP-1 complex	2, 3		
Twist	1, 2, 3		
LEF-1	1, 2, 3		
Ets-1	1, 2, 3		
FOXC2	1, 2		
Goosecoid	1, 2		
MicroRNAs			
miR10b	2	Mir-200 family	2
miR-21	2, 3		

ZEB1, zinc finger E-box binding homeobox 1.

[1)] Types of EMT 1: embryonic, 2: wound healing, 3: carcinogenesis
*Adapted from [150]

The changes in gene expression that occur during EMT are influenced by environmental factors [152] [153] [154]. In adult tissues, stromal signals such as transforming growth factor β (TGF-β) can induce EMT and lead to downregulation of epithelial products such as E-cadherin and upregulation of EMT-promoting transcription factors including twist and snail [155] [156]. In cancer, EMT can be triggered by the inflammatory immune response [157] and by the hypoxic tumour environment [158] [159]. EMT in different types of cancer cells *in vitro* leads to increased activity in assays of migration and invasion [160] [161]. Collectively, these findings suggest that EMT is likely to play a significant role in cancer metastasis by allowing tumour cells to migrate away from the primary tumour to initiate metastases at distant body

sites. Although *in vivo* evidence has been lacking for a long time, newer studies confirm a role of EMT in cancer spread and metastasis. For example, Kallergi and co-workers found circulating cancer cells that stained positively for vimentin and twist, both classic markers of EMT, in the blood of breast cancer patients [162].

Some studies have also linked EMT to cancer stem cells [153] [163] and to therapy resistance [164] [165]. A link between CSCs and EMT has been established for breast-cancer cells, where the CSCs phenotype ($CD44^{+}CD24^{low/-}$) has been found to coincide with the expression of EMT markers [166] [152] [153]. Mani and co-workers reported the acquisition of stem cell-like phenotype upon induction of EMT [153]. However, our recent findings suggest that rather than inducing stem cell functions, EMT can occur in CSCs present in tumours to generate an alternative stem cell phenotype [160]. We have demonstrated [160] that CSCs that have undergone EMT are present both in fresh samples of head and neck cancers and in cell lines derived from HNSCC and skin SCC. Thus, CSCs exist as at least two distinct phenotypes; one, which is preferentially proliferative, has a $CD44^{high}ESA^{high}$ surface phenotype, and displays epithelial characteristics; and another that has a migratory phenotype, is $CD44^{high}ESA^{low/-}$, and shows mesenchymal features. Using EMT and the reverse process of mesenchymal to epithelial transition (MET) cells are able to switch between these two phenotypes [160]. It is suggested that these properties, if present in tumours *in vivo*, would allow translocation of primary tumour cells to distant body sites and the development of metastases.

In summary, the evidence cited above suggests that EMT plays an important role in the metastasis of OSCC [158], breast cancer [167], and several other types of carcinoma and that EMT, by inducing therapeutic resistance is likely to be implicated in tumour recurrence [90].

3.3.3.1 Integrin αVβ6 in carcinogenesis-associated EMT

One of the surface proteins upregulated during EMT is integrin αVβ6 (Table 3.5). Unlike other integrin heterodimers, αVβ6 is not constitutively expressed by adult epithelial cells. However, its expression has been reported on epithelial cells after wounding [168] and also in various types of carcinoma including carcinoma of the lung, breast, pancreas, colon, oral and skin squamous cell carcinoma [169] [170] [168] [171]. For some of these tumours, high abundance of integrin αVβ6 has been observed particularly at the invading edge of the tumour [172]. In OSCC, integrin αVβ6 has been shown to promote migration and matrix metallopeptidase 9 (MMP9)-dependent invasion [173] [174], suggesting a role for integrin αVβ6 in the EMT occurring during tumour invasion and spread.

4. Materials and Methods

4.1 Cell culture

4.1.1 Cell lines and standard culture conditions

4.1.1.1 Cell lines

Established cell lines used in the study are listed in the table below (Table 4.1). Epithelial and fibroblastic cultures, generated from a number of OSCC specimens in course of the study, were also used and are listed in table 4.2 (Table 4.2). The newly generated cell lines were either given a laboratory number or were labelled with a code unique to each OSCC patient. The letter "n" at the end of the cell line name indicates that the cell line has been produced from cells isolated from a lymph node metastasis. Fibroblastic cultures were designated by the code followed by "fibs" in order to distinguish them from cultures of primary keratinocytes derived from the same tumour (Table 4.2). All fibroblastic cultures were examined for expression of pan-Cytokeratin to confirm their mesenchymal origin and stained negative. Cell lines Luc4 and Luc11 were produced by a colleague (Dr Luke Gammon), the remaining cell lines were produced by me. A list of clinical and pathological parameters of tumour specimens the cell lines have been generated from can be found in the appendix (Appendix Table 1 and Table 2).

Table 4.1: Established cell lines and other cell types used in the study

Cell line	Tissue of origin	Source/comment
CA1	OSCC of the tongue	generated in our laboratory
5PT	laryngeal cancer (supraglottis)	cisplatin resistant; kindly provided by Dr. Thomas Carey, University of Michigan
H357	OSCC of the tongue	integrin αV negative [175] [176]
Met2	cutaneous SCC	generated in our department [177]
normal skin fibroblasts	healthy skin biopsy	generated in our laboratory
3T3 fibroblasts	mouse embryo fibroblasts	[178]

Table 4.2: Tumour-derived epithelial cell lines and fibroblast cultures generated in course of the study

Tumour cell line	OSCC tissue of origin
24	floor of mouth
24*n	lymph node
25	tongue, oropharynx
30	retromolar region
33	mandibular alveolus
42	maxilla
50	mandible
54	tongue
57	buccal mucosa, palate
57n	lymph node
AB	floor of mouth
EM	retromolar and tonsilar region
GR	tongue
LK	gingiva
LM	mandible
Luc4	floor of mouth
Luc11	buccal mucosa
MKn	lymph node
NA	tongue
NK	tongue
PB	mandible

Fibroblast culture	OSCC tissue of origin
17fibs	manbible, gingiva
20fibs	soft palate
21fibs	cheek, mandible
22*fibs	mandible, palate
23fibs	buccal mucosa
30fibs	retromolar region
32fibs	floor of mouth, mandible
33fibs	mandibular alveolus
37fibs	maxilla, buccal mucosa
40fibs	mandible
41fibs	tongue
42fibs	maxilla
55fibs	gingiva
56fibs	floor of mouth, ventral tongue
57fibs	buccal mucosa, palate
Afibs	tongue, oropharynx
Anfibs	lymph node
ABfibs	floor of mouth
GRfibs	tongue
JFfibs	floor of mouth
JNfibs	floor of mouth
LMfibs	mandible
NAfibs	tongue
NKfibs	tongue
PBfibs	mandible

Normal skin fibroblasts and 3T3 fibroblasts were grown in DMEM/Ham's F12 medium (PAA laboratories) mixed in a ratio 3:1, supplemented with Glutamine (PAA laboratories, final concentration in medium 2 mM), penicillin/strepomycin (PAA laboratories, final concentration of 100 U/ml and 0.1 mg/ml, respectively) and 10% fetal calf serum (FCS, Biosera). This medium formulation was termed "E4 medium". All other cell lines (including the newly generated epithelial and fibroblastic cultures) were grown in the same medium (E4) with additional supplements (Table 4.3). This medium was termed "RM+ medium". For some experiments, cells were grown in the commercially-available CnT24 medium ("CnT24 progenitor cell targeted oral epithelium medium", CellnTec Advanced Cell Systems) supplemented with additives provided by the supplier (including 100 U/ml Penicillin, 100 µg/ml Streptomycin and 250 ng/ml Amphotericin B).

Table 4.3: RM+ supplements

Product name	Source	Concentration in medium
Cholera toxin	Sigma	10^{-10} M
Epidermal Growth Factor (Mouse)	Serotec	10ng/ml
Hydrocortisone	Sigma	0.4µg/ml
Insulin	Sigma	5µg/ml
Transferrin	Sigma	5µg/ml
3,3′,5-Triiodo-L-thyronine sodium salt	Sigma	$2*10^{-11}$ M

For established cell lines, cells were usually plated at clonal density (2000 cells per ml or 20,000 cells per T75 plate) in a plastic cell culture flask. For the newly generated malignant epithelial cell lines, cells were co-cultured with non-proliferative (irradiated) mouse 3T3 feeder cells during the initial few passages. In the early passages cells were plated at high density (50-60% confluence) and subsequently allowed to become 80-90% confluent. All cultures were kept in a humid incubator at 37°C in 5% carbon dioxide. When cultures reached 70-80% confluency, they were washed with phosphate buffered saline (PBS, without Ca^{2+} and Mg^{2+}) (PAA laboratories) and detached from the dish following a 10 min incubation with trypsin/EDTA (PAA laboratories, 0.025% and 2.0 g/l EDTA•4Na in 0.9% sodium chloride) at 37°C. Trypsin was neutralized by addition of an equal amount of RM+ medium. Cells were counted and centrifuged at 380 g for 5 min. The supernatant was removed and the cell pellet resuspended in RM+ medium at a concentration of 1x106 cells per ml. Cells were then either used for further experiments, re-plated, or frozen for long-term storage.

4.1.1.2 Freezing cells for long-term storage

When freezing cells, 10% dimethyl sulfoxide (DMSO) was added to the RM+ medium in which the cell pellet was resuspended. Cells were transferred to a cryovial and placed in a -80°C freezer. When freezing newly generated cell lines, DMSO-containing cryopreservation medium CryoMaxx S (PPA

laboratories) was used and, in order to increase the survival rate, cryovials were wrapped in tissue paper to allow the cells to cool and freeze slowly. After 3-14 days storage at -80°C cryovials were transferred to the liquid nitrogen till further use.

4.1.1.3 Thawing cells

Immediately after their removal from liquid nitrogen, cryovials containing cells were put in a 37°C water bath for 1 min. When the content had thawed completely, 5 ml RM+ medium was added to dilute the toxic DMSO. Cells were centrifuged at 1500 rmp for 5 min. Supernatant was aspirated and the cell pellet was resuspended in fresh RM+ medium. Depending on the number of cells in the cryovial, cells were plated in T25 or T75 flasks. Cells were passaged at least once before they were used for flow analysis or other experiments.

4.1.2 Growth in non-adherent conditions (sphere formation assay)

4.1.2.1 Poly-HEMA-coated plates

To prevent cells from attaching to the bottom of the culture wells, 48 well plates were coated with poly(2-hydroxyethylmethacrylate) (also known as poly-HEMA). 300 mg of poly-HEMA (Sigma) was dissolved in 25 ml absolute alcohol (Fisher Scientific) using a magnetic stirrer overnight to give a final concentration of 12 mg/ml. 250 µl of that solution were added into the middle 26 wells of a 48 well plate, leaving one row of wells empty at each side. To avoid the “edge effect” these wells were not used for growing spheres. The plates were left with the lids off in the hood overnight, allowing poly-HEMA to solidify. Next morning the plates were removed from the hood, wrapped in parafilm (Santa Cruz Biotechnology) and stored at room temperature till further use.

4.1.2.2 Preparation of cells and media

Cells were first grown at clonal density for 4-6 days and were then detached with trypsin/EDTA. Cells were centrifuged and resuspended in RM+ medium at a concentration of 1000-10,000 cells per 30 µl. Cells were then put through a 70 µm filter to remove clumps. To thicken the culture medium, methylcellulose (Sigma) was added to RM+ medium to create a 1% solution. To completely dissolve the methylcellulose, the solution was left on a shaker overnight. The tube was then left in an upright position with no agitation for a few hours to let the remaining undissolved methylcellulose settle. 500 µl of methylcellulose in RM+ solution were added to poly-HEMA-coated wells. Then 30 µl of RM+ medium containing 1000 to 10,000 cells were added to the wells. The number of cells plated per well depended on the size of the sphere-forming cell fraction in a given cell line. The empty wells at the edge of the plate were filled with PBS. Cells were left to grow until sphere formation could be seen, which usually took 2-3 weeks. Spheres were counted in each well and expressed as a proportion of the total number of cells plated.

4.2 Flow cytometry

4.2.1 Flow analysis

For flow analysis, cells were washed with PBS and detached from culture dishes using trypsin/EDTA. Trypsin was neutralized with RM+ medium. Cells were counted, centrifuged and resuspended either in PBS or unsupplemented DMEM/Ham's F12 (3:1) medium. Typically $5x10^5$ cells in 500 µl PBS or DMEM/Ham's F12 medium were incubated with 5 µl of the antibody for 15 minutes at room temperature. 2 ml PBS were then added to dilute the antibody. Cells were centrifuged at 380 g for 5 minutes, PBS containing the remaining unbound antibody was aspirated and the cell pellet was resuspended in 500 µl PBS containing 100 ng/ml DAPI to mark dead cells. Cells were then analysed on LSR II analyser or FACS Canto II analyser (both by BD Bioscience).

All FACS-antibodies (fluorochrome-conjugated and unconjugated) used in the study are listed in table 4.4 and table 4.5. When unconjugated primary antibodies were used, after the incubation with the primary antibody, cells were washed with PBS and resuspended in 500 µl fresh medium. A second incubation step with fluorochrome-conjugated secondary antibody was then performed at room temperature for 15 min.

Table 4.4: Primary antibodies used for flow analysis

Antigen	Clone	Isotype	Conjugate	Source
CD24	ML5	mouse IgG2a, κ	FITC, PE	BD Pharmingen
CD44	C26	mouse IgG2b, κ	PE, FITC, APC	BD Pharmingen
EGFR	EGFR.1	mouse IgG2b, κ	PE	BD Pharmingen
ESA (CD326)	HEA-125	mouse IgG1	APC, PE, FITC	MACS Miltenyi Biotec
ESA (CD326)	VU-1D9	mouse IgG1	FITC	AbD Serotec
Integrin αVβ6	10D5	mouse IgG2a	--	Millipore
Integrin β4	439-9B	rat IgG2b, κ	PE	BD Pharmingen
Integrin β6	437211	mouse IgG2b, κ	PE	R&D Systems
Human hematopoietic cocktail: CD2 (RPA-2.10) CD3 (OKT3) CD14 (61D3) CD16 (CB16) CD19 (HIB19) CD56 (CB56) CD235a (HIR2)		--	APC	eBioscience
PECAM1 (CD31)	WM59	mouse IgG1, κ	APC	eBioscience
PDGFRβ (CD140b)	18A2	mouse IgG1, κ	APC	Biolegend
PDGFRβ (CD140b)	APB5	rat IgG2a, κ	APC	eBioscience

Table 4.5: Secondary antibodies used for FACS and immunohistochemistry (IHC)

Antigen	Species	Conjugate	Dilution	Source
Mouse IgG	Rabbit	Alexa-488	1:1000 (FACS) 1:700 (IHC)	Invitrogen
Mouse IgG	Goat	Alexa-488	1:1000 (FACS) 1:700 (IHC)	Invitrogen
Rabbit IgG	Goat	Alexa-546	1:700 (IHC)	Invitrogen

For some assays cells were co-stained with two or three different antibodies. If only conjugated antibodies were used, cells were incubated with all the different antibodies at the same time. When unconjugated antibodies (i.e. anti- integrin αVβ6) were used, staining was carried out sequentially. In the first incubation step only the unconjugated primary antibody was added to the sample. Second incubation step included the secondary antibody and the third incubation step included all the other primary conjugated antibodies. After each incubation step 2 ml PBS were added, cells were centrifuged and after PBS was aspirated the cell pellet was resuspended in 500 µl of fresh PBS.

Flow cytometric analysis of cells isolated from tumour tissue was carried out according to the protocol as above, except all antibody incubations were performed at room temperature for 30 minutes.

4.2.2 Isotype controls and non-stained control samples

To assess the degree of unspecific cell binding of the FACS antibodies, flow analysis was performed on different types of cells (keratinocytes and fibroblasts) that were incubated with different fluorochrome-conjugated IgG isotypes (Table 4.6).

Table 4.6: Isotype controls used for flow cytometric analysis

Isotype	Clone	Conjugate	Source
mouse IgG1, κ	MOPC-21	APC, FITC, PE	BD Pharmingen
mouse IgG2a, κ	G155-178	APC	BD Pharmingen
mouse IgG2b, κ	27-35	FITC	BD Pharmingen
mouse IgG2b, κ	MPC-11	PE	BD Pharmingen
rat IgG2b, κ	R35-95	Pacific Blue	BD Pharmingen

The signal intensity of the isotype stained control samples was compared with the signal intensity of non-stained control samples, which was entirely due to auto-fluorescence. None of the isotype controls showed a detectable difference in signal intensity compared to the non-stained control sample (Appendix Figure 1 and Figure 2). Therefore, it was considered unnecessary to use an isotype control sample in each FACS experiment. Instead, a non-stained control sample containing 1-2x10^5 cells was used in each experiment to set up machine voltages and to draw gates for sample analysis. For integrin αVβ6 (unconjugated primary antibody) a sample stained only with the secondary antibody was used as negative control to assess non-specific background signal.

4.2.3 Compensation

When combinations of fluorochromes were used for which emission spectra overlap (e.g. FITC and PE), manual or automatic compensation was carried out in order to correct spill-over. Briefly, cells were stained with each antibody separately and flow analysed. Spill-over into the wrong channel (i.e. PE signal detected in the FITC channel and vice versa) was corrected by adjusting the median fluorescence intensity (MFI) in the wrongly detected channel by bringing it to the MFI level of the non-stained control sample.

4.2.4 Assessing the CD44 median fluorescent intensity (MFI)

Samples stained for CD44 were flow analysed according to the standard protocol. The MFI value for the CD44 signal was determined by the FACS machine for both the non-stained control sample and the sample

immunolabelled with anti-CD44 PE-conjugated antibodies. The ΔMFI was calculated by subtracting the CD44 MFI value of the non-stained sample from the MFI value of the labelled sample. Because the MFI depends on the calibration and the settings of the FACS machine, all samples were analysed during the same session.

4.2.5 Cell sorting experiments to test negative and positive selection

4.2.5.1 Cultured cells

CA1 cells and cultured fibroblasts derived from fresh tumour tissue were trypsinised and mixed in a ratio 1:1. After staining the cell mix with epithelial-specific antibodies (used in positive selection) or antibodies against non-epithelial-specific antigens (used in negative selection) epithelial and non-epithelial cell fractions were sorted. Following sorting, cells were centrifuged at 380 g for 5 min and $3*10^4$ – $5*10^4$ cells per well were plated in a 24 well plate. The following day cells were fixed with ice-cold acetone-methanol (1:1) at -20°C for 5 min and stained for pan-Cytokeratin (see below).

4.2.5.2 Cells isolated from fresh tumour tissue

Tumour cells isolated from fresh tumour tissue were stained and sorted according to the same protocol as above. Following sorting, cells were deposited on poly-L-lysin coated microscope slides (VWR international) using the cytospin centrifuge (Thermo Scientific). Briefly, the slides were labelled and mounted with a paper pad. The plastic cuvette was placed on top of the paper pad and secured with the metal holder. 250 µl of RM+ medium containing the sorted cells were pipetted into the cuvette and centrifuged at 200 g for 10 min. The slides were left to dry, cells were then fixed with ice-cold acetone-methanol (1:1) at -20°C for 5 minutes and stained for pan-Cytokeratin according to the standard protocol (see below).

4.3 Immunofluorescence and immunohistochemistry

4.3.1 Cultured cells and cells isolated from tumour tissue

Cells were grown in a 12 well culture plate (VWR International) and, when cell colonies reached the required size, the plate was washed with PBS and cells were fixed in ice-cold acetone-methanol (1:1) at -20°C for 5 minutes. After fixing, cells were washed with PBS three times and the blocking solution (1% BSA, 0.5% TritonX100 in PBS) was added for 1 hour at room temperature. The primary antibody was diluted in blocking solution and left on the cells overnight at 4°C. Plates were then washed with PBS three times and the secondary antibody in blocking solution was applied for 3-4 hours at room temperature. The plate was then washed with PBS twice and incubated with PBS containing 300 ng/ml DAPI. Cells were again washed with PBS and mounted with Immumount (Thermo Scientific). All antibody incubations and blocking were performed with a slow agitation on a shaker. All primary and secondary antibodies and dilutions used are listed in table 4.7 and table 4.5.
When fresh tumour cells were stained, cells were deposited onto a microscope slide prior to staining using the cytospin centrifuge. The area containing the cells was delineated with a hydrophobic pen (DAKO) and cells stained according to the standard protocol described above.

Table 4.7: Primary antibodies used for immunohistochemistry

Antigen	Clone	Isotype/Species	Dilution	Source
CD44	C26	mouse IgG2b, κ	1:100	BD Pharmingen
Wide spectrum cytokeratin	polyclonal	Rabbit, IgG	1:100	Abcam
Vimentin	RV202	Mouse IgG1	1:100	BD Pharmingen
EGFR	111.6	IgG1	1:100	Thermo Scientific
E-Cadherin	polyclonal	Rabbit IgG	1:100	Santa Cruz
β-Catenin	6F9	Mouse IgG1	1:100	Sigma

4.3.2 Tumour tissue sections

4.3.2.1 DAB staining for CD44

Resected tumour tissue was fixed in 4% paraformaldehyde (PFA) and embedded in paraffin. 5 µm thick sections were cut from tumour blocks and put on poly-lysine coated microscope slides. Fixation, embedding and cutting of the tissue was done by the staff of the Royal London Hospital pathology department.

Tissue sections were first deparaffinised by immersing the slides in xylene, two times for 5 min each, and then rehydrated by incubating in decreasing strengths of ethanol (100%, 90% and 70%) for two min each. The slides were then washed in distilled water for 5 min. Tissue sections were delineated using a hydrophobic pen. In a humidified chamber, 300-400 µl of a 3% H_2O_2 solution (Sigma) were pipetted onto the tissue sections and left on for 10 min to quench the endogenous peroxidase activity. Slides were rinsed in distilled water, placed in a container, and immersed in 300-350 ml of 10 mM citrate buffer (tri-sodium citrate (dihydrate) in dH_2O, pH 6) to unmask antigenic epitopes. The container was heated in a microwave at maximum power for 3 min. The container was removed from the microwave, refilled with citrate buffer and allowed to cool down for 20 min at room temperature.

After washing the slides twice for 5 min in PBS, they were placed into a humidified chamber and incubated with blocking buffer (10% goats serum in PBS) for 1 h to block the non-specific antibody binding sites. The blocking buffer was flicked off and 200-300 µl (depending on the size of the tissue section) of blocking buffer containing the mouse-anti-human-CD44-antibody (BD Pharmingen, diluted 1:70) was added. After incubation at 4°C overnight, slides were washed in PBS and incubated with the secondary HRP-conjugated goat-anti-mouse-antibody (DAKO) for 2 h at room temperature. Following two washes in PBS the slides were then treated with 3,3'-diaminobenzidine (DAB) substrate kit for peroxidase (Vector Laboratories) according to the manufacturer's instructions. Briefly, immediately before use,

2 drops of the buffer stock solution, 4 drops of the DAB stock solution and 2 drops of hydrogen peroxide solution were added to 5 ml of distilled water and mixed well. The solution was applied on the tissue sections. The colour development was monitored and the reaction was stopped by immersing the slides in fresh distilled water. A sufficient staining intensity was observed after 3-5 min. The slides were then washed in water and counter-stained with hematoxylin and eosin (H&E).

4.3.2.2 H&E staining

Upon completing the DAB staining for CD44 detection, slides were submerged in hematoxylin (DAKO) for 2-5 minutes to stain the nuclei. Slides were rinsed in tap water for 5 minutes to oxidise the dye and give it the blue colour. Slides were then dipped briefly in 1% acid alcohol and counterstained with eosin (DAKO) for 2-3 minutes to stain the cytoplasm and connective tissue. This was followed by rinsing in water and rehydrating in a series of alcohols of decreasing strength (100%, 90%, 70%) for 2 min each. Finally, sections were fixed through incubation in xylene for two times, 2 min each. Immediately after fixation, slides were mounted with coverslips (VWR International) using DPX mounting medium (Sigma).

4.4 Microscopy

Pictures of stained cultured cells or cells isolated from tumours were taken on the Nikon eclipse TE 2000 microscope connected to QIClick™ digital CCD camera. Typically photographs were taken at 100x or 200x magnification. The microscope was used for both fluorescent and bright field photographs. Pictures were processed and analysed using QCapture Suit software, Image J graphics package and Photoshp CS4.

4.5 Processing the tumour tissue

OSCC tissue was sampled at St Bartholomew's Hospital and the Royal London Hospital with patients' informed consent under the Ethics approval

from East London and The City Research Ethics Committee (study number P/03/122, principal investigator: Prof Farida Fortune). The specimens were placed in a 15 ml falcon tube containing 6 ml transport medium (RM+ medium containing 200 U/ml penicillin and 0.2 mg/ml streptomycin) and were kept at 4°C until further use. The tissue was usually processed and analysed on the next day after resection.

4.5.1 Isolating cells from tumour specimens

Tissue samples were washed, minced with a scalpel and transferred to a falcon tube for dissociation in type III collagenase (Sigma) at a final concentration of 200 U/ml for up to 2 hours (Figure 4.1). Every 15 minutes the suspension was put through a 5 ml pipette (Fisher Scientific) in order to mechanically enhance disintegration of the tissue. Every 30 minutes the solution containing the cells that had broken out from the tissue was removed and neutralized with RM+ medium. Fresh medium containing collagenase was added to the remaining tissue fragments. The last round of digestion was performed in 1x trypsin/ETDA for 5 min.

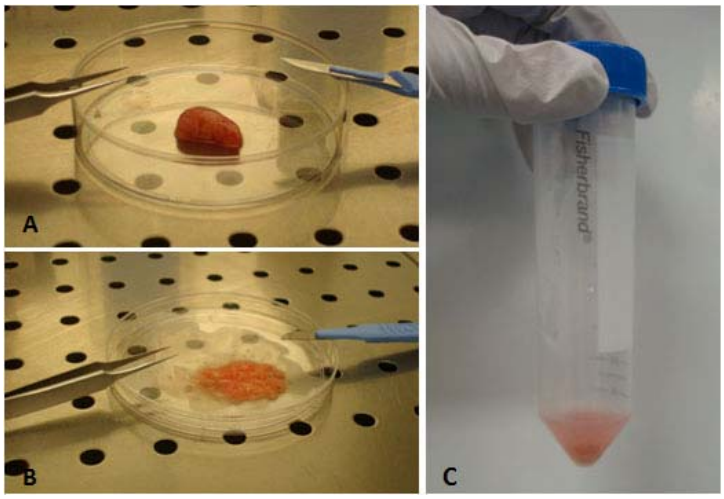

Figure 4.1: Processing of the tumour tissue. After three rounds of washes in PBS the tumour tissue was placed on a plastic cell culture dish (A). The tissue was finely minced using sterile scalpel and forceps (B). The tissue fragments were transferred into a 50 ml Falcon tube containing type III collagenase (200 U/ml) in unsupplemented DMEM/F12 medium (C).

All procedures were carried out in a laminar flow hood to minimise the risk of infecting the isolated tumour cells. Only sterile/autoclaved instruments were used to handle the tissue.

Cells extracted from the tissue in this manner were centrifuged at 380 g for 7 minutes. The supernatant was aspirated and the cell pellet was resuspended in 1-2 ml red cell lysis buffer (Sigma), which was left on for 2 min. 10 ml PBS was added to the tube and cells were pipetted up and down a few times to encourage the lyses of the red blood cells. Cells were then centrifuged at 1500 for 5 min. After the supernatant was removed, the pellet was resuspended in a small volume (500 µl – 1 ml) of PBS or RM+ medium. Isolated tumour cells were either plated on a layer of irradiated 3T3 fibroblasts in RM+ medium or immunolabelled with antibodies for FACS analysis.

4.6 Generating cell lines from OSCC specimens

4.6.1 Preparation of feeder cells

In preparation for irradiation, mouse 3T3 fibroblasts were grown in DMEM/Ham's F12 medium supplemented with 2 mM glutamine, penicillin/streptomycin (final concentration of 100 U/ml and 0.1 mg/ml, respectively) and 10% FCS in T175 flasks. Upon reaching confluency, cells were washed in Versene (Gibco) and trypsinised. After centrifugation at 380 g for 5 min cells were resuspended in fresh medium. For irradiation, typically 50-60*10^6 cells were trypsinised and resuspended in 20-25 ml medium. Cells were irradiated with γ-rays at a total dose of 60 Gy. Following irradiation, cells were frozen in FCS containing 10% DMSO till further use.

4.6.2 Establishing tumour-derived cell lines

4.6.2.1 Explant method

The tissue specimen was cut into pieces of approximately 1mm^3 in size, which were placed on a plastic cell culture dish. When they dried and adhered RM+ medium was added. After 4-10 days, epithelial cells started growing out from the tissue pieces and could be passaged after reaching 70-80% confluency. This initial cell expansion step was referred to as “passage 0”. Successive rounds of trypsinisation and re-plating gave rise to passages 1, 2, 3 etc. Medium was changed every 2-3 days. For the first few passages cells were grown as co-culture with non-proliferative 3T3 feeder cells, but from passage 8-10 feeders were no longer required.

4.6.2.2 Enzymatic method

Tumour cells were isolated from the surgical specimens of OSCC using collagenase III and trypsin (see section 4.5) and were plated on a subconfluent layer of irradiated 3T3 fibroblasts in a T25 flask in RM+ medium. Typically, 5x10^5 – 6x10^5 feeder cells were plated one day before seeding the tumour cells. On following days, 1x10^5 –2x10^5 feeder cells were added when necessary, to maintain them at a subconfluent level. The medium was changed for the first time 3 days after starting the culture. Afterwards the medium was changed every 2nd-3rd day. After 4-14 days for some cultures epithelial colonies could be seen in the flask amongst the feeder cells. When epithelial colonies grew and nearly reached confluency (after 10-25 days) cells were trypsinised. Half of the harvested cells was frozen and half was re-plated, either on a subconfluent layer of irradiated 3T3 fibroblasts in RM+ medium or in CnT24 medium without feeder cells.

4.7 Immunoblotting

4.7.1 Cell preparation and protein extraction

Flasks or dishes containing up to 70-80% confluent cell cultures were washed with PBS. To lyse the cells, RIPA Buffer (50 mM Tris pH 7.3, NaCl, 0.1% SDS, 1% NP40) containing protease inhibitor (Roche Diagnostics) and 1% phosphatase inhibitor (Sigma) was added to just cover the surface of the flask. After 30 min on ice, cell scrapers (BD Falcon) were used to disrupt the cells and release intracellular proteins. The lysates were collected and centrifuged at 21,912 g for 20 min at 4°C. The supernatant was collected into 1.5 ml eppendorf tubes and kept at -80°C till further use.

Protein concentration in lysates was determined using Bio-Rad D_C Protein Assay (Bio-Rad Laboratories). Briefly, 25 µl of reagent D_C were added to 1 ml of reagent A producing reagent A'. 25 µl of reagent A' were pipetted into wells of a 96 well plate. Protein lysates were diluted 1:10 with RIPA buffer and 10 µl were then added to the wells followed by 200 µl of reagent B. After 15 min at room temperature absorbance was measured at 595 nm and converted to protein concentration in the lysate, using standards of known concentrations of bovine serum albumin between 0-10 µg.

4.7.2 Western blotting

7.5 -10 µg of total cell protein were mixed with SDS-PAGE 2x buffer and heated at 95°C for 5 min to denature the proteins. Samples were then centrifuged for 30 sec and loaded onto the 4-12% NuPAGE Bis-Tris gels (Life Technologies). The Precision Plus Protein Standards ladder (Bio-Rad Laboratories) was loaded in the first gel slot and the electrophoresis chamber was filled with SDS running buffer (Life Technologies). Electrophoresis was performed at 200 mV for approximately 1h 40 min until all bands of the protein standards ladder have completely resolved. The gel was removed from the cassette and placed in a blotting chamber. The blotting sandwich was assembled as follows: sponge, two layers of blotting paper, gel,

polyvinylfluoride membrane (Hybond-C Extra, Amersham Pharmacia Biotech) followed by another two layers of blotting paper. All materials were pre-soaked in transfer buffer (Bio-Rad Laboratories) containing 20% methanol (Fisher Scientific). Air bubbles were removed by gently rolling a FACS tube over the assembly. The blotting sandwich was placed in the transfer tank filled with transfer buffer and connected to the power supply in such way that the current was flowing through the gel to the membrane. Transfer was performed at 400 mA for 90 min.

Following transfer, the membrane was separated from the gel and stained with Poinceau (Sigma) red to visualise the proteins and check whether the transfer was successful. After rinsing in tris buffered saline (TBS, see below) the membrane was incubated with blocking buffer (TBS-T, 5% dry milk powder in TBS with 0.1% Tween) on the shaker for 1 h at room temperature to block non-specific protein binding sites on the membrane. The membrane was then incubated under slow agitation, overnight at 4°C, with the primary antibodies diluted (Table 4.8) in blocking buffer.

Table 4.8: Primary and secodary antibodies used for western blotting

Antigen	Clone	Species/Conjugate	Dilution	Source
CD44	156-3C11	mouse IgG2a	1:1000	Cell Signalling
β actin	8226	mouse IgG1	1:10,000	Abcam
EGFR	polyclonal	Rabbit IgG	1:1000	Santa Cruz Biotechnology
EGFR-P (Tyr 1173)	9H2	mouse IgG1	1:200	EMD Chemicals
mouse immunoglobulins	polyclonal	goat, HRP-conjugated	1:1000	DAKO
rabbit immunoglobulins	polyclonal	goat, HRP-conjugated	1:1000	DAKO

Following three 5 min washes in TBS, the membrane was incubated with appropriately diluted secondary antibodies conjugated to horseradish peroxidase (HRP) for 1 h at room temperature. The membrane was again washed in TBS buffer for three times, 5 min each. The membrane (protein

side up) was then placed in an X-ray film cassette and up to 1 ml ECL plus blotting detection reagent (GE-Healthcare) was pipetted onto the membrane covering it completely. The ECL reagent was left on for 2 min and the surplus was gently wiped off with a tissue paper. An autoradiography film was placed on top of the membrane, left on for 15 sec to 5 min and then developed.

4.7.2.1 Buffers and reagents for immunoblotting

Transfer Buffer 1x

Transfer buffer (Bio-Rad 10x)	200 ml
Methanol (Fisher Scientific)	400 ml
	In 2 L dH_2O

TBS 10x

Tris (500 mM)	60.57 g
NaCl (1.5 M)	87.66 g
	in 1 L dH_2O, pH was adjusted to 7.6 with HCL

4.8 Clinical data acquisition

Full clinical reports, produced by the pathologist who examined the tumour tissue for diagnostic purposes, were obtained for all 34 patients included in the study. The names of the patients were coded, but all the other relevant information was available. The reports contained information about pathological features of the tumour describing TNM staging, extracapsular spread, invasion pattern, perineural and lymphovascular invasion, tumour depth, tumour grade and host inflammatory response. Sex and age of the patient as well as the description of the surgical margin of the tumour were also stated.

4.9 Statistics

Clinical and pathological parameters were examined for a correlation with the frequency of CD44 expressing cells in tumour samples using statistical package “R”.

Spearman's ranked test and Fisher's exact test (the most common non-parametric tests) were chosen for the statistical analyses of the data. The correlations were considered significant when p-values were below 0.05.

5. Results

5.1 Negative and positive selection in analysis of surgical specimens of OSCC

In recent years, analysis of cells isolated from fresh tumour tissue has been performed for a number of solid cancers. Most of these studies focused on identification and isolation of cancer stem cells (CSCs) from cell suspensions generated through enzymatic dissociation of the tumour tissue. Flow cytometry is the most common approach and has been used in identification and isolation of CSCs from various solid malignancies, including cancers of breast [76], HNSCC [82], bladder [75], colon [80] and pancreas [86]. To my knowledge, the method of selecting the epithelial cell fraction containing the CSCs amongst other tumour cells of non-epithelial cell lineages such as fibroblasts, endothelial cells, inflammatory cells and pericytes was never investigated in great detail. The accuracy of this selection, however, is very important as expression of stem cell markers may not be exclusive to the epithelial CSCs. Here, I test the standard method (negative selection) and attempt to develop a novel method (positive selection) for identifying the epithelial fraction amongst cells isolated from the tumour tissue.

5.1.1 Flow cytometric analysis of specimens of OSSC. Negative Selection

Oral squamous cell carcinoma (OSCC) and other solid tumours contain multiple diverse cell types, including (epithelial) tumour cells, fibroblasts, endothelial cells and infiltrating inflammatory cells. The non-epithelial components of the tumour are collectively referred to as tumour stroma (Figure 5.1 A). Because SCC is a cancer of epithelial origin, CSCs reside in the epithelial fraction of these tumours. Prior to assessing the presence and the proportion of CSCs in specimens of OSCC, the epithelial cell fraction must be identified within all cells isolated from the specimen through enzymatic digestion of the tumour tissue (Figure 5.1 B). The standard technique used for identification and isolation of epithelial cells in a mix of cells of different lineages by flow cytometry is based on the exclusion of all

non-epithelial cells. This technique was described by Al Hajj and co-workers for analysing breast cancer tissue [76] and was used in 2007 by Prince and colleagues for analysis of HNSCC specimens [82]. Isolated tumour cells are stained with a mix of different antibodies against non-epithelial components of the tumour, including antibodies against hematopoietic, mesenchymal and endothelial antigens. These antigens act as lineage markers for non-epithelial cells (referred to as “lineage markers”) and the method is known as “negative selection”, because the cell fraction of interest (epithelial fraction) is not labelled by the antibodies used.

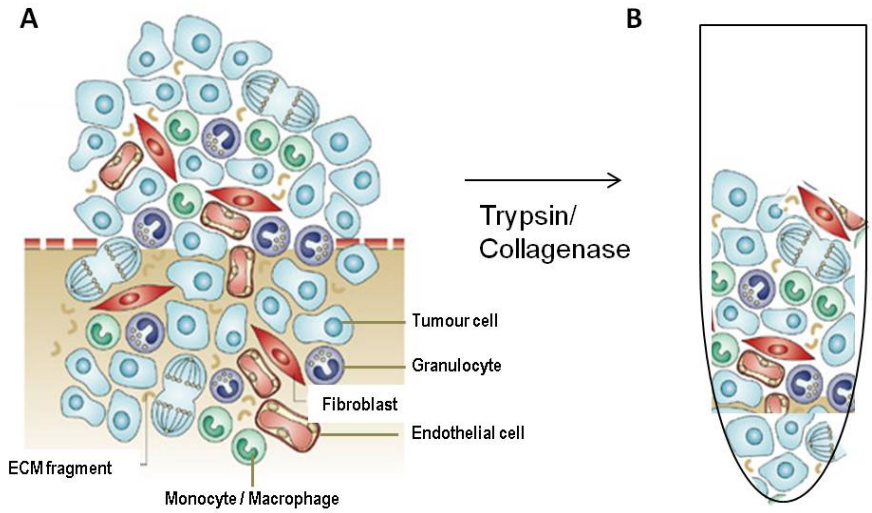

Figure 5.1*: Schematic representation of a carcinoma with its stroma consisting of cells of different cell lineages. A carcinoma consisting of different cell types is shown. The stroma contains inflammatory cells (monocytes/macrophages), granulocytes, fibroblasts and endothelial cells (A). An enzymatic digestion of the tumour specimen produces a single cell suspension containing cells of all the different cell lineages (B). *Modified from [179]

5.1.1.1 Expression of the negative selection markers by CA1 cells

The lineage markers, commonly used in the negative selection, were assessed for their specificity using an established OSCC cell line CA1. All lineage markers used in this study to identify lineage$^+$ cells are listed in table 5.1 together with specific cell types by which they are typically expressed (Table 5.1). Expression of these lineage markers (CD2, CD3, CD14, CD16,

CD19, CD56, CD235a, CD31 and CD140b) by CA1 cells was analysed on an mRNA microarray and by flow cytometry. All of these antigens are reported to be specific for cells of various non-epithelial cell lineages (Table 5.1) and were not expected to be expressed on cells from an epithelial cell line such as the tongue SCC-derived cell line CA1.

Table 5.1: Lineage markers used in negative selection and cell types by which they are typically expressed*

Antigen	Cell type
CD2	T, B lymphocytes, thymocytes natural killer cells, monocytes subset
CD3	mature T lymphocytes, thymocytes
CD14	monocytes, macrophages, Langerhans cells, granulocytes
CD16	neutrophils, natural killer cells, activated monocytes, macrophages, dentritic cells
CD19	B lymphocytes, follicular dentritic cells
CD31 (PECAM)	monocytes, platelets, granulocytes, endothelial cells, lymphocytes subset, dendritic cells
CD56 (NCAM)	neural tissues
CD140b (PDGF Receptorβ)	fibroblasts, mesenchymal cells, platelets, glial cells and chondrocytes
CD235a	erythrocytes

*Antibodies against CD31 and CD140b were supplied as separate monoclonal antibodies. All the other antibodies were part of the human hematopoietic cocktail.

We performed an mRNA microarray looking at expression of lineage markers in several types of CA1 clones and sorted cell populations with different phenotypes. Cell preparations and the microarray analysis were performed by a colleague (Dr Adrian Biddle), who made the data available to me for analysis. The clones were generated through single cell cloning from the parental cell line (CA1par). The generated clones differed in their morphologies and FACS phenotypes (Table 5.2, Figure 5.2). Clone 1 was a purely epithelial clone, whereas clone 23 was a purely migratory clone with

an EMT phenotype. In addition to these clones, distinct cell populations with epithelial and EMT phenotypes were isolated by flow-sorting the parental line and were also included in the microarray. Figure 5.2 and table 5.2 describe the sorted populations. All sorted CA1 populations used for the mRNA microarray analysis have been extensively studied and are described in detail in Biddle et al. 2011 [160]. Because of their different morphological and differentiation states, these different CA1 clones and populations can be regarded as representing different cell populations present in a tumour.

Surprisingly, expression of the lineage markers CD14, CD31, CD56 and CD140b was detected in all or some of the CA1 clones and populations. Figure 5.3 summarises the findings.

Table 5.2: CA1 clones and cell populations used for the mRNA microarray analysis

Clone/cell line	Properties/Phenotype
Clone 1 (C1)	CA1 clone 1, epithelial phenotype
Clone 23 (C23)	CA1 clone 23, EMT phenotype
Parental hihi (Par hihi)	CA1par $CD44^{high}ESA^{high}$, epithelial phenotype
Parental hilo (Par hilo)	CA1par $CD44^{high}ESA^{low}$, EMT phenotype
Parental lo (Par lo)	CA1par $CD44^{low}$, differentiating

A **B**

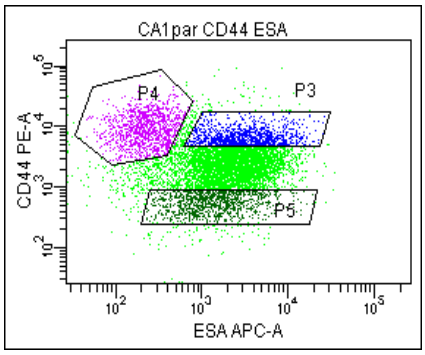

Gate	Phenotype	Characteristics
P3	$CD44^{high}ESA^{high}$	Epithelial stem phenotype: small, round, stationary, self-renewing
P4	$CD44^{high}ESA^{low}$	EMT stem phenotype: spindle shaped, migratory, self-renewing
P5	$CD44^{low}$	Large and flat, no self-renewing potential, differentiating

Figure 5.2: CA1 populations used for the mRNA microarray analysis. Gated populations (A) were isolated through flow-sorting. Sorted populations represent cell fractions with distinct morphological and behavioural features (B). In P3 and P4 there are the two types of stem cells with the stationary ($CD44^{high}ESA^{high}$) and the migratory ($CD44^{high}ESA^{low}$) phenotypes, respectively. P5 is the differentiating CD44 low fraction ($CD44^{low}$).

High expression level of CD14 (average signal between 1944 and 3392) was observed in all samples (Figure 5.3). Its highest expression (average signal above 2000) was detected in samples Par hilo, Par lo and C23. A low level of CD31 expression just above the background signal of 100 was detected in all samples (average signal between 135 and 165). CD56 was also expressed at low levels in all samples (average signal between 179 and 249). CD140b was expressed in the samples Par hilo and C 23 (average signal 292 and 261) (Figure 5.3)

A

	Par hihi	Par hilo	Par lo	C 1	C 23
CD14	1944	2568	3392	1219	3055
CD31	151	135	165	146	149
CD56	239	237	179	249	207
CD140b	103	292	90	96	261

B

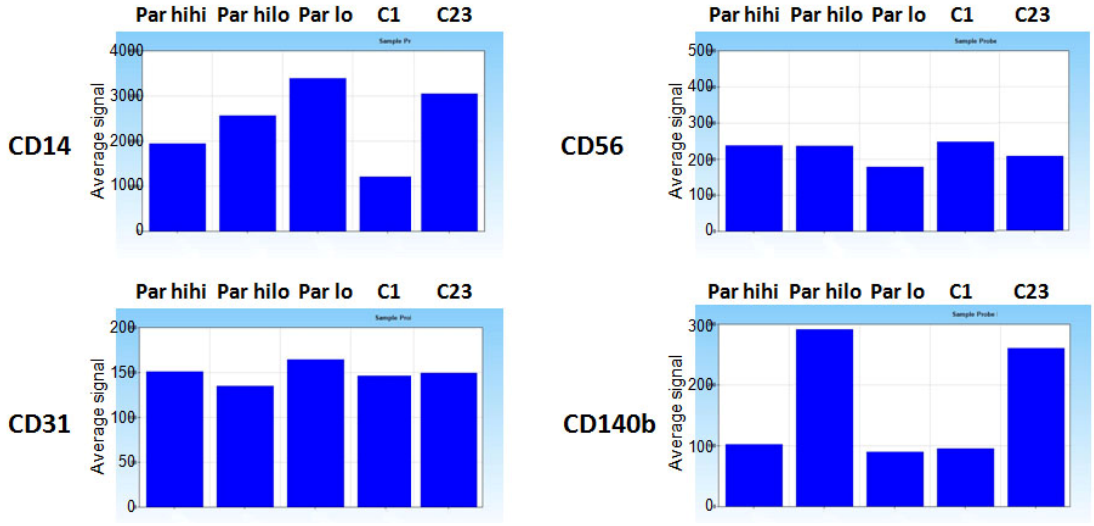

Figure 5.3: mRNA microarray analysis of the expression of negative selection markers by different CA1 clones and populations (average signal). (A) The table shows detected average signal values after normalisation and p value corrections. Detectable background signal was around 100. For genes with more than one probe on the array, numbers for the probe with the highest expression are shown. (B) Above background expression of CD14, CD31 and CD56 was detected in all samples. CD14 was expressed at a higher level in the samples Par hilo, Par lo and C 23. CD31 and CD56 were expressed at a low level in all samples. CD140b signal was detected in the samples Par hilo and C 23.

In summary, all samples analysed on the mRNA microarray were found to express detectable levels of CD14, CD31 and expression of CD56 and CD140b was seen in the samples Par hilo and C 23. Highest CD14 expression was detected in the differentiating $CD44^{low}$ population of the parental CA1 line (Par lo), highest levels of CD56 were observed in clones and populations with the epithelial phenotype, whereas the EMT-phenotype clones were highest for CD140b (Table 5.2, Figure 5.3). Consequently, in each population (epithelial, EMT and differentiating) expression of at least one of the putative non-epithelial lineage markers was detected by the mRNA microarray. If expression of these non-epithelial markers was also present at

the protein level on the cell surface, these cell populations, if present in the tumour, would be lost from the epithelial fraction identified for further analysis.

To analyse this problem further, expression of negative selection markers by CA1 cells was examined at the protein level. CA1 cells were flow-analysed for the expression of all lineage markers listed in table 5.1. Antibodies against CD2, CD3, CD14, CD16, CD19, CD56 and CD235a were included in the human hematopoietic cocktail, whereas antibodies against CD31 (PECAM) and CD140b (PDGFRβ) were supplied as two separate monoclonal antibodies. Consistent with the mRNA microarray, expression of some of the lineage markers by CA1 cells was detected by flow cytometry (Figure 5.4). Markers included in the human hematopoietic cocktail were found to be expressed by 6.3% of CA1 cells (Figure 5.4, D), PECAM was detected on 9.9% and CD140b on 7.7% of cells (Figure 5.4 E, F). To confirm that detected fluorescence was the result of specific antibody binding, cells were stained with two different APC-conjugated isotype controls (Figure 5.4 B and C). There was no difference in signal distribution and intensity between the non-stained and the isotype-stained samples (compare Figure 5.4 A and B, C).

Staining with other isotype controls relevant for flow cytometric experiments in this study was also performed (Appendix Figure 1 and Figure 2). Because no difference in signal intensities between the non-stained and isotype stained samples was observed, the non-stained samples were used to set the gates in the subsequent experiments.

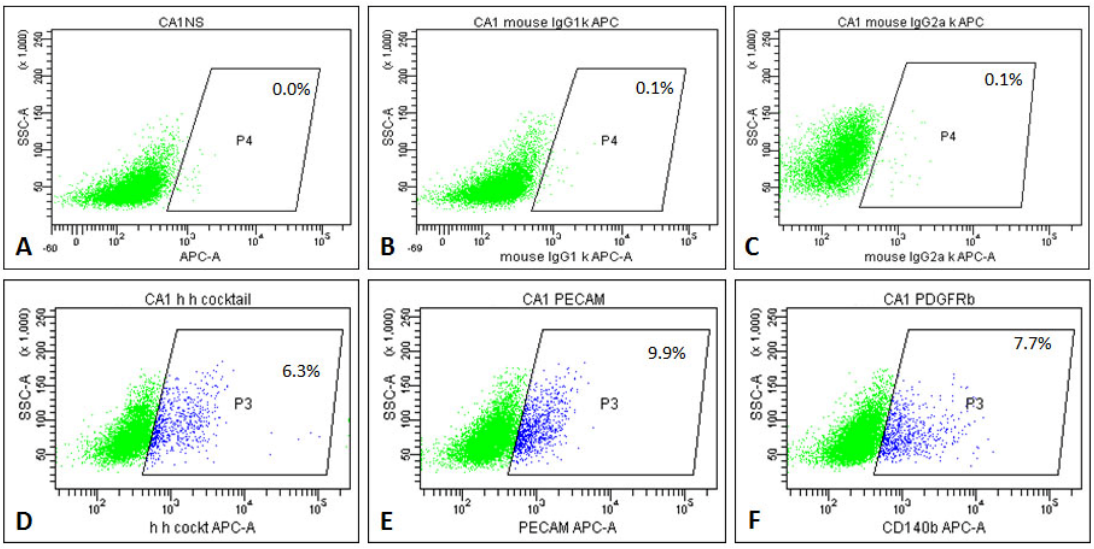

Figure 5.4: Flow-analysis of CA1 cells for the expression of lineage markers. The non-stained negative control is shown in A (A). B and C show cells stained with two different APC-conjugated isotype controls, mouse IgG1 κ (B) and mouse IgG2α κ (C). There was no difference in signal intensity between non-stained and isotype-stained samples. 6.3% of all cells were positive for the markers included in the human haematopoietic cocktail (D). 9.9% were positive for PECAM (E) and 7.7% stained positively for CD140b (F).

5.1.1.2 Expression of negative selection markers by tumour-derived cell lines

Because CA1 is a long-established OSCC cell line, it is possible that its cells have altered expression of lineage markers as a consequence of prolonged cell culture. Ideally, fresh tumour cells should be used to examine whether or not lineage markers are present on their surface. However, with fresh tumour cells it is difficult to tell whether stained cells are epithelial cells aberrantly expressing the lineage markers or belong to non-epithelial cell lineages of the tumour stroma. Hence I chose to analyse early passage cell lines derived from oral tumours to test the specificity of the lineage markers. Unlike fresh tumour tissue these early passage tumour-derived cell lines are not contaminated with cells of non-epithelial lineages and are genetically and phenotypically much closer to the tumours of origin than the long-established OSCC lines such as CA1.

These early passage tumour-derived cell lines contain cells with morphologically different phenotypes identified as small, regularly shaped

epithelial cells that form tight epithelial colonies or larger, spindle-shaped cells that form more loosely spaced colonies or appear as single cells (Figure 5.5). In some of the early passage cell lines a differentiating cell fraction can also be observed. These cells appear larger and flatter. Entire colonies of differentiating cells (Figure 5.5 A, C, black arrow heads) as well as single differentiating cells that are usually located at the edge of the colony are seen (Figure 5.5 D, black arrow head).

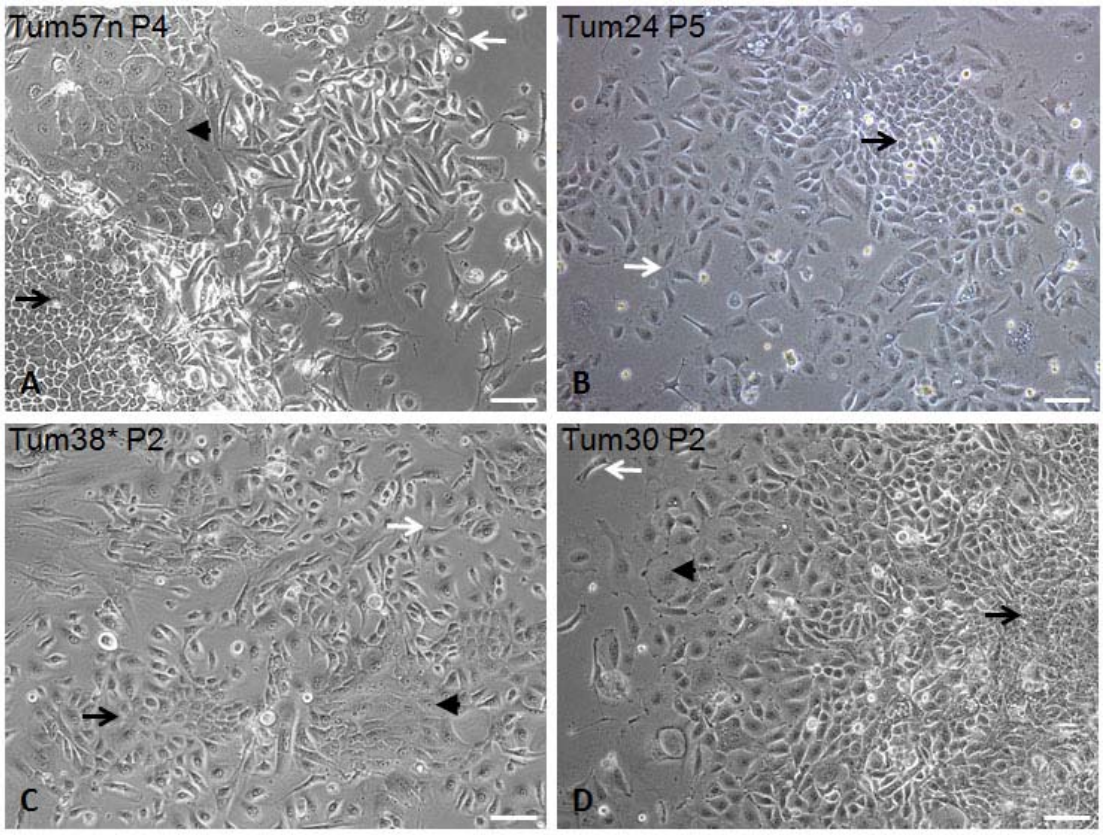

Figure 5.5: Morphologically different cell populations in early passage tumour-derived cell lines. Three morphologically different types of cells are present in all four early passage (passage 2 to 4) cultures: 1) small, regularly shaped cells in tight epithelial colonies (black arrows), 2) spindle-shaped, loosely packed cells (white arrows) and 3) differentiating colonies with large and flat cells (black arrow heads). Scale bar 100 µm

Expression of the lineage markers was examined in three early passage tumour-derived cell lines. In cell line TumNA (generated from a primary non-metastatic OSCC) 5.9% of cells were found to express the lineage markers

(Figure 5.6 B). In cell line TumLM (derived from a primary metastatic OSCC) 12.2% of cells and in cell line Tum57n 12.5% of cells stained positive for the lineage markers (Figure 5.6 D and F).

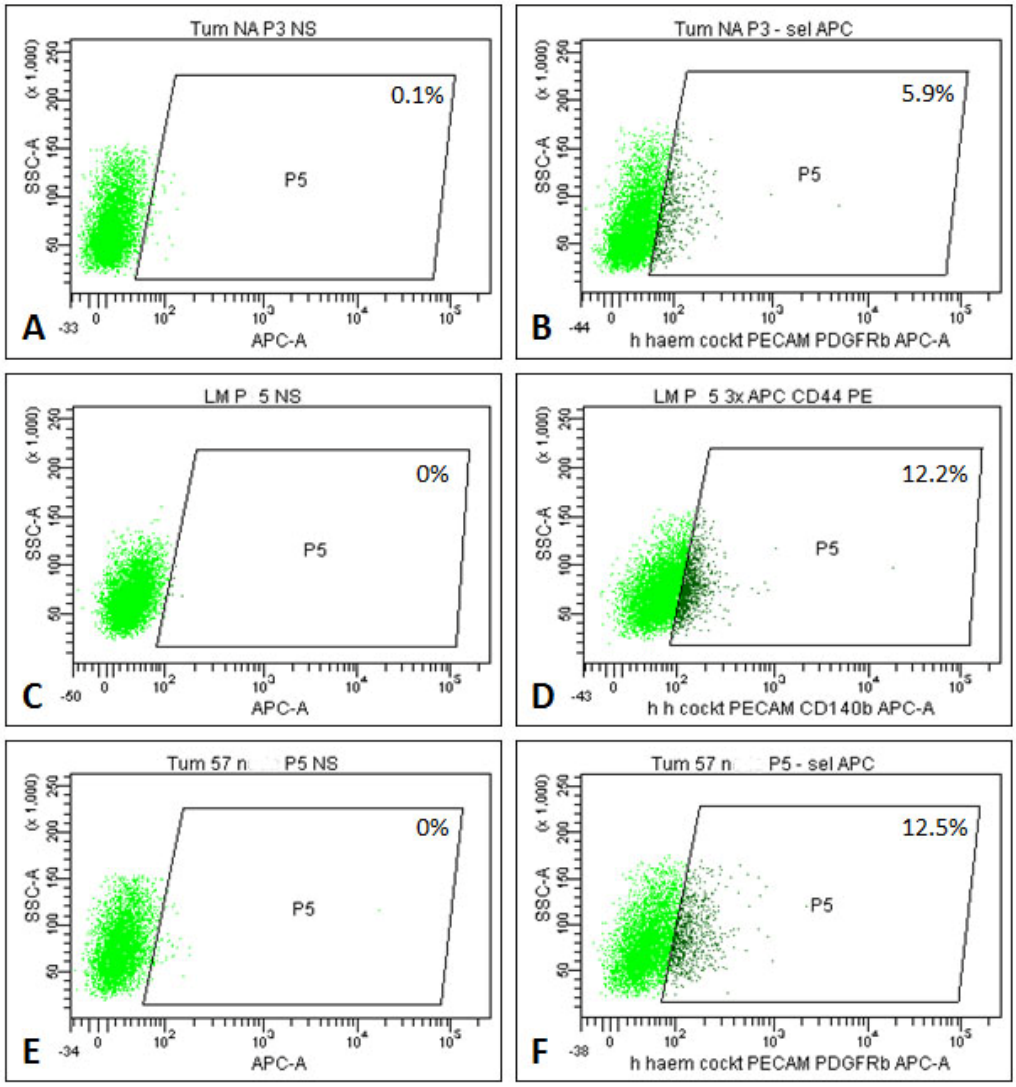

Figure 5.6: Expression of lineage markers by tumour-derived cell lines. Three tumour-derived cell lines were stained with antibodies against human haematopoietic cocktail combined with CD31 and CD140b antibodies (all APC-conjugated). The gates were set using a non-stained negative control sample (A, C and E). 5.9% in Tum NA (B), 12.2% in Tum LM (D) and 12.5% in Tum57 node (F) of cells stained positively for at least one lineage marker.

To test whether expression of lineage markers was linked to a particular morphological cell phenotype (Figure 5.5), cells were co-stained with antibodies against the lineage markers and CD44. This co-staining

established whether the lineage markers were expressed by $CD44^{high}$ or $CD44^{low}$ cells and we have previously reported that different levels of CD44 expression are associated with the morphologically different cell phenotypes present in HNSCC lines (Figure 5.5) [160] [180]. Immunohistochemical staining of a number of HNSCC lines revealed a strong surface CD44 expression in cells forming tight epithelial colonies as well as scattered spindle-shaped cells. The large and flat differentiating cells had very low levels of surface CD44, hardly detectable by immunohistochemistry [160] [180]. The association between cell morphology and expression levels of surface CD44 was confirmed by examining the morphological phenotype of flow-sorted cells with different levels of CD44 expression [160]. These observations imply that different levels of CD44 detected by flow cytometry give indications about cell and colony morphology.

There was no association between expression of lineage markers and expression levels of CD44 in the tumour-derived cell line TumLM with cells positive for lineage markers showing a wide range of CD44 expression levels (Figure 5.7). Consequently, expression of the lineage markers was not associated with a specific morphological phenotype.

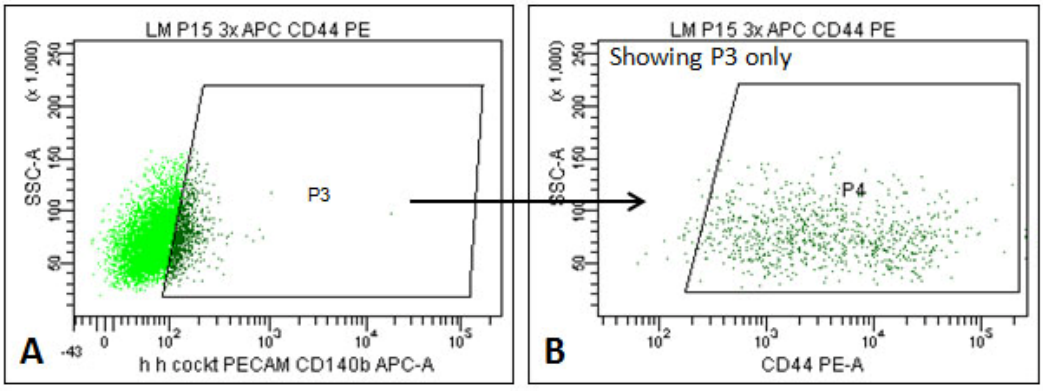

Figure 5.7: Co-expression of lineage markers and CD44 in tumour-derived cell line TumLM. Cells of the cell line TumLM (passage 5) were stained with antibodies against lineage markers and CD44. Lin^+ cell fraction, gated in P3 (A) is shown on the CD44 plot with CD44 expressing cells gated in P4 (B).

5.1.1.3 Expression of negative selection markers by tumour-derived fibroblasts

As the negative selection technique relies on the principle of sparing all epithelial cells while excluding all cells of all non-epithelial cell lineages, I tested the efficiency of negative selection in excluding cells of non-epithelial cell lineages using tumour-derived fibroblasts.

It was observed that fibroblasts isolated from oral tumour tissue express high levels of CD44 (Figure 5.8). This implies that in cell suspensions containing both, fibroblasts and epithelial cells, fibroblasts can be mistaken for $CD44^+$ cancer cells leading to wrong estimates of the size of CD44 expressing cancer cell fraction. Therefore, fibroblasts and other stromal components need to be separated from the epithelial fraction of the tumour.

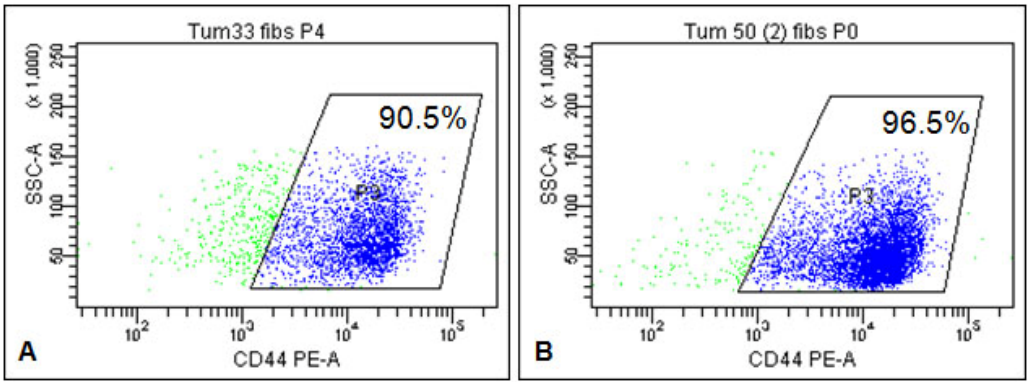

Figure 5.8: Flow cytometric analysis of CD44 expression on tumour-derived cultured fibroblasts. Fibroblasts were isolated from samples of OSCC and grown under standard culture conditions. Cells were trypsinised and immunolabelled with antibodies against CD44. FACS plots for two primary fibroblastic cultures are shown. 90.5% of Tum33 fibroblasts (A) and 96.5% of Tum50(2) (B) are $CD44^+$.

Cultured fibroblasts derived from fresh specimens of OSCC were stained with antibodies used in the negative selection. Apart from CD140b, which is a typical fibroblastic marker [76] [82], the cocktail also included antibodies against PECAM and a number of hematopoietic markers (Table 5.1). The fraction of cells that stained positively varied between the fibroblastic cultures

derived from different tumours with only one out of three cultures being completely positive (Figure 5.9).

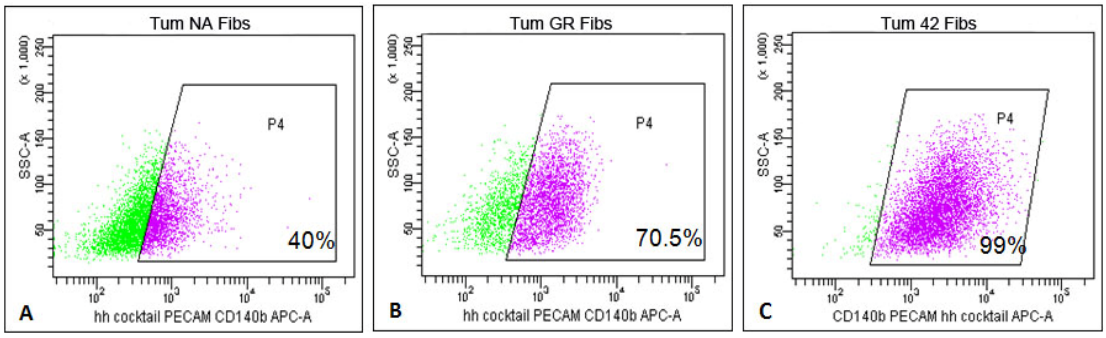

Figure 5.9: Expression of negative selection markers by tumour-derived fibroblasts. FACS plots for early passages of three fibroblastic cultures are shown. Expression of lineage markers was detected on 40% of fibroblasts isolated from the tumour NA (A), 70.5% of cells from tumour GR (B) and 99% of cells from tumour 42 (C).

From these data it can be seen that the negative selection fails to identify the entire epithelial tumour fraction leading to loss of some tumour cell populations. Moreover, negative selection can yield an epithelial fraction contaminated with cells of non-epithelial cell lineages such as fibroblasts.

5.1.2 Flow cytometric analysis of specimens of OSSC. Positive Selection

As negative selection was not fully efficient in isolating a pure cell fraction containing all epithelial cells of the tumour, I tried to use a different approach termed “positive selection”. In this method tumour cells were stained with antibodies against epithelial-specific antigens such as CD24, ESA and epithelial integrins. All epithelial cells present in the total cell suspension isolated from the tumour were expected to be positively stained, whereas no cells forming the tumour stroma were expected to be labelled.

5.1.2.1 Expression of the positive selection markers by established and newly generated OSCC cell lines

Similar to negative selection, a combination of epithelial-specific antibodies was used for positive selection as all epithelial cells in a tumour might not express a given marker, but are likely to express at least one of the epithelial-specific antigens selected. This implies that the more epithelial-specific antibodies that are included in the positive selection, the more likely is the identification of the entire epithelial tumour fraction. Figure 5.10 shows passage 11 of the tumour-derived cell line LM stained with different combinations of epithelial-specific antibodies: ESA (A), ESA and CD24 (B), ESA, CD24 and integrin β4 (C). The more antibodies were included, the more cells moved into the positive gate. When labelled with 1, 2 or 3 antibodies 45.2%, 49,2% and 82.7% of cells appeared positively stained (Figure 5.10). However, even by inclusion of three epithelial-specific antibodies about 17% of the cells remained unlabelled (Figure 5.10 C).

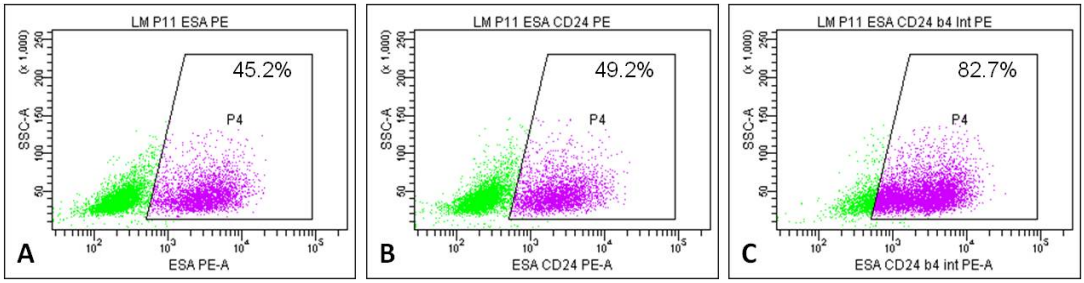

Figure 5.10: Expression of positive selection markers by tumour-derived cell lines. Tumour-derived cell line LM (passage 11) was stained with different combinations of epithelial-specific antibodies and analysed by FACS. ESA was expressed by 45.2% of cells (A). ESA and CD24 together marked 49.2% of cells (B) and the combination of ESA, CD24 and integrin β4 stained 82.7% of cells (C).

Recently, we reported that CSCs in HNSCC and skin SCC switch between two distinct phenotypes [160]: $CD44^{high}ESA^{high}$, which is a preferentially proliferative epithelial phenotype, and $CD44^{high}ESA^{low/-}$, which is a preferentially migratory mesenchymal phenotype. $CD44^{high}ESA^{low/-}$ cells were found to be cells that have undergone epithelial-to-mesenchymal-transition

(EMT cells). Cells with the $CD44^{high}ESA^{low/-}$ EMT phenotype were also found in OSCC tumour tissue [160]. Because EMT cells downregulate their epithelial markers, it is possible that they will not be recognised by the epithelial-specific antibodies used in the positive selection. This is an important issue, as the EMT fraction appears to be highly relevant to tumour invasion and therapeutic resistance.

The additional use of markers associated with EMT could help include EMT cells. I modified the positive selection by inclusion of an additional antibody against integrin αVβ6, which has been reported to promote invasion and migration in OSCC and has been associated with EMT in colon carcinoma [170] [168] [171]. To confirm expression of integrin αVβ6 by EMT cells, its expression pattern was analysed in several established HNSCC and skin SCC cell lines known to have an EMT cell fraction (identifiable by the $CD44^{high}ESA^{low}$ FACS phenotype). In CA1 (OSCC cell line) and Met2 (skin SCC cell line) integrin αVβ6 was expressed on the surface of the great majority of cells including EMT cells (Figure 5.11).

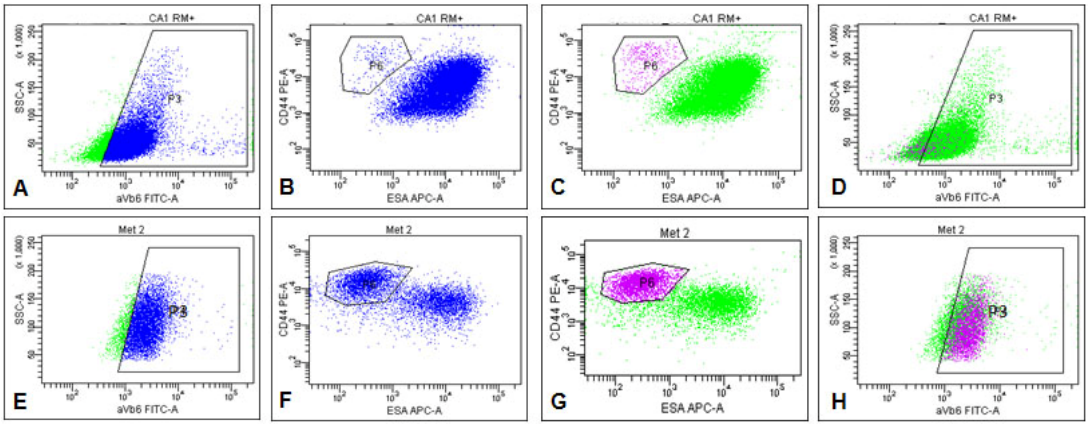

Figure 5.11: Integrin αVβ6 expression in NHSCC and skin SCC cell lines. FACS plots for CA1 (A-D) and Met2 (E-H) cell lines are shown. The great majority of cells in both cell lines stain positively for integrin αVβ6 (gated blue cells in A and E). These integrin αVβ6 positive cells are shown in CD44 vs. ESA plot revealing the $CD44^{high}ESA^{low/-}$ EMT fraction (B and F, gated in P6). Both, EMT and epithelial fractions include integrin $\alpha V\beta 6^{+}$ cells. In C and G the EMT cells were gated (pink cells) which are shown on the integrin αVβ6 plot in D and H.

Next, I tested the combination of epithelial antibodies (ESA, CD24 and integrin β4) with the antibody against integrin αVβ6 on the tumour-derived cell line LM. When immunolabelled with these four antibodies and analysed by FACS, 92% of cells appeared positively stained (Figure 5.12). Figure 5.12 shows FACS plots of the cell line LM stained with anti- integrin αVβ6 (FITC-conjugated), ESA, CD24 and integrin β4 (all PE-conjugated). Quadrant Q3 contains double-negative cells, i.e. cells that did not bind any of the four antibodies and were therefore not labelled with FITC or PE. Cells in the quadrants Q1, Q2 and Q4 represent cells that have been stained with at least one of the four antibodies.

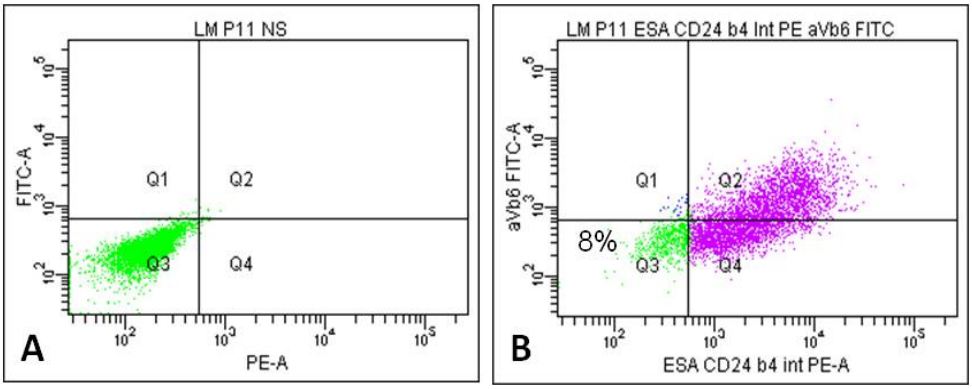

Figure 5.12: Use of integrin αVβ6 in the positive selection technique. A non-stained control sample is shown in A (A). Cells from the tumour-derived cell line LM (passage 11) were immunolabelled with antibodies against integrin αVβ6 (FITC-conjugated), ESA, CD24 and integrin β4 (all PE- conjugated) and analysed by FACS (B). In the stained sample 8% of cells did not stain for any of the four markers (Q3, B).

When stained with the three epithelial-specific antibodies only, 82.7% of cells were labelled. Inclusion of the integrin αVβ6 antibody led to an increase of the positively stained fraction to 92% (compare figure 5.10 C and 5.12 B). FACS plots in figure 5.10 and 5.12 show passage 11 of the tumour-derived cell line LM. During 11 passages in culture tumour cells might have altered expression of their surface antigens. To mimic the fresh tumour, cells as closely as possible, I tested the same combination of antibodies on early-passage (<5) tumour-derived cell lines.

Figure 5.13 shows FACS plots of early passage tumour-derived cell lines stained with antibodies against ESA, CD24, integrin β4 and integrin αVβ6. The non-stained cells account for 2.3% of all cells in the cell line TumNA (Figure 5.13 B), 5.4% of cells in cell line TumLM (Figure 5.13 D) and for 1.5% of cells in the cell line Tum57n (Figure 5.13 F).

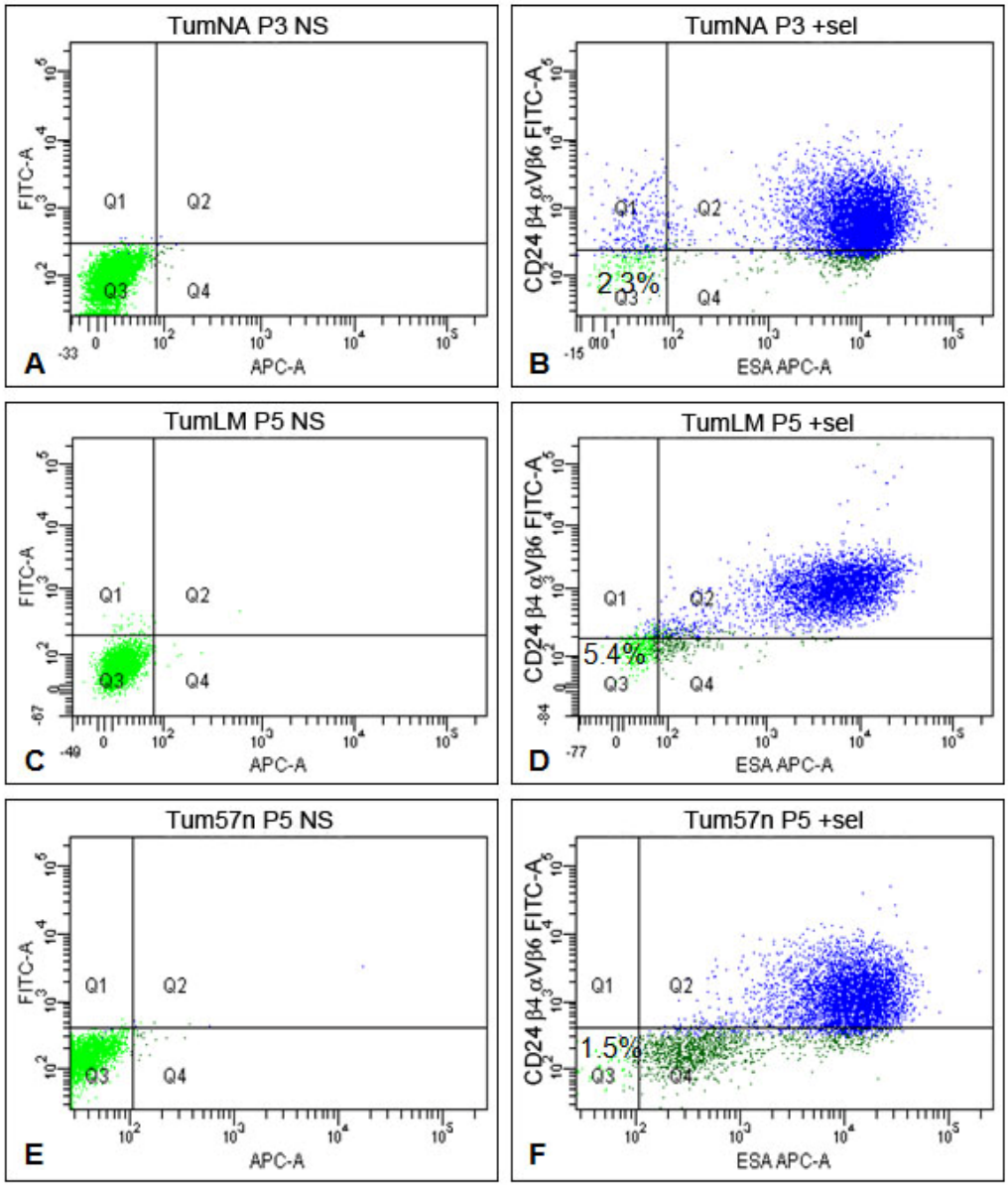

Figure 5.13: Expression of positive selection markers by early passage tumour-derived cell lines. Cell lines TumNA (passage 3) TumLM (passage 5) and Tum57n (passage 5) were stained with antibodies against ESA (APC-conjugated), CD24, integrin β4 and integrin αVβ6 (all FITC-conjugated). The cross-gate was set based on the autofluorescence signal of the non-stained control samples (A, C, E). In the stained samples the fraction of unlabelled cells (in Q3) was 2.3% in TumNA (B) 5.4% in TumLM (D) and 1.5% in Tum57 node (F).

5.1.2.2 Expression of positive selection markers by tumour-derived fibroblasts

Two tumour-derived fibroblastic cultures were used to assess the specificity of antibodies used in the positive selection. Surprisingly, CD24 expression was detected on 2.4% of cells in the culture derived from tumour specimen NA and on 9% of cells in the culture derived from tumour sample GR (Figure 5.14 B, F). No other epithelial-specific antigen used in the positive selection (ESA, integrin β4 and integrin αVβ6) was found to be present on tumour-derived fibroblasts (Figure 5.14).

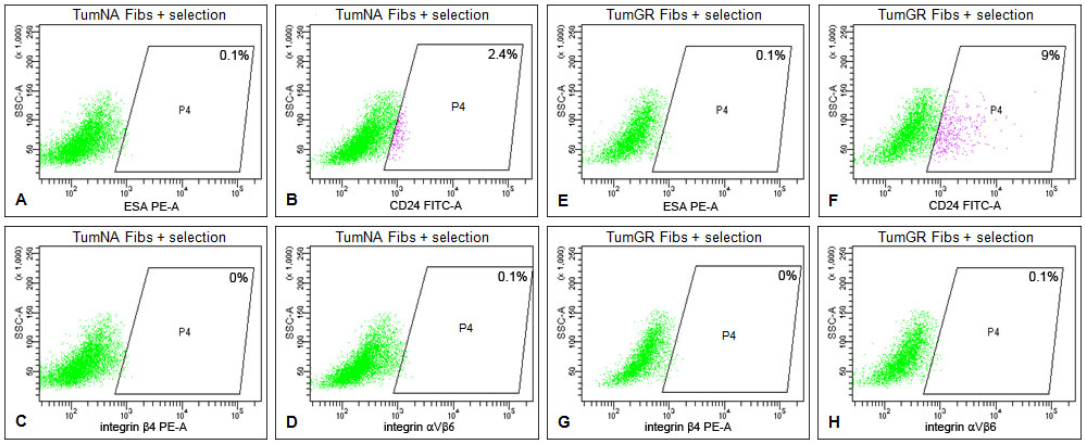

Figure 5.14: Expression of positive selection markers by tumour-derived fibroblasts. Fibroblasts derived from tumour NA (A-D) and tumour GR (E-H) were cultured under standard conditions. Cells were stained with antibodies against ESA (A, E), CD24 (B, F), integrin β4 (C, G) and integrin αVβ6 (D, H). In both cultures a fraction of cells was positive for CD24: 2.4% in TumNA fibs (B) and 9% in TumGR fibs (F). No other markers were found to be expressed in the two cultures.

In summary, antibodies used in the positive selection seem to mark the great majority of cells in early passage tumour-derived cell lines. Only 2.3%, 5.4% and 1.5% of cells did not stain when immunolabelled with a cocktail of four antibodies used in the positive selection (Figure 5.13). Expression of CD24, but no other epithelial-specific antigens exploited in the positive selection, was detected on 2.4% and 9% of fibroblastic cultures derived from tumour specimens (Figure 5.14).

5.1.3 Positive and negative selection in comparison

In the three cell lines tested for the expression of the negative selection markers 5.9%, 12.2%, and 12.5% of cells stained positively (Figure 5.6), whereas only 2.3%, 5.4% and 1.5% of cells were non-stained when immunolabelled with antibodies used in the positive selection (Figure 5.13). In the negative selection from 1% to 60% of fibroblasts could wrongly be identified as epithelial cells (Figure 5.9). For the positive selection this number is much lower with 2.4%-9% (Figure 5.14 B, F). These observations suggest that the positive selection more specifically identifies the epithelial fraction amongst cells of different cell lineages isolated from a tumour.

5.1.3.1 Separation of two cell types by FACS using negative and positive selection

To be able to compare directly the efficiency and accuracy of the negative and the positive selection I performed the following experiment. Separately cultured fibroblasts and keratinocytes were mixed in a ratio 1:1. These were then immunolabelled with the markers used for negative or positive selection. Positive and negative fractions from each tube were collected, representing the epithelial (keratinocytes) and the non-epithelial (fibroblasts) fractions as identified by the negative or the positive selection. All four collected cell fractions were plated on a cell culture dish. 24 hours after plating, cells were fixed and stained with an antibody against pan-Cytokeratin to identify epithelial cells (Figure 5.15). By counting the cytokeratin^{+} cells in sorted fractions it was possible to quantify the purity/degree of contamination of each fraction.

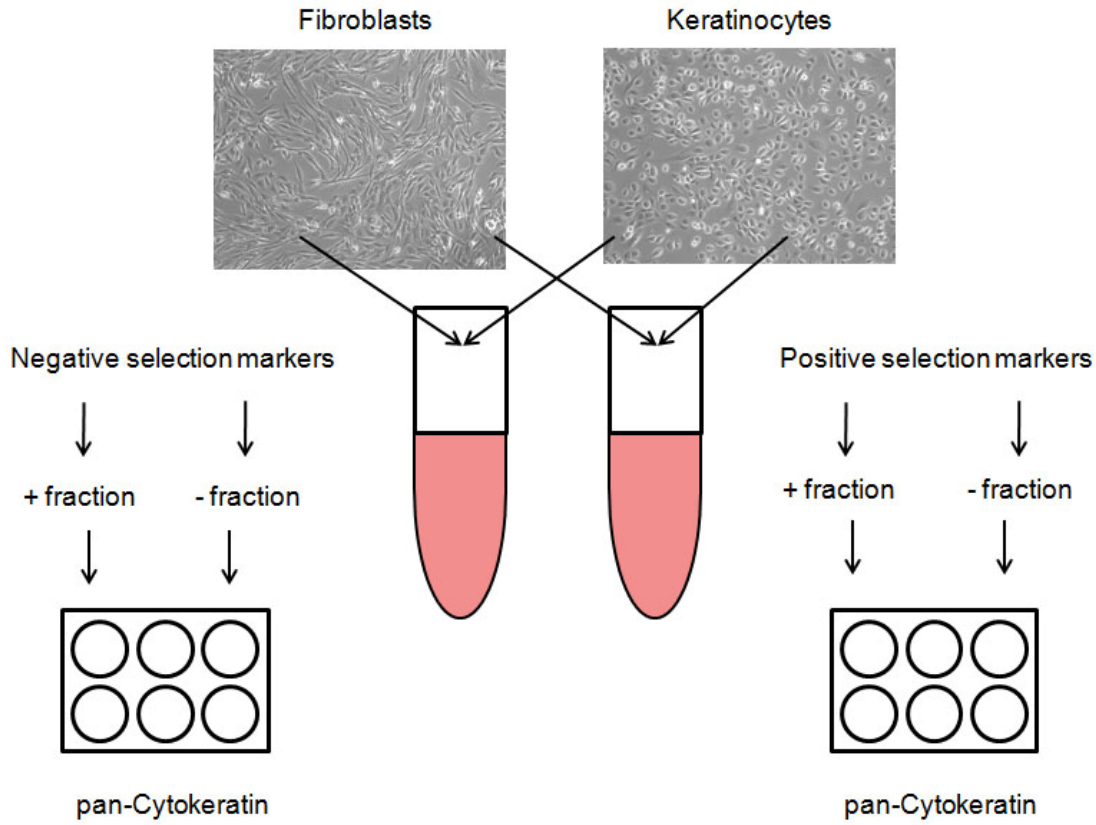

Figure 5.15: Separating two cell types using negative and positive selection. Separately cultured fibroblasts and keratinocytes were trypsinised, mixed 1:1 and stained with the markers used for negative and positive selection. Positive and negative fractions were collected from each of the two samples. Cells were plated, let to adhere overnight and stained with an antibody recognising pan-Cytokeratin.

Fibroblasts used in this experiment were early passage fibroblasts derived from an oral tumour biopsy. Cells from an established oral cancer cell line CA1 were used as keratinocytes. The two cell types (fibroblasts and CA1 cells), cultured separately, were first flow-analysed for the expression of the negative and the positive selection markers (Figure 5.16). Furthermore, the presence of cytokeratin was analysed in the two cultures by immunohistochemistry (Figure 5.17).

In agreement with previous observations (see section 5.1.1.1) the cell line CA1 revealed a small subpopulation (6.8%) of cells expressing negative selection markers (Figure 5.16 A). As expected, when immunolabelled with antibodies used in the positive selection, nearly the entire CA1 cell population (99.1%) stained positively (Figure 5.16 B). Similarly, almost the entire

fibroblastic population (98%) was labelled, when stained with negative selection antibodies (Figure 5.16 C). A small fraction of fibroblasts was found to be positive when analysed by positive selection (Figure 5.16 D). As described above, when the expression of the positive selection markers by fibroblasts was analysed for each of the markers separately, CD24 was found to be the only detectable antigen (Figure 5.14).

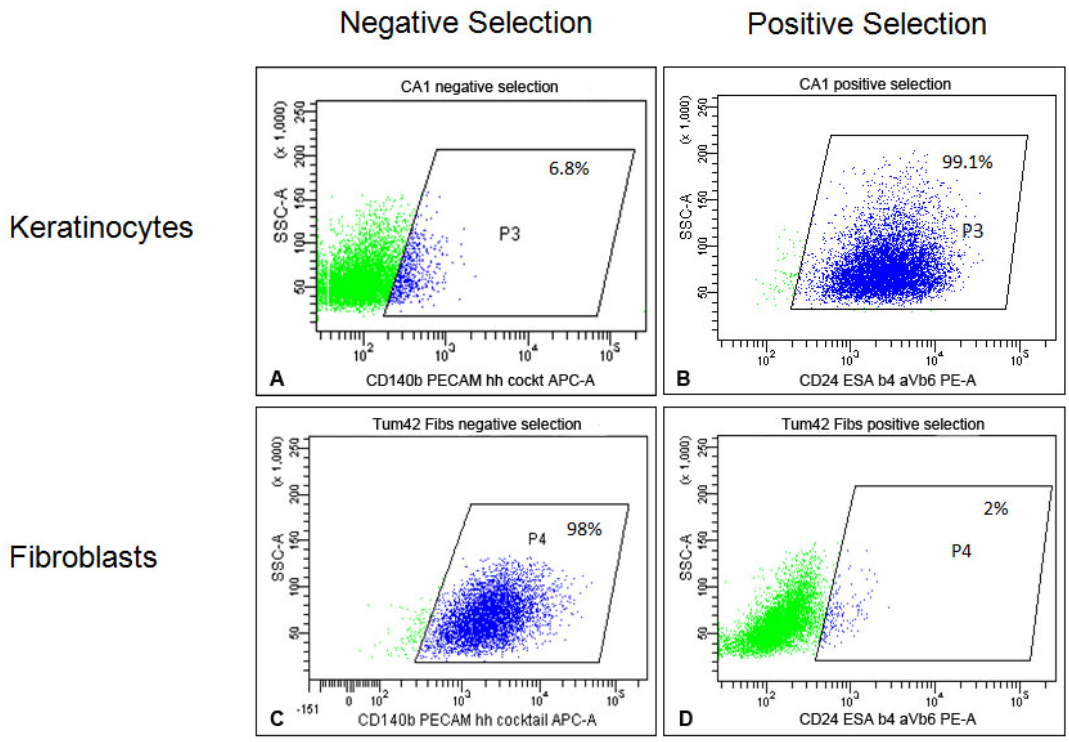

Figure 5.16: Expression of positive and negative selection markers on cultured keratinocytes and fibroblasts. Cells were immunolabelled with antibodies against lineage markers (A and C) or epithelial-specific antigens (B and D). Expression of the lineage markers was detected on 6.8% of CA1 cells (A), whereas nearly all cells (99.1%) in the cell line CA1 stained positively for the positive selection markers (B). 98% of fibroblasts were positive for lineage markers (C) and 2% stained positively for the positive selection markers.

Expression of cytokeratin was detected in all cells in CA1 (Figure 5.17 A, B), whereas no cells in the fibroblast culture stained positively for pan-Cytokeratin when analysed by immunohistochemistry (Figure 5.17 C, D).

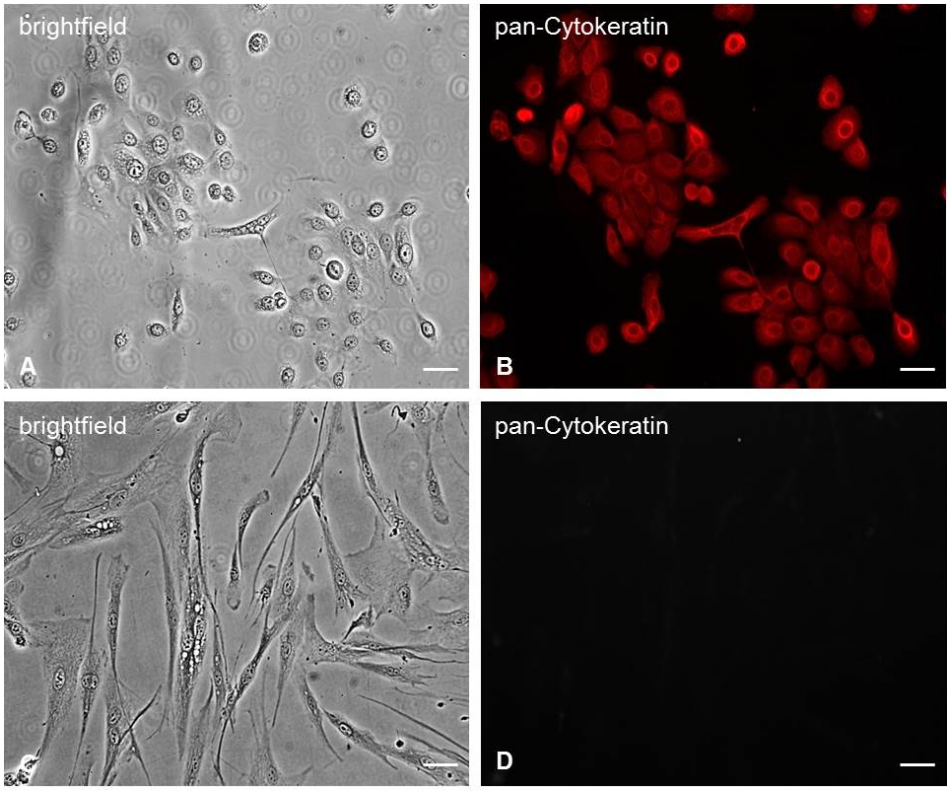

Figure 5.17: pan-Cytokeratin expression in CA1 cells and tumour-derived fibroblasts. Cells were fixed and stained with a pan-Cytokeratin antibody. Expression was detected in all cells in the CA1 cell line (B). No signal was seen in tumour-derived fibroblasts (D). A and C show the corresponding brightfield images (A, C). Scale bar 50 µm

When the two cell types were mixed and flow-analysed, for both selection techniques two distinct cell populations were visible on the FACS plot (Figure 5.18). Interestingly, the positive selection achieved a clearer separation of the two cell types with the two distinct populations lying further apart from each other and being more clearly defined on the FACS plot as compared to populations identified by the negative selection (compare Figure 5.18 B and A).

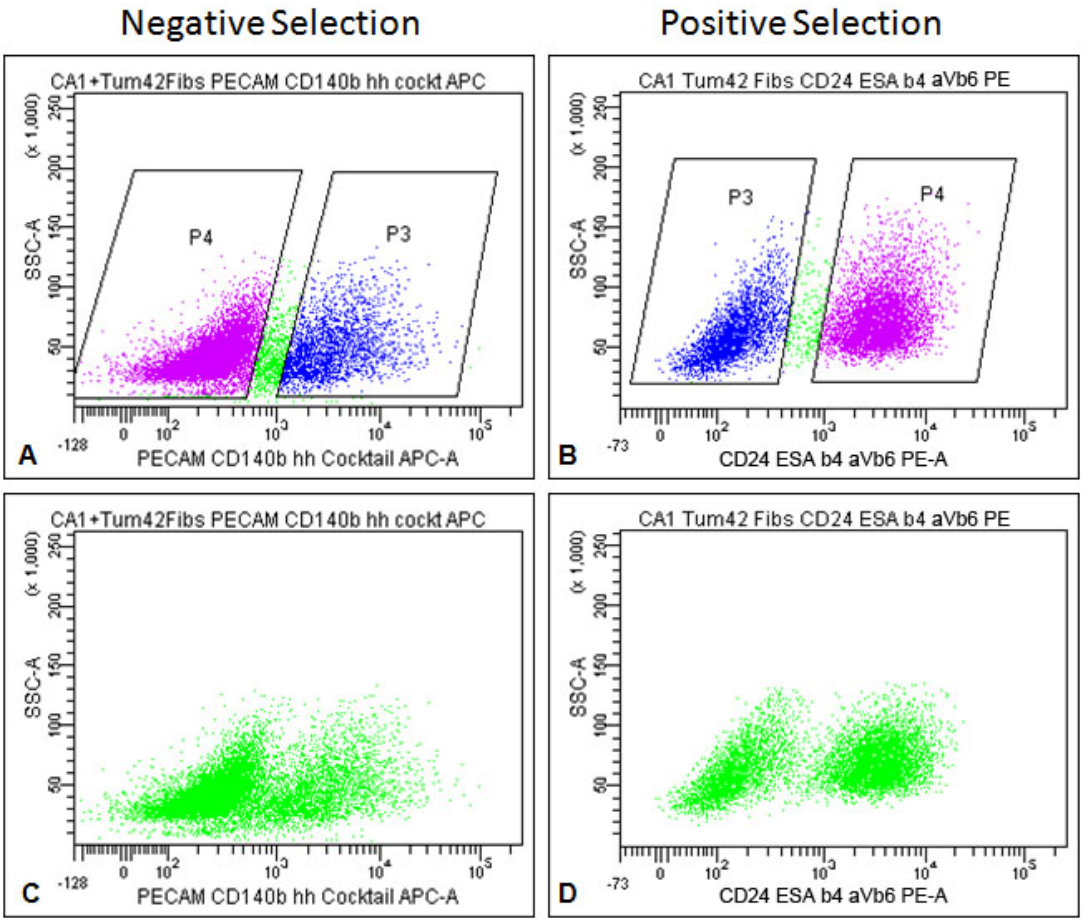

Figure 5.18: Separation of keratinocytes and fibroblasts using positive and the negative selection methods. Separately cultured keratinocytes and fibroblasts were mixed and immunolabelled with antibodies used for negative (A, C) or the positive selection (B, D). Positive selection achieved a clearer separation of the two cell populaions (B) as compared to the negative selection method (A). C and D show the gates from which the fibroblastic population (gated in P3) and the keratinocyte population (gated in P4) were sorted.

Presence of cytokeratin expressing cells in sorted cell fractions was analysed to identify epithelial cells. Figure 5.19 and figure 5.20 show representative pictures of the epithelial fraction (keratinocytes) and the non-epithelial fraction (fibroblasts) as identified by the negative and the positive selection, respectively.

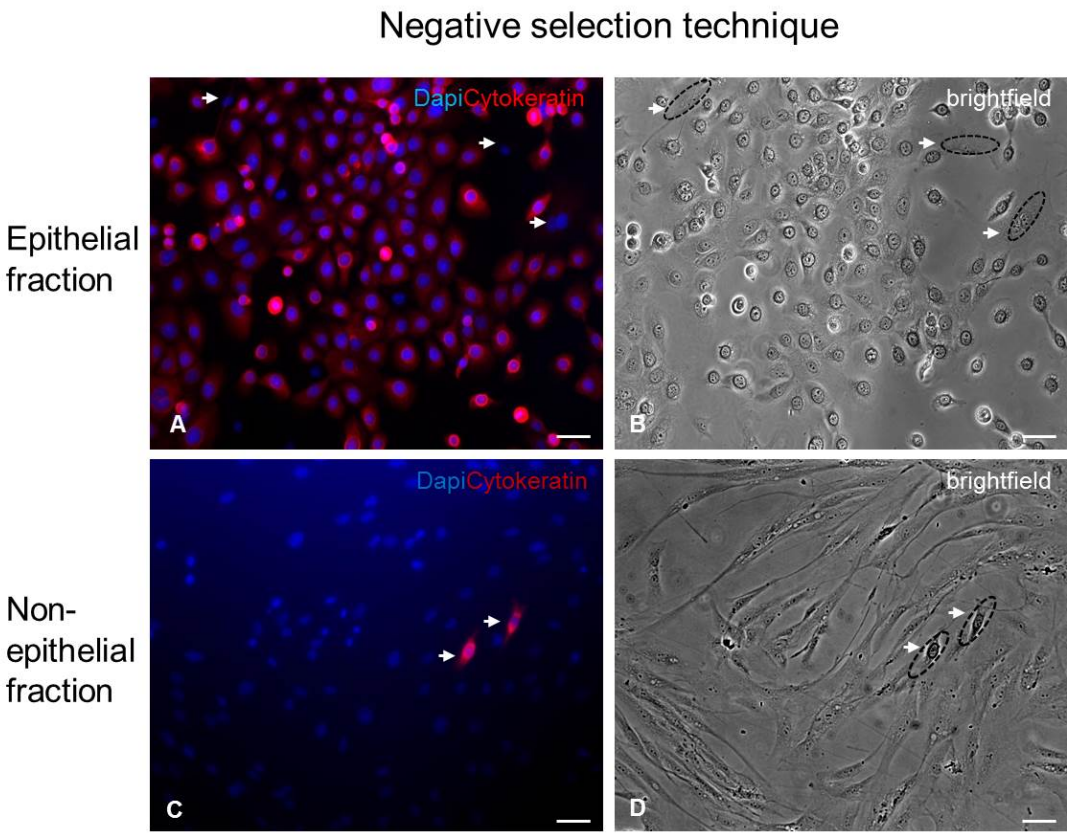

Figure 5.19: Presence of cytokeratin^{+} cells in the epithelial and the fibroblastic fractions identified by means of the negative selection. Sorted epithelial (A, B) and non-epithelial (C, D) cell fractions were stained for pan-Cytokeratin (red). Cytokeratin expression was detected in the majority of cells in the epithelial fraction, which contained only a few cytokeratin^{-} cells (A, white arrows; B, white arrows and dotted ovals). In the non-epithelial fraction cytokeratin was detected in a small number of cells (C, white arrows; D, white arrows and dotted ovals) and was absent in most cells. DAPI (blue) (A, C) and brightfiled images (C, D) show location and morphology of cells. Scale bar 50 µm

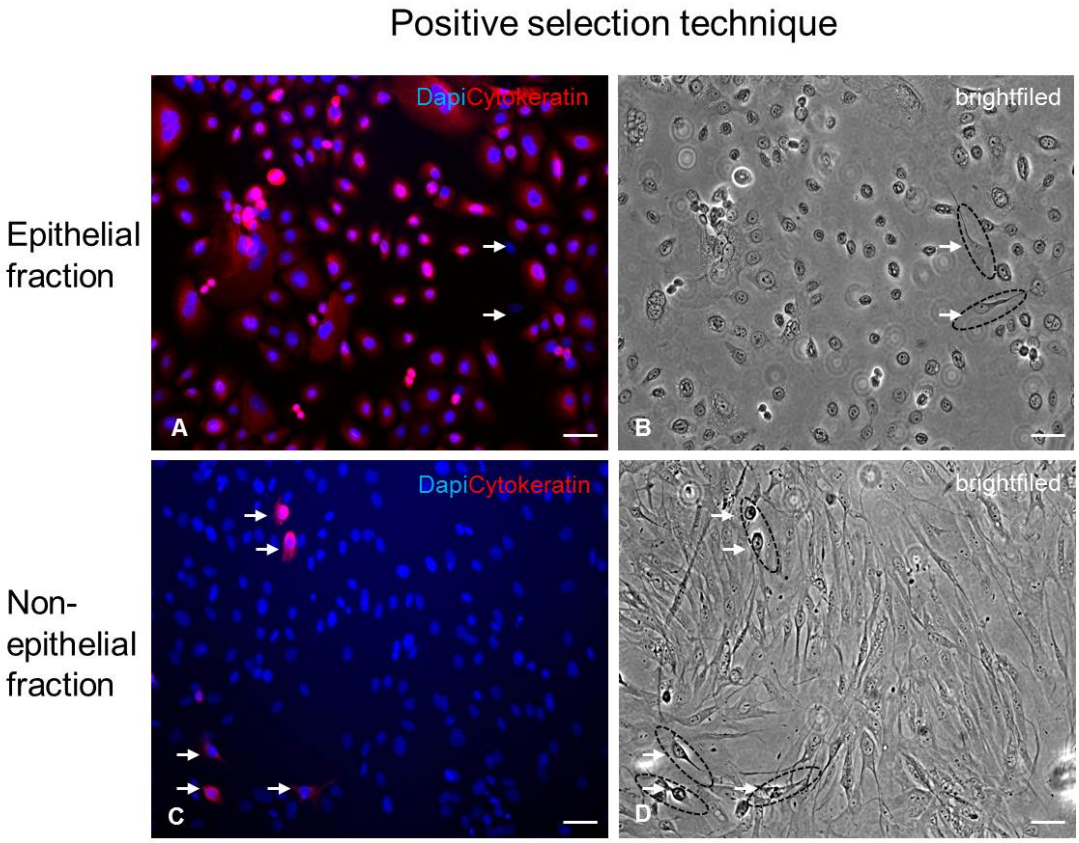

Figure 5.20: Presence of cytokeratin$^+$ cells in the epithelial and the fibroblastic fractions identified by means of the positive selection. Epithelial (A, B) and non-epithelial (C, D) cell fractions were stained for pan-Cytokeratin (red). Cytokeratin expression was detected in the majority of cells in the epithelial fraction, which contained only a few cytokeratin$^-$ cells (A, white arrows; B, white arrows and dotted ovals). In the non-epithelial fraction cytokeratin was detected in a small number of cells (C, white arrows; D, white arrows and dotted ovals) and was absent in most. DAPI (blue) (A, C) and brightfiled images (C, D) show location and morphology of cells. Scale bar 50 µm

For each of the four sorted fractions, pictures were taken from at least 6 fields of view and a total of approximately 500 cells were counted in each of the three separate sorting experiments. The number of contaminating cells (cytokeratin$^-$ cells in the epithelial fraction and cytokeratin$^+$ cells in the non-epithelial fraction) was determined and calculated as a percentage of the total cells counted (Table 5.3). The purity of sorted fractions identified by the two methods was similar. The epithelial fraction was contaminated with fibroblasts to 1.60±0.51% and 1.38±0.50% in the negative and the positive selection techniques, respectively. The contamination of the fibroblastic cell fraction with epithelial cells was slightly higher with 5.75±2.08% and

5.05±1.44% for the negative and the positive selection, respectively (Table 5.3). There was no statistically significant difference in the accuracy of the two methods according to the unpaired Student's t-test.

Table 5.3: Quantification of the purity of sorted cell fractions identified by the positive and the negative selection techniques*

Negative selection			**Positive selection**	
(-ve) epithelial fraction		*(+ve) non-epithelial fraction*	*(+ve) epithelial fraction*	*(-ve) non-epithelial fraction*
CK^- cells/total cells counted		CK^+ cells/total cells counted	CK^- cells/total cells counted	CK^+ cells/total cells counted
8/410 (2.0%)		54/551 (9.8%)	13/548 (2.4%)	11/445 (5.1%)
11/488 (2.3%)		14/490 (2.9%)	9/868 (1.0%)	61/818 (2.5%)
3/498 (0.6%)		24/522 (4.6%)	4/543 (0.7%)	21/517 (0.8%)
Average	1.60%	5.75%	1.38%	5.05%
StDev	0.88%	3.61%	0.87%	2.50%
SEM	0.51%	2.08%	0.50%	1.44%

* Cell counts for three separate sorting experiments are shown. StDev: standard deviation, SEM: standard error of the mean

For both selection techniques the contamination of the sorted keratinocyte fraction with fibroblasts was below 2% and the contamination of the fibroblastic fraction with keratinocytes was between 5% and 6%. However, it is reasonable to assume that the error in the negative selection could have been much larger than that of the positive selection if a different fibroblastic culture had been used. In the fibroblastic culture derived from Tum42 that was used in this experiment over 98% of cells expressed the lineage markers (Figure 5.9 C and Figure 5.16 C). In comparison, in cultures of fibroblasts generated from tumour NA and tumour GR only 40% and 70.5% of cells respectively were found to have detectable levels of the lineage markers when analysed by FACS (Figure 5.9 A, B). If used in the cell separation experiment, the lin^- cell fraction of these cultures would probably contaminate the sorted keratinocyte fraction to a higher degree. Unlike negative selection, positive selection does not rely on lineage marker expression by fibroblasts.

Furthermore, the fraction of cells expressing positive selection markers in different fibroblastic cultures did not differ considerably across fibroblasts derived from three different tumours with 2% in Tum42 fibroblasts (Figure 5.16 D), 2.4% in TumNA fibroblasts (Figure 5.14 B) and 9% in TumGR fibroblasts (Figure 5.14 F). Consequently, for the positive selection, using different fibroblasts in the cell separation experiment would probably not significantly change the degree of contamination of sorted cell fractions.

5.1.3.2 Testing negative and positive selection on cells isolated from fresh tumour tissue

Having established that both positive and negative selection techniques can achieve similar efficiency in separating cultured fibroblasts and keratinocytes, I tested both methods on cells isolated from fresh tumour samples.
Cells were isolated from samples of OSCC according to the standard protocol. Isolated cells were immunolabelled with antibodies used for negative or positive selection. Cells were flow-sorted collecting the positive and the negative fractions identified by each selection method. Sorted cells were centrifuged onto microscope slides using the cytospin centrifuge, fixed and stained for pan-Cytokeratin (Figure 5.21). Photographs of stained cells were taken and used to count the cells. The purity of each fraction was quantified by expressing the number of contaminating cells (cytokeratin$^-$ cells in the epithelial fraction and cytokeratin$^+$ cells in the non-epithelial fraction) as a percentage of the total cell number counted (Table 5.4; Appendix Table 4).

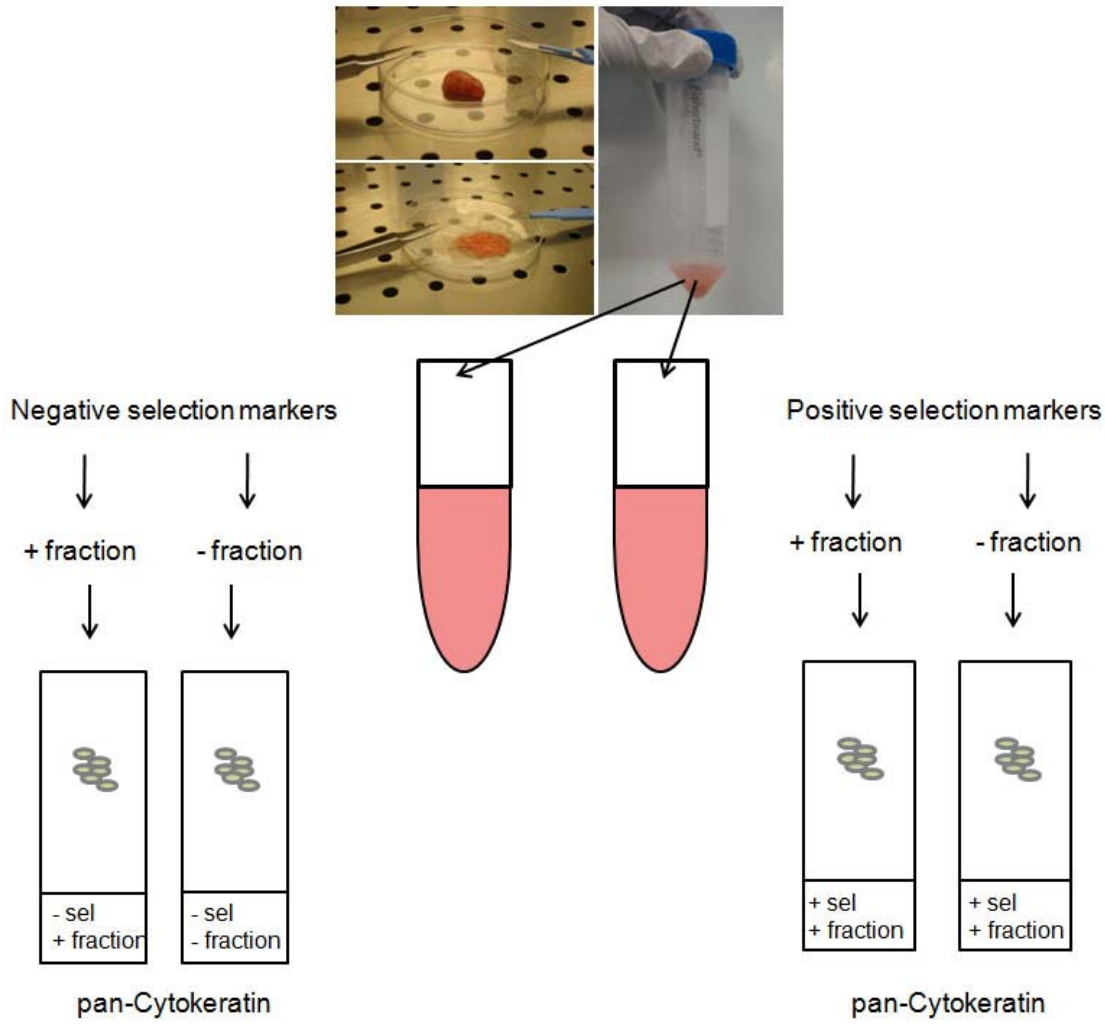

Figure 5.21: Separating epithelial and non-epithelial cell fractions from fresh tumour tissue by means of negative and positive selection techniques. Cells isolated from large tumour specimens were split into two parts and immunolabelled with antibodies used in negative and positive selection techniques, respectively. Positive and negative fractions were collected from each of the two samples, cytospun onto a microscope slide, fixed and stained for pan-Cytokeratin.

Six surgical specimens of OSCC were analysed. Three of the six tumour samples (TumLM, TumAB and TumRM) were large enough to allow both negative and positive selection techniques to be performed on the same specimen. For the remaining three specimens, two (TumABn and TumEG) were analysed by negative selection and one (TumGR) by positive selection.

Similar to cultured cells, for some tumour samples (TumLM, TumRM and TumGR) a clear separation of the epithelial and the non-epithelial cell fractions was achieved with fractions being visible as two distinct cell

populations on the FACS plot (Figure 5.22 A, D, C, F and I). For specimens TumAB, TumABn and TumEG the separation of the epithelial from the non-epithelial cell fraction was less clear (Figure 5.22 B, E, G and H).

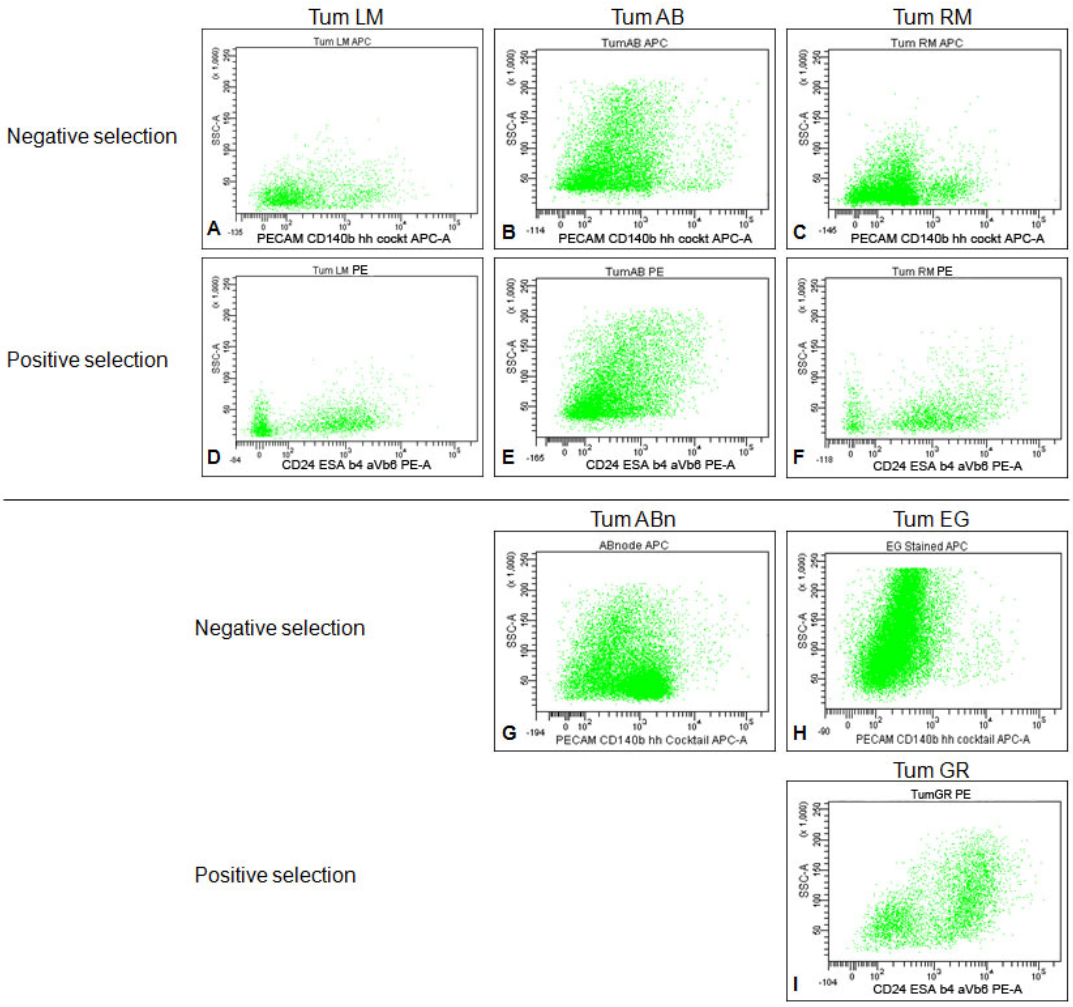

Figure 5.22: Analysis of fresh tumour cells using the negative and the positive selection techniques. Cells isolated from fresh tumour samples were stained with antibodies used for positive or negative selection. All FACS plots show cell distribution after exclusion of dead cells. For tumour specimens TumLM (A and D), TumAB (B and E) and TumRM (C and F) both selection methods were performed. Tumour specimens TumABn (G), TumEG (H) were analysed by means of the negative and TumGR (I) by means of the positive selection only. The epithelial and the non-epithelial fractions were visible as two distinct cell populations for samples TumLM and TumRM analysed by both methods (A, D an C, F) and for TumGR analysed by the positive selection (I).

Gates for sorting the cells were set based on a non-stained sample of cells isolated from the same tumour (Figure 5.23 A and D). Tumour specimen TumAB was one of the larger samples and a sufficient number of cells could be isolated allowing both selection techniques to be performed. The size of the putative epithelial cell fraction identified by the negative and the positive selection was similar with 58.5% and 56.6%, respectively. The size of the non-epithelial cell fraction was also similar with 25.4% and 29.5% for the negative and the positive selection, respectively (compare Figure 5.23 B and E). For other tumour specimens analysed by both selection techniques, the size of the corresponding fractions identified by the two different methods was also similar (Table 5.4).

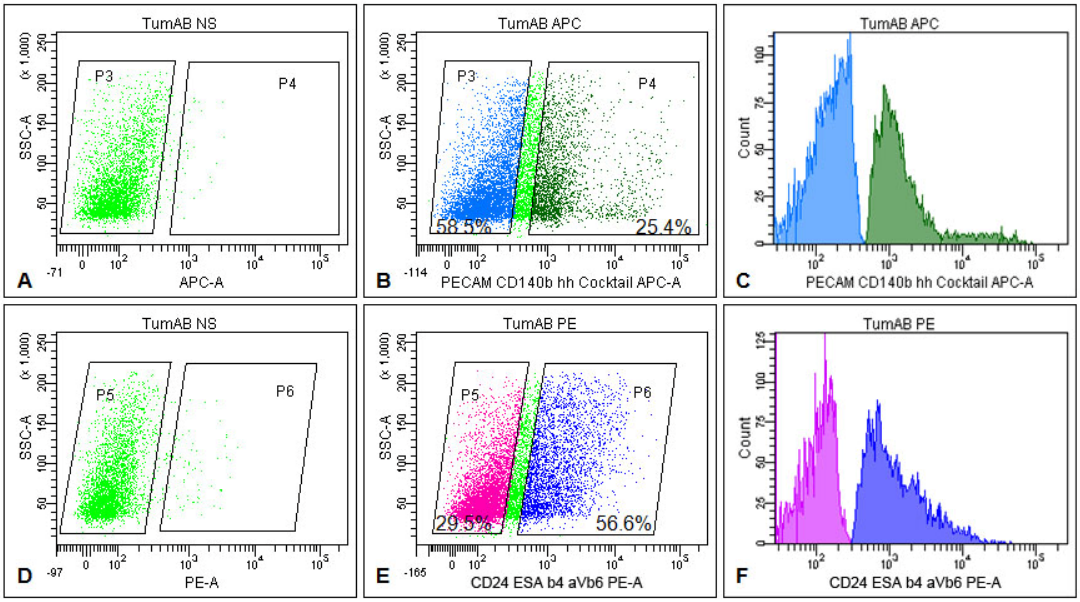

Figure 5.23: FACS-sorting tumour cells using negative and positive selection techniques. Cells isolated from tumour specimen TumAB were stained with antibodies used in the negative (A-C) and the positive (D-F) selection techniques. Positive and negative fractions were sorted from each sample. Gates for cell sorting were set based on the non-stained control sample (A and D). When setting the gates care was taken for the gated populations not to overlap (count diagrams in C and F).

Table 5.4: Size of epithelial and non-epithelial cell fractions in fresh tumour tissue

	Negative selection		Positive selection	
	Epithelial fraction	Non-epithelial fraction	Epithelial fraction	Non-epithelial fraction
TumLM	54.2%	34.7%	52.6%	43.1%
TumAB	58.5%	25.4%	56.6%	29.5%
TumRM	68.8%	21.1%	61.5%	21.3%

Epithelial and non-epithelial cells isolated from fresh specimens of OSCC, as identified either by positive or negative selection, were phenotypically distinctly different from each other. Cells of the putative epithelial fraction were much larger than cells of the non-epithelial fraction (Figure 5.24). Furthermore, for one tumour, cells in the non-epithelial fraction were more granular than epithelial cells isolated from the same tumour (compare Figure 5.24, E and F).

Sorted cells were fixed and stained for pan-Cytokeratin to quantify the degree of contamination of each fraction. For both selection methods, the majority of cells in the putative epithelial fraction was found to express cytokeratin, whereas no cytokeratin was present in most cells of the putative non-epithelial fraction (Figure 5.25, Figure 5.26). For some samples, sorted cells deposited on a microscope slide for immunohistochemical staining were lost in course of the staining procedure. This was probably due to the frequent washing of the slides in PBS after the incubation with primary and secondary antibodies and DAPI. Loss of cells resulted in low cell numbers available for quantification. Samples, in which less than 200 cells were counted per fraction (samples TumLM, TumRM and TumEG) were excluded from the final statistical analysis, as such low cell numbers might not be representative of the complete sorted fraction (for the full list of samples see Appendix Table 4).

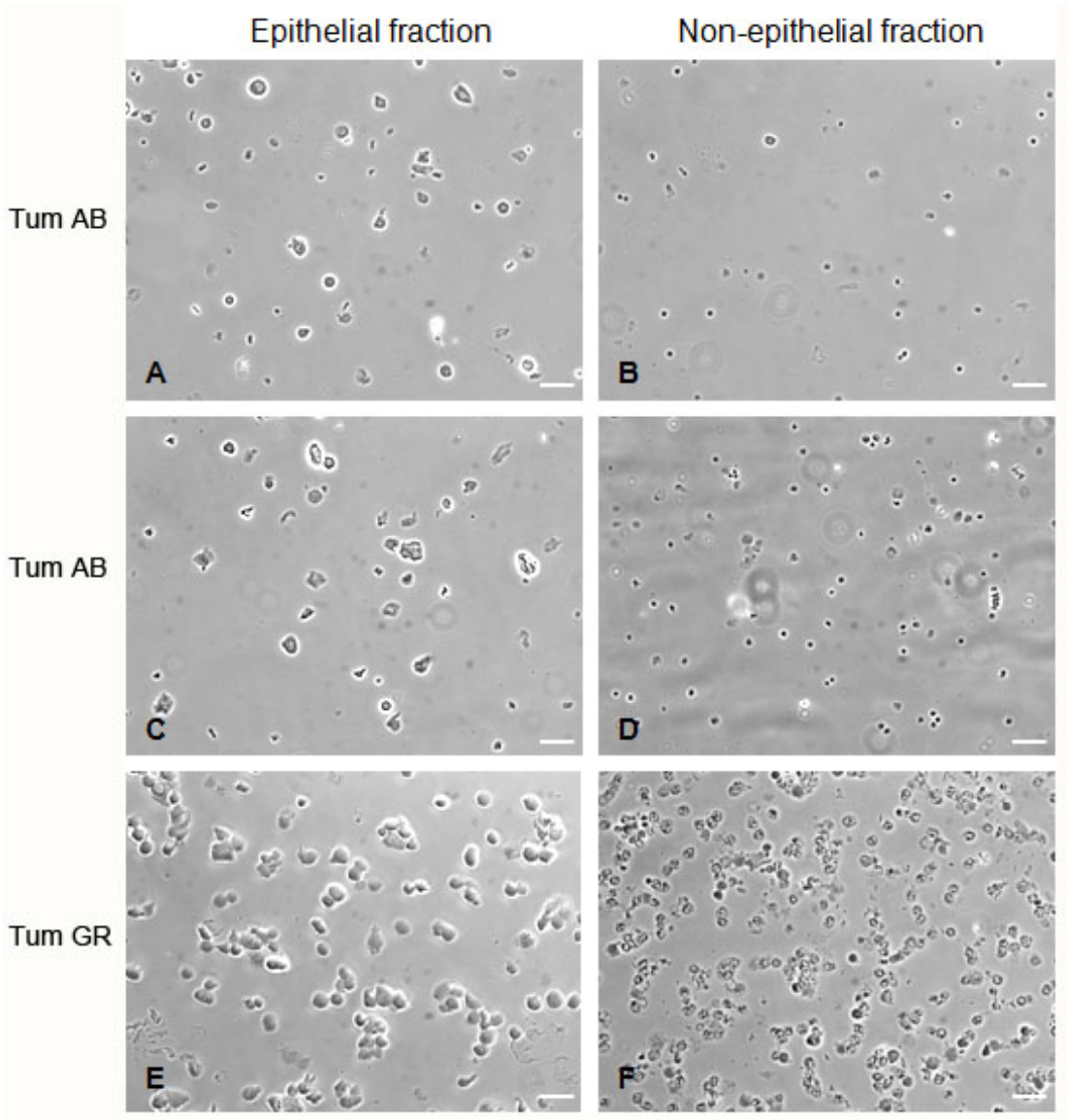

Figure 5.24: Morphology of epithelial and non-epithelial tumour cells identified by negative and positive selection. Cells isolated from tumour AB were subjected to both negative (A, B) and positive (C, D) selection, cells from tumour GR were analysed by means of the positive selection only (E, F). Photographs were taken from sorted epithelial (A, C and E) and non-epithelial (B, D and F) fractions as identified by means of negative (A, B) or positive (C-F) selection. Cells of the putative non-epithelial fraction were a lot smaller and for TumGR more granular than cells of the putative epithelial fraction. Scale bars 50 µm

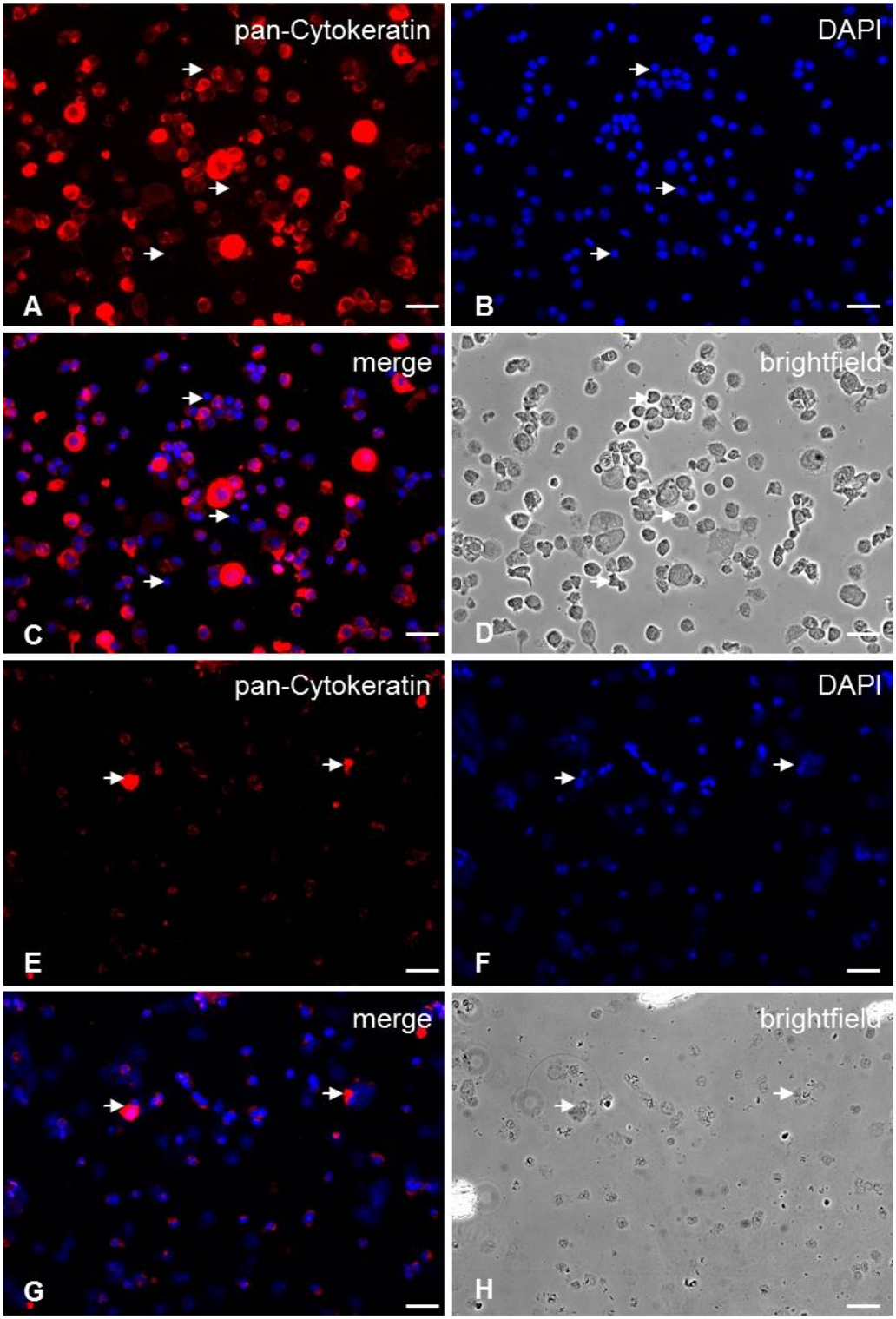

Figure 5.25: Cytokeratin expression in epithelial and non-epithelial tumour cells identified by the negative selection. Putative epithelial (A-D) and non-epithelial (E-H) tumour cell fractions were sorted and stained with antibodies against pan-Cytokeratin (red). A few cytokeratin negative cells were present in the epithelial fraction (white arrows, A-D). A small number of cytokeratin positive cells were seen in the non-epithelial fraction (white arrows, E-H). DAPI (B, F) and brightfield (D, H) images show the localisation and the shape of cells.

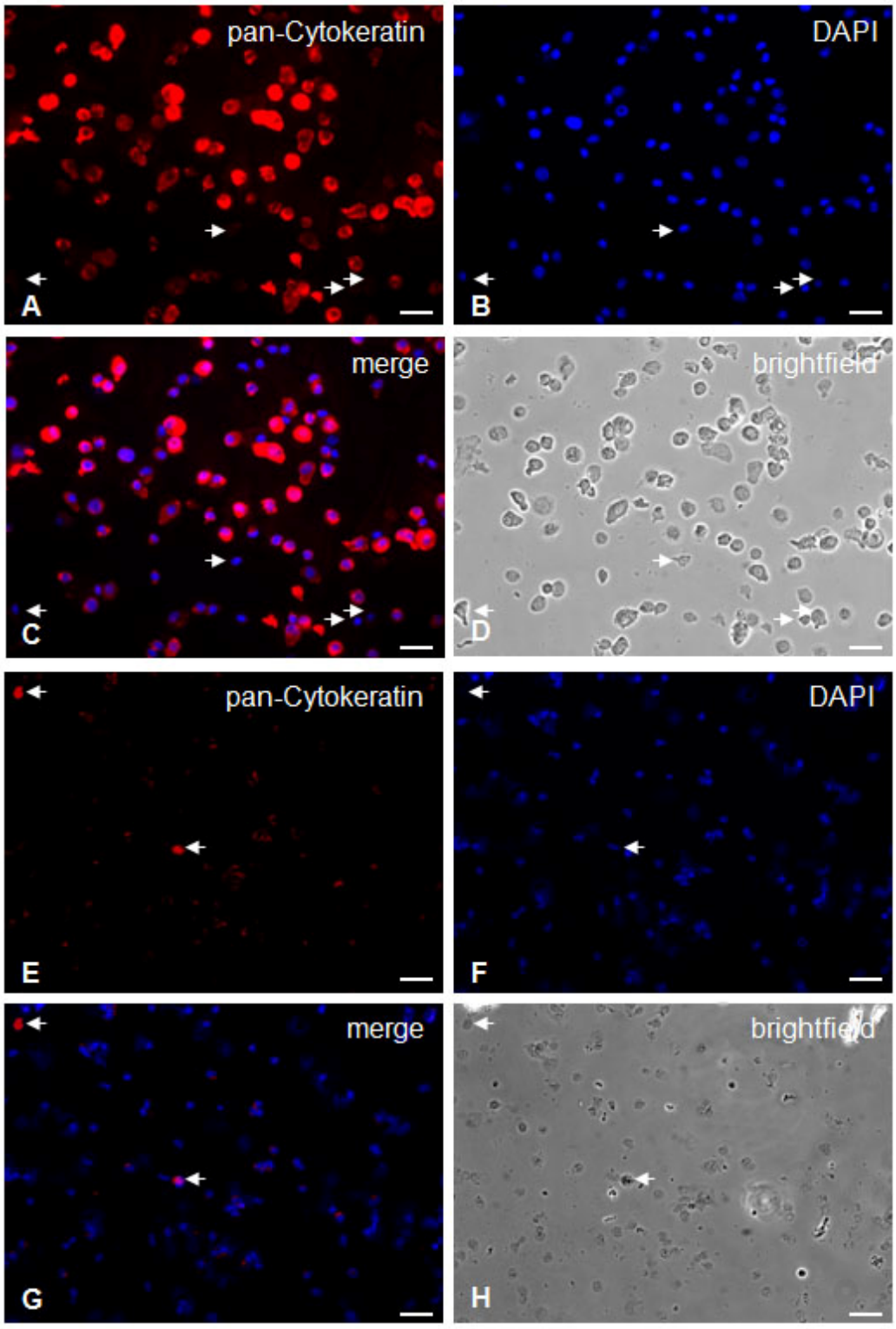

Figure 5.26: Cytokeratin expression in epithelial and non-epithelial tumour cells identified by the positive selection. Putative epithelial (A-D) and non-epithelial (E-H) tumour cell fractions were sorted and stained with antibodies against pan-Cytokeratin (red). A few cytokeratin negative cells were present in the epithelial fraction (white arrows, A-D). A small number of cytokeratin positive cells were seen in the non-epithelial fraction (white arrows, E-H). DAPI (B, F) and brightfield (D, H) images show the localisation and the shape of cells.

Despite keeping the FACS staining and sorting conditions as consistent as possible, the purity of sorted fractions varied considerably between the individual tumour specimens (Table 5.5). The cell fraction with the highest purity was the putative epithelial fraction of the tumour GR identified by positive selection. 94.4% of cells in this fraction were found to express cytokeratin and were therefore classified as epithelial cells. The epithelial fraction of the tumour ABn, identified by negative selection, consisted to 68.5% of cytokeratin expressing cells. The proportion of cytokeratin$^+$ cells contaminating the non-epithelial fraction was 4.6% for tumour GR and 1.8% for tumour ABn (Table 5.5). For the tumour specimen AB both selection methods were performed. The epithelial fraction identified by positive selection had a higher purity (75.9%) than the same fraction identified by negative selection (62.9%). The contamination of the non-epithelial fraction identified by negative and positive selection methods was 8.8% and 3.1%, respectively (Table 5.5).

In summary, the purity of the epithelial cell fraction identified by negative selection was on average 65.7±2.8%, whereas the epithelial fraction identified by positive selection consisted to 85.2±3.6% of cytokeratin$^+$ cells (Table 5.6). These numbers suggest that the positive selection yielded a purer epithelial fraction than the negative selection. However, this difference has not been found to be statistically significant (according to the Student's t-test), which was probably due to the small number of samples. No directional trend was present in the degree of contamination of the putative non-epithelial fraction. In the direct comparison (negative and positive selection performed on cells isolated from the same specimen) positive selection seemed slightly more accurate with the degree of contamination of the non-epithelial fraction with cytokeratin$^+$ cells of 8.8% for the negative and 3.1% for the positive selection respectively. In the indirect comparison (two selection methods performed on cells from two different samples) negative selection appeared superior with 1.8% of contamination cells as compared to 4.6% for the positive selection (Table 5.6).

Table 5.5: Quantification of the purity of epithelial and non-epithelial fractions of tumour cells separated by the negative or the positive selections (selected samples)*

	Negative selection		**Positive selection**	
	CK^- cells in negative (epi) fraction	CK^+ cells in positive (non-epi) fraction	CK^- cells in positive (epi) fraction	CK^+ cells in negative (non-epi) fraction
Tum AB	117/315 (37.1%) **epi 62.9%**	20/226 (8.8%) **epi 8.8%**	67/278 (24.1%) **epi 75.9%**	14/458 (3.1%) **epi 3.1%**
Tum GR	NA	NA	40/709 (5.6%) **epi 94.4%**	17/367 (4.6%) **epi 4.6%**
Tum ABn	177/562 (31.5%) **epi 68.5%**	11/627 (1.8%) **epi 1.8%**	NA	NA

* Cells in up to 8 different fields of view were counted. The number of contaminating cells per total number of cells counted in each sorted fraction is shown and degree of contamination is given in brackets as a percentage. The percentage of epithelial cells (epi) in each sorted fraction is also shown in bold. NA: not analysed

Table 5.6: Purity of the sorted cell fractions identified by negative and positive selection (summary)

	Negative selection		Positive selection	
	negative fraction	positive fraction	positive fraction	negative fraction
CK^+ cells	62.9% (TumAB)	8.8% (TumAB)	75.9% (TumAB)	3.1% (TumAB)
CK^+ cells	68.5% (TumABn)	1.8% (TumABn)	94.4% (TumGR)	4.6% (TumGR)
Average	**65.7%**	**5.3%**	**85.2%**	**3.9%**
StDev	4%	4.9%	13.1%	1.1%
SEM	**2.8%**	**2.2%**	**3.6%**	**1%**

5.1.4 Discussion

In the above sections I aimed to test and compare two methods used to identify the epithelial fraction of a tumour amongst cells of non-epithelial lineages. I tested the antibodies used in negative and positive selection on a number of OSCC cell lines, including cell lines that I had recently generated from fresh tumour specimens.

The longer cells isolated from a tumour specimen are maintained in culture, the more likely they are to undergo physiological changes under the influence of growth conditions imposed by cell culture medium [181] [182]. These changes might be associated with down- or up-regulation of certain surface antigens. Cells, that have been grown in culture for a few passages only, are more likely to resemble the original tumour cells in their physiological and biological characteristics than cells that have been passaged many times. Testing the two selection techniques on early passage tumour-derived cell lines offers a unique opportunity to work with a pure epithelial cell fraction (as opposed to a mix of cells of different cell lineages isolated from the tumour) that closely parallels the tumour cells of origin.

Cells from early passage tumour-derived cell lines were not expected to be immunolabelled with antibodies used in negative selection, because these antibodies are specific for cells of non-epithelial lineages. In contrast, all cells were expected to be positively stained when immunolabelled with antibodies used in positive selection, as these antibodies recognise epithelial-specific antigens. However, in the three cell lines tested for the expression of the negative selection markers 5.9%, 12.2%, and 12.5% of epithelial cells stained positively (Table 5.7). In the same cell lines, 2.3%, 5.4% and 1.5% of cells were unstained when immunolabelled with antibodies used in positive selection (Table 5.7). This shows that neither of the two methods is flawless. However, the size of the cell fraction that was mistakenly identified as non-epithelial (positively stained in the negative selection and unlabelled in the positive selection) suggests that the positive selection is more accurate (compare 5.9%, 12.2% and 12.5% vs. 2.3%, 5.4% and 1.5%).

Table 5.7: Expression of negative and positive selection markers by early passage tumour-derived epithelial and fibroblastic cultures*

Culture	Negative selection (lineage markers)		Positive selection (epithelial markers)	
	positive	negative	positive	negative
TumNA	5.9%	*~94.1%*	*~97.7%*	2.3%
TumLM	12.2%	*~87.8%*	*~94.6%*	5.4%
Tum57n	12.5%	*~87.5%*	*~98.5%*	1.5%
TumNA fibs	40%	*~60%*	2.4% (CD24)	*~97.6%*
TumGR fibs	70.5%	*~20.5%*	9% (CD24)	*~91%*
Tum42 fibs	99%	*~1%*	2% (CD24)	*~98%*

*Numbers given *in italics* have been calculated by subtracting the experimentally determined numbers describing the size of the reciprocal fraction from 100%.

An accurate analysis of $CD44^+$ cells in tumour samples requires selection of the entire epithelial cell fraction and efficient exclusion of cells of non-epithelial cell lineages, particularly CD44 expressing lymphocytes and fibroblasts. In a reverse strategy, the specificity of antibodies used in negative and positive selection was tested on fibroblasts, a cytokeratin-negative cell type forming a major component of the tumour stroma. Three tumour-derived fibroblast cultures were flow-analysed for their surface expression of negative and positive selection markers. Surprisingly, only one of the three cultures showed labelling of the entire culture (99% of cells) with antibodies used in negative selection (Table 5.7). In the other two tumour-derived fibroblast cultures the fraction of stained cells was 40% and 70.5% (Table 5.7). Thus, for some tumours analysed by negative selection, a large fraction of unlabelled fibroblasts could contaminate the epithelial fraction. Of the positive selection markers, only CD24 was expressed by fibroblasts (at 2%, 2.4% and 9%, Table 5.7). This antibody could be removed from analyses but as CD24 is strongly expressed by a large fraction of tumour cells (Figure 5.27) the risk of CD24 leading to fibroblastic contamination was thought to be outweighed by its potential to assist identification of the complete epithelial fraction.

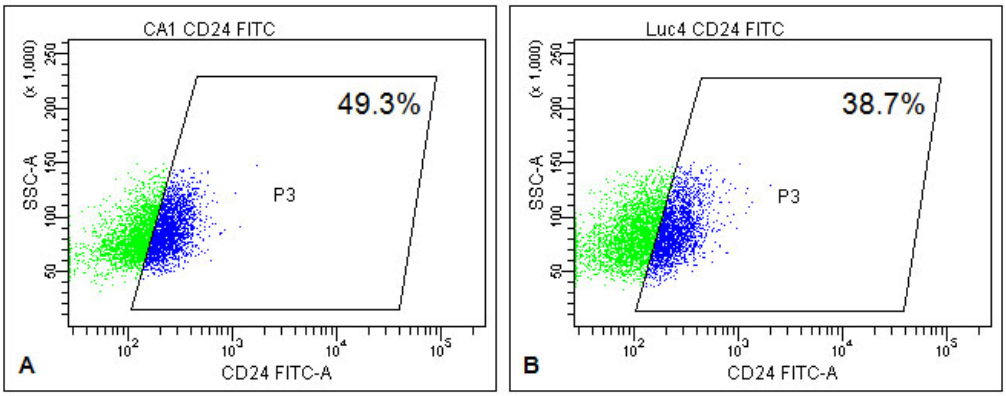

Figure 5.27: Expression of CD24 on established OSCC cell lines. Cells were trypsinised, counted and stained for CD24. 49.3% of cells stained positively in the cell line CA1 (A) and 38.7% of cells were labelled in the cell line Luc4 (B).

In summary, the size of the fibroblastic fraction in the three cultures that was identified as epithelial (not labelled in the negative selection and labelled in the positive selection) was ~0%, 29.5% and 60% for the negative selection and 2%, 2.4% and 9% for the positive selection. These numbers suggest that the positive selection is more specific for epithelial cells, producing an epithelial fraction with a lower extent of fibroblastic contamination.

It is important that epithelial tumour cells that have undergone EMT are also included in the epithelial fraction identified for further analysis, as these cells appear to be highly relevant to tumour invasion and therapeutic resistance. Because EMT cells downregulate expression of epithelial antigens their detection by epithelial-specific antibodies was uncertain. Antibodies known to recognise EMT cells need to be used and integrin αVβ6 was therefore included (Figure 5.11). Individual OSCC lines differed in their expression patterns of integrin αVβ6. For the skin SCC line Met2 all EMT cells expressed integrin αVβ6, whereas for the OSCC line CA1 some EMT cells were negative, localising to an area outside the gate encompassing the integrin $\alpha V\beta 6^{+}$ fraction on the FACS plot (Figure 5.11, pink cells in H and D). An additional cell-surface antibody specific for EMT cells could be added to enhance selection of EMT cells present in the tumour, but in an extensive literature search did not identify a marker that would select epithelial EMT cells and would not be expressed by fibroblasts.

5.1.4.1 Assessing the efficiency of positive and negative selection methods

Tests on cultured cells showed that both selection methods appropriately identify cells of epithelial and non-epithelial lineages. Testing the two methods on fresh tumour cells is more relevant for their potential use in research studies and clinical applications but, unfortunately, quantification of the two methods on fresh tumour cells proved technically difficult. The small size of tumour samples available for analyses was a major limitation. Only a small number of cells could be isolated and loss of sorted cells occurred for some samples during immunohistochemical staining. This did not happen for cultured cells, because these cells could be plated to adhere to the culture dish. They could then be easily fixed, stained and counted. The tumour cells did not adequately survive the process of cell isolation to give uniform adhesion and a cytospin centrifuge was therefore used to deposit sorted cells onto microscope slides. However, cells did not adhere well and for some samples many cells were lost during subsequent staining procedures. Only for three out of six samples could a sufficient number of cells be counted to quantify the purity/degree of contamination of the sorted fraction.

5.1.4.2 Positive selection. Implications in research and clinics

The use of flow cytometry for analysing cells isolated from fresh tumour tissue has not been used as frequently as detection of antigens of interest by immunohistochemistry (IHC) on sectioned tissue. Many studies have attempted to establish correlations between CD44 expression (detected by IHC) and pathological parameters of the tumour and the clinical outcome for the patient. A study by Wang reported a positive correlation between expression levels of CD44 (standard and/or variant isoforms) and advanced T stage, regional and distant metastasis and perineural invasion [183]. Other studies observed a negative correlation, i.e. a reduced expression of CD44 in aggressive HNSCC tumours. For example, reduced CD44 expression in the primary tumour was reported to be associated with the presence of cervical lymph node metastases [184] [185]. Reduced expression of one or more of the variant CD44 isoforms in OSCC samples, in particular in poorly

differentiated tumours, has also been described [186]. Some studies did not find any correlation with aggressive tumour features such as T or N stage [187] or with 5 year survival of OSCC patients [188]. These discrepancies are possibly due to the heterogeneity of the examined patient cohorts, the use of different antibodies, and different fixation and staining techniques.

Assessing CD44 expression by FACS offers a number of advantages over immunohostochemistry as it relies on the analysis of single isolated tumour cells. The complete exposure of surface antigens allows better antibody binding compared to epitopes in tissue sections. There is also less confusion concerning the surface staining of adjacent cells. As signal intensity can be more easily and accurately analysed, FACS analysis is expected to produce more accurate and consistent results. However, there are two major limitations that can lead to false estimates of the size of a CD44 expressing fraction. First, cell surface antigens can be damaged or destroyed by enzymatic dissociation of the tissue employed to obtain cell suspensions. Second, the identity of $CD44^+$ stromal cells cannot be determined by their position in relation to the tumour. We recently reported that trypsinisation causes destruction of some CD44 epitopes and that this can be avoided by alternative non-enzymatic treatments [189]. To exclude stromal cells the epithelial fraction of the tumour needs to be identified by either negative or positive selection. The findings described above suggest that, with existing antibodies and technologies, the standard method (negative selection) is imperfect with the average purity of the epithelial fraction obtained being only 65% (Table 5.5). The novel method described here (positive selection) improved the average purity of the epithelial fraction to 85% (Table 5.5).

Discrepancies in published data also suggest that the standard selection technique (negative selection) may be inconsistent. The first study to use negative selection to analyse CD44 expression on cells isolated from HNSCC tumours reported that the $CD44^+$ cell population in 25 tumour samples was less than 10% of all epithelial cells [82]. A later article published by the same group reported that the $CD44^+$ cell fraction varied from 0.4% to 81% in 31 HNSCC samples [190]. As the size of the patient cohort was

similar and the same selection technique was used (negative selection with the same antibodies), statistically the frequency of CD44 expressing cells ought to be of a similar range. Due to inaccuracy of the negative selection, the putative epithelial fraction may have been contaminated with $CD44^+$ and/or $CD44^-$ non-epithelial cells. This would lead to wrong estimates of the size of the $CD44^+$ cell fraction detected in the putative epithelial fraction of the tumour. Contamination with $CD44^+$ non-epithelial cells would result in larger numbers and contamination with $CD44^-$ cells in lower numbers describing the size of the $CD44^+$ cell fraction. However, it is unclear to which extent the large differences between the two studies were due to inconsistent identification of the epithelial fraction and to biological variability of the tumour samples.

Contamination with non-epithelial cells could significantly distort results when analysing small sub-fractions of tumour cells and such studies make accurate identification of the tumour fraction particularly necessary. For a few tumours I attempted to assess the size of the EMT cell fraction as defined by the $CD44^+ESA^{low/-}$ FACS phenotype, which ranged from 0% to 27% in the 11 samples analysed (see section 5.2.5, Table 5.14 and Figure 5.39). The $CD44^+ESA^{low/-}$ phenotype is also typical for fibroblasts (Figure 5.28) and fibroblasts contaminating tumour cell suspensions can be mistaken for $CD44^+ESA^{low/-}$ EMT tumour cells leading to wrong estimates about presence and proportion of EMT cells in the tumour.

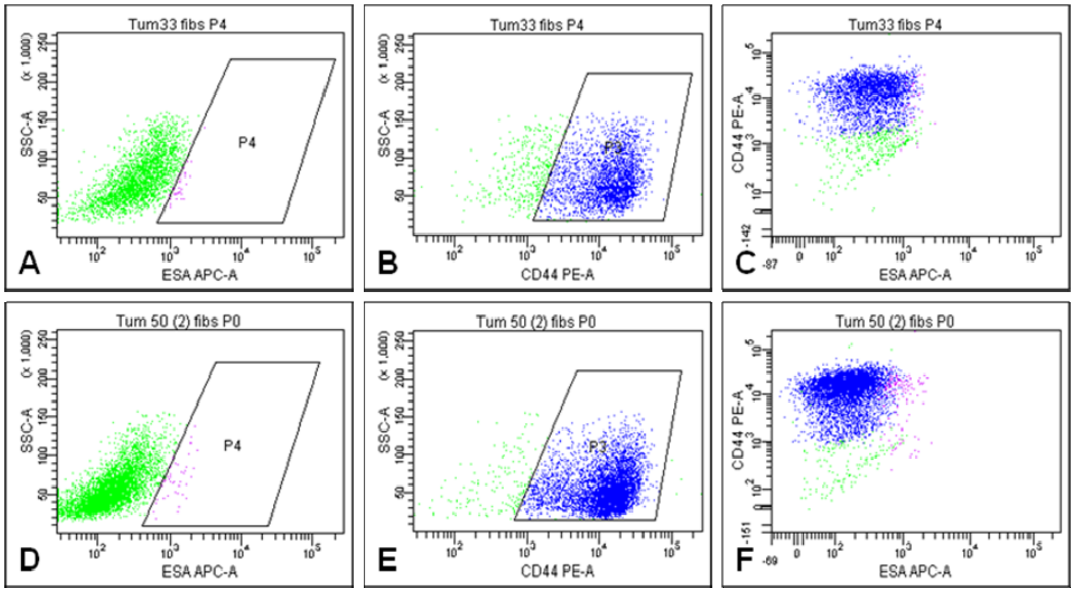

Figure 5.28: CD44 and ESA expression by tumour-derived cultured fibroblasts. Cells were detached with EDTA and immunolabelled with antibodies against ESA (APC-conjugated) and CD44 (PE-conjugated). FACS plots for two primary fibroblast cultures are shown. Detected ESA positivity is below 1% in both cultures (A, D). 90.5% of Tum33 fibroblasts (B) and 96.5% of Tum50(2) (E) are $CD44^{+}$.

The average purity of the epithelial tumour fraction identified by negative or positive selection was 65.7±2.8% and 85.2±3.6% respectively (Table 5.6). Consequently, the epithelial fraction was contaminated with cells of non-epithelial cell lineages to 34.3% and 14.8% respectively. Given the small size of the EMT fraction (0-27%) relative to the degree of contamination, presence of fibroblasts (or other cells with $CD44^{+}ESA^{low/-}$ phenotype) amongst the contaminating cells would significantly falsify estimates of the size of the EMT cell fraction of the tumour.

In conclusion, while FACS analysis of fresh tumour cells may offer a more reliable way of examining expression levels of the antigens of interest as compared to IHC, the identification of the epithelial fraction needs further improvement. This study could provide an important milestone by introducing a new selection technique which seems more efficient and reliable than the standard method currently used.

5.2 The CD44$^+$ cell population is associated with aggressive features of OSCC

One of the objectives of this study was to examine the frequency of CD44 expressing cells in samples of OSCC and to assess the findings for a possible correlation to clinical and pathological parameters of tumours of origin. Having tested negative and positive selection on cultured cells and on cells isolated from tumours (described in 5.1), here I used both methods to identify the epithelial fraction in tumour samples prior to its assessment for the presence and the size of CD44$^+$ cell fraction.

The frequency of CD44 expressing cells was analysed in 34 surgical specimens of oral squamous cell carcinoma and 5 specimens of lymph node metastases. Tumour specimens were obtained with informed consent from patients who were undergoing surgical resection of their tumour at St Bartholomew's Hospital and the Royal London Hospital. Tumour tissue was sampled for research whenever the size of the resected tumour allowed. Samples were usually analysed on the next day after the surgery. Tissue was dissociated into single cells using Collagenase and/or Trypsin according to the protocol described in detail in section 4.3. After disintegration of the tumour tissue the isolated cells were analysed by flow cytometry. The epithelial fraction of each specimen was identified using either negative or positive selection and was then analysed for the presence and the size of the CD44 expressing cell fraction. For all 34 primary OSCC samples analysed in this study full clinical reports could be obtained from the hospital. The proportion of CD44 expressing cells was evaluated for a correlation with the following clinical and pathological parameters: T stage, N stage, extracapsular spread, invasion pattern, perineural and lymphovascular invasion, tumour depth and tumour grade.

5.2.1 Patient cohort and tumour specimens

The patient cohort examined in this study consisted of 14 female (41.2%) and 20 male (58.8%) patients. Patients' mean age at the time of diagnosis with OSCC was 66 years with the youngest patient being 40 and the oldest being 88 years old.

The OSCC tumours, with which these patients were presented varied widely in their location, size and spread (Table 5.8). Primary tumour sites included tongue, mandible, floor of mouth, buccal mucosa, maxilla and the retromolar region. All five lymph node metastases were surgically removed at the same time as the primary tumours they were associated with which were also included in the study. Table 5.8 summarises clinical and pathological features of all patients and tumour specimens.

Table 5.8: Summary of samples and parameters analysed in the study.

Parameter	No of samples	%
Sex		
female	14	41.2
male	20	58.8
Age		
40-55 years	4	11.8
56-70 years	19	55.9
71-88 years	11	32.4
Tumour site		
Tongue	15	44.1
Mandible	7	20.6
Buccal	4	11.8
Flour of mouth	4	11.8
Maxilla	3	8.8
Retromolar region	1	2.9
T classification		
T1	5	14.7
T2	15	44.1
T3	2	5.9
T4	12	35.3
N classification		
N0	11	32.4
N1	8	23.5
N2	15	44.1
N3	0	0
Extracapsular spread		
Yes	15	65.2
No	8	34.8

Parameter	No of samples	%
Grade		
poorly differentiated	3	8.8
poor to moderately differentiated	17	50.0
moderately differentiated	8	23.5
moderate to well differentiated	4	11.8
well differentiated	2	5.9
Invasion Pattern		
cohesive	10	29.4
discohesive	24	70.6
Tumour depth		
≤ 8 mm	11	32.4
9-16 mm	14	41.2
< 16 mm	6	17.6
unknown	3	8.8
Perineural Invasion		
yes	16	47.1
no	18	52.9
Lymphovascular Invasion		
yes	6	17.6
no	28	82.4
Surgical margin		
clear (> 5 mm)	16	47.1
close (1 - 5 mm)	13	38.2
involved (< 1mm)	5	14.7

The clinical and pathological parameters summarised in the table above existed as many different permutations in the patients included in the study. For example, patient “EB” was a 79 year old man who was diagnosed with squamous cell carcinoma of the mandible. His tumour was staged as T4N0. It was moderately differentiated with no perineural or lymphovascular invasion and showed a largely cohesive invasion front. The patient underwent a unilateral selective neck dissection and no metastatic deposit

was detected in the 33 lymph nodes removed from the neck. Patient “56” was a 47 year old female patient presented with the squamous cell carcinoma of the tongue, which was diagnosed as a T2N2c moderately differentiated tumour with no perineural or lymphovascular invasion and a discohesive invasion front. The bilateral selective neck dissection yielded 34 lymph nodes, of which metastatic disease was detected in 3 of 15 lymph nodes on the left and 3 of 19 lymph nodes on the right. Extracapsular tumour spread was found in two lymph nodes. Many other different types of OSCC tumours with varying clinical and pathological parameters were also amongst the specimens examined. For a full list of tumours analysed in the study see Appendix Table 3.

5.2.1 Variable frequency of $CD44^+$ cells in samples of OSCC

Cell suspensions isolated from the tumour tissue were co-stained with antibodies against CD44 and antibodies used in either negative or positive selection. DAPI was used to exclude dead cells. Amongst all $DAPI^-$ cells the epithelial fraction was identified and examined for the presence of CD44 expressing cells (Figure 5.29 and Figure 5.30).

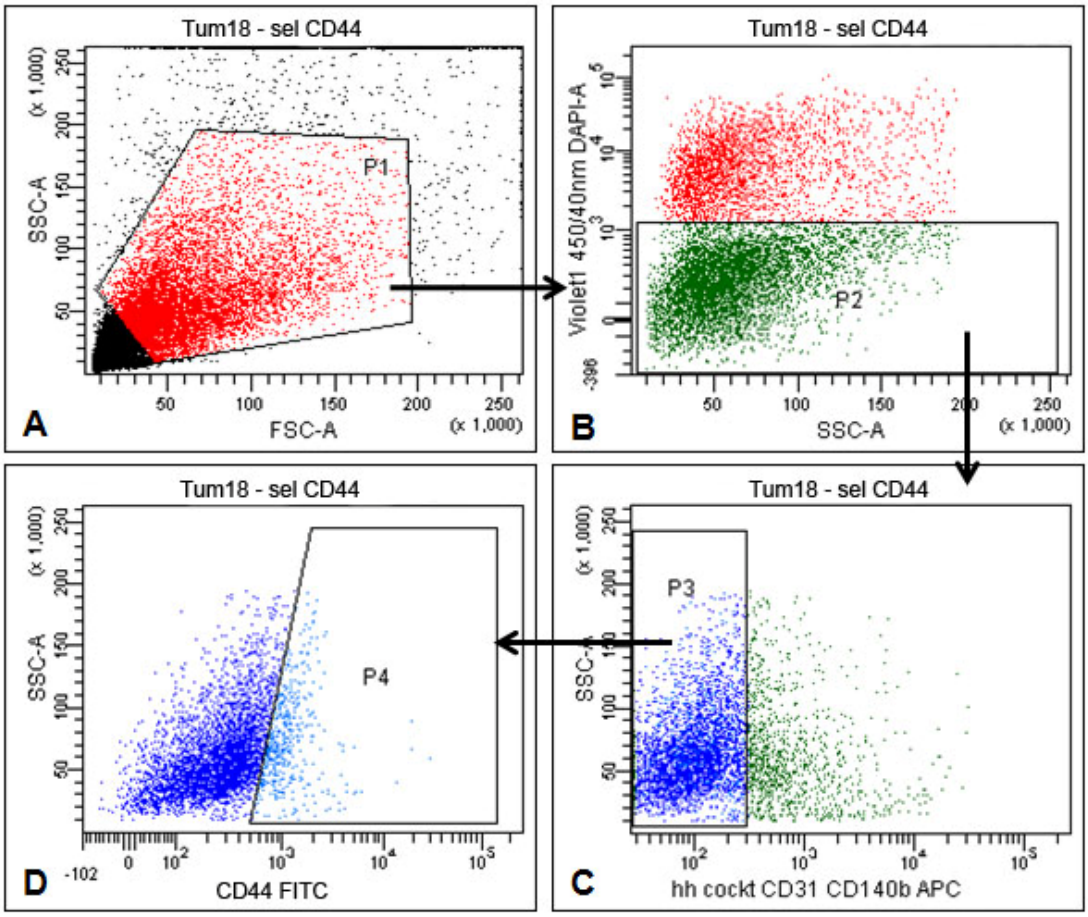

Figure 5.29: Flow cytometric analysis of a typical OSCC sample using negative selection to identify the epithelial fraction. All cells (A) were sequentially gated on viable cells (B) with DAPI as a dead cell marker. Within all viable cells the epithelial cell fraction was gated (C) based on the absence of signal for lineage markers CD2, CD3, CD14, CD16, CD19, CD56, CD235a CD32 and CD140b (all APC-conjugated). Finally, linage-negative cells were assessed for the presence of $CD44^+$ cells with an anti-CD44 antibody conjugated to FITC (D, gated in P4).

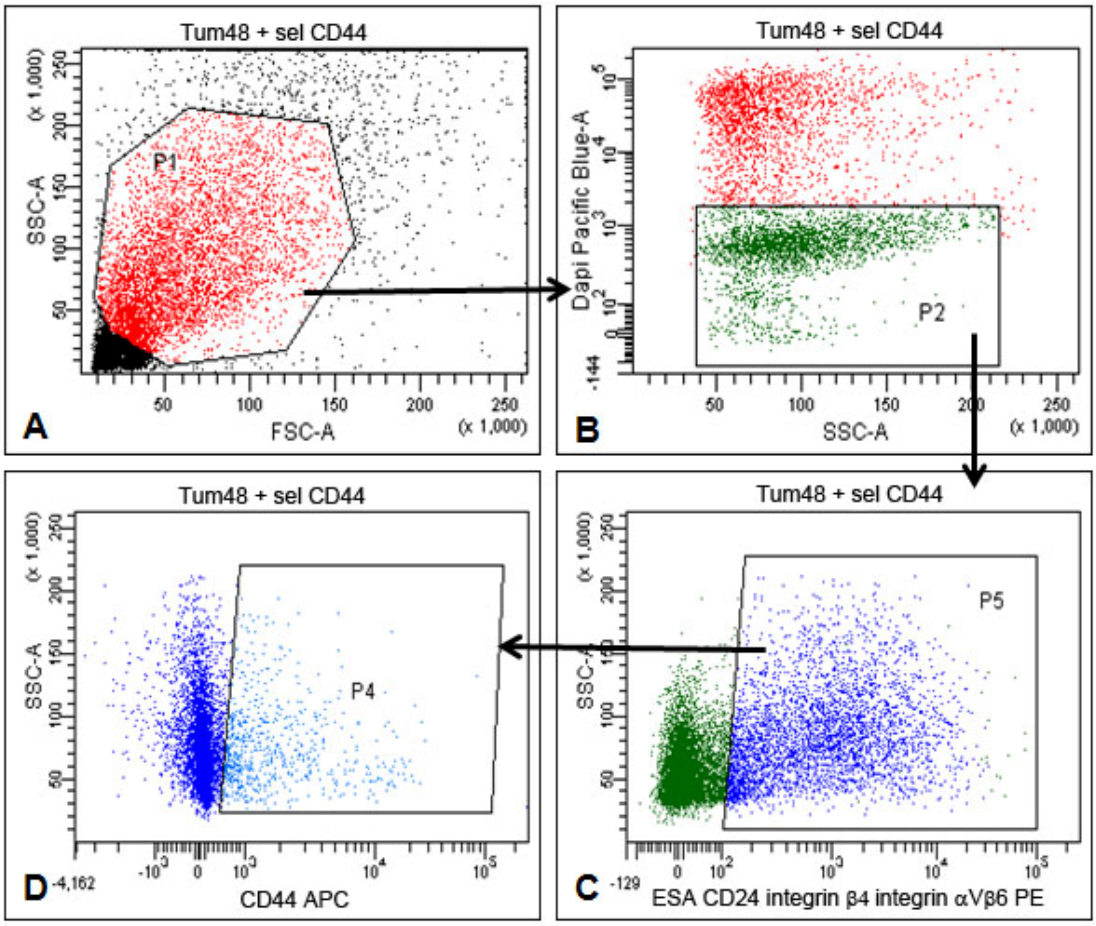

Figure 5.30: Flow cytometric analysis of a typical OSCC sample using positive selection to identify the epithelial fraction. All cells (A) were sequentially gated on viable cells (B) with DAPI as a dead cell marker. Within all viable cells the epithelial cell fraction was gated (C) based on positivity for epithelial markers ESA, CD24, integrin β4 and integrin αVβ6 (all FITC-conjugated). Finally, FITC-positive cells were assessed for the presence of $CD44^+$ with an anti-CD44 antibody conjugated to APC (D, gated in P4).

The frequency of $CD44^+$ cells was highly variable amongst individual tumour specimens (Table 5.9, Figure 5.31). The proportion of $CD44^+$ cells in the primary tumour samples varied between 3% and 97.7% (Table 5.9 A). The frequency of CD44 expressing cells in metastatic lymph node specimens varied between 21.7% and 96.8% (Table 5.9 B). Figure 5.31 shows representative FACS plots with a small (Figure 5.31 A-B), a medium (Figure 5.31 C-D) and a large (Figure 5.31 E-F) CD44 expressing cell fraction.

Table 5.9: Frequency of CD44 expressing cells in samples of primary OSCC and associated lymph node metastases*

A

Tumour (primary)	$CD44^+$ cells [%]
42 (2)	3
27	3.9
PB	5
IS	5.3
LK	5.4
47	5.9
23	6.1
NA	7
21	7.7
EB	8.5
52	9.2
18	9.9
24	10.5
46	10.8
56	11.6
KR	13.1
MB	16.3

Tumour (primary)	$CD44^+$ cells [%]
46 (2)	19.1
48	22.2
30	22.7
56 CM	23.3
RA	23.7
MP	25
CB	25
A	27.2
MK	31.5
NK	34
AB	43.1
IV	51.9
25	65.2
60	67.1
57JK	74.3
44	77.5
BKK54+	97.7

B

Lymph node	$CD44^+$ cells [%]
NKn	21.7
Bn	31.7
24n	43.3
MKn	54.9
57n	96.8

* A: frequency of $CD44^+$ cells in fresh samples of human OSCC. B: frequency of $CD44^+$ cells in samples of lymph node metastases.

The size of the epithelial fraction of the examined tumour specimens varied between 30% and 85% of all cells isolated from the tissue sample. The CD44 expressing fraction varied between 3% and 97.7% as described above. The size of $CD44^+$ cells in the non-epithelial fraction varied from 2% to 83% of all non-epithelial cells. This means that for some tumours a large proportion of cells identified as non-epithelial by either negative or positive selection was expressing CD44, whereas for others only a small fraction of non-epithelial cells was $CD44^+$. In some specimens the proportion of $CD44^+$ cells was higher in the epithelial fraction, in others it was higher in the non-epithelial cell fraction.

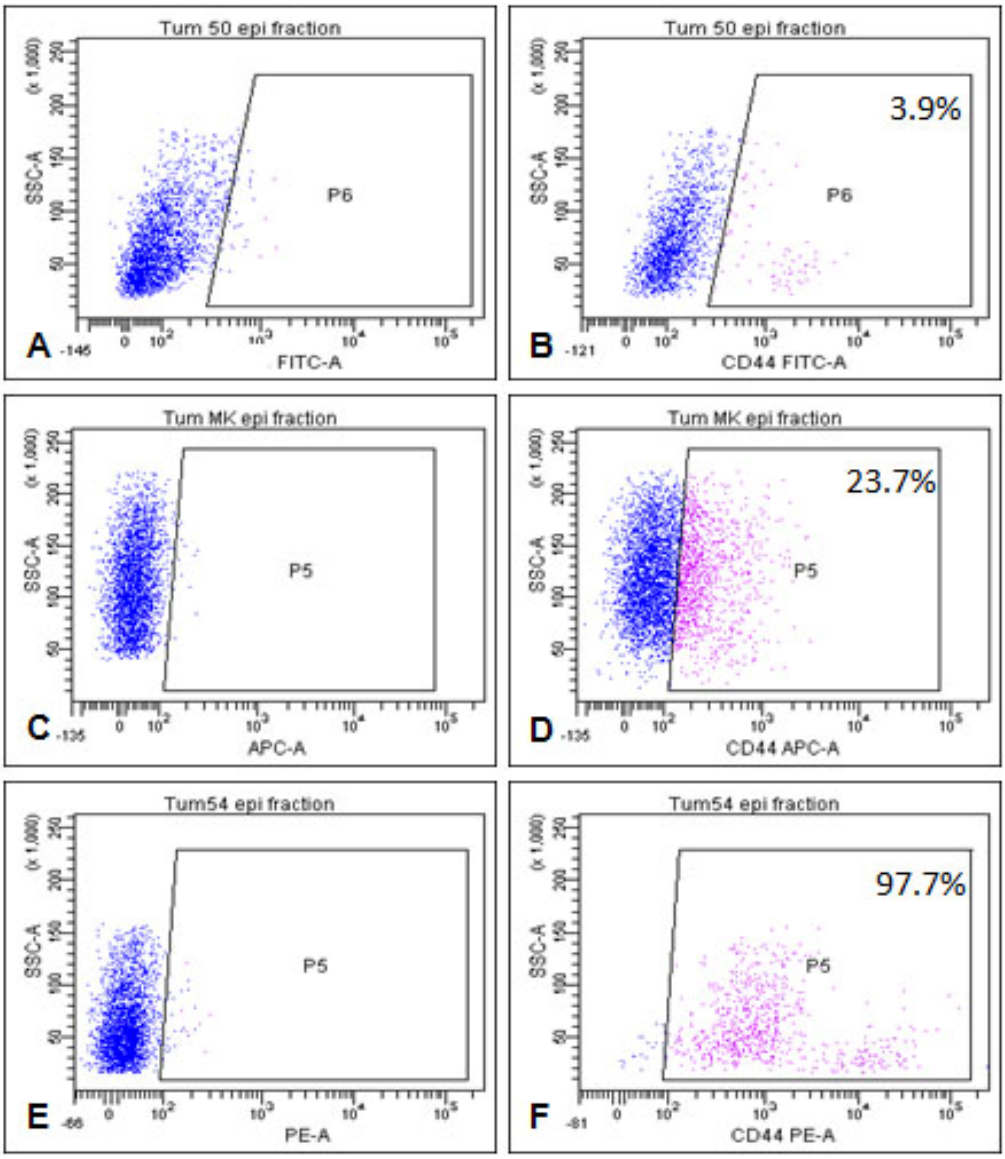

Figure 5.31: Different size of the CD44$^+$ fraction in the epithelial fraction in OSCC specimens. Representative FACS plots are shown for tumours with small (B), medium (D) and large (F) fraction of CD44 expressing cells in the epithelial fraction. Gates were set based on autofluorescence signal of non-stained control samples (A, C, E).

5.2.2 Frequency of CD44$^+$ cells in primary metastatic and non-metastatic tumours

Visual examination of the data indicated a different distribution of the frequency of CD44 expressing cells in primary metastatic tumours as compared to primary non-metastatic tumours. All OSCC specimens were grouped based on the absence (N0) or the presence (N1 and N2) of lymph

node metastasis. The frequency of CD44 expressing cells in the non-metastatic tumours (N0) varied between 3% and 23.3% (Table 5.10 A). In metastatic tumours (N1/2) the proportion of $CD44^+$ cells ranged from 5.9% to 97.7% (Table 5.10 B). The median values for each group were 7% for N0 and 25% for N1/2, respectively. Values representing proportions of $CD44^+$ cells in samples in N0 and N1/2 groups were plotted in a scatter plot shown in figure 5.32.

Table 5.10: Frequency of CD44 expressing cells in metastatic vs. non-metastatic tumours*

A

Tum No	TNM	% $CD44^+$ cells	Selection method
42	T4 **N0**	3	+
27	T4 **N0**	3.9	+
PB	T4a **N0**	5	+
IS	T2 **N0**	5.3	-
LK	T2 **N0**	5.4	-
NA	T2 **N0**	7	-
EB	T2 **N0**	8.5	-
18	T4 **N0**	9.9	-
46	T2 **N0**	10.8	-
MB	T1 **N0**	16.3	-
56CM	T1 **N0**	23.3	+

B

Tum No	TNM	% $CD44^+$ cells	Selection method
47	T2 **N2b**	5.9	-
23	T4a **N1**	6.1	-
21	T4 **N2b**	7.7	-
52	T2 **N2b**	9.2	-
24	T2 **N2b**	10.5	-
56	T2 **N2c**	11.6	-
KR	T2 **N1**	13.1	+
46(2)	T4 **N2b**	19.1	-
48	T4 **N2a**	22.2	+
30	T2 **N1**	22.7	+
RA	T2 **N1**	23.7	-
MP	T3 **N2b**	25	-
CB	T2 **N2b**	25	-
NK	T3 **N2a**	26.4	+
A	T4a **N1**	27.4	-
MK	T4a **N2c**	31.5	+
AB	T2 **N1**	43.1	-
25	T2 **N2b**	51.7	+
IV	T1 **N1**	51.9	-
60	T2 **N2b**	67.1	+
44	T4 **N2b**	77.5	+
57JK	T1 **N2a**	77.9	+
54	T1 **N1**	97.7	+

C

	N0	N1+N2
Median (%$CD44^+$ cells)	7%	25%
n > 10% CD44+	3 / 11 (27%)	19 / 23 (83%)
n > 15% CD44+	2 / 11 (18%)	16 / 23 (70%)

*A: non metastatic tumours (N0), B: metastatic tumours (N1/2); C: median values and number of samples in each group with proportion of $CD44^+$ cells higher than 10% or higher than 15%.

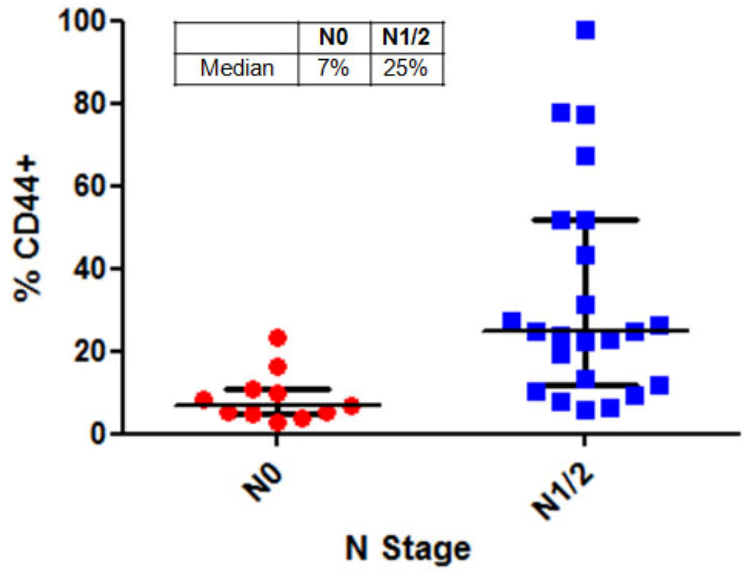

Figure 5.32: Scatter plot showing proportions of CD44$^+$ cells in the groups N0 and N1/2. Values representing frequencies of CD44$^+$ cells in non-metastatic (N0, red) and metastatic (N1/2, blue) tumour samples are shown. The horizontal line with error bars shows the median value for each group. Plot and calculations were made using the GraphPad Prism 5 software.

These observations show that primary oral tumours that have formed early lymph node metastases have a higher proportion of CD44 expressing cells than primary tumours that did not metastasise. Presence of a possible correlation between the proportion of CD44$^+$ cells and other clinical and pathological parameters could not be as easily established and statistical tests were needed to examine this.

5.2.3 Correlation between the proportion of CD44$^+$ cells and clinical and pathological parameters

To examine other possible correlations between the proportion of CD44 expressing cells and clinical and pathological parameters of the tumour, the data was analysed using the statistical package “R”. To choose a suitable statistical test it was first established how the data was distributed. The numbers, representing the frequency of CD44 expressing cells in tumour samples were plotted as a cumulative function of the number of specimens

analysed (Figure 5.33). The plot showed that the probability function of the data points does not correspond to that of a normal distribution.

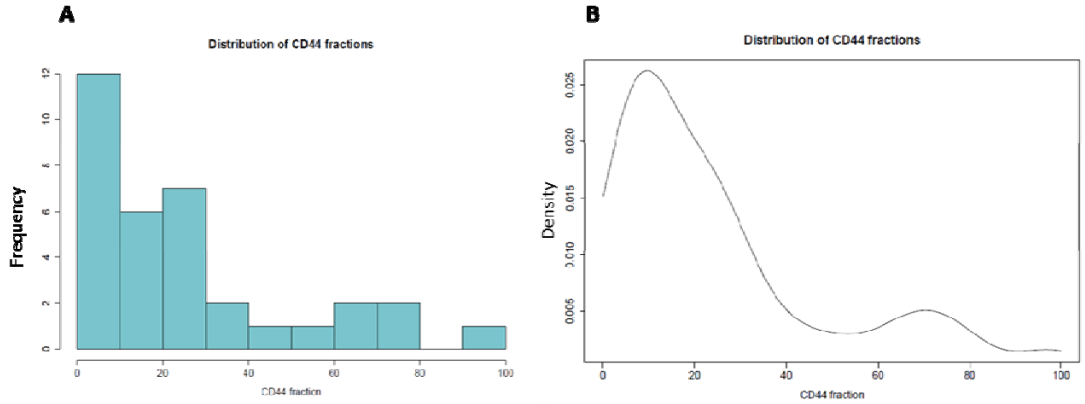

Figure 5.33: Distribution of data points describing the proportion of CD44$^+$ cells in fresh samples of primary OSCC. The frequency of different proportions of CD44$^+$ cells (A) and the corresponding probability density function (B) show that the data points are not normally distributed.

Because the data points were not normally distributed Spearman's ranked test and Fisher's exact test, which are the two most common non-parametric tests, were chosen for the statistical analyses of the data. Clinical parameters examined for a correlation with the frequency of CD44 expressing cells included T stage, N stage, grade of the tumour, depth of the tumour, nature of the invasion front, presence of perineural and lymphovascular invasion and extracapsular spread. With both tests, the positive correlation observed between the frequency of CD44 expressing cells in OSCC specimens and the presence of lymph node metastases (see above) was confirmed. Moreover a correlation between high proportion of CD44$^+$ cells and discohesive invasion front as well as high tumour grade (poorly differentiated tumours) was found.

Figure 5.34 shows the Spearman correlation matrix from which the presence or the absence of a correlation between the frequency of CD44$^+$ cells and selected clinical and histological parameters can be seen (for a full matrix, including all parameters mentioned above, see Appendix Figure 3). The

parameters of interest are shown in squares forming the diagonal of the matrix. Every other square gives the relationship between the two parameters framing the square in question. For example, the third square from the left in the first row represents the relationship between the T stage and the frequency of $CD44^+$ cells in OSCC samples (shown as “CD44” in the matrix) (Figure 5.34). Different shades of green of the squares represent different strengths of correlation between the two parameters in question, with dark green showing a strong correlation and white showing no correlation. The numbers (Spearman's rank correlation coefficients) also quantify the strength of the correlation with 1 and -1 representing the strongest positive or negative correlation and numbers close to 0 showing no correlation. The p-values for the established correlations are given in brackets. The strongest correlation was observed between the frequency of $CD44^+$ cells and the presence of lymph node metastases (p=0.0001). The proportion of CD44 expressing cells also correlated with a discohesive invasion front (0.009) and with a high tumour grade (representing poorly differentiated tumours, p=0.05) (Figure 5.34). No correlation was observed with the T stage (Figure 5.34), the depth of the tumour, perineural and lymphovascular invasion and extracapsular spread (Appendix Figure 3).

With the Fisher’s exact test the strongest correlation was observed between the frequency of $CD44^+$ cells and high tumour grade (odds ratio: 23.1, p-value 0.001). Figure 5.35 shows the distribution of the data points describing the frequency of $CD44^+$ cells in tumour samples (depicted on the y-Axis) arranged in five groups representing the different differentiation states of the tumour (shown on the x-Axis) (Figure 5.35). A weaker but statistically significant correlation was found with the presence of lymph node metastases (odds ratio: 20.6, p-value: 0.002) and discohesive invasion front (odds ratio: 12.6, p-value 0.02). The representative plots are shown in figure 5.36 and figure 5.37, respectively.

Figure 5.34: Spearman correlation matrix. Different shades of green represent different strengths of correlation between high frequency of CD44 expressing cells and the clinical parameter in question (see text for a detailed explanation). The p-values for each correlation are given in brackets. The strongest correlation (dark green) was found with the presence of lymph node metastases. A weaker but significant correlation (lighter green) was found with the discohesive invasion front and high grade of the tumour. No correlation (white) was observed with T stage.

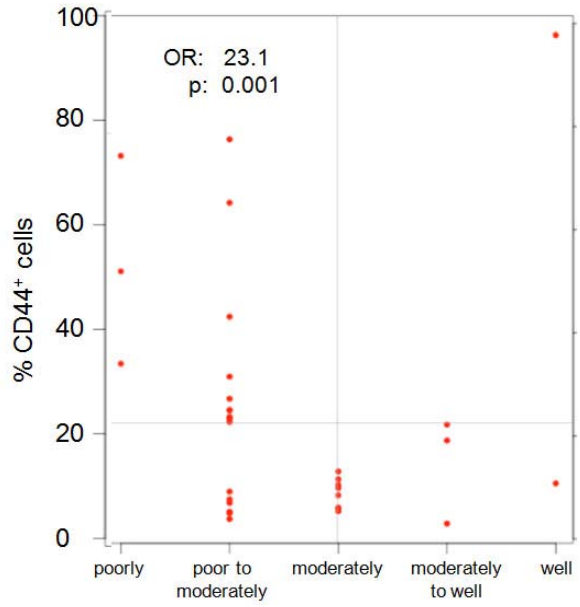

Figure 5.35: The frequency of CD44$^+$ cells in samples with a different tumour grade. Tumour specimens were grouped into 5 groups based on their grade. The majority of the specimens in the groups containing poorly and poor to moderately differentiated tumours showed a proportion of CD44$^+$ cells above the cut-off point of 22.5% (grey horizontal line). No specimens in the groups with moderately, moderately to well and well differentiated tumours contained more than 22.5% of CD44$^+$ cells.

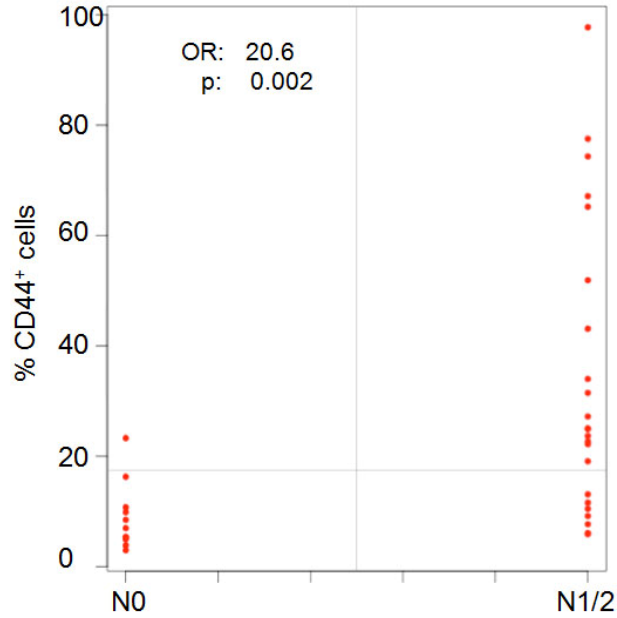

Figure 5.36: Frequency of CD44$^+$ cells in non-metastatic and metastatic tumours. The proportion of CD44$^+$ cells in tumour samples without (N0) or with (N1/2) lymph node metastases is shown. The majority of samples in the N1/2 group and only one sample in the N0 group had a frequency of CD44$^+$ cells above the cut-off point (grey horizontal line) of 17.5%.

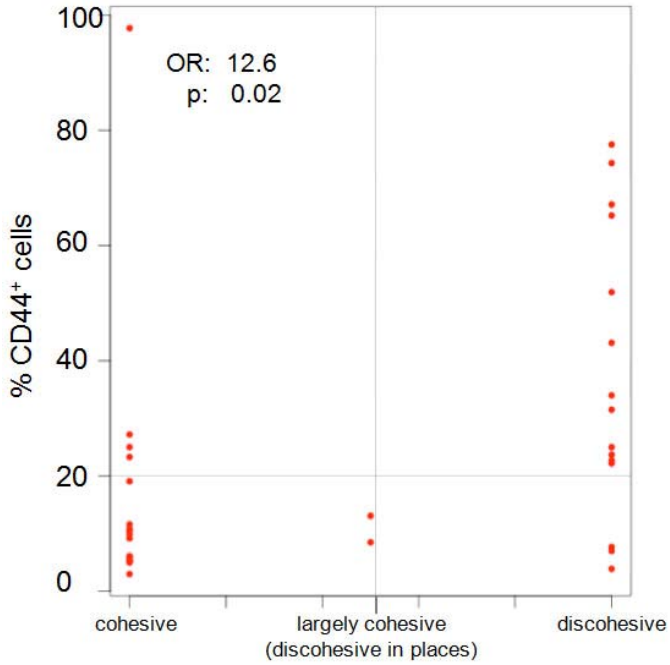

Figure 5.37: The frequency of CD44$^+$ cells in samples with different invasion pattern. The tumour specimens were grouped into 3 groups based on their invasion pattern. In the group with a discohesive invasion front the majority of samples showed a high proportion (above the cut-off point of 20%, grey horizontal line) of CD44$^+$ cells. Only 3 samples with a cohesive invasion front and no samples with a largely cohesive invasion front had a proportion of CD44$^+$ cells higher that 20%.

Mann-Whitney U test is another commonly used statistical test for comparison of two sets of samples. It is used when the sample data are not normally distributed and when they cannot be transformed to a normal distribution. The Mann-Whitney U test (also known as Mann-Whitney-Wilcoxon test, Wilcoxon rank-sum test or Wilcoxon–Mann–Whitney test) combines and ranks the data from sample set 1 and sample set 2 and calculates a statistic on the difference between the sum of the ranks of sample set 1 and sample set 2. A cut-off value for the independent variable 'frequency of CD44$^+$ cells' was determined to differentiate the two sample sets: CD44 high and CD44 low. This cut-off CD44 value was calculated so as to minimize the p-value and maximize the effect size for each sample set.

Similar to the Spearman's ranked test and the Fisher's exact test, the Mann-Whitney U test, when performed on the data set described above, showed a statistically significant correlation between the frequency of CD44$^+$ cells in the

tumour sample and the presence of lymph node metastases, discohesive invasion front and the tumour grade (Table 5.11). In addition, a statistically significant correlation was observed between high frequency of $CD44^+$ cells and perineural invasion, which was not established when Spearman's ranked test or the Fisher's exact test were used (Table 5.11).

In summary, all three tests (Spearman's ranked test, Fisher's exact test and Mann-Whitney U test) showed that OSCC tumours with a high frequency of $CD44^+$ cells are more likely to have lymph node metastases, a discohesive invasion front and a high tumour grade. In addition, using the Mann-Whitney test, the high frequency of $CD44^+$ cells was also found to correlate with perineural invasion. Table 5.11 gives the p-values for the different correlations as established by the three different tests. Differences in p-values calculated for the same parameter/correlation by the different tests are likely due to the tests' methodological differences.

Table 5.11: P-values for statistically significant correlations established by three different tests

Tumour parameter	Spearman's ranked test	Fisher's exact test	Mann-Whitney U test
Lymph node metastases	0.0001	0.002	0.0002
(discohesive) Invasion front	0.009	0.02	0.004
(high) Tumour grade	0.05	0.001	0.0006
Perineural invasion	Not significant	Not significant	0.02

The statistical analysis described above was performed on all 34 samples, pooling the samples where negative or positive selection was applied to identify the epithelial fraction of the tumour. In the previous section (5.1) positive selection was described as more efficient and accurate than the negative selection. Because the two selection techniques were different in their efficiency, the selection method used might have affected the detection

of CD44$^+$ cells. To justify pooling the samples despite different selection techniques, I looked at whether there was a statistically significant difference in the proportion of CD44 expressing cells between samples analysed by positive and negative selection. Figure 5.38 shows the proportion of CD44 expressing cells in tumour samples in relation to the selection method used (Figure 5.38). A trend line fitted to the data points is an ascending line suggesting a positive correlation between the frequency of CD44 expressing cells and the positive selection technique. This would mean, that a sample analysed with positive selection might be expected to show a higher proportion of CD44 positive cells than if analysed with negative selection. However, this correlation was not found to be statistically significant.

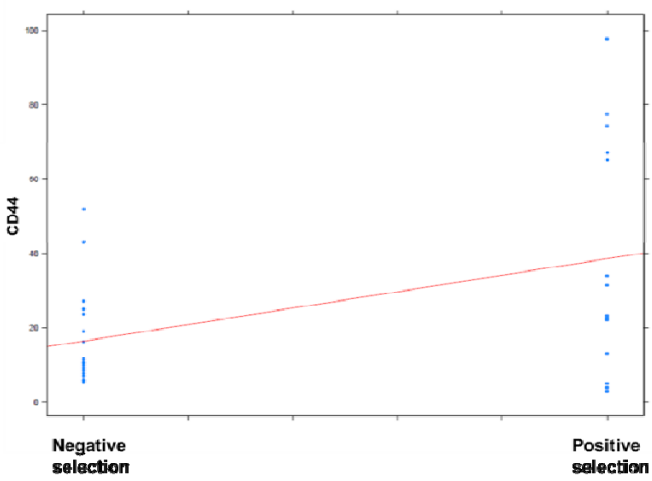

Figure 5.38: Frequency of CD44+ cells in relation to the selection method used to identify the epithelial fraction. The tumour specimens were grouped according to the selection method used. Specimens analysed by negative selection are shown on the left, samples analysed by positive selection are shown on the right. The trend line fitted to the data points indicates that samples analysed by positive selection were more likely to have a higher proportion of CD44$^+$ cells. However, this trend was not statistically significant.

Because of the observed trend between the proportion of CD44 positive cells in tumour samples and positive selection, the Fisher's exact test was run on the two sets of data separately. The results for the two data sets were essentially similar to those obtained from the analyses of the combined data set. Due to a smaller number of samples, the correlations observed using a

single selection method were statistically weaker (Table 5.12), but for the group analysed by negative selection, which included 20 samples, all three correlations were still statistically significant ($p \leq 0.05$). For the group analysed by positive selection, including 14 samples, only the correlation with lymph node metastases was found to be statistically significant.

Table 5.12: Statistical analyses of samples analysed by negative and positive selection*

	Combined data set (34 samples)	Negative selection (20 samples)	Positive selection (14 samples)
Tumour grade	OR: 23.1 (p=0.009)	OR: Inf (p=0.01)	OR: 8.4 (p=0.22)
Lymph node metastases	OR: 20.6 (p=0.0024)	OR: Inf (p=0.04)	OR: 18 (p=0.04)
Discohesive invasion front	OR: 12.6 (p=0.02)	OR: 9.3 (p=0.046)	OR: 9.5 (p=0.09)

* OR: odds ratio, inf: infinity

5.2.4 Frequency of CD44 expressing cells in lymph node metastases

Five pairs of matching primary OSCC and associated lymph node metastases were analysed in this study. Due to their small number, a statistical analysis could not be performed on lymph node samples. However, as seen in Table 5.13, no consistent difference in the proportion of $CD44^+$ cells appeared related to the sample origin from either a primary tumour or a lymph node metastasis. For some pairs the frequency of CD44+ cells was higher in the primary tumours, for others it was higher in the lymph node metastases (Table 5.13).

Table 5.13: Frequency of CD44+ cells in primary tumours vs. associated lymph node metastases

Sample	Sample type	%CD44+ cells	Selection method	Δ %CD44+ cells
A	Primary OSCC	27.2	-	
Bn	Lymph node	31.7	-	+4.5
25	Primary OSCC	51.7	+	
24n	Lymph node	43.3	+	-8.4
57	Primary OSCC	74.3	+	
57n	Lymph node	96.8	+	+22.5
MK	Primary OSCC	31.5	+	
MKn	Lymph node	54.9	+	+23.4
NK	Primary OSCC	26.4	-	
NKn	Lymph node	21.7	-	-4.7

5.2.5 Frequency of $CD44^{+}ESA^{-/low}$ EMT cells in OSCC specimens

Cell suspensions isolated from fresh OSCC tumours were also examined for the presence of EMT cells that can be identified by their $CD44^{+}/ESA^{low/-}$ FACS phenotype. The epithelial fraction of the tumours was identified either by negative or positive selection as described above prior to examining the EMT cell fraction.

Because three different fluorophores were used when examining the EMT fraction, compensation needed to be done and therefore a lot of cells were required. Hence, detection of the EMT cell fraction was only possible for large tumours from which a sufficient number of cell could be isolated. In the 11 OSCC specimens analysed the EMT cell fraction varied in size from 0% to 27% of all epithelial cells (Table 5.14). Figure 5.39 depicts examples of FACS plots showing the $CD44^{+}$ cell fraction and the EMT cell fraction of three different tumour specimens.

There was no statistically significant correlation between the size of the EMT fraction and the clinical and pathological parameters of the respective tumours, which was probably due to the small number of specimens analysed. Presence of EMT cells in these tumour samples gives evidence of

EMT occurring in human tumours *in vivo*, a topic that has been, and still remains, highly controversial [191].

Table 5.14: EMT cell fraction in fresh tumour specimens

Tum No	TNM	% EMT cells
Tum30	T2 N1	~0
Tum47	T2 N2b	2.0
TumMK	T4a N2c	4.8
Tum23	T4a N1	5.7
TumC	unknown	5.2
Tum48	T4 N2a	9.7
Tum24	T2 N2b	7.3
Tum25	T2 N2b	12.8
Tum54	T1 N1	20.1
TumA	T4a N1	20.4
TumJK	T1 N2a	27.0

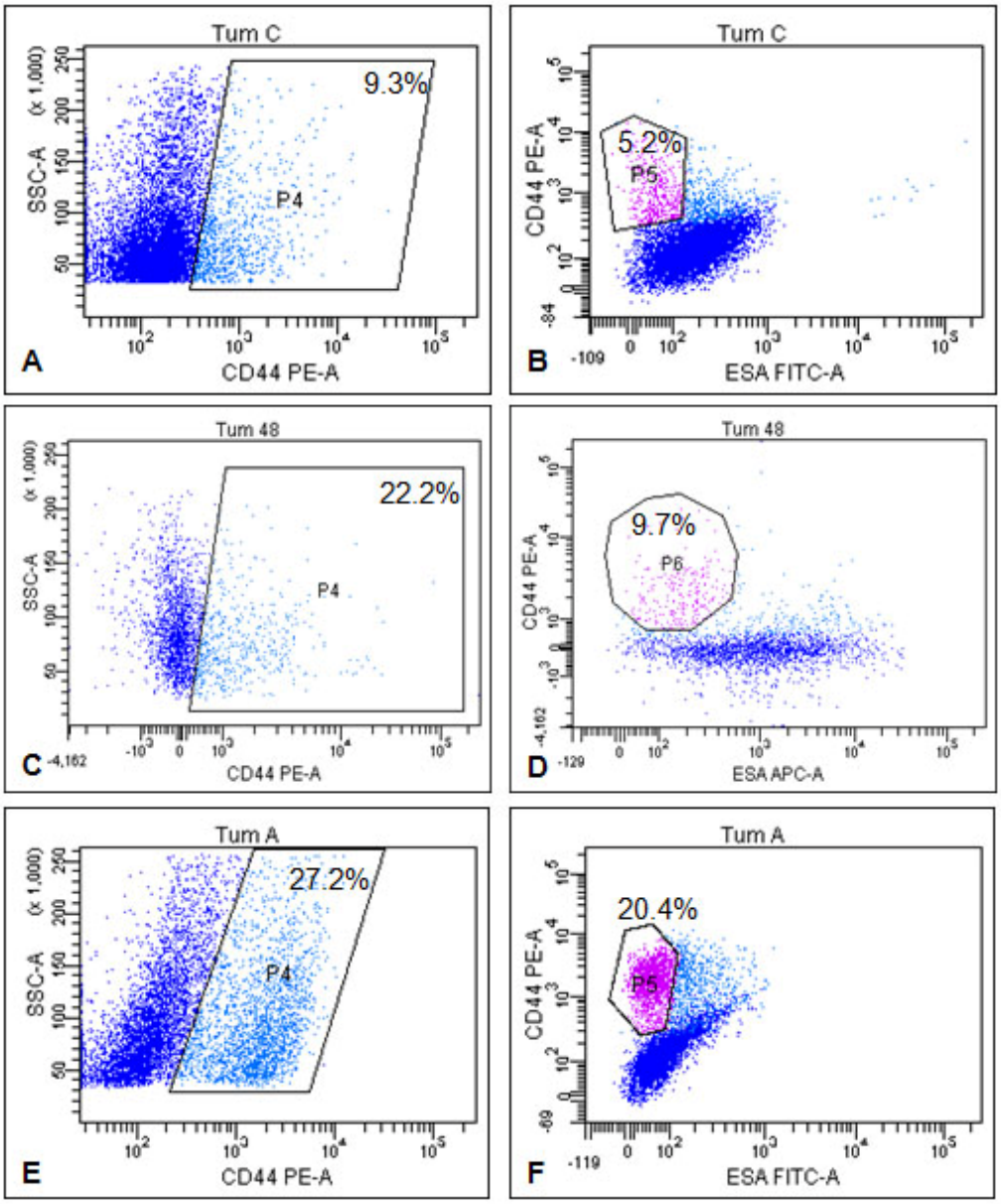

Figure 5.39: CD44$^+$ and EMT cells in fresh tumour tissue. Cells were isolated from 3 different OSCC specimens. The epithelial fraction was identified using negative selection for the specimens TumC and TumA and using positive selection for the specimen Tum48. The EMT cell fraction constituted 5.2% of all epithelial cells in TumC (B), 9.7% in Tum48 (D) and 20.5% in TumA (F).

5.2.6 Discussion

5.2.6.1 Sampling the tumour tissue

A major limitation of the study was the scarce availability of tumour tissue. Usually the OSCC tumours were not very large in size and tissue sufficient for a full pathological examination was required before a resected tumour could be sampled for research. For pathological analysis of fresh tumour tissue, part was usually processed for embedding in paraffin and part snap-frozen in liquid nitrogen. These two ways of tissue processing were used to reduce the uncertainty of histology. After tissue sampling for pathological examination, often there was no or very little tissue to spare for research. Another limiting factor in tissue acquisition was the often necrotic area in the centre of the tumour, which further reduced the size of the available usable tissue. The pathologist attempted consistent sampling from the tumour edge to make the samples less necrotic and to collect as many viable cells as possible. Sampling was always performed by the same pathologist and the risk of contamination with normal oral mucosal cells, was similar for all tumour samples. All other variables that related to processing and analysing the tissue (such as the choice of enzyme, incubation time, etc.) were kept unchanged for all tumour specimens to provide maximum possible consistency.

5.2.6.2 Distinguishing between normal and malignant oral mucosa

During sampling, the tumour margin was located macroscopically by the pathologist and tissue was always sampled from the edge of the tumour. There was thus a chance of including adjacent non-malignant oral mucosa in the samples. The distribution of $CD44^+$ cells in the normal oral tissue might be different from that in the malignant tissue. Consequently, presence of normal cells in the tumour cell fraction could falsify the estimates about the proportion of $CD44^+$ tumour cells. Reports of tumour cell analysis found in the literature do not seem to have approached this problem and it is not clear whether antibodies capable of consistently distinguishing normal from

malignant epithelial cells exist. T and Tn antigens are precursors in normal complex carbohydrate chains, and, in normal tissues, these antigens are masked and not accessible to the immune system. However, they have been reported as uncovered and immuno-reactive in most carcinomas [192] [193]. Possibly antigens of this type could be used to distinguish normal from malignant epithelial cells. However, further work in this direction is needed.

5.2.6.3 Influence of the selection method on detection of $CD44^+$ tumour cells

The frequency of CD44 expressing cells in individual tumour samples varied widely and independently of the selection method used to identify the epithelial fraction. The slight differences in the strength of the correlations (Table 5.12) observed in the analysis of the combined data set and the analysis of the two groups of data separately are most likely due to a smaller number of specimens included. Although not statistically significant, samples analysed with the positive selection tended to have a higher proportion of $CD44^+$ cells (median 27.4%) that samples analysed with the negative selection (median 10.7%) (Figure 5.38). As described in section 5.1 the positive selection seems to be slightly more accurate in identifying the epithelial cell fraction. The larger proportions of $CD44^+$ cells in samples analysed with the positive selection could be explained through the negative selection yielding an impure epithelial fraction contaminated with $CD44^-$ cells of non-epithelial cell lineages. The presence of $CD44^-$ non-epithelial cells in the putative epithelial fraction would dilute the epithelial fraction and lower the estimates of the proportion of $CD44^+$ cells.

5.2.6.4 The use of CD44 as a prognostic marker in OSCC

The present study established a statistically significant correlation between high frequency of CD44 expressing epithelial tumour cells and the presence of neck lymph node metastases, discohesive invasion front and high tumour grade. In a recent study by Joshua and co-workers, the frequency of lin^- $CD44^+$ cells was analysed in 31 samples of primary human OSCC using negative selection, and was found to correlate with T stage and local

recurrence of the tumours according to the Spearman's ranked test [190]. A strong correlation was also observed with successful xenograft implantation (p=0.001). There was a trend towards higher proportion of $CD44^+$ cells in poorly differentiated tumours as compared to moderately and well differentiated tumours (p=0.09) and tumours with perineural invasion (p=0.12). In contrast to the present study the work by Joshua did not find a correlation with the presence of lymph node metastases. The disparity between the findings of the two studies could be based on the heterogeneity of the tumour samples. The study by Joshua was performed on head and neck tumours, which included cancers of the oral cavity but also cancers of the oropharynx, larynx and hypopharynx, nose and sinuses, whereas the current study examined tumours of the oral cavity only. Importantly, both studies found correlations between the frequency of $CD44^+$ epithelial cells in tumour samples and aggressive features of the tumours stressing the role of CD44 in cancer progression.

5.3 Analysis of malignant cell lines derived from surgical specimens of OSCC and lymph node metastases

Major limitations of analysing fresh tumour cells include the usually small size of the specimen and the inaccuracy of the epithelial selection. Cell lines generated from fresh tumour tissue can provide large numbers of cells and allow a more standardised analysis of the progeny of cells isolated from the tumour.

In this section I describe generation, cultivation and analysis of malignant cell lines derived from specimens of primary OSCC and associated lymph node metastases. Furthermore, the data obtained from analysis of cells isolated from fresh tumour tissue, presented in the previous chapter (section 5.2), is compared with the data obtained from the analysis of cell lines generated from these tumours and malignant cell lines are evaluated as suitable models for studying cancer stem cells.

5.3.1 Influence of the medium composition on cultured cells

To find the optimal conditions for isolation and cultivation of cells form OSCC tissue I first compared growth, proliferation and differentiation patterns of established head and neck cancer cell lines grown under different culture conditions. Cell and colony morphology as well as proliferation and differentiation pattern were examined in established cell lines cultured in the routinely used RM+ medium and in a serum-free, low-calcium medium formulation, termed CnT24 medium (CellnTec Advanced Cell Systems). Both, adherent as well as non-adherent culture conditions were tested.

5.3.1.1 Colony morphology, proliferation and differentiation patterns in established head and neck cancer cell lines

Cell and colony morphology have been extensively studied in primary cultures of keratinocytes isolated from many epithelial tissues. Three types of colonies characteristic for cell lines derived from epithelial tissues were first

discovered by clonal analysis in primary epidermal keratinocytes [194]. These colony types, termed holoclone, meroclone and paraclone, were reported to be formed by cells with distinct morphological features and different proliferative capacities. Holoclone colonies contained small, round, tightly packed cells, which had a great reproductive capacity. Paraclone colonies contained loosely spaced, large cells with a low reproductive capacity. Meroclone colonies were identified as a transition state between holoclone and paraclone colonies, containing a mix of cells of different sizes and different reproductive capacities [194]. Holo-, mero- and para-clones were classified as stem cells, amplifying cells and early differentiating cells, respectively [194] [195].

Holo-, mero- and para-clone colonies have been since described in cell lines derived from many epithelial tissues including hair follicles [196], ocular surface epithelium [197] and the oral mucosa [198]. Our own laboratory was first to provide evidence for the existence of the three colony types in cancer cell lines [180]. Similar to epidermal primary keratinocytes, holo-, mero- and para-clones in head and neck cancer cell lines displayed morphological differences and had different proliferative potential. In addition, Harper and co-workers reported a distinct expression pattern of stem cell-related and differentiation-related markers for each type of colony [180]. The holoclone colonies showed strong expression of the stem cell-related markers CD44, β-catenin and integrin β1. In contrast, markers associated with differentiation, such as keratin 6 [180] were mainly present in paraclone colonies. Vimentin expression was detected in meroclone colonies [180]. These findings extended the proposed hierarchy model of epithelial differentiation to head and neck cancer cell lines with holo- mero- and para-clones corresponding to stem, transit amplifying and early differentiating cells, respectively.

Studies describing the existence of the three characteristic colony types in cell lines derived from epithelial tissues have been performed on cells cultured in a standard serum-containing medium [199]. The method of serial cultivation of keratinocytes, including composition of the standard medium formulation, was described almost 30 years ago [199]. Although the original

method is still successfully and widely used, today, there exist many alternative commercially-available cell culture media. Some of these media have been developed to support the growth of epithelial cells isolated from specific tissues. For example, the “CnT24 progenitor cell targeted oral epithelium medium” (CellnTec Advanced Cell Systems) has been specifically designed for isolating and culturing oral mucosal keratinocytes. CnT24 is a fully-defined, serum-free medium that contains low levels of calcium (0.07 mM). According to the manufacturer CnT24 supports the growth of oral epithelial stem and early progenitor cells, maintaining their undifferentiated and immature state by causing a delay in the onset of terminal differentiation.

It is well known that the composition of the culture medium has a significant impact on cell growth, cell differentiation and maturation state. I tested the suitability of the CnT24 medium for culturing established head and neck cancer cell lines available in our laboratory, comparing CnT24 to the routinely used RM+ medium. Cells were seeded at clonal density in both media and cultures were monitored daily. A marked difference in colony morphology was observed for cells grown in CnT24 medium as compared to growth in RM+ medium. Grown in RM+ medium cell lines for CA1, 5PT and H357 formed the three characteristic types of colonies: holoclones, meroclones and paraclones previously described (Figure 5.40). In contrast, in the CnT24 medium this pattern of colony formation was not observed. Instead, the cell lines formed three distinct types of colonies (termed colony types I, II and III) containing one, two or three morphologically distinct cell types (cell type 1, 2 and 3) arranged in concentric rings (termed zones 1, 2 and 3) (Figure 5.41, Figure 5.42). Each of the three cell lines grown in the CnT24 medium showed colonies with such morphologies (Figure 5.43).

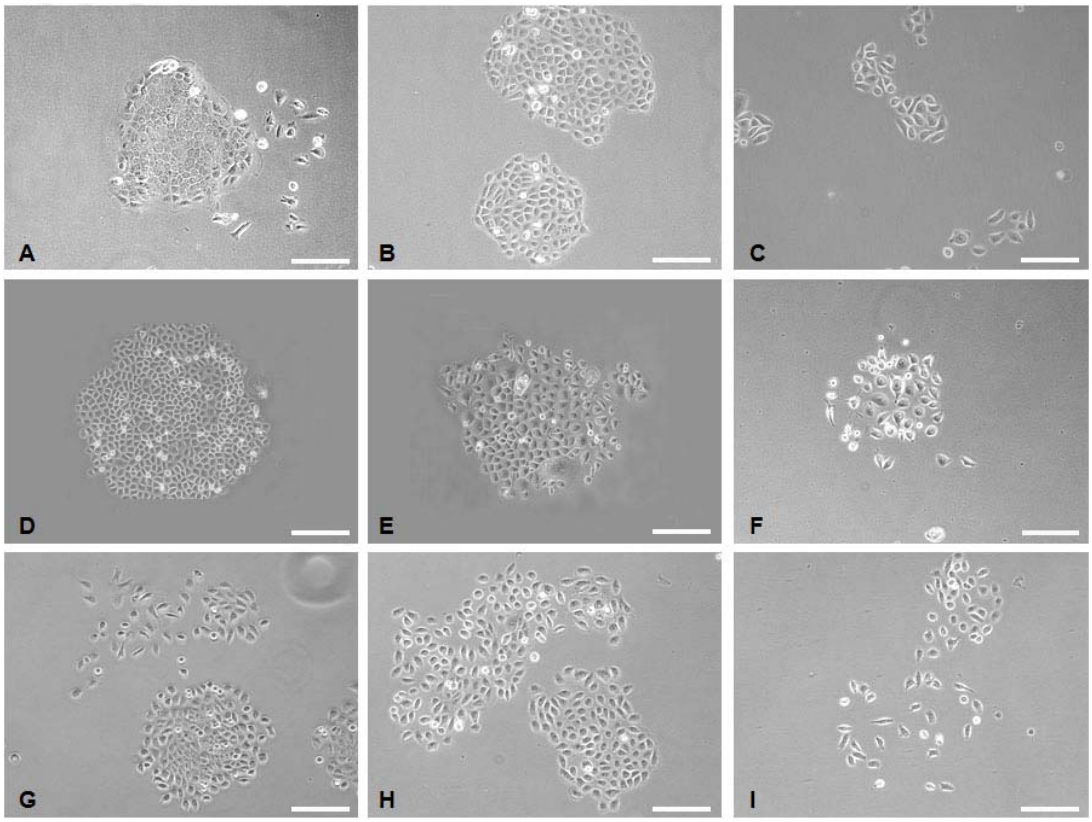

Figure 5.40: Different types of colonies in head and neck cancer cell lines grown in RM+ medium. Oral cancer cell lines CA1 (A-C), 5PT (D-F) and H357 (G-I) were grown in RM+ medium. In each cell line three morphologically different types of colonies were present**:** holoclone colonies with a circular outline and tightly packed "cobblestone" cells (A, D and bottom G), meroclone colonies containing larger irregularly sized cells (B, E, H) and paraclone colonies with large loosely spaced cells (C, F, I). Scale bar 100 µm

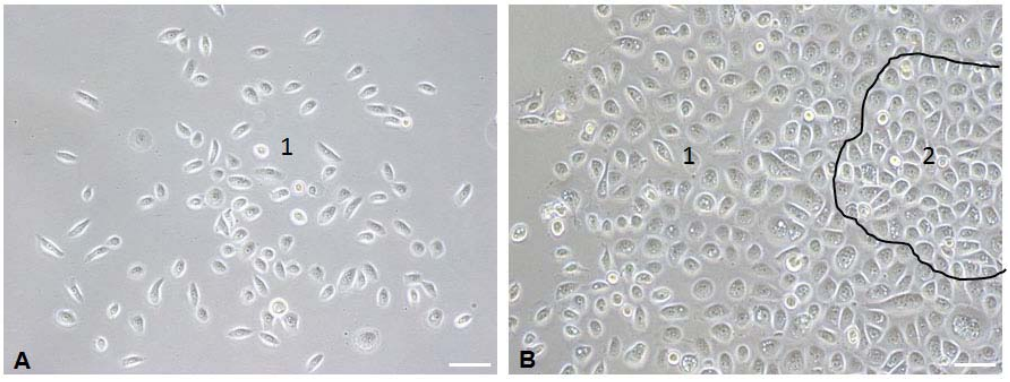

Figure 5.41: Type I and II CA1 colonies present in the CnT24 medium. Cells were grown at clonal density in CnT24 medium for 14 days before photographs were taken. The type I colony contained irregularly shaped, loosely spaced type 1 cells (A). Type II colony consisted of smaller tightly packed type 2 cells in the centre and type 1 cells in the periphery (B) Scale bar 100 µm (A), 50 µm (B)

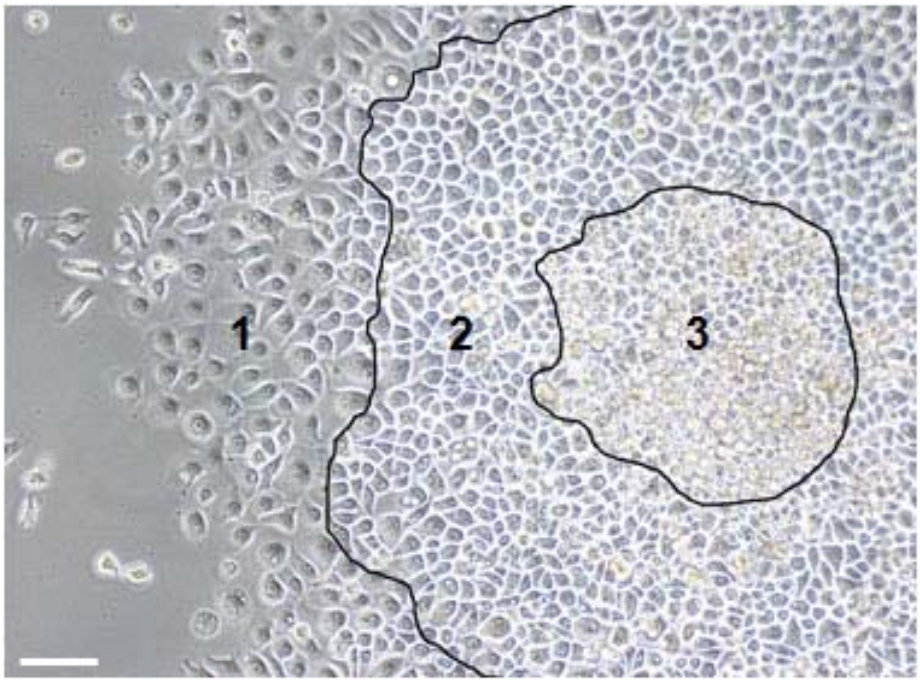

Figure 5.42: Type III 5PT colony present in CnT24 medium. Type III colony contained three different types of cells arranged in concentric circles or zones. The outer circle (zone 1) is formed by type 1 cells which are large and loosely spaced. Small and round type 2 cells form the intermediate circle (zone 2). The central zone (zone 3) consists of yet smaller and more closely packed type 3 cells. Scale bar 50 µm

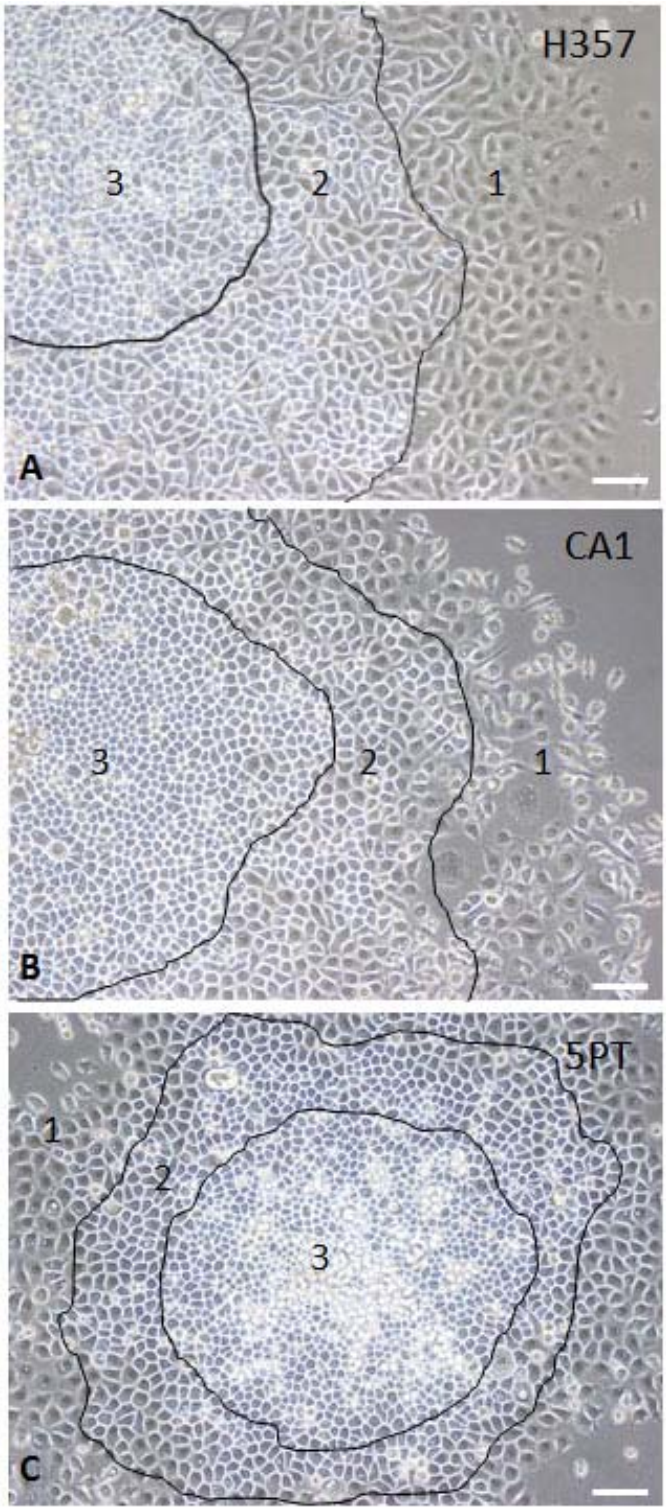

Figure 5.43: Colony morphology of head and neck cancer cell lines in CnT24 medium. All three cell lines H357, CA1 and 5PT (A, B and C, respectively) formed colonies consisting of cells with different morphologies arranged in concentric circles. The centre of the colony was made up of very small, round cells that were tightly packed type 3 cells (zone 3). It was surrounded by larger irregularly shaped type 2 cells (zone 2). The outer circle (zone 1) consisted of even larger, more loosely spaced type 1 cells. Scale bar 50 µm

Similar colony morphologies have been described for murine epidermal and oral epithelium grown under serum-free, low-calcium culture conditions. Tudor and co-workers reported colonies of keratinocytes comprising three different types of cells arranged in concentric circles [200]. They also studied the differentiation and proliferation patterns in these colonies. They observed that type 3 cells did not express keratins associated with differentiation but expressed keratin 15, a keratin that is found in some epidermal and mucosal stem cell zones [201] [202]. On the contrary, type 1 and type 2 cells stained for mucosal (Keratin 4, Keratin 13) or epidermal (Keratin 1 and Keratin 10) differentiation markers. Clonogenic assays and BrdU labelling revealed that type 2 and in particular type 3 cells were highly proliferative, whereas type 1 cells could only divide once or twice. Furthermore, Tudor and co-workers reported that qPCR indicated expression of Oct-4, considered a classic stem cell marker, to be restricted to type 3 cells, and c-myc expression, which is associated with commitment of stem cells to differentiation [203], was found in type 1 and type 2 cells only. Based on these findings the authors proposed a model in which zone 3, zone 2 and zone 1 cells correspond to stem cells, amplifying cells and early differentiating cells, respectively [200].

To determine whether this model could be applied to human malignant oral keratinocyte cultures grown in a serum-free, low-calcium medium formulation such as CnT24, I examined their expression patterns of markers associated with stemness and differentiation. Expression patterns of CD44, EGFR, β-catenin, E-cadherin and vimentin were examined by immunohistochemistry. Differential expression of each of these markers was observed across the different cell zones. In zone 3 cells a high level of markers associated with stemness (CD44, EGFR, membrane β-catenin and E-cadherin) was detected (Figures 5.44, 5.45, 5.46 and 5.48). Nuclear β-catenin, which has been linked to increased proliferation in basal cell carcinoma [204] and observed in differentiated keratinocytes [205] was found in zone 2 cells. High levels of vimentin were observed in zone 1 cells (Figure 5.47). A striking reciprocal E-cadherin and vimentin localisation in zone 3 and zone 2/1 was seen in concentric colonies (Figure 5.48).

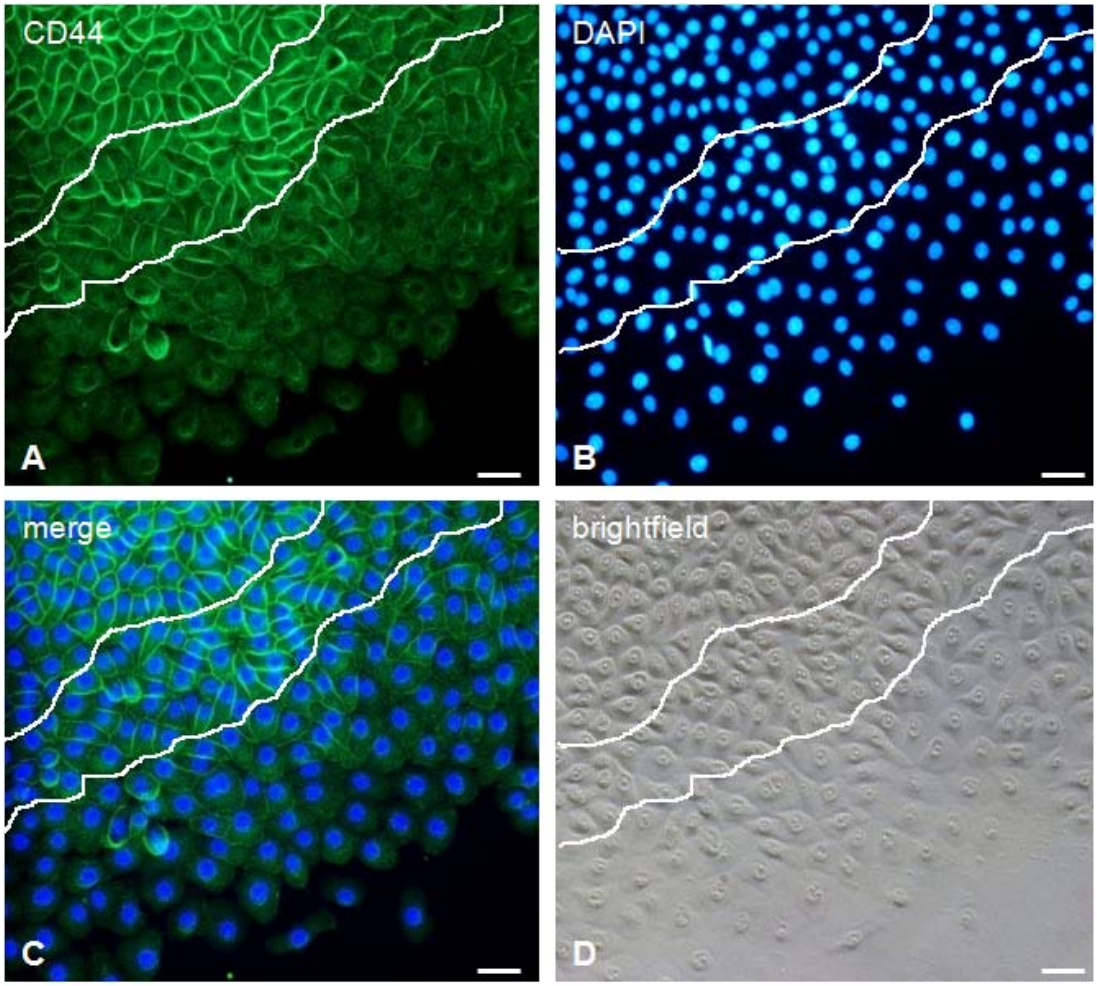

Figure 5.44: CD44 expression pattern in a concentric CA1 colony. CA1 cells were grown in CnT24 medium for 14-20 days. Cells were fixed and stained with DAPI and an antibody against CD44. Concentric rings (zones 1-3) of the colony are outlined, with zone 3 in top left and zone 1 in bottom right corner of the image. Immunostaining for CD44 (green, A, C) shows a strong membrane staining in cells in zones 3 and zone 2 in the middle of a colony. The signal gets weaker towards the periphery of the colony and is only present in a few cells in the outermost area (zone 3) of the colony. DAPI and brightfield images (B and D) reveal concentric colony morphology. Scale bar 50 µm

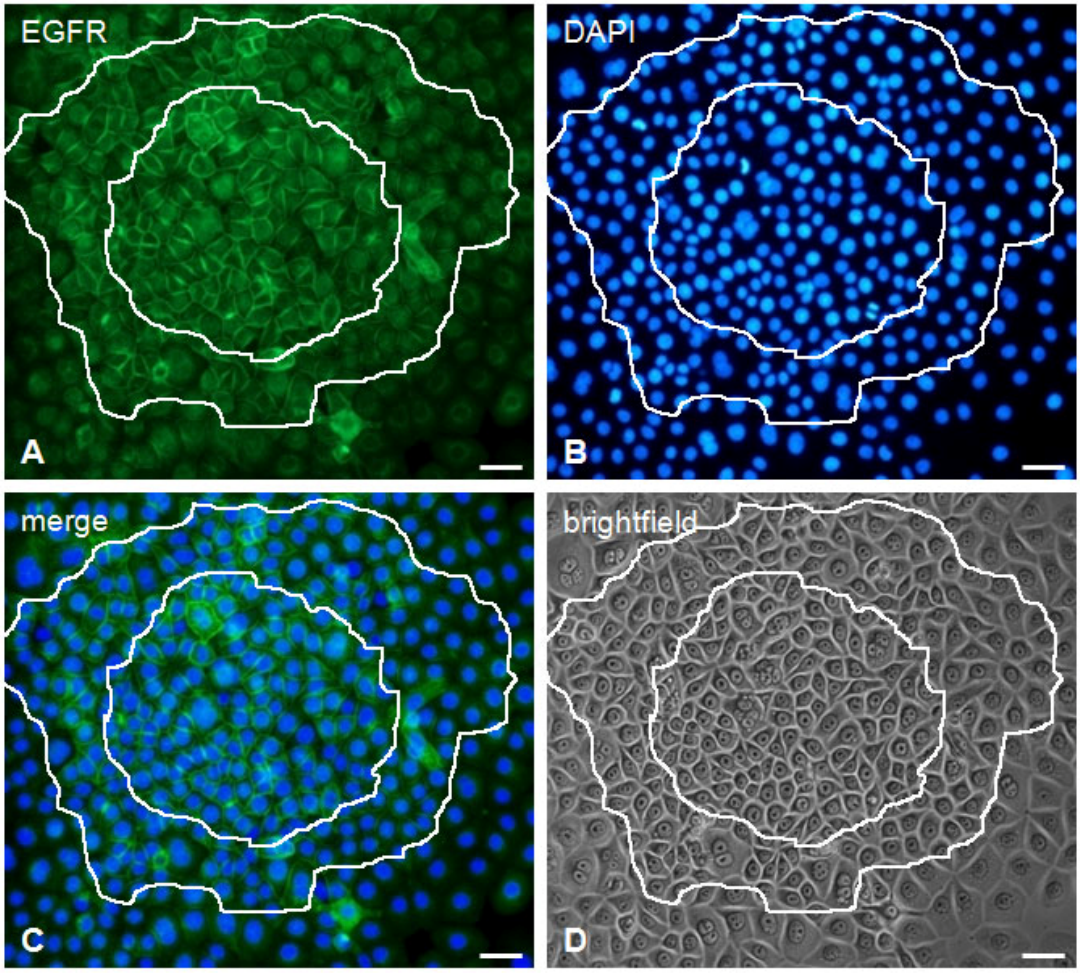

Figure 5.45: EGFR expression pattern in a concentric CA1 colony. Concentric rings (zones 1-3) of the colony are outlined, with the central zone 3, intermediate zone 2 and peripheral zone 1. Immunostaining for EGFR (green, A, C) shows a strong membrane staining in cells in the innermost zone in the middle of the colony. In zone 2 EGFR is also present in some cells. Almost no signal is seen in cells in the outermost zone 1 at the periphery of the colony. DAPI and brightfield images (B and D) reveal concentric colony morphology. Scale bar 50 µm

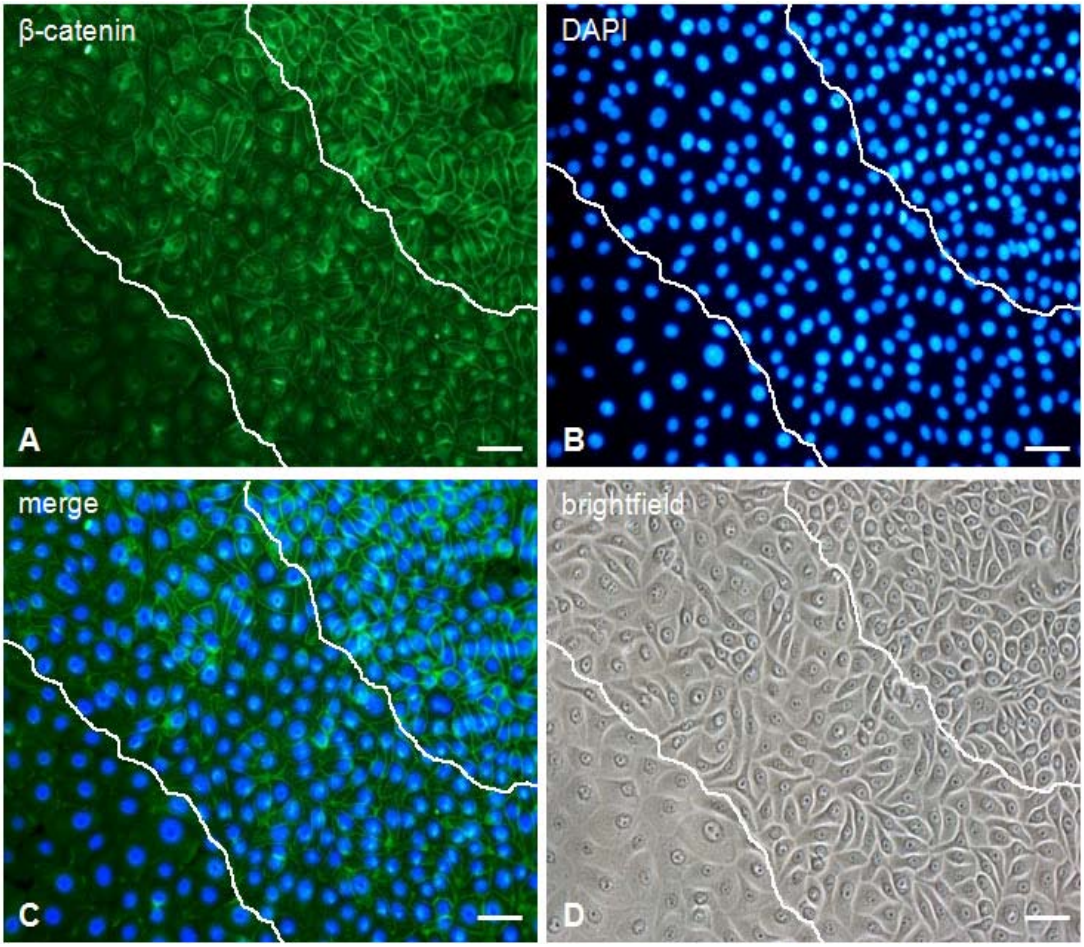

Figure 5.46: β-catenin expression pattern in a concentric CA1 colony. Concentric rings (zones 1-3) of the colony are outlined, with zone 3 in top right and zone 1 in bottom left corner of the image. β-catenin (green, A, C) is seen in the membrane of most zone 3 cells and some zone 2 cells. β-catenin is also present in the nuclei of zone 2 cells and a few zone 1 cells. Neither nuclear nor membrane β-catenin is seen in zone 1 cells. DAPI and brightfield images (B and D) reveal concentric colony morphology. Scale bar 50 μm

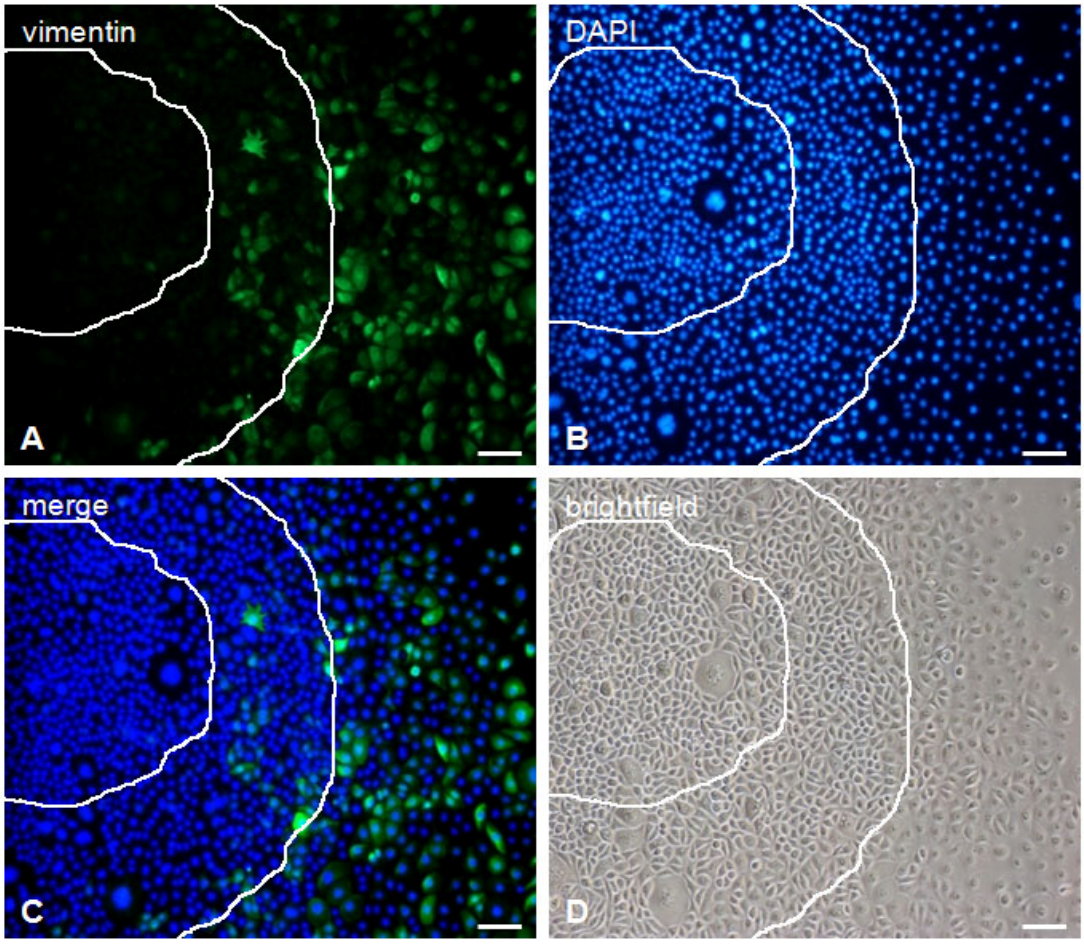

Figure 5.47: Vimentin expression pattern in a concentric CA1 colony. Concentric rings (zones 1-3) of the colony are outlined, with the central zone 3, intermediate zone 2 and peripheral zone 1. Vimentin expression (green, A, C) is seen in zone 1 cells at the periphery and a few zone 2 cells. No vimentin is present in zone 3 in the centre of the colony. DAPI and brightfield images (B and D) reveal concentric colony morphology. Scale bar 100 μm

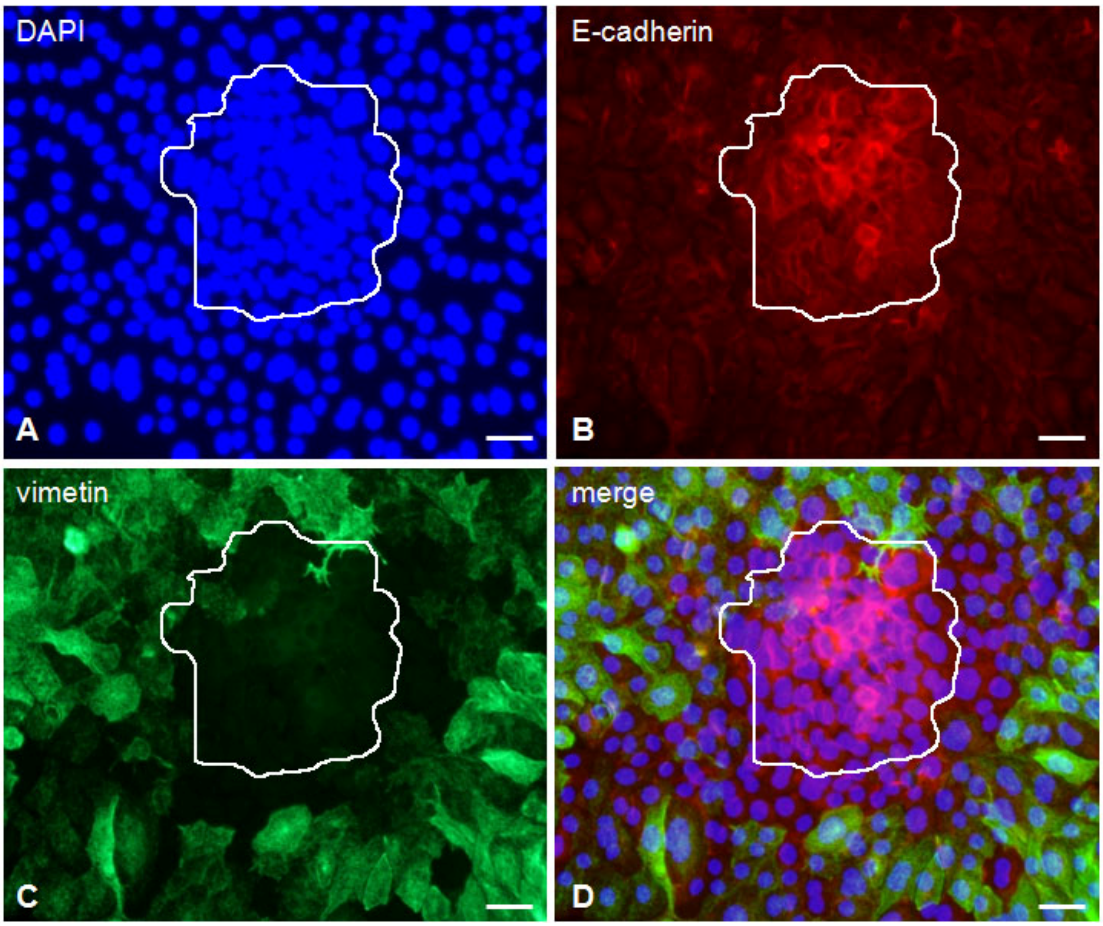

Figure 5.48: Reciprocal E-cadherin and vimentin expression patterns in a concentric CA1 colony. Concentric rings (zones 2 and 3) of the colony are outlined, with the central zone 3 and the peripheral zone 2. Dapi signal (A) reveals a concentric colony with small tightly packed cells in the centre. Immunostaining for E-cadherin (red, B) shows a strong signal in the middle of a colony. Vimentin immunostaining (green, C) reveals a bulk of vimentin negative cells in the centre and strongly positive cells at the periphery of the colony. A merged picture of all three channels shows reciprocal expression of E-cadherin and vimentin (D). Scale bar 50 µm

Expression patterns of stem cell-related and differentiation-related markers in different types of colonies observed in RM+ medium (as previously published by Harper et al. [180]) and in CnT24 medium are summarised in table 5.15.

Table 5.15: Expression of stemness- and differentiation-related markers in head and neck cancer cell lines grown under different culture conditions

Medium	Marker	Cell type	Marker association	Reference
CnT 24	CD44	3	stemness	[82]
	EGFR	3	stemness	[206]
	β-catenin	3 (membrane) 2 (membrane, nuclear)	proliferation, differentiation	[204], [205]
	E-cadherin	3	stemness	[207]
	Vimentin	1	differentiation	[208]
RM+	CD44	holoclone	stemness	[82]
	Integrin β1	holoclone	stemness	[209], [210]
	β-catenin	holoclone (membrane)	stemness	[204], [205]
	Keratin 6	paraclone	differentiation	[180]
	Vimentin	paraclone	differentiation	[180]

Expression patterns of the various marker proteins suggest that the three cell types found in concentric colonies in CnT24 medium (type 1, 2 and 3 cells) correspond to the paraclone, meroclone and holoclone cells present in RM+ medium, respectively. The analogy between zone 3 cells and holoclones, zone 2 cells and meroclones and zone 1 cells and paraclones is backed up by similarities in cell morphology, such as cell size and cell spacing within the colony. In RM+ cultures the progression from holoclones to mero- and then paraclones is associated with increase in cell size and cell spacing and a decrease in the nuclear-to-cytoplasmic ratio. The same changes can be observed in CnT24 medium during progression from type 3 cells to type 2 and type 1 cells. Consequently, type 3 cells appear to represent stem cells, type 2 cells represent transit amplifying cells and type 1 cells correspond to early differentiating cells.

These findings indicate that head and neck cancer cell lines have different colony morphology when cultured in adherent conditions in RM+ medium and CnT24 medium. However, the same three cell types with distinct proliferation and differentiation patterns are present in both media.

5.3.1.2 Non-adherent growth of established head and neck cancer cell lines

In addition to adherent growth on a plastic cell culture dish, some cells in head and neck cancer cell lines are capable of growth in non-adherent culture condition as so called tumour spheres [71]. I examined the sphere-forming ability of established head and neck cancer cell lines in RM+ and CnT24 medium. All three cell lines included in this experiment were able to form spheres when grown in non-adherent conditions on poly-HEMA coated plates in RM+ medium (Figure 5.49). The fraction of sphere-forming cells varied between the cell lines and was highest for H357, intermediate for 5PT and lowest for CA1 (Figure 5.50). Spheres formed by the different cell lines also varied in size with larger spheres being formed by H357 and 5PT and with CA1 spheres being much smaller (Figure 5.49). Interestingly, the size of the sphere-forming fraction in a cell line directly correlated with the size of its EMT fraction.

In CnT24 medium the sphere growth was considerably reduced in all cell lines. A marked decrease in the number of spheres as well as their size was observed for CA1 and 5PT. For both cell lines the size of the sphere-forming fraction was too low to quantify and H357 did not produce any spheres in CnT24 medium (Figure 5.49).

In summary, serum-free low-calcium CnT24 medium proved suitable for culturing established head and neck cancer cell lines in adherent conditions, but did not support their non-adherent growth. In comparison, RM+ medium was found to support adherent and non-adherent growth of established head and neck cancer cell lines.

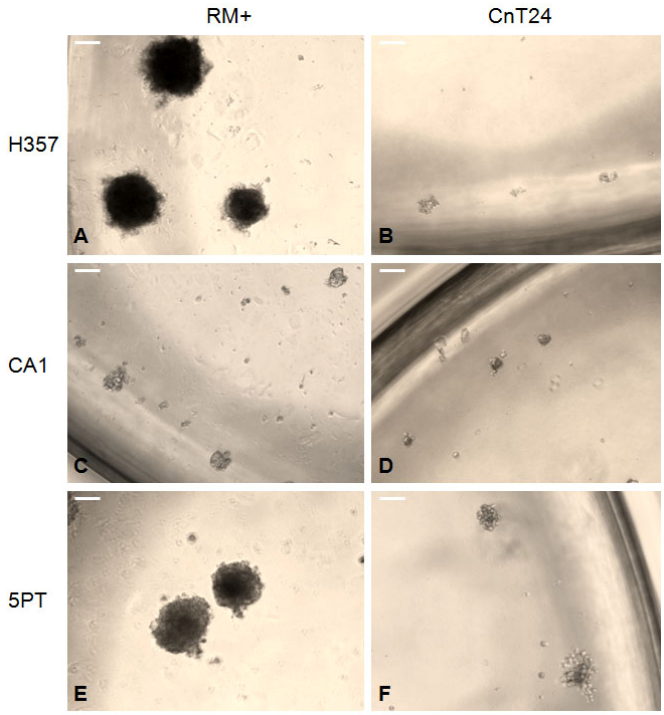

Figure 5.49: Ability of head and neck cancer lines to grow in non-adherent culture conditions as tumour spheres in RM+ and CnT24. Cells were grown on poly-HEMA coated plates in RM+ medium (A, C, E) or CnT24 medium (B, D, F) containing 1% methyl-cellulose. Photographs show spheres 14 days after plating. Lines H357 and 5PT formed large, round spheres in RM+ (A and E), whereas CA1 formed very small irregularly shaped spheres in this medium (C). In CnT24 medium CA1 and 5PT produced very small irregularly shaped spheres (D and F), H357 did not produce any spheres at all (B). Scale bar 100 µm

A

Cell line	Average no of spheres per 1000 cells	% sphere-forming fraction (± SEM)
CA1	16±3	1.6±0.3
5PT	79±8	7.9±0.8
H357	92±7	9.3±0.7

B

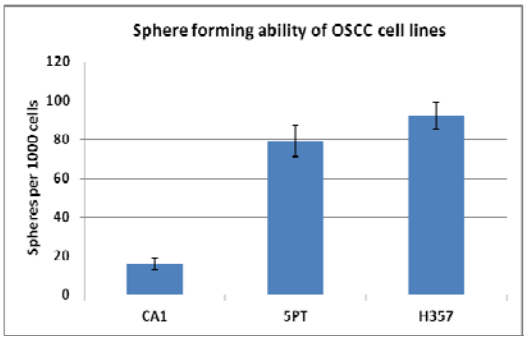

Figure 5.50: Number of spheres formed by CA1, 5PT and H357 in RM+ medium. CA1, 5PT and H357 cells were seeded in poly-HEMA coated 96-well plates at a density 1000 cells per well. Spheres were counted 14 days after plating. The table (A) and the graph (B) show the average number of spheres counted in each well (A).

5.3.1.3 Epithelial to mesenchymal transition under different culture conditions

Another comparison between the two culture media (RM+ and CnT24) was made by examining the EMT cell fraction present in cell lines cultured in RM+ and CnT24. I examined established oral cancer cell lines for the presence of the two distinct cell populations: the epithelial population, which is characterised by the $CD44^{+}ESA^{+}$ FACS phenotype, and the EMT cell population, that can be identified by its $CD44^{high}ESA^{low/-}$ phenotype. Figure 5.51 shows expression of CD44 and ESA and the EMT cell fraction identified by these two markers in the established oral cancer cell line CA1 cultured in RM+ or in CnT24. There was no significant difference in the size of the CD44 expressing and the ESA expressing cell fractions between the RM+ and the CnT24 media (Figure 5.51). The size of the EMT fraction was also similar in RM+ and CnT24 with 6.9% and 7.4% of cells, respectively (Figure 5.51 E, F). However, in the RM+ medium there was a clearer separation between the EMT fraction and the epithelial fraction on the FACS plot. The clearly defined EMT fraction was gated (p9 in Figure 5.51 E) in RM+ medium and the same gate was used to identify the EMT fraction in CnT24. There were no distinctly separate EMT and epithelial cell populations visible on the FACS plot in the CnT24 culture (compare Figure 5.51 E and F).

An early passage tumour-derived cell line was also examined for the expression of CD44 and ESA and the presence of EMT fraction when grown in RM+ or CnT24. No difference was observed in the size of the CD44 expressing fraction with all cells being CD44 positive (Figure 5.52 A, D). The ESA expressing fraction was smaller in CnT24 with 64.4% of cells as compared to 85.9% in RM+ (Figure 5.52 B, E). In both types of cultures there was no distinct EMT cell fraction seen on the FACS plot (Figure 5.52 C, F).

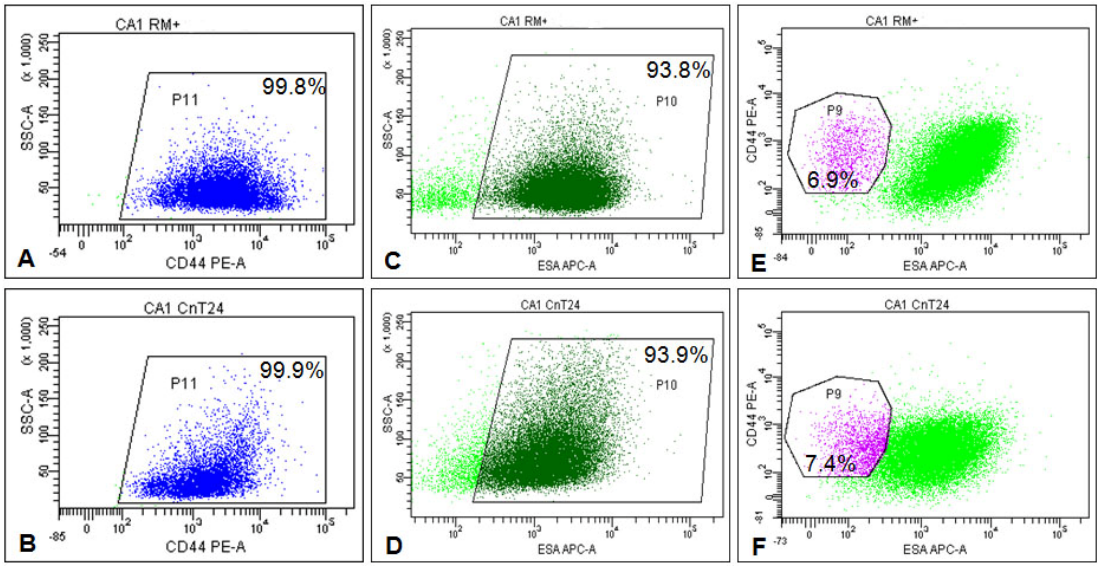

Figure 5.51: Expression of CD44 and ESA in CA1 line cultured in RM+ and CnT24 media. In both media CD44 expression was detected in the vast majority of cells: 99.8% and 99.9% of cells in RM+ and CnT24, respectively (A, B). Size of the ESA expressing fraction was also similar in both media 93.8% and 93.9% in RM+ and CnT24, respectively (C, D). The ESA positive and ESA negative populations were more clearly separated in RM+ medium (compare C and D). The size of the EMT cell fraction (gated in P9 in E and F) was comparable in the two media with 6.9% and 7.4% in RM+ and CnT24 respectively. The EMT cell fraction was more clearly separated from the epithelial fraction in RM+ medium (Compared E and F).

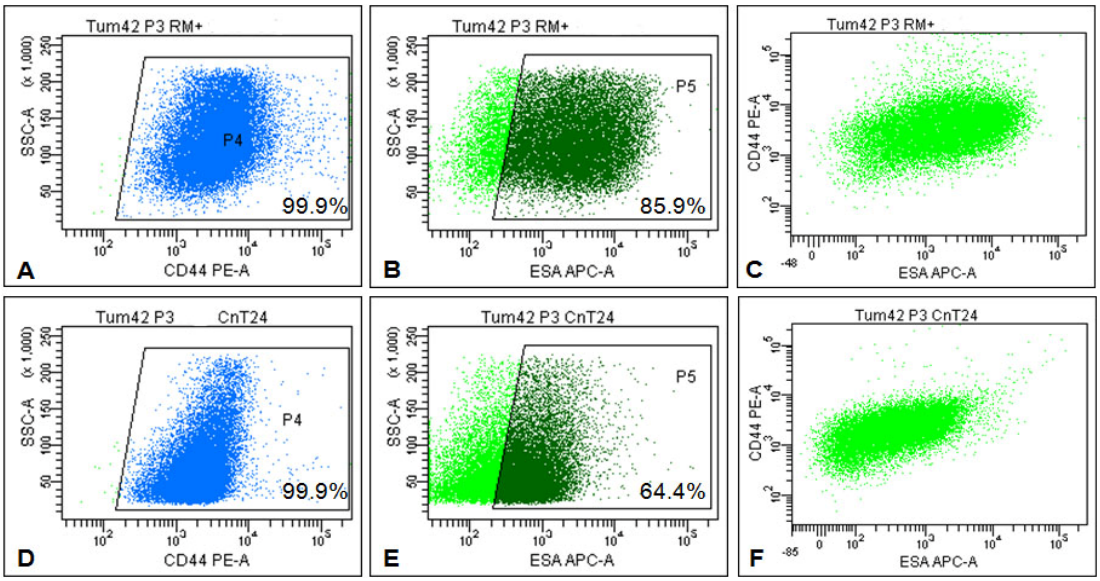

Figure 5.52: Expression of CD44 and ESA in early passage tumour-derived cell line cultured in RM+ and CnT24 media. Tum42 cells, passage 3, grown in RM+ or CnT24 were trypsinised and stained with antibodies against CD44 and ESA. In both media CD44 expression was detected in 99.9% of cells (A, D). 85.9% and 64.4% of cells were positive for ESA in RM+ and CnT24 respectively (B, E). In neither cultures was a distinct EMT fraction was detectable on the CD44 vs. ESA FACS plot (C and F).

In summary, the FACS phenotype of cells cultured in RM+ and in CnT24 did not differ significantly. However, it appeared that the EMT cell fraction could be easier identified by flow cytometry in cell lines grown in RM+.

In conclusion, adherent growth of the established head and neck cancer cell lines was supported by both, the routinely used RM+ medium as well as the serum-free, low-calcium CnT24 medium. In both media there existed a similar hierarchy of epithelial proliferation and differentiation, which included stem cells, amplifying cells and early differentiating cells. For non-adherent growth RM+ medium seemed to be more suitable than CnT24. RM+ medium also proved superior in maintaining a distinct $CD44^{high}ESA^{low/-}$ EMT fraction in established oral cancer cell lines.

I next compared the suitability of the RM+ medium and the CnT24 medium for isolation and cultivation of primary malignant keratinocytes isolated from samples of oral squamous cell carcinoma.

5.3.2 Expansion of tumour cells in cell culture and generation of cell lines

5.3.2.1 Isolation and initial expansion of tumour cells from OSCC samples

I attempted to generate cell lines from the tumour specimens I received from the hospital. There are two techniques that are commonly used to isolate cells from normal oral tissue: the direct explant technique [211] and the enzymatic technique [199] (for a detailed description see section 4.6.2).
I tested both methods for culturing malignant oral keratinocytes. The direct explant method, although widely used for normal epidermal and oral keratinocytes, did not prove successful for malignant keratinocytes. Out of 18 specimens only 4 grew in an explant culture (Figure 5.53). For 2 of the 4 specimens growth arrest occurred after initial expansion and it was not possible to maintain cells in culture for prolonged periods of time. Most specimens grown as explants gave rise to pure fibroblastic cultures. On the contrary, the enzymatic method produced a number of viable cultures.

Dissociated cells from 19 out of 54 specimens grew on irradiated 3T3 feeder cells in RM+ medium. This method allowed viable, fibroblast-free keratinocyte clones to be isolated and propagated in culture (Figure 5.54).

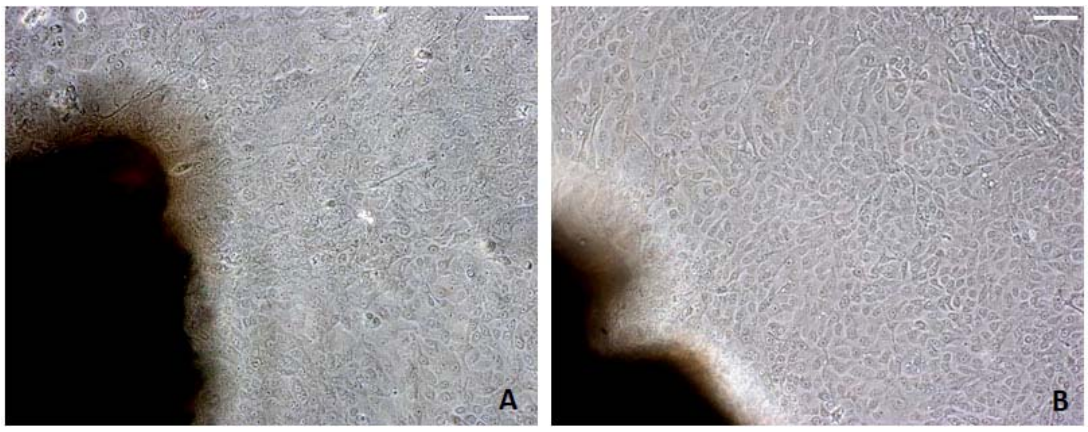

Figure 5.53: Explant cultures from surgical specimens of OSCC. Tissue samples were cut into pieces of 1 mm^3 in size and placed on a plastic culture dish. After the tissue pieces adhered to the dish RM+ medium was added. After 4-10 days keratinocytes outgrowth could be seen around the tissue pieces, which are seen as dark, opaque structures in the bottom left corner (A, B). Scale bars 50 µm

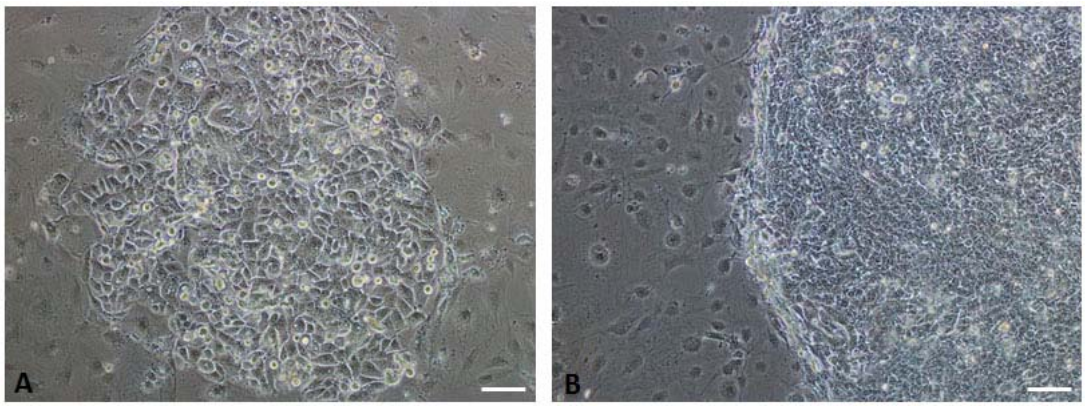

Figure 5.54: Co-cultures of primary keratinocytes isolated from a tumour biopsy with 3T3 feeder cells in RM+. The tumour biopsy was digested with trypsin-EDTA. Isolated tumour cells were plated in RM+ medium together with irradiated 3T3 feeder cells. The figure shows photographs of cell colonies 15 days (A) and 24 days (B) after plating. Scale bar 50 µm (A), 100 µm (B)

The choice of the enzyme(s) for the enzymatic method did not appear to be crucial. Three different dissociation conditions have been tested: trypsin (with or without EDTA), collagenase and the enzyme free buffer. All three

protocols allowed isolation of viable cells that were able to form colonies of keratinocytes when plated together with irradiated 3T3 feeder cells in RM+ medium.

Surprisingly, isolated tumour cells failed to adhere to the culture dish when plated in CnT24 medium straight after their isolation from the tumour tissue. However, after the initial expansion on 3T3 feeder cells in RM+ medium for 2-3 passages, tumour-derived keratinocytes could be switched to the CnT24 medium and propagated in culture without the use of feeder cells for at least 8 passages.

It was also attempted to grow tumour cells in non-adherent conditions as spheres. Cells isolated from tumour tissue were plated on poly-HEMA coated plates in RM+ medium or in CnT24 medium. In RM+ medium, for 2 out of 5 tumour samples, spheres formed within 2 weeks after plating. For the remaining 3 tumours no spheres could be seen. Figure 5.55 shows representative pictures of sphere growth in RM+ medium. There were differences in number and size of the formed spheres between cells isolated from different tumours (Figure 5.55). Similar to observations made with established cell lines (see section 5.3.1.2), sphere formation in CnT24 medium could not be detected for any of the tumours.

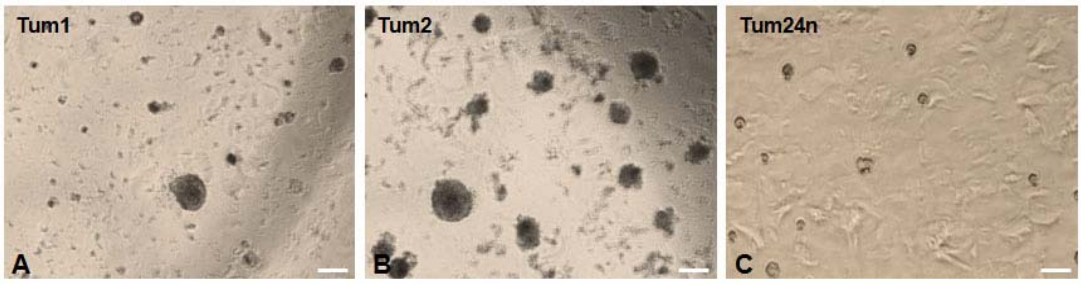

Figure 5.55: Cells isolated form fresh tumour tissue grown as spheres in RM+ medium. Tissue was dissociated with trypsin/collagenase and the isolated cells were plated on poly-HEMA coated plates in RM+ medium. After 2 weeks spheres have formed from cells isolated from tumour specimens tum1 (A) and tum2 (B) but not tum24n (C). Scale bar 50 µm

The sphere formation assay was performed with the total cell suspension isolated from the tumour, which could contain cells of different cell lineages present in the tumour and the tumour stroma. To find out which type(s) of cells gave rise to spheres, spheres were transferred to an uncoated plastic culture dish and grown in RM+ medium. Adherent growth allowed the cell morphology, which is indicative of the cell lineage, to be examined. Within 24 h after plating spheres adhered to the plastic surface and cells forming the spheres switched to adherent growth migrating away from the sphere body (Figure 5.56 A). Eventually, the sphere completely dissolved giving rise to a confluent layer of adherent cells (Figure 5.56 D). In all repetitions of this experiment, including spheres formed by cells isolated from different tumours, cells growing out of spheres had a spindle-shaped morphology strongly resembling fibroblasts (Figure 5.56). Alternatively, the spindle-shaped cells could be epithelial cells that have undergone an epithelial to mesenchymal transition. To reveal their lineage, cells were stained for cytokeratin as an epithelial marker and vimentin as a fibroblastic marker (Figure 5.57). All cells from each examined sphere had high expression levels of vimentin (Figure 5.57 A, C), but were negative for cytokeratin (Figure 5.57 B, D). This suggests that none of the tumour spheres were formed by keratinocytes.

To test whether sphere-forming ability is a feature of cancer associated fibroblasts or all fibroblasts regardless of their association with malignant epithelia, the sphere formation assay was performed with normal skin fibroblasts. Formation of many round spheres of different sizes was observed within 2 weeks after the normal skin fibroblasts were plated on poly-HEMA coated plates in E4 medium (Figure 5.58). These results suggested that malignant as well as normal fibroblasts have the ability to grow in non-adherent conditions as spheres.

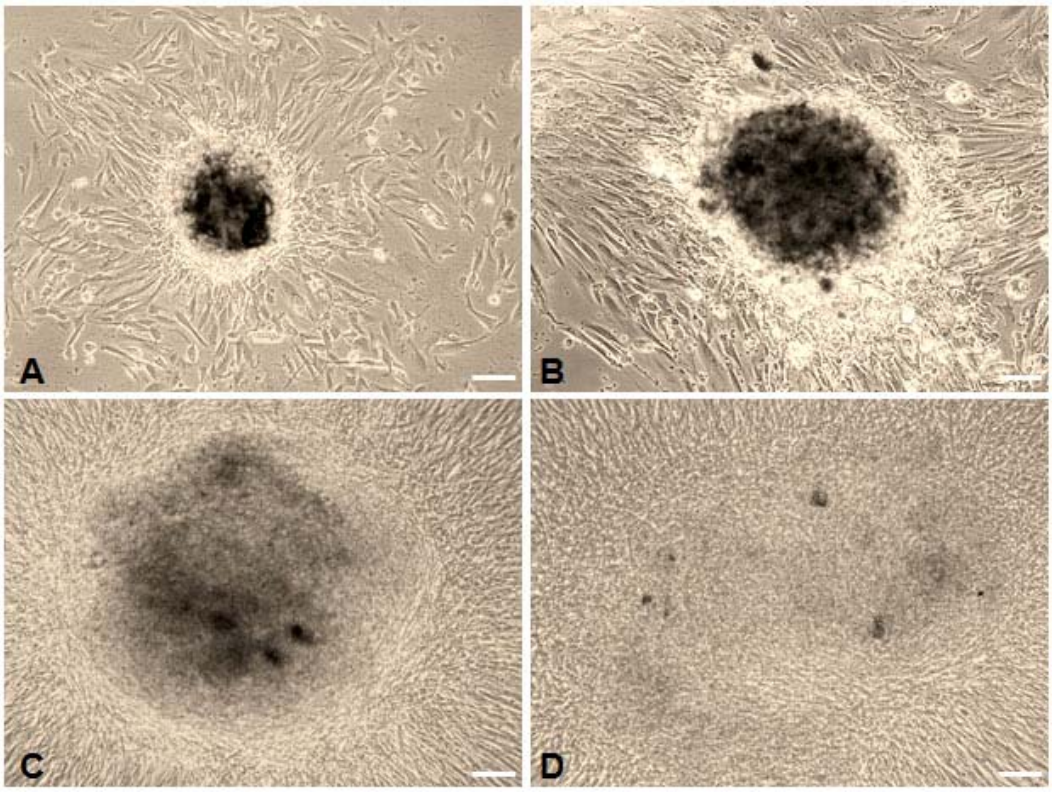

Figure 5.56: Growth of tumour spheres after their transfer to a non-coated culture dish. The spheres were transferred to a non-coated culture dish. 24 h later spheres attached and gave rise to adherent cells with a spindle-shaped morphology (A). Within the next few days in culture more cells adhered and migrated out of the sphere body (B, C) which eventually completely dissolved (D). Scale bar 100 µm (A), 50 µm (B-D)

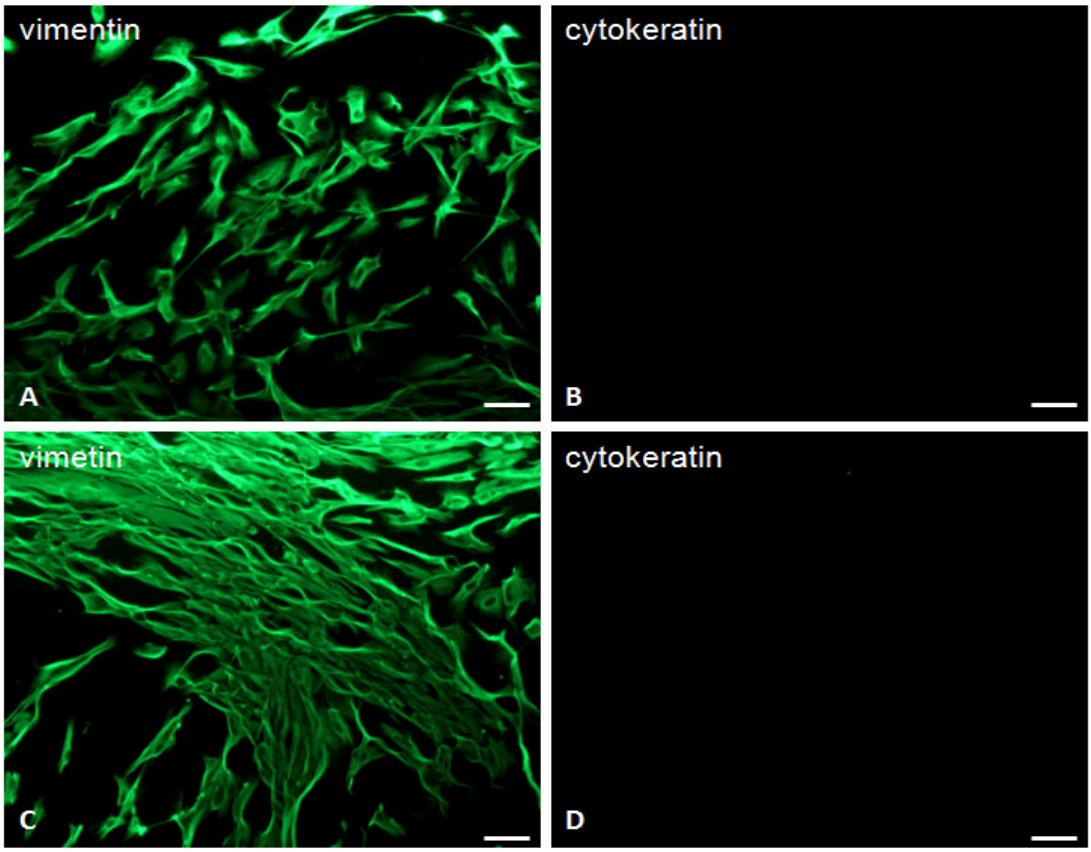

Figure 5.57: Vimentin and cytokeratin expression in cells that grew from spheres in adherent conditions. Cells growing out from spheres formed by tumour cells isolated from two different OSCC samples are shown. In both cultures all cells were positive for vimentin (green) (A, C). No cytokeratin (red) expression was detected in the two cultures (B, D). Scale bar 50 µm

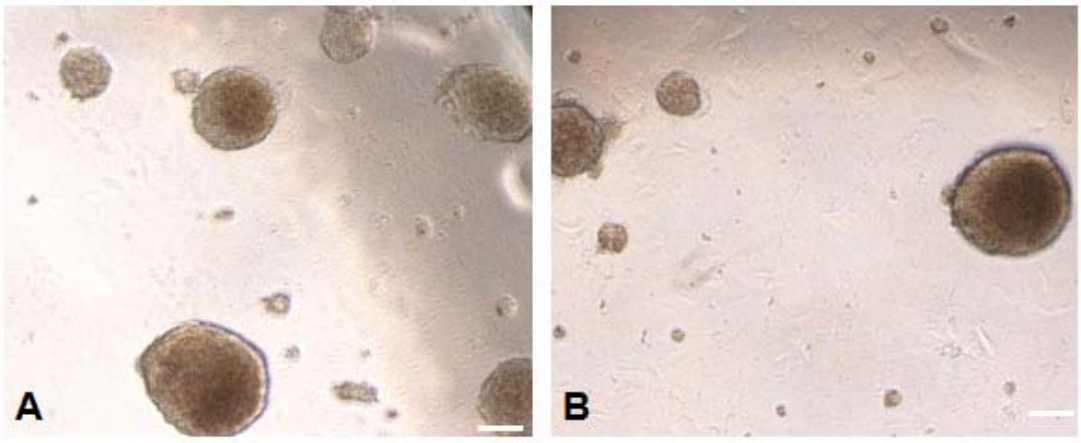

Figure 5.58: Normal skin fibroblasts grown in non-adherent conditions as spheres. Normal skin fibroblasts were plated on poly-HEMA coated plates in E4 medium. Sphere formation was observed within 2 weeks after plating. Many small and large round spheres with a smooth edge were formed (A, B). Cells that didn't form spheres appear as small, slightly transparent dots (A, B).

Based on the observations described above the enzymatic dissociation method followed by cell cultivation in RM+ medium together with non-proliferative 3T3 feeder cells appeared to be the most efficient approach for culturing cells isolated from samples of OSCC.

5.3.2.2 Establishment of long-term cultures

Cells were isolated from surgical specimens of OSCC according to the enzymatic method described above. As described above the initial expansion of these cells was only possible in RM+ medium as a co-culture with non-proliferative 3T3 feeder cells. After 2-3 passages in the initial culture system cells were trypsinised and re-plated either under the same conditions or in CnT24 medium. For a few cultures a feeder-free expansion in RM+ medium has also been attempted.

Differences in cell and colony morphology between the different culture systems became apparent from the first passage. Colonies present in RM+ medium with feeder cells had a round shape and a smooth edge and contained very small, round, tightly packed cells (Figure 5.59 A, B). Colonies in RM+ without feeders were made up of cells with varied morphological features. As well as small, round cells these colonies contained larger, elongated cells (Figure 5.59 C, D). In the CnT24 cultures, cells of different morphologies were also present: small round cells along with larger elongated cells could be seen (Figure 5.59 E, F). Colonies consisting of morphologically different cells arranged in concentric circles could also sometimes be observed in CnT24 (Figure 5.59 F).

Cultures that were switched to the feeder free system in RM+ at the first passage (i.e. after only one round of initial expansion on feeder cells) lost their proliferative capacity and could not be maintained in culture beyond passage 1. The other two systems (RM+ with feeder cells and CnT24) seemed to produce viable cultures that could be propagated in culture for a prolonged period of time. A switch to a feeder free RM+ based system was

attempted at a later stage again and proved successful for nearly all cultures if performed after passage 8-10.

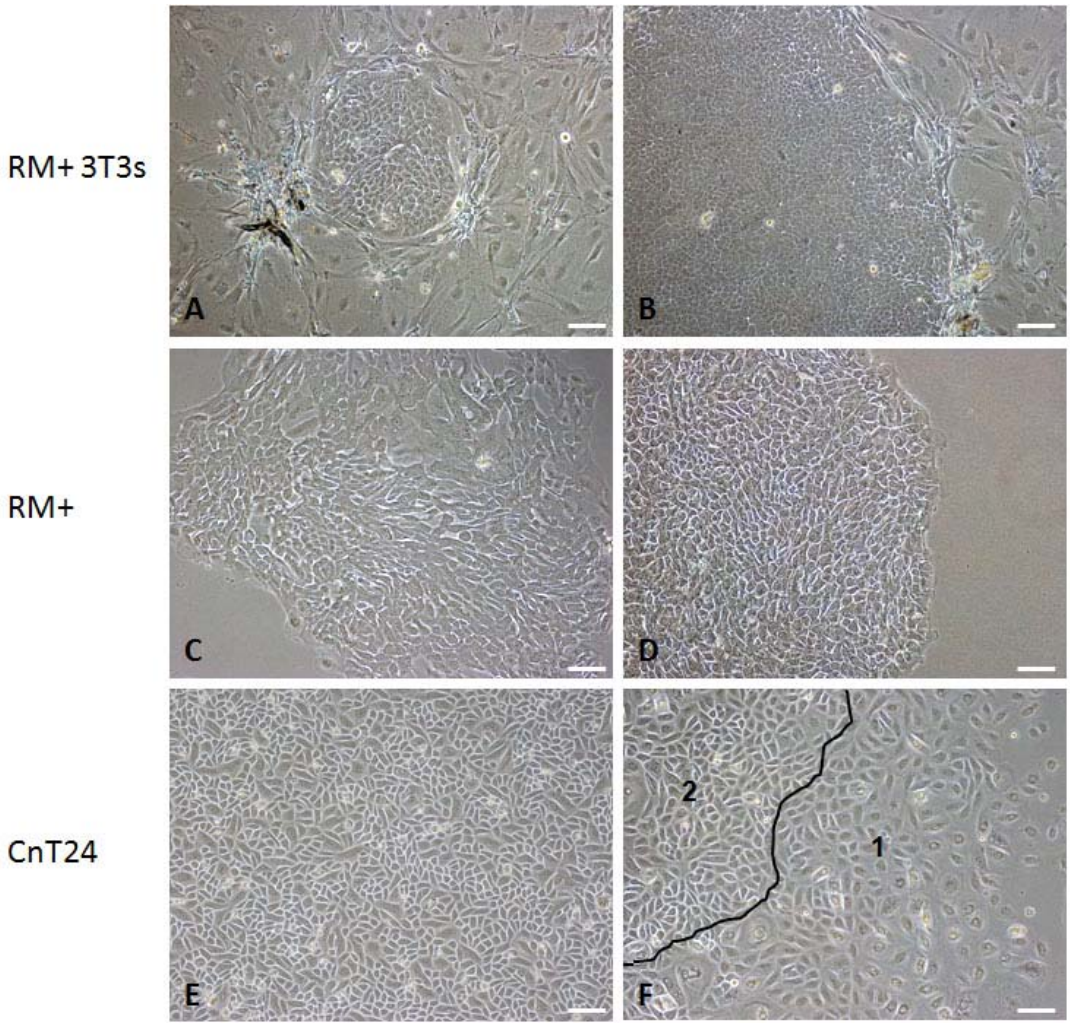

Figure 5.59: Cells isolated from an OSCC sample (Tum30) cultured under different conditions. After initial expansion in RM+ medium with feeders, cells were trypsinised and re-plated in RM+ with or without feeders and in CnT24. All three cultures were photographed a few days after plating. Cells in CnT24 were larger and more loosely spaced than cells in RM+ medium with feeders (compare A, B and E, F). In CnT24 colonies with concentric morphology were present (F). Colonies in RM+ without feeders showed heterogeneous morphology with small and round cells as well as larger elongated cells. Scale bar 50 µm

Based on the findings described above, the enzymatic technique was chosen as a routine method of isolating cells from fresh tumour tissue. RM+ medium was chosen as the standard culture medium. Non-proliferative 3T3 feeder cells were used to support the initiation of keratinocytes cultures up until

passage 7-8. Hereafter, the newly generated cell lines were routinely grown in RM+ without the need of feeder cells.

Using isolation and cultivation techniques described above, cell line generation was attempted with a total of 91 specimens of OSCC and lymph node metastases (Figure 5.60). 19 early cultures were lost due to bacterial or fungal infections, presumably caused by microorganisms present in the patient's mouth. 2 out of 18 specimens gave rise to viable cultures when plated as explants. 19 out of 54 grew when the enzymatic digestion of the tumour tissue was performed, followed by co-culture of the isolated cells with non-proliferative 3T3 feeder cells in RM+ medium. Growing cells isolated from the tumour tissue in non-adherent conditions as spheres in either RM+ or CnT24 did not result in generation of viable epithelial cultures (Figure 5.60).

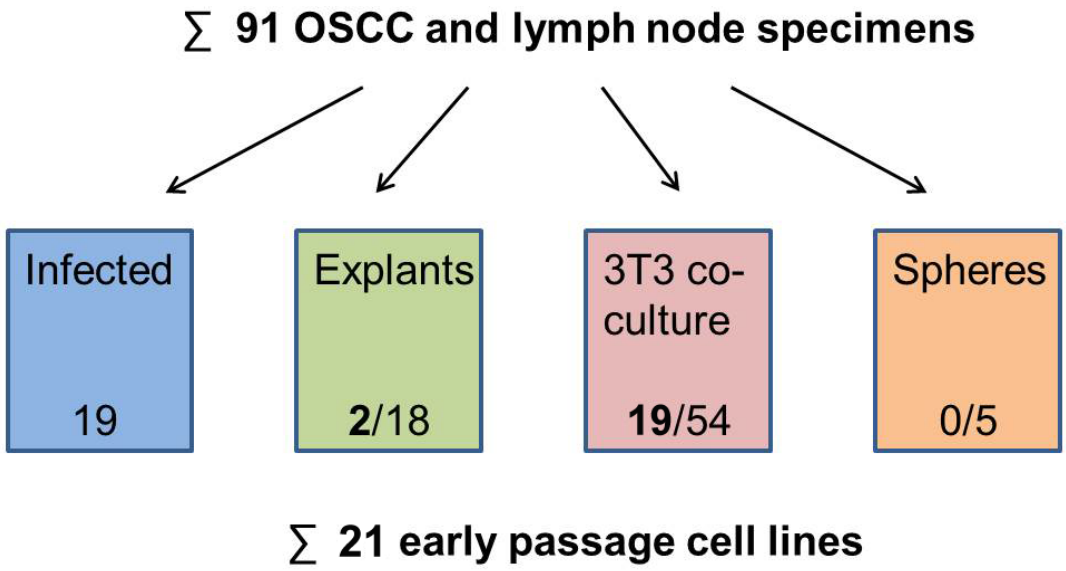

Figure 5.60: Number of cell lines generated from OSCC and lymph node samples with the different techniques used.

5.3.3 Expression of the cancer stem marker CD44 in tumour-derived cell lines

It is now well established that tumours are heterogeneous and consist of different cell populations. It is highly controversial, however, whether cell lines generated from the tumour tissue mirror the heterogeneity of the tumours of origin. Here, I describe data obtained from analysis of malignant cell lines generated from specimens of oral squamous cell carcinoma (OSCC) and lymph node metastases. The available cell lines are compared with each other and also compared with the data obtained from analysis of fresh tumour tissue (see section 5.2).

5.3.3.1 Frequency of CD44 expressing cells in tumour-derived cell lines

Tumour-derived cell lines were analysed for the expression of the cancer stem cell marker CD44. For these assays, the cell lines used had been maintained in culture for 10 or more passages, a point at which cells have acclimatised to culture conditions and show a stable phenotype. All cell lines were cultured under standard cell culture conditions in RM+ medium. Upon reaching 70-80% confluency cells were trypsinised, immunolabelled with an antibody against CD44 and analysed by flow cytometry. A series of FACS experiments with all relevant isotype controls was initially performed (Appendix Figure 1 and Figure 2) and showed no difference between the autofluorescence signal of non-stained control samples and samples stained with the isotype control. Therefore, non-stained control samples were used for all subsequent FACS experiments.

Figure 5.61 shows FACS plots for 3 different tumour-derived cell lines generated from lymph node metastases (cell line 24n), primary metastatic (cell line LM) and primary non-metastatic (cell line NA) oral tumours, respectively (Figure 5.61 A-C). Large fractions of CD44 expressing cells (>90%) were found in all tumour-derived cell lines, including cell lines that had been generated from tumours with a low frequency of $CD44^+$ cells in the

fresh tumour specimen (Table 5.16). For example, tumour specimens PB, LK and NA had low fractions of CD44 expressing cells (5%, 5.4% and 7%, respectively) in the fresh tumour tissue, whereas cell lines derived from these specimens showed 98.6%, 93.6% and 99.8% of cells expressing CD44 (Table 5.16).

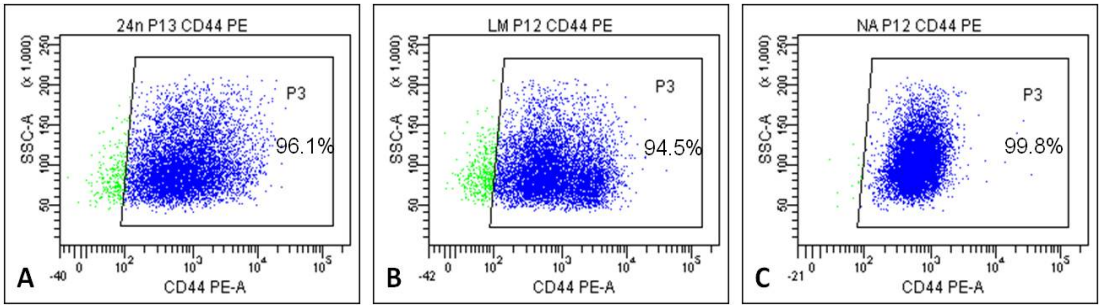

Figure 5.61: CD44 expression in tumour-derived cell lines. FACS plots for three different tumour-derived cell lines are shown (A-C). Gates were set based on the autofluorescence signal from a non-stained control sample. The CD44 expressing cell fraction amounts to 96.1% in cell line 24n (A), 94.5% in cell line LM (B) and 99.8% in cell line NA (C).

Table 5.16: CD44 expression in tumour specimens and cell lines derived from them*

Tum line	% CD44+ in tumour	% CD44+ in cell line
PB	5	97.3
LK	5.4	98.1
NA	7	99.8
42	3	99.8
25	51.7	98.3
30	22.7	98.9
33	NA	96.3
50	10.2	97.9
54	98.6	97.7
57	77.9	94.2
AB	NA	97.6
LM	NA	98.3
NK	34	88.9 (P1)
Luc4	NA	98.2
Luc11	NA	99.7
MKn	21.7	98.1
24n	18.6	97.3
57n	94.7	95.5
NKn	29.8	91.2 (P2)

* Frequency of CD44 expressing cells refers to cell lines that have been passaged for at least 5 passages, unless otherwise stated. “n” (node) annotates cell lines derived from lymph node metastases. NA: not analysed.

There are several possible explanations for the percentage of $CD44^+$ cells isolated fresh tumours not corresponding with the frequency of CD44 expressing cells in cell lines generated from them. It could be, that only the CD44 expressing cell fraction of a tumour is capable of growing and proliferating in cell culture. Alternatively, expression of CD44 could be induced in cells, which were initially CD44 negative, by the components of the culture medium. In the first case, all cells, surviving the transition from the tissue to the culture dish, would initially express CD44, i.e. from passage 0. In contrast, the second possibility would be associated with a gradual increase in the size of the CD44 positive fraction with passaging, at a rate depending on how fast cultured cells adapt to their new environment. CD44 expression was analysed at different passages of several tumour-derived cell lines, three of which are shown in figure 5.62. Initially (e.g. P0 or P2) a very large CD44 positive population was detected by FACS in all three cell lines

(Figure 5.62 A, D and G). There was a slight increase in the size of the CD44 expressing population in the later passages of these lines so that by passage 10 the CD44 expressing cell fraction reached 97.3% in cell line TumPB, 98% in cell line TumLK and 99.5% in cell line Tum50 (Figure 5.62 C, F and I)

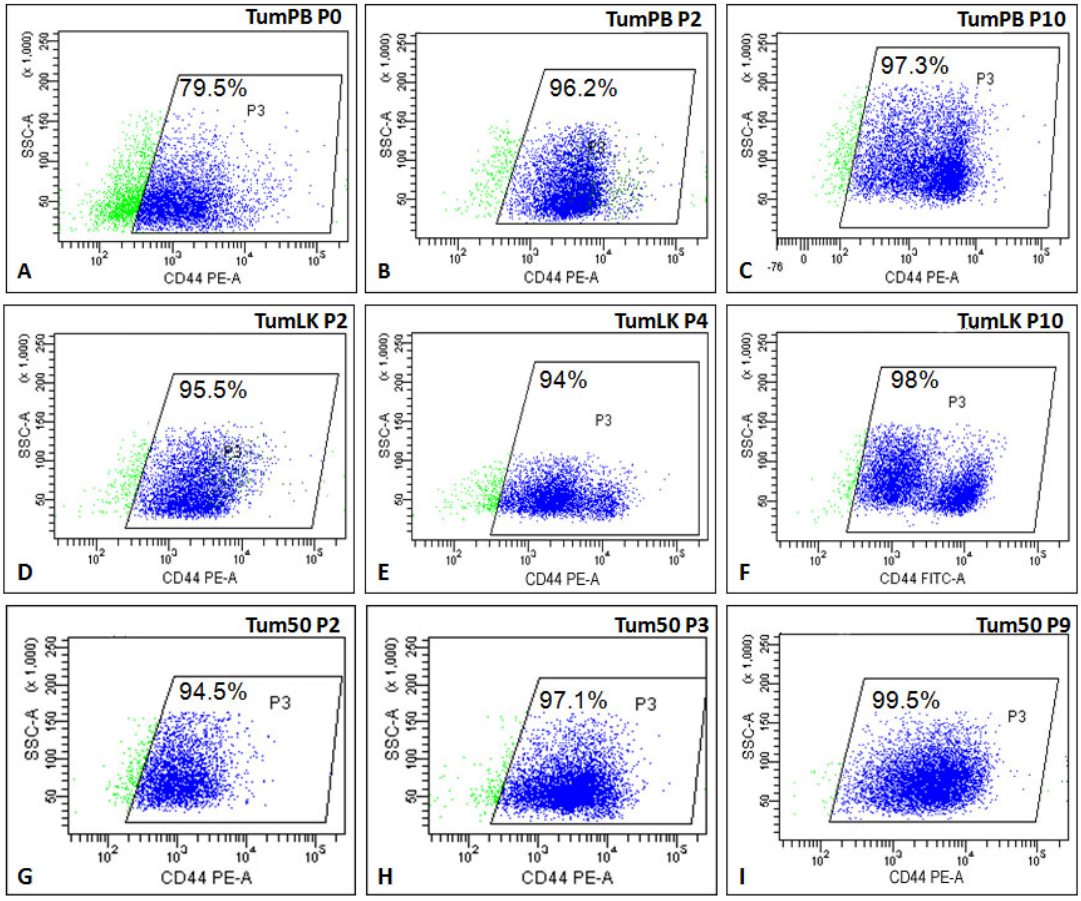

Figure 5.62: CD44 expression in different passages of tumour-derived cell lines. Different passages of tumour-derived cell lines TumPB, TumLK and Tum50 were FACS-analysed for CD44 expression. In cell line TumPB the $CD44^+$ cell fraction increased from 79.5% in passage 0 to 96.2% in passage 2 to 97.3% in passage 10 (A-C). In cell line TumLK 95.5% of cells in passage 2, 94% of cells in passage 4 and 98% of cells in passage 10 stained positively for CD44 (D-F) and in cell lne Tum50 the $CD44^+$ cell fraction increased from 94.5% in passage 2 to 97.1% in passage 3 to 99.5% in passage 9 (G-I).

Because of the large CD44 positive cell fraction in the very early passages, it seems likely, that only CD44 positive cells have the extensive ability to grow and proliferate in culture and that, under these conditions, they produce only a few differentiating cells that are losing their CD44 expression.

In summary, all tumour-derived cell lines were found to have a large fraction of CD44 expressing cells which did not correspond to the frequency of CD44 expressing cells in the tumours of origin and did not correlate to the type of tumour (primary non-metastatic, primary metastatic, lymph node metastasis). A slight increase in the size of the CD44 positive cell population was observed in the later passages of tumour-derived cell lines as compared to earlier passages of the same lines.

5.3.3.2 Expression level of CD44 in early passage tumour-derived cell lines

As well as the frequency of the CD44 expressing cells, the level of CD44 expression was also assessed in tumour-derived cell lines. Analysing cells by flow cytometry, I looked at the median fluorescent intensity (MFI) for the CD44 signal, a value that can be regarded as a measure of CD44 expression level. The MFI value for each sample was taken as a reading from the FACS machine and the ΔMFI was calculated as a difference between the MFI value of the stained sample and the MFI value of the non-stained control. The ΔMFI values detected for various cell lines were then compared.

The median fluorescence intensity for cell surface CD44 found in early passage cell lines generated from metastatic OSCC and from lymph node metastases was considerably higher than for cell lines generated from non-metastatic OSCC specimens (Table 5.17). Cell lines generated from non-metastatic specimens (N0 stage), metastatic primary tumours (N1/2 stage) and from lymph node metastases had average ΔMFI values of 2127.33, 5337.33 and 3977.33, respectively (Table 5.17).

Table 5.17: CD44 median fluorescence intensity (MFI) in early passage tumour-derived cell lines.

Tum line	Passage	TNM	% CD44+ cells	Δ MFI (CD44)	Mean ± STDev Δ MFI (CD44)
LK	**P3**	T2 **N0**	88.7	1613	2127.33 ±451.947
NA	**P3**	T2 **N0**	92.6	2308	
PB	**P2**	T4a **N0**	79.7	2461	
54	**P5**	T1 **N1**	86	3894	5337.33 ± 1284.3
25	**P2**	T2 **N2b**	78.4	5764	
LM	**P5**	T4a **N2b**	91.1	6354	
24n	**P5**	Node	90.3	3531	3977.33 ± 391.881
MKn	**P2**	Node	85.4	4136	
57n	**P4**	Node	87.4	4265	

This difference in CD44 MFI between the cell lines could only be observed in early passage cell lines (passage < 5). At later passages, when the CD44 positive cell fraction increased in size, no distinct difference between the cell lines generated form metastatic and non-metastatic tumours could be detected. At later passages all cell lines showed relatively high MFI value for extracellular CD44.

5.3.4 Epithelial to mesenchymal transition in tumour-derived cell lines

A very important aspect of cancer progression is cancer metastasis. High mortality figures are reported particularly for types of cancer that are highly metastatic. In other words, metastases are usually the reason why cancer is so difficult to treat. Cell lines derived from cancerous tissue might represent suitable models to study cancer metastases allowing the elucidation of mechanistic traits of the metastatic tumour progression. Epithelial-to-mesenchymal-transition (EMT) has been associated with cancer metastasis as the first step of the metastatic process (see also 3.3.3). Therefore, the presence of cells that have undergone EMT (EMT cells) in tumour-derived cell lines could indicate the ability of a given tumour to metastasise.

5.3.4.1 Variable size of the EMT fraction in tumour-derived lines

I analysed 10 tumour-derived cell lines for the presence of EMT cells. All cell lines had been maintained in culture for at least 8 passages and were grown in RM+ medium without feeder cells. Four of these cell lines were generated from primary non-metastatic tumours, three from primary metastatic tumours and the remaining three were derived from lymph node metastases. Four of the primary tumours had a discohesive invasion pattern, three had a cohesive invasion pattern and all three lymph node metastases had extracapsular spread. EMT cells in OSCC lines cells can be identified by flow cytometry by their $CD44^{high}ESA^{low/-}$ phenotype [160].

The size of the EMT fraction varied considerably between individual cell lines. A few tumour-derived cell lines did not have an EMT fraction at all, whereas others contained a very large fraction of EMT cells amounting in one case to 72% (cell line Luc4). Figure 5.63 shows examples of FACS plots depicting the EMT cell fraction and table 5.18 summarises these findings.

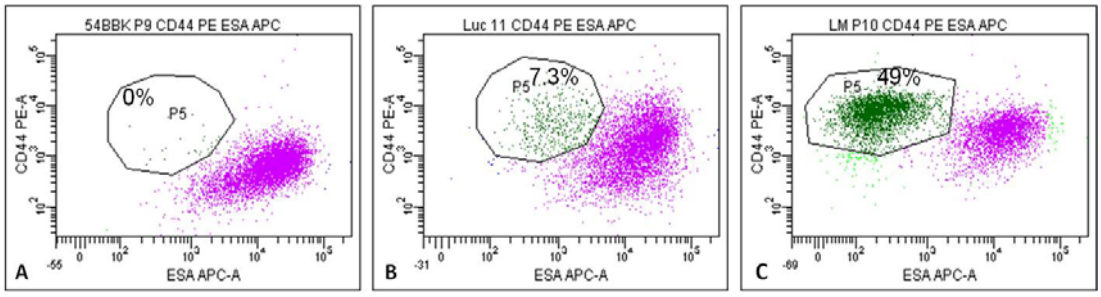

Figure 5.63: Variable size of the EMT cell fraction in tumour-derived cell lines. Cell lines were stained with antibodies against CD44 and ESA and analysed by FACS. In cell line 54 no cells with the $CD44^{high}ESA^{low}$ EMT phenotype were present (A). In cell line Luc11 the EMT fraction formed 7.3% of the total cell population (B) and in cell line LM 49% of all cells were EMT cells (C).

Table 5.18: Highly variable size of the EMT cell fraction in tumour-derived cell lines

Tum line	TNM	Passage	Invasion front	% EMT cells
NA	T2 **N0** Mx	13	discohesive,	0
LK	T2 **N0** Mx	12	discohesive	38
PB	T4a **N0** Mx	10	discohesive	57
Luc11	T2 **N0** Mx	>10	cohesive	9
54BBK	T1 **N1** Mx	9	cohesive	0
LM	T4a **N2b** Mx	10	cohesive	49
Luc4	T3 **N2b** Mx	>10	discohesive	72
57n	node	9	ECS	29
24n	node	14	ECS	36
MKn	node	9	ECS	43

ECS: extracapsular spread

The size of the EMT fraction in tumour-derived cell lines was reflected in their morphological phenotype. Differences in cell size, cell shape and the shape of cell colonies were found (Figure 5.64). The proportion of spindle-shaped fibroblastic-like cells seen on the culture dish corresponded to the size of the EMT cell fraction detected by flow cytometry.

The size of the EMT fraction in tumour-derived cell lines is determined by the ability of the cultured cells to undergo EMT in cell culture. From the observations described above it becomes apparent, that despite being cultured under identical growth conditions, some cell lines are able to undergo EMT to a greater extent than others, resulting in considerable differences in the size of the EMT cell fraction in individual cell lines. These findings imply that there exist intrinsic differences between the tumour-derived cell lines cultured under the standard cell culture conditions.

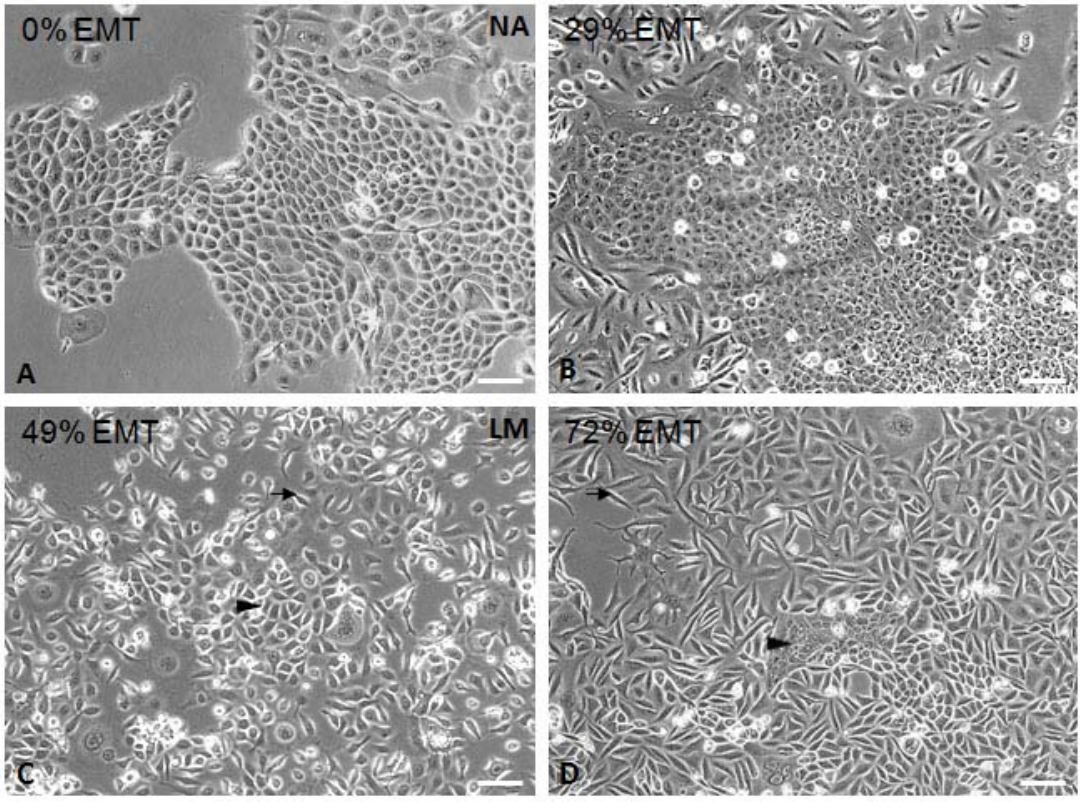

Figure 5.64: Morphological differences of cells in tumour-derived cell lines. Cells of the line NA are oval, medium-sized cells forming irregularly shaped epithelial colonies (A). Cell line 57n contains two types of cells: small round cells that form tightly packed epithelial colonies and larger elongated cells that are loosely spaced or seen as single cells (B). The epithelial colonies in the line LM consist of larger, oval, relatively loosely packed cells (black arrow head), whereas spindle-shaped cells are also seen (black arrow) (C). In Luc4 most of the cells have a spindle-shaped fibroblastic appearance; the few epithelial colonies consist of small, round, closely-packed cells (black arrow head) (D).

5.3.4.2 EMT fraction in correlation to clinical parameters

Our recently published findings indicate that EMT cells are much more migratory than cells with a purely epithelial phenotype [160] and it can be therefore assumed that cell lines with a larger EMT fractions are more migratory than cell lines with a small EMT cell fraction. If the ability of cell lines to migrate is predetermined by the invasiveness of the tumour from which they were generated, then cell lines with the largest EMT fraction would be expected to arise from the most invasive tumours.

I examined a possible correlation between the size of the EMT fraction in cell lines and the nature of the invasion front as well as the spread of the tumour of origin to neck lymph nodes. Against my expectations, there was no obvious correlation between the presence or the size of the EMT fraction in the cell line and the discohesive invasion front or the presence of neck lymph node metastases in the patient (Table 5.18, Figure 5.65). For example, cell line NA from the N0 group and cell line 54 from the N1/2 group were found to have fairly small EMT cell fractions (Figure 5.65 A and C). Furthermore, in both groups there were cell lines containing a very large EMT fraction, e.g., cell line LK (belonging to the N0 group) and line LM (belonging to the N1/2 group) (Figure 5.65 B and D). Similarly, cohesive and discohesive invasion pattern did not correlate to the presence or the size of the EMT cell fraction (Table 5.18).

Interestingly, a large EMT cell fraction was consistently found in all cell lines derived from lymph node metastases. For example, cell lines 24n and 57n contained quite a large, clearly defined EMT cell fraction (Figure 5.65 E and F).

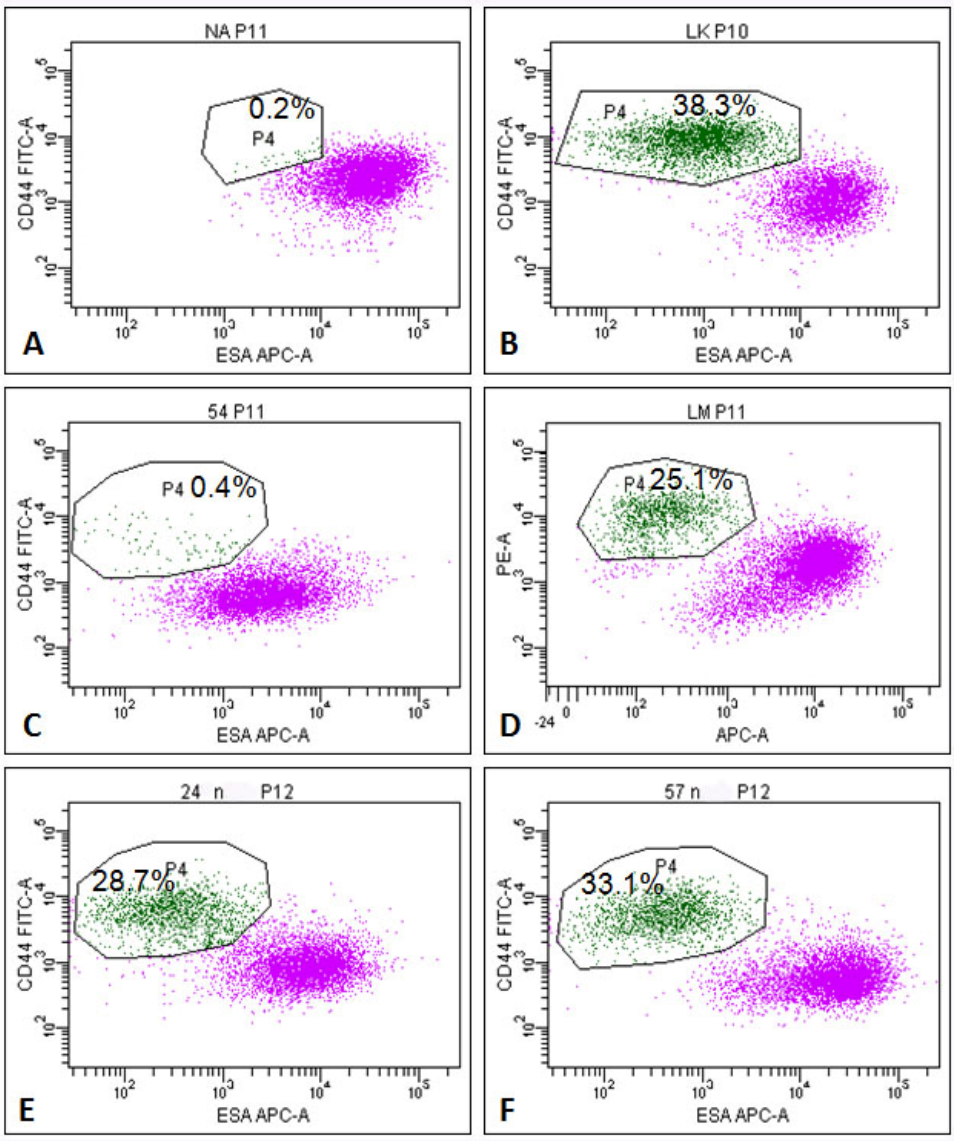

Figure 5.65: Variable size of the EMT fraction in cell lines generated from specimens of primary OSCC and lymph node metastases. Representative FACS plots for cell lines generated from primary non-metastatic tumours (A, B), primary metastatic tumours (C, D) and lymph node metastases (E, F) are shown. Cell line NA and cell line 54 had a very small EMT fraction of 0.2% and 0.4%, respectively (A, C).The EMT cell fraction in cell line LK amounted to 38.3% and in cell line LM to 25.1% of cells (B-D). Both cell lines derived from lymph node metastases (24n and 57n) had a well-defined EMT fraction with 28.7% and 33.1%, respectively (E, F).

5.3.4.3 Changes in the EMT cell fraction with passaging

Next, I tried to establish whether the size of the EMT fraction changes with prolonged passaging. In order to do so, cells from different passages of tumour-derived cell lines were flow analysed for the expression of CD44 and

ESA. An increase in the size of the EMT fraction in later passages in some cell lines but not in others was observed. Figure 5.66 shows FACS plots for three different passages of three tumour-derived cell lines. In the lines LK and PB the EMT fraction ($CD44^{high}ESA^{low/-}$ cells gated in P5) gradually increased over the passages (Figure 5.66 A-C and D-F), whereas in the line NA an EMT fraction did not develop even after14 passages (Figure 5.66 G-I).

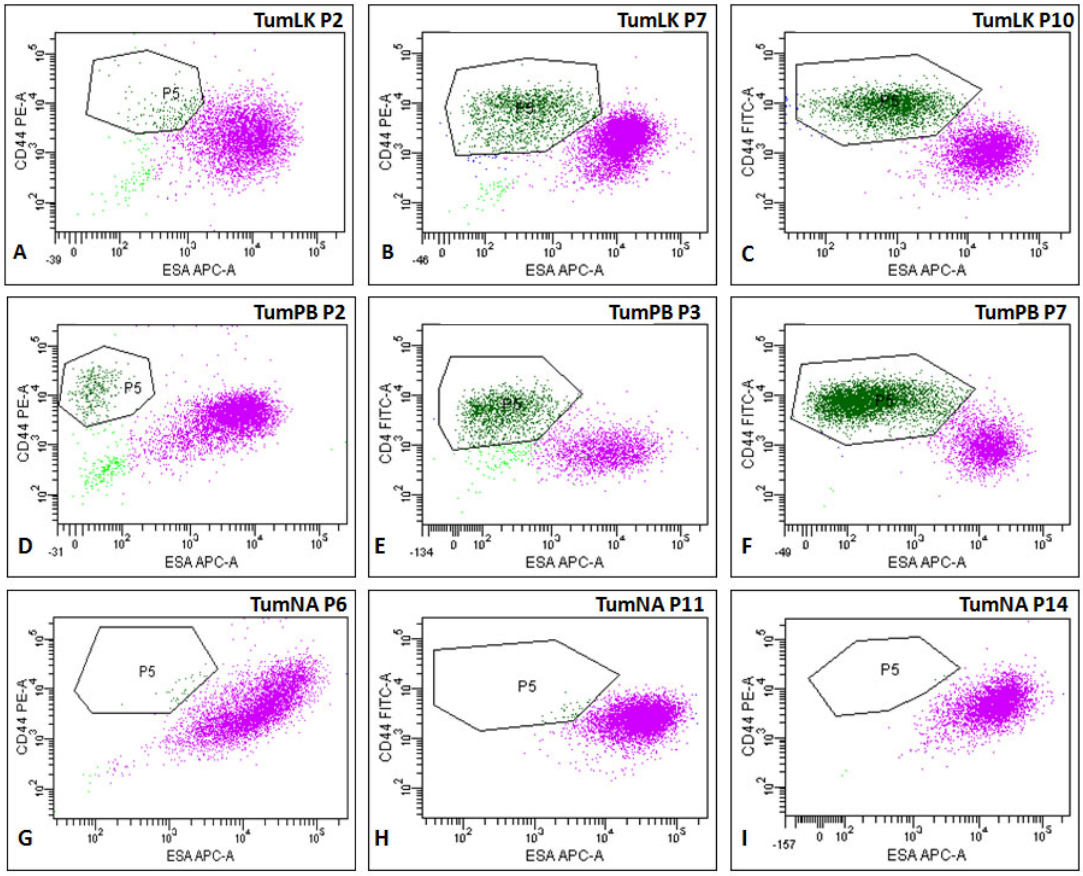

Figure 5.66 Changes in the size of the EMT fraction in tumour-derived cell lines with passaging. FACS plots for three different passages of three tumour-derived cell lines are shown: passage 2, 7 and 10 for the line LK (A-C); passage 2, 3 and 7 for the line PB (D-F) and passage 6, 11 and 14 for the line NA (G-H). The size of the EMT cell fraction (gated in P5) increased from 3.5% to 25.1% to 38.3% in the cell line LK (A-C) and from 4.8% to 25.9% to 60.3% in the cell line PB (D-F), but remained unchanged for the line NA (G-I).

These observations suggest that EMT is induced and/or enhanced in culture, but that some cell lines are not responsive to stimuli imposed by the cell culture and do not develop or increase their EMT cell fraction.

In summary, the size of the EMT cell fraction varied from 0% to 72% between individual tumour-derived cell lines. There seemed to be no correlation between the size of the EMT cell fraction and the TNM stage and the nature of the invasive front of the tumour. However, a large EMT fraction was consistently found in all cell lines generated from lymph node metastases. This observation supports the role of the epithelial to mesenchymal transition in metastatic tumour progression. The size of the EMT fraction changed with passaging for some cell lines but not for others. This and differences in size of the EMT fraction suggest, that tumour-derived cell lines may retain biological and physiological features that are predetermined by the tumour of origin.

5.3.4.4 High levels of cellular CD44 and phosphorylated EGFR in cell lines with a large EMT fraction

To examine the intrinsic differences in tumour-derived cell lines, and more specifically to establish what may account for the considerable differences in size of the EMT cell fraction, I performed a series of western blotting experiments. Protein lysates were isolated from 10 cell lines derived from primary metastatic and primary non-metastatic tumours as well as from lymph node metastases. Levels of cellular CD44 and phosphorylated epidermal growth factor receptor (P-EGFR) were analysed. Expression levels of the total EGFR were also examined. Western blotting revealed that all 10 cell lines had detectable levels of all three proteins (Figure 5.67 A, note that CD44 could also be detected in cell lines 54 and NA after a longer exposure). In cell lines MKn, Luc4, LM, LK and PB a much higher level of P-EGFR was detected as compared to the remaining cell lines. The level of the total EGFR was also higher in these five cell lines, but the difference to the level of the total EGFR in the remaining cell lines was less pronounced. The same five cell lines were found to have very high levels of cellular CD44 (Figure 5.67 A) and a comparatively large EMT cell fraction (Figure 5.67 B). In cell lines where no distinct CD44 band was seen on the blot after a short exposure time (cell line 54 and cell line NA), no EMT cells could be detected by FACS

(Figure 5.67 A and B). These observations suggest a role of CD44 and EGFR in the process of EMT.

A

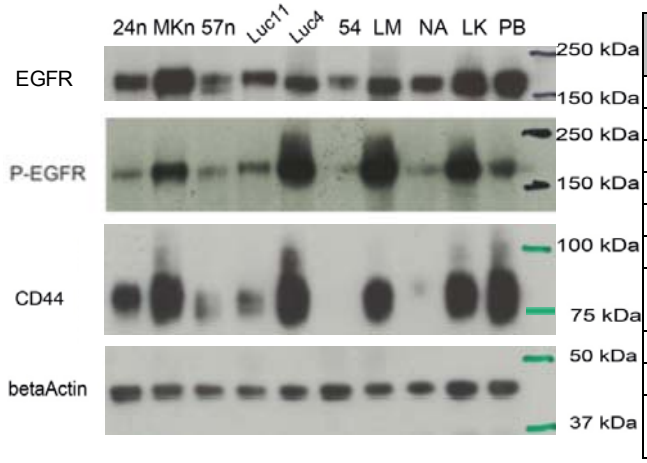

B

Tum	TNM	Pass	% EMT cells
24n	Node	14	36
MKn	Node	9	43
57n	Node	9	29
Luc11	T2 N0	>10	9
Luc4	T3 N2	>10	82
54	T1 N1	9	0
LM	T4a N2	10	49
NA	T2 N0	13	0
LK	T2 N0	12	38
PB	T4a N0	10	57

Figure 5.67: Western blot analysis for EGFR, P-EGFR and CD44 levels in tumour-derived cell lines. (A) Western blotting was performed on protein lysates isolated from 10 tumour-derived cell lines. Strong signal for total EGFR, P-EGFR and CD44 was seen in the lines MKn, Luc4, LM, LK and PB. Apart from the standard CD44 isoform (80-90kDa) these five cell lines also contained detectable amounts of larger variant CD44 isoforms, seen as a smear. (B) In the same five cell lines a large EMT cell fraction was present as detected by FACS.

CD44 glycoproteins vary in size due to extensive post-translational modification (N- and O-glycosylation in the extracellular domains) and to alternative splicing. The estimated molecular mass of the smallest isoform known as the standard isoform (CD44s) is 80-90 kDa [212]. The human CD44 gene contains at least 10 exons that can be alternatively spliced to generate multiple variant CD44 isoforms with a molecular mass of up to 250 kDa [212] [145].

Apart from the prominent signal for the standard CD44 isoform, cell lines MKn, Luc4, LM, LK and PB also contained a number of variant CD44 isoforms, seen as a smear (Figure 5.67 A). The differences in the detected levels of EGFR, P-EGFR and CD44 present another finding that suggests that individual tumour-derived cell lines, even when grown under identical cell

culture conditions, express distinct biological and physiological characteristics.

5.3.5 Discussion

5.3.5.1 Generation of malignant cell lines

This section addressed several technical aspects related to the process of generating cell lines from surgical specimens of oral squamous cell carcinoma and their associated lymph node metastases. Two different methods of isolating cells from tumour samples were tested and two different culture media were assessed for their suitability for culturing primary keratinocytes isolated from the tumour tissue. The enzymatic dissociation technique followed by cultivating isolated tumour cells in RM+ medium as a co-culture with non-proliferative 3T3 feeder cells achieved the highest success rate in generating stable cell lines (Figure 5.60).

As well as different culture media, different growth conditions (i.e. adherent and non-adherent growth) were tested. Attempts to expand epithelial cells isolated from patient tissues in non-adherent conditions were unsuccessful, although this has been reported by others [213]. It could be that the proportion of sphere-forming keratinocytes was so low that it was technically difficult to detect this cell fraction when performing a sphere formation assay using the total cell suspension isolated from the tumour. Enrichment of epithelial cells could possibly facilitate detection of the sphere-forming keratinocyte fraction. Purification of the epithelial fraction of the tumour was attempted through either excluding cells of all other cell lineages by flow sorting using antibodies against lineage markers (negative selection) or selecting epithelial cells using epithelial-specific antibodies (positive selection). Unfortunately, all efforts to recover epithelial cells after the sort were unsuccessful. Despite the lowest flow rate settings on the FACS sorter and the minimal time cells spent in the collection tube before being transferred into a pre-warmed medium (for adherent or non-adherent

growth), the isolated tumour cells never seemed to survive the sorting procedure.

In total, cell line generation was attempted from 91 tumour specimens that were received from the Royal London Hospital and the St Bartholomew's Hospital in course of the study (Figure 5.60). 19 out of 91 early cultures, corresponding to 21%, were lost at the initial expansion stage due to bacterial and/or fungal infections. These infections were presumably caused by microorganisms present in the patients' mouths. Despite multiple rounds of thorough washing of the tumour tissue with PBS prior to cell isolation, microorganisms were sometimes carried over to the culture dish where they infected the entire culture. Addition of antibiotic and antimycotic drugs to the culture medium in order to prevent bacterial and fungal contamination seemed only to delay the onset of infection and the subsequent culture loss.

The success rate of generating cell lines from tumour tissue could possibly be improved by using other methods of isolating and cultivating primary keratinocytes, for example, growing cells isolated from the tumour as organotypic cultures [214]. In the organotypic gel culture system tumour cells are plated on a synthetic stroma composed of a collagen gel and fibroblasts, creating an environment similar to the natural environment of the tumour in the patient's body. This method might improve cell survival during the transition from human tissue to the culture dish.

5.3.5.2 CD44 expression in tumour-derived cell lines

A very large $CD44^+$ cell fraction (>90%) was detected in all passages of all cell lines generated from samples of OSCC and associated lymph node metastases. A slight increase occurred during early passaging bringing the $CD44^+$ fraction to over 95% by passage 3-4. In all cell lines the frequency of CD44 expressing cells was markedly higher than the frequency of $CD44^+$ cells in the tumour tissue the cell lines had been derived from (Table 5.16). Interestingly, cultured keratinocytes isolated from normal oral mucosa also contained a very large fraction of CD44 expressing cells (Figure 5.68).

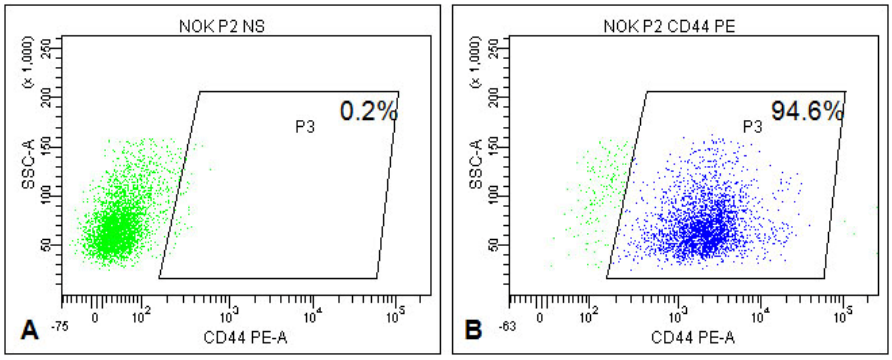

Figure 5.68: CD44 expression patterns in normal oral keratinocyes. Normal oral keratinocytes (passage 2) were trypsinised and stained with a PE-conjugated antibody against CD44. The gate (P3) was set based on autofluorescence of the non-stained control sample (A). CD44 expression was detected on 94.6% of cells in the stained sample (B).

In the normal oral mucosa, CD44 expression was observed to be restricted to the basal and the epi/para-basal layers of the epithelium (Figure 5.69 A, B) where the undifferentiated stem and amplifying cells are located (see section 3.1). Figure 5.69 shows the pattern of CD44 expression detected in paraffin-embedded sections of tumour-adjacent normal tissue (A, B) and of an OSCC of the floor of mouth and the ventral tongue (C, D). In malignant epithelium CD44 expression was not restricted to the basal and para-basal layers, but was also present in cells of the supra-basal layers of the epithelium (Figure 5.69 C, D).

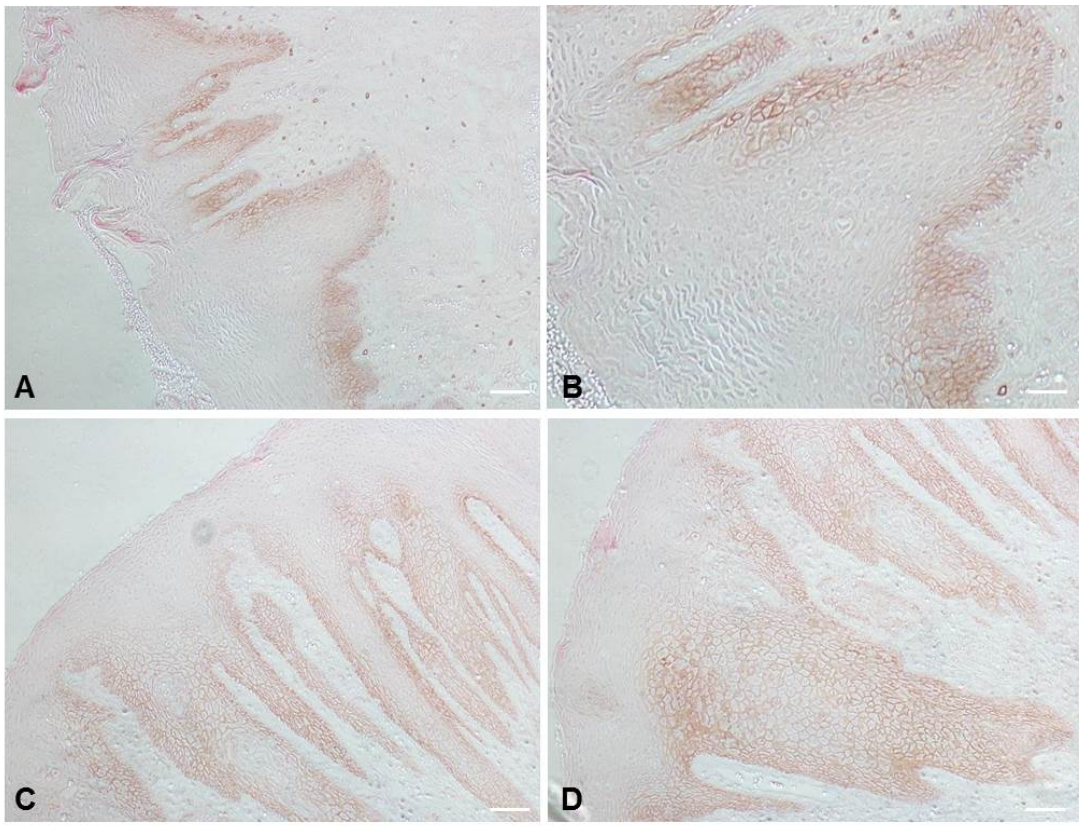

Figure 5.69: CD44 expression in normal and malignant epithelium of the floor of mouth/ventral tongue. Cross-sections through the tumour-adjacent normal epithelium (A, B) and OSCC of floor of mouth/ventral tongue (C, D) were stained with an antibody against CD44 using the DAB detection kit. In the normal epithelium CD44 (brown) is only present on the surface of cells in the basal and the para-basal layers, at the edge of the epithelial ridges (A, B). In malignant epithelium CD44 expression is also present in the suprabasal layers of the epithelium (C, D). Scale bar 100 µm (A, C), 50 µm (B, D)

In the hierarchical model postulated for continuously regenerating epithelia, such as the oral mucosa, the epithelium consists of a series of clonal units with each unit representing the progeny of a single stem cell (Figure 5.70 A) [215] [216] [217]. There are three types of cells in each clonal unit, stem cells, amplifying cells and post-mitotic terminally differentiating cells that are separated by two transitions (Figure 5.70 A, dotted lines). In normal homeostasis each stem cell division usually generates one stem cell and one amplifying cell which undergoes a series of further divisions and eventually produces terminally differentiating cells [218]. The first transition (T1) controls stem cell homeostasis; lack of T1 would lead to augmentation of stem cells and increased transition would lead to stem cell loss [218]. The T2 transition

determines the number of differentiated cells generated per stem cell division. Loss or gain of amplification rounds before T2 would result in decrease or increase in the total number of cells produced [218]. In mouse epidermis the stem cell fraction has been estimated to be 1 in 10 to 1 in 30 of basal cells [219]. The CD44 expression levels are high in stem cells and decrease with differentiation (Figure 5.69). In culture, it appears that only stem cells and less differentiated $CD44^{+}$ cells are present and that senescence or cell death occur before cells reach a terminally differentiated state where they lose their CD44 expression. The balance between stem cells and differentiating cells appears to be shifted with a greater proportion of stem and immature amplifying cells and with fewer early and late differentiating cells being present per total number of cells (Figure 5.70 B). Presumably this shift occurs due to the increased number of symmetric divisions by stem and amplifying cells and a reduced rate of terminal differentiation *in vitro*.

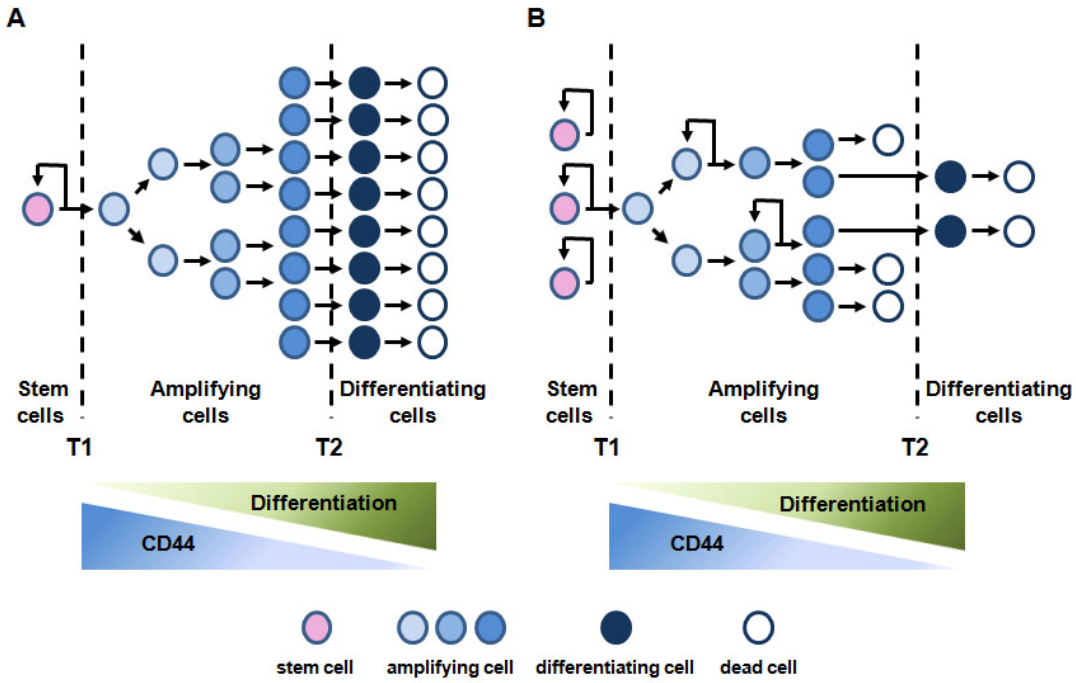

Figure 5.70: A model of hierarchical cell renewal in normal epithelia *in vivo* and *in vitro*. (**A**) In normal homeostasis *in vivo* each stem cell divides assymmetrically giving rise to one stem cell and one other cell that goes through the T1 transition point and enters a differentiation programme. This amplifying cell undergoes a series of divisions and finally crosses another transition point T2 to terminally differentiate and eventually die. (**B**) In cell culture the balance is shifted towards stem and amplifying cells through increased number of their symmetric divisions. The majority of cells does not undergo terminal differentiation but die before reaching the T2 transition point. In both systems CD44 expression is high in stem cells and decreases with differentiation.

Similar to normal oral mucosa, as well as to other types of cancers, OSCC tumours have a distinct hierarchy of cells. There is only a small sub-population of cells that can initiate new tumour growth [82]. The bulk of tumour consists of rapidly dividing cells and post-mitotic differentiated cells which arise through differentiation of CSCs and do not possess a tumour-initiating ability. It has been demonstrated through xenograft transplantation experiments that the immature tumourigenic cells of the tumour express CD44, whereas the differentiating, non-tumourigenic cells do not [82]. $CD44^-$ cells although abundantly present in the tumour tissue as detected by flow cytometry and immunohistochemistry are not present in later passages of cell lines generated from the tissue. Similarly to normal oral keratinocyte cultures, there appears to be a shift towards the immature, undifferentiated cells in

cultures of malignant keratinocytes compared to the hierarchical organisation of cells in the tissue.

Concomitant with the increase in the $CD44^+$ fraction during early passaging, the $CD44^-$ fraction decreases and almost completely disappears in later passages (Figure 5.62). This suggests that some $CD44^-$ cells in the tumour tissue are able to survive the transition from the tissue to the culture dish and to undergo a limited number of cell divisions. These cells are present in culture during the first few passages. However, when these cells further differentiate and die they are not replenished from the pool of amplifying/early differentiating cells as it would be the case *in vivo*, presumably because culture conditions do not allow the cells to fully differentiate *in vitro*.

Interestingly, some authors observed abundant expression of CD44 in the great majority of cells in normal and malignant head and neck tissues reporting that on average two thirds of the thickness of normal mucosa samples were positive for CD44 as detected by immunohistochemistry [220]. Other studies found decreased levels of CD44 in cell lines as compared to head and neck cancer tissues [221]. Both observations contradict the findings of the present study. This is probably due to inclusion of other head and neck squamous cell carcinoma samples such as oro-pharyngeal cancers, which are known to behave differently from oral cancers. [222].

In summary, cells isolated from normal or malignant oral epithelium can be maintained in cell culture for prolonged periods of time. Standard cell culture conditions seem to enrich for cells with phenotype of stem cells and of immature amplifying cells, both of which express CD44. *In vitro* terminal differentiation of keratinocytes occurs at a much reduced rate resulting in very small numbers of $CD44^-$ cells present in cell lines.

5.3.5.3 Changes in tumour-derived cell lines during prolonged passaging

Early and later passages of tumour-derived cell lines were compared with regard to the size of their $CD44^+$ cell fraction and the size of the EMT cell

fraction. In all lines an increase of the CD44 expressing cell fraction was observed with passaging. The $CD44^+$ cell fraction increased from around 80% at passage 0 to over 95% in all cell lines analysed at passage 10 (Figure 5.62, Table 5.16). An increase of the EMT fraction with passaging was also seen in the majority of cell lines with exception of lines where no EMT cells were present at the start of the culture (Figure 5.66). Both $CD44^+$ and EMT cell fractions stabilised by passage 8-10 and no further changes occurred beyond this point.

The changes that occurred in cells under culture conditions facilitated the development of feeder-independent cell lines. Tumour-derived cell lines were not able to grow without feeder cells during the early passages but acquired this ability by passage 8-10. After passage 10 cells appeared to have completely acclimatised to the culture conditions becoming feeder-independent and showing a stable phenotype.

The differences in the median fluorescent intensity (MFI) for CD44 between cell lines derived from primary metastatic tumours, non-metastatic tumours and lymph node metastases were only detected in early passages and were not seen in the later passages of the same lines. In the early passages the MFI values were higher for cell lines generated from primary metastatic tumours and lymph node metastases as compared to lines generated from primary non-metastatic tumours.

The observations described above indicate that cells change when maintained in culture for long periods of time. However, different cell lines cultured under the same conditions remain different in some aspects such as the presence/size of the EMT fraction and the levels of intracellular CD44 as detected by western blotting (Figure 5.67). These distinctive features are probably indicative of genetic and/or epigenetic characteristics of fresh tumour cells the cell lines have been generated from.

6. General Discussion

Recognition of cancer stem cells has changed our understanding of cancer progression and spread, opening up new avenues to improving cancer diagnostics and treatment. Analysis of cancer stem cells requires their accurate identification and it is surprising that this topic has not received more attention.

Here I showed that the isolation technique used for analysis of epithelial cancers can be improved by performing positive selection with epithelial-specific antibodies instead of the commonly used negative selection with lineage markers. Negative selection was used in identification of CSCs in a number of solid malignancies including cancers of the bladder [75], breast [76], colon [80], liver [83], pancreas [86] and head and neck [82]. These studies identified CSCs based on their ability to give rise to tumours in immunocompromised mice and postulated the surface phenotype of these cells as the CSCs phenotype for the particular type of cancer. However, these findings need to be interpreted carefully, as the flow sorted cell fractions that were isolated from tumours and injected into mice might have contained stromal cells, that may influence the tumour-initiating ability of cancer cells [223].

The new method described here (positive selection) is more accurate, bringing the purity of the epithelial cell fraction to 85% (as compared to 65% achieved by the negative selection), but still needs further improvement in order to accurately identify/isolate the entire epithelial fraction of the tumour. Inclusion of more epithelial-specific antibodies would possibly lead to binding of different antibodies to every epithelial cell and would therefore increase the signal intensity of labelled cells detected by flow cytometry. This would result in a clearer separation of labelled (epithelial) and non-labelled (non-epithelial) cells and improve the purity of sorted cell fractions.

In this study both selection methods were used to examine the proportion of the $CD44^+$ cell fraction in fresh OSCC specimens. It is unclear to which extent the imperfectness of the selection methods affected the data

presented in this work. There was no statistically significant correlation between the size of the $CD44^+$ cell fraction in the tumour sample and the selection method used. Furthermore, correlations observed with the combined data set were also observed when samples examined by positive or negative selection were analysed separately. This suggests that the selection method did not bias the size of the CD44 expressing cell fraction detected in cell suspensions isolated from tumour specimens.

The present study linked high frequency of CD44 expressing cells in OSCC tumours to aggressive tumour features, such as discohesive invasion front, high tumour grade and presence of lymph node metastases. These findings, in particular the association with the presence of metastatic lymph nodes, could be clinically relevant and could present a useful tool in the diagnosis of metastatic deposits in the neck lymph nodes. Up to 95% of metastatic lymph nodes can be diagnosed prior to surgery by both clinical examination and imaging techniques such as ultrasonography (US), computed tomography (CT), magnetic resonance (MR), positron emission tomography (PET) [224]. However, it was reported that in up to 50% of lymph nodes, clinically diagnosed as negative, micrometastases were found in OSCC patients undergoing a neck dissection [224]. At present, no clinical tests, imaging techniques or biological markers are available to diagnose nodal micrometastases. Molecular markers such as CD44, which I found to be expressed by a larger proportion of cells in metastatic primary tumours compared to non-metastatic primary tumours, could be used to predict the risk of lymph nodes involvement and help make informed decisions about the necessity of a neck dissection.

Association of CD44 with aggressiveness of HNSCC tumours has also been described by others. Joshua and co-workers reported that HNSCC tumours containing a high proportion of CD44 expressing cells had an advanced T stage, higher xenograft implantation efficiency and were more likely to recur [190], confirming a role for CD44 in cancer progression. A study by Wang found expression of variant CD44 isoforms to be associated with advanced T stage, regional and distant metastases, radiation failure and shorter disease-

free survival [183]. In larynx cancer expression of CD44 variant isoforms correlated with local recurrence after radiotherapy [119].

Stem cell properties such as self-renewal are extremely difficult to study in vivo. Therefore, since the discovery of CSCs in tumour tissue, many studies have aimed to develop cancer cell lines and to validate their use to study cellular and molecular characteristics of these cells. A cell fraction with characteristics of CSCs has been described in cell lines generated from many different cancers including breast [225] [226], head and neck [227] and prostate [228] [229]. These studies identified populations of cells in cancer cell lines that possess the defining properties of malignant stem cells including self-renewal, expression of stem cell-related markers and tumour initiation ability upon xenograft transplantation. Furthermore, mutations similar to those discovered in primary HNSCC tumours (such as mutations in TP53) were found in HNSCC cell lines, suggesting that CSCs present in culture very closely mirror the CSCs found in tumour tissue [230].

However, whether or not stem cells persist in cell lines derived from tumour tissue has also been questioned and some investigators point out that therapeutically relevant information derived from cell lines has to be interpreted with caution [231]. It has been suggested that the cellular diversity observed in cancer cell lines was due to genetic instability [232]. This, and the uncertainty about the effects of cell adaptation to *in vitro* conditions [233] led to doubts about the value of cell lines for studies of cancer stem cell properties [231].

Present work supports the notion that tumour cells change in culture. For example, I found that the proportion of $CD44^+$ cells increased when OSCC cells were maintained *in vitro*. In all newly generated cell lines the $CD44^+$ cell fraction was a lot larger than in samples of OSCC that cell lines were generated from. This suggests that one of the differences between behaviour of CSCs *in vitro* and *in vivo* is the shift towards more frequent symmetric cell division occurring in culture, resulting in a larger fraction of (CD44 expressing) stem cells and amplifying cells.

The intrinsic mechanisms controlling CSC proliferation and the type of cell division are likely to be the same *in vivo* and *in vitro*. Signalling pathways regulating symmetric and asymmetric cell division during embryonic development such as Notch, Hedgehog and Wnt may be involved. Hijioka and co-workers observed an accumulation of the Notch intracellular domain in the nucleus of cells in OSCC cell lines and in OSCC biopsies and reported that blocking the Notch signalling pathway prevents growth of OSCC cells *in vitro* [234]. In a different study, Notch1 and Notch3 were found to be overexpressed in OSCC of the tongue and their expression directly correlated with pathological grade of the tumours [235]. An additional study also reported Notch1 to be upregulated in OSCC, particularly at the invasive front of tumours, and to correlate with their T stage [236].

In contrast, other investigators reported that active Notch signalling inhibited proliferation of OSCC cell lines and that the Notch pathway is defective in 66% of OSCC patients [237]. Whole-exome sequencing of 32 OSCC specimens identified loss-of-function mutations in the components of the Notch pathway in a large proportion of specimens [238] [239], suggesting that *NOTCH1* may function as a tumor suppressor gene rather than an oncogene in this tumour type. Evidence supporting this idea has also been reported for breast cancer. It was reported that CSCs in breast tumours exhibit loss of the two components of the Notch signalling pathway, Musashi1 and Notch1. Both factors are the key regulators of asymmetric cell division and both are abundantly expressed in the normal breast stem cells [240]. Downregulation of Musashi1 and Notch1 could lead to an increase in the frequency of symmetric cell division and an increase in the size of the stem cell fraction in breast cancer tissue as compared to stem cells in normal tissue.

The contradictory findings described above indicate that more work needs to be done to elucidate the role of Notch and possibly other developmental pathways in OSCC *in vitro* and *in vivo*.

In addition to developmental pathways, ErbB signalling could also be responsible for the expansion of the pool of stem (and amplifying) cells in cell cultures of OSCC. ErbB signalling activation has been shown to play an important role in stem-cell proliferation in the intestinal crypts [241]. EGFR (ErbB1, ErbB family member) is strongly expressed in OSCC cell lines and its activated form (phosphorylated EGFR) was detected by western blot in all cell lines examined (Figure 5.67). The constitutive activation of the EGFR signalling by EGF that is present in culture medium could explain the expansion of the stem cell pool occurring *in vitro*. Similarly, other growth factors and cytokines present in the culture medium as well as epithelial autocrine factors produced by the cells themselves could activate signalling pathways that promote proliferation and stem cell maintenance in cell lines.

The fact that OSCC cell lines contain a much larger fraction of CD44 expressing cells than the tumours of origin could be explained with an expansion of the pool of stem cells and amplifying cells *in vitro* as compared to *in vivo.* Due to the enrichment of CSCs *in vitro,* and their parallels to the CSCs present in tumours *in vivo*, cell lines can be used to investigate drugs targeting CSC-specific processes. New ways of targeting and killing CSCs would potentially contribute to the development of new therapies for treatment of OSCC.

Although nearly all cells in OSCC cell lines were $CD44^{+}$, there was a large difference (several units on a log scale) in the CD44 expression levels among individual cells detectable by FACS. There is extensive evidence that low CD44 expression is associated with differentiation [160] [180]. Thus, cell lines could be used to study molecular mechanisms associated with differentiation, which in turn can be easily measured via changes in the CD44 expression levels. The potential of known drugs and other chemical and biological compounds to induce differentiation could also be explored. Induced differentiation could lead to a complete depletion of the CSC pool resulting in elimination of a tumour.

Changes occurring in cultured cells are likely to be of genetic as well as epigenetic nature. These changes occur over time and it is reasonable to assume that cells in early passage cell lines are closer to the cells of the tumour of origin in their genetic and epigenetic make-up than the later passages of the same cell lines. Elucidating these changes would provide useful information to further support the use of cell lines as suitable models for studying tumour behaviour.

7. Conclusions and Future Work

Today, over 15 years after their discovery in haematological malignancies [64], the concept of CSCs in solid tumours is widely accepted. We now need to focus on the characterisation of the properties of these cells that could be exploited for developing new therapeutic interventions. One of these properties concerns the stability of the CSC phenotype. The question whether differentiated cells can de-differentiate and return to a stem cell state is of tremendous importance for our understanding of tumour growth and spread and consequently for developing anti-tumour therapies. Another relevant question is the plasticity of the CSC phenotype. Our work showed that CSCs in head and neck SCC and SCC of the skin exist in at least two distinct phenotypes (EMT and epithelial phenotype) [160]. The EMT CSC phenotype is regarded as the only CSC phenotype by many investigators. This notion emerged due to the wide utilisation of the sphere formation assay for identification and isolation of CSCs. However, it is important to remember that the sphere assay predominantly identifies the EMT CSC population, which forms a fraction of the total CSC pool [160]. Alternative CSC phenotypes might also exist and more CSC-specific markers and isolation assays need to be developed for the identification of other CSC sub-types.

These finer discriminations of CSC phenotypes require isolation of purer cell populations for analysis. To date, negative selection has always been the method of choice for isolation of CSCs from fresh tumour specimens. The present study showed the negative selection to be less than satisfactory in identifying the epithelial fraction of the tumour. The positive selection described here, yielded better results but still needs further improvement in order to accurately identify/isolate the epithelial tumour fraction.

This work presents evidence that CD44 is associated with CSC properties in OSCC. The proportion of $CD44^+$ cells in OSCC tumours was found to correlate with a poor differentiation state, presence of neck lymph node metastasis (and a discohesive invasion front). These findings are perhaps not surprising as CD44 has many functions [126] and we (amongst others)

show that its expression is related to control of CSC phenotype and differentiation [148]. More specimens need to be examined to confirm the findings described in this study. Expression of CD44 variant isoforms, properties of the EMT population and other potentially relevant CSC phenotypes could also be studied in fresh tumour tissue and may prove associated with tumour invasion and metastases. Investigating MET associated mechanisms would also add to our understanding of the metastatic process.

HNSCC is the 6th most common type of cancer worldwide. Current therapies are lacking efficacy, leaving HNSCC patients with a poor prognosis. The concept of CSCs provides a better understanding of tumour biology and might help elucidate mechanisms responsible for tumour growth, tumour dissemination and resistance to therapy. Cell lines derived from tumour specimens, in particular in their early passages, present valuable models for studying CSCs in OSCC. In the past, *in vitro* studies have significantly contributed to our understanding of mechanisms driving cell division and ultimately tumour growth *in vivo*. Continued use of cell lines would allow studying therapeutic responses and resistance mechanisms leading to the discovery of new therapeutic targets and may ultimately improve clinical outcomes for OSCC patients.

8. References

1. Smart, J.D., *Buccal drug delivery.* Expert Opin Drug Deliv, 2005. **2**(3): p. 507-17.
2. Squier, C.A. and M.J. Kremer, *Biology of oral mucosa and esophagus.* J Natl Cancer Inst Monogr, 2001(29): p. 7-15.
3. Liu, S.C., et al., *Markers of cell proliferation in normal epithelia and dysplastic leukoplakias of the oral cavity.* Cancer Epidemiol Biomarkers Prev, 1998. **7**(7): p. 597-603.
4. Gibbs, S. and M. Ponec, *Intrinsic regulation of differentiation markers in human epidermis, hard palate and buccal mucosa.* Arch Oral Biol, 2000. **45**(2): p. 149-58.
5. Watt, F.M., *Epidermal stem cells: markers, patterning and the control of stem cell fate.* Philos Trans R Soc Lond B Biol Sci, 1998. **353**(1370): p. 831-7.
6. Steven, A.C. and P.M. Steinert, *Protein composition of cornified cell envelopes of epidermal keratinocytes.* J Cell Sci, 1994. **107 (Pt 2)**: p. 693-700.
7. Candi, E., R. Schmidt, and G. Melino, *The cornified envelope: a model of cell death in the skin.* Nat Rev Mol Cell Biol, 2005. **6**(4): p. 328-40.
8. Agarwal, M.L., et al., *p53 controls both the G2/M and the G1 cell cycle checkpoints and mediates reversible growth arrest in human fibroblasts.* Proc Natl Acad Sci U S A, 1995. **92**(18): p. 8493-7.
9. Girod, S.C., et al., *p53 expression in the carcinogenesis in the oral mucosa.* J Cell Biochem, 1994. **56**(4): p. 444-8.
10. Cruz, I.B., et al., *p53 expression above the basal cell layer in oral mucosa is an early event of malignant transformation and has predictive value for developing oral squamous cell carcinoma.* Journal of Pathology, 1998. **184**(4): p. 360-368.
11. Schmitt, C.A., et al., *Dissecting p53 tumor suppressor functions in vivo.* Cancer Cell, 2002. **1**(3): p. 289-298.
12. Todd, R., et al., *Cellular sources of transforming growth factor-alpha in human oral cancer.* Journal of Dental Research, 1991. **70**(5): p. 917-23.
13. Scully, C., *Oncogenes, Tumor Suppressors and Viruses in Oral Squamous Carcinoma.* Journal of Oral Pathology & Medicine, 1993. **22**(8): p. 337-347.
14. Alroy, I. and Y. Yarden, *The ErbB signaling network in embryogenesis and oncogenesis: Signal diversification through combinatorial ligand-receptor interactions.* Febs Letters, 1997. **410**(1): p. 83-86.
15. McDonald, J.S., et al., *Immunohistochemical detection of the H-ras, K-ras, and N-ras oncogenes in squamous cell carcinoma of the head and neck.* J Oral Pathol Med, 1994. **23**(8): p. 342-6.
16. Kiaris, H., et al., *Mutations, expression and genomic instability of the H-ras proto-oncogene in squamous cell carcinomas of the head and neck.* Br J Cancer, 1995. **72**(1): p. 123-8.
17. Roberts, P.J. and C.J. Der, *Targeting the Raf-MEK-ERK mitogen-activated protein kinase cascade for the treatment of cancer.* Oncogene, 2007. **26**(22): p. 3291-3310.
18. Hahn, W.C. and R.A. Weinberg, *Mechanisms of disease: Rules for making human tumor cells.* New England Journal of Medicine, 2002. **347**(20): p. 1593-1603.
19. Reya, T., et al., *Stem cells, cancer, and cancer stem cells.* Nature, 2001. **414**(6859): p. 105-11.
20. Bello, I.O., Y. Soini, and T. Salo, *Prognostic evaluation of oral tongue cancer: means, markers and perspectives (II).* Oral Oncol, 2010. **46**(9): p. 636-43.
21. Patel, S.G. and J.P. Shah, *TNM staging of cancers of the head and neck: Striving for uniformity among diversity.* Ca-a Cancer Journal for Clinicians, 2005. **55**(4): p. 242-258.

22. Pisani, P., D.M. Parkin, and J. Ferlay, *Estimates of the worldwide mortality from eighteen major cancers in 1985. Implications for prevention and projections of future burden.* Int J Cancer, 1993. **55**(6): p. 891-903.
23. Saintigny, P., et al., *Gene expression profiling predicts the development of oral cancer.* Cancer Prev Res (Phila), 2011. **4**(2): p. 218-29.
24. Pavia, M., et al., *Association between fruit and vegetable consumption and oral cancer: a meta-analysis of observational studies.* American Journal of Clinical Nutrition, 2006. **83**(5): p. 1126-1134.
25. Scully, C. and J. Bagan, *Oral squamous cell carcinoma overview.* Oral Oncol, 2009. **45**(4-5): p. 301-8.
26. Maier, H., et al., *Dental status and oral hygiene in patients with head and neck cancer.* Otolaryngol Head Neck Surg, 1993. **108**(6): p. 655-61.
27. Balaram, P., et al., *Oral cancer in southern India: the influence of smoking, drinking, paan-chewing and oral hygiene.* Int J Cancer, 2002. **98**(3): p. 440-5.
28. Johnson, N.W. and K.A. Warnakulasuriya, *Epidemiology and aetiology of oral cancer in the United Kingdom.* Community Dent Health, 1993. **10 Suppl 1**: p. 13-29.
29. Hindle, I., M.C. Downer, and P.M. Speight, *The epidemiology of oral cancer.* Br J Oral Maxillofac Surg, 1996. **34**(5): p. 471-6.
30. Carvalho, A.L., et al., *Trends in incidence and prognosis for head and neck cancer in the United States: a site-specific analysis of the SEER database.* Int J Cancer, 2005. **114**(5): p. 806-16.
31. Robbins, K.T., et al., *Neck dissection classification update: revisions proposed by the American Head and Neck Society and the American Academy of Otolaryngology-Head and Neck Surgery.* Arch Otolaryngol Head Neck Surg, 2002. **128**(7): p. 751-8.
32. Herbst, R.S. and C.J. Langer, *Epidermal growth factor receptors as a target for cancer treatment: The emerging role of IMC-C225 in the treatment of lung and head and neck cancers.* Semin Oncol, 2002. **29**(1): p. 27-36.
33. Christensen, M.E., et al., *Epidermal growth factor receptor expression on oral mucosa dysplastic epithelia and squamous cell carcinomas.* Eur Arch Otorhinolaryngol, 1992. **249**(5): p. 243-7.
34. Yu, X., et al., *Ligand-independent dimer formation of epidermal growth factor receptor (EGFR) is a step separable from ligand-induced EGFR signaling.* Mol Biol Cell, 2002. **13**(7): p. 2547-57.
35. Hansen, A.R. and L.L. Siu, *Epidermal growth factor receptor targeting in head and neck cancer: have we been just skimming the surface?* J Clin Oncol, 2013. **31**(11): p. 1381-3.
36. Cripps, C., et al., *Epidermal growth factor receptor targeted therapy in stages III and IV head and neck cancer.* Curr Oncol, 2010. **17**(3): p. 37-48.
37. Cerniglia, G.J., et al., *Epidermal growth factor receptor inhibition modulates the microenvironment by vascular normalization to improve chemotherapy and radiotherapy efficacy.* PLoS One, 2009. **4**(8): p. e6539.
38. Naruse, T., et al., *Immunohistochemical study of VEGF expression in oral squamous cell carcinomas: correlation with the mTOR-HIF-1alpha pathway.* Anticancer Res, 2011. **31**(12): p. 4429-37.
39. Riedel, F., et al., *Serum levels of vascular endothelial growth factor in patients with head and neck cancer.* Eur Arch Otorhinolaryngol, 2000. **257**(6): p. 332-6.
40. Smith, B.D., et al., *Prognostic significance of vascular endothelial growth factor protein levels in oral and oropharyngeal squamous cell carcinoma.* J Clin Oncol, 2000. **18**(10): p. 2046-52.
41. Uehara, M., et al., *Expression of vascular endothelial growth factor and prognosis of oral squamous cell carcinoma.* Oral Oncol, 2004. **40**(3): p. 321-5.

42. Pernas, F.G., Resto, V. A. et al., , *EGFR Therapy in Head and Neck Cancer, available at http://www.utmb.edu/otoref/grnds/EGFR-H&N-Ca-2011-0331/EGFR--2011.pdf*, 2011, Grand Rounds Presentation, The University of Texas Medical Branch, Department of Otolaryngology.
43. PF, D., *Tumour, Node and Metastasis (TNM).* Bull Inst Nat Hug (Paris), 1944. **1944;1:1-69**(1): p. 1-69.
44. P, O.c., et al., *Tumour thickness predicts cervical nodal metastases and survival in early oral tongue cancer.* Oral Oncol, 2003. **39**(4): p. 386-90.
45. Genden, E.M., et al., *Neck disease and distant metastases.* Oral Oncol, 2003. **39**(3): p. 207-12.
46. Shingaki, S., et al., *Impact of lymph node metastasis on the pattern of failure and survival in oral carcinomas.* Am J Surg, 2003. **185**(3): p. 278-84.
47. Greenberg, J.S., et al., *Extent of extracapsular spread: a critical prognosticator in oral tongue cancer.* Cancer, 2003. **97**(6): p. 1464-70.
48. Woolgar, J.A., et al., *Cervical lymph node metastasis in oral cancer: the importance of even microscopic extracapsular spread.* Oral Oncol, 2003. **39**(2): p. 130-7.
49. Gregoire, V., et al., *Squamous cell carcinoma of the head and neck: EHNS-ESMO-ESTRO Clinical Practice Guidelines for diagnosis, treatment and follow-up.* Ann Oncol, 2010. **21 Suppl 5**: p. v184-6.
50. National Institute for Health and Care Excellence (NICE), *Improving Outcomes in Head and Neck Cancers, available at http://www.nice.org.uk/nicemedia/live/10897/28851/28851.pdf*, 2004.
51. Scottish Intercollegiate Guidelines Network (SIGN), *Diagnosis and management of head and neck cancer. A national clinical guideline, available at http://www.sign.ac.uk/pdf/sign90.pdf*, 2006.
52. National Comprehensice Cancer Network (NCCN), *NCCN guidelines for treatment of head and neck cancers, available at http://www.nccn.org/professionals/physician_gls/f_guidelines.asp#site*, 2013.
53. Lomax, M.E., M.K. Gulston, and P. O'Neill, *Chemical aspects of clustered DNA damage induction by ionising radiation.* Radiat Prot Dosimetry, 2002. **99**(1-4): p. 63-8.
54. Fuertes, M.A., et al., *Cisplatin biochemical mechanism of action: From cytotoxicity to induction of cell death through interconnections between apoptotic and necrotic pathways.* Current Medicinal Chemistry, 2003. **10**(3): p. 257-266.
55. Grem, J.L., *5-Fluorouracil: forty-plus and still ticking. A review of its preclinical and clinical development.* Investigational New Drugs, 2000. **18**(4): p. 299-313.
56. Longley, D.B., D.P. Harkin, and P.G. Johnston, *5-Fluorouracil: Mechanisms of action and clinical strategies.* Nature Reviews Cancer, 2003. **3**(5): p. 330-338.
57. Rose-Ped, A.M., et al., *Complications of radiation therapy for head and neck cancers. The patient's perspective.* Cancer Nurs, 2002. **25**(6): p. 461-7; quiz 468-9.
58. Vera-Llonch, M., et al., *Oral mucositis in patients undergoing radiation treatment for head and neck carcinoma.* Cancer, 2006. **106**(2): p. 329-36.
59. Lacouture, M.E., *Dermatologic Principles and Practice in Oncology: Conditions of the Skin, Hair, and Nails in Cancer Patients*. 2013.
60. Grundmann, O., G.C. Mitchell, and K.H. Limesand, *Sensitivity of salivary glands to radiation: from animal models to therapies.* Journal of Dental Research, 2009. **88**(10): p. 894-903.
61. Vissink, A., et al., *Oral sequelae of head and neck radiotherapy.* Crit Rev Oral Biol Med, 2003. **14**(3): p. 199-212.
62. Formenti, S.C. and S. Demaria, *Systemic effects of local radiotherapy.* Lancet Oncol, 2009. **10**(7): p. 718-26.
63. Virchow, R.L.K., *Cellular Pathology* 1858: (ed.Hirschwald A), Berlin

64. Bonnet, D. and J.E. Dick, *Human acute myeloid leukemia is organized as a hierarchy that originates from a primitive hematopoietic cell.* Nat Med, 1997. **3**(7): p. 730-7.
65. Zhang, P., et al., *Side population in oral squamous cell carcinoma possesses tumor stem cell phenotypes.* Cancer Lett, 2009. **277**(2): p. 227-34.
66. Sobreira, T.J., et al., *Structural shifts of aldehyde dehydrogenase enzymes were instrumental for the early evolution of retinoid-dependent axial patterning in metazoans.* Proc Natl Acad Sci U S A, 2011. **108**(1): p. 226-31.
67. Ginestier, C., et al., *ALDH1 is a marker of normal and malignant human mammary stem cells and a predictor of poor clinical outcome.* Cell Stem Cell, 2007. **1**(5): p. 555-567.
68. Rasper, M., et al., *Aldehyde dehydrogenase 1 positive glioblastoma cells show brain tumor stem cell capacity.* Neuro-Oncology, 2010. **12**(10): p. 1024-1033.
69. van den Hoogen, C., et al., *High Aldehyde Dehydrogenase Activity Identifies Tumor-Initiating and Metastasis-Initiating Cells in Human Prostate Cancer.* Cancer Research, 2010. **70**(12): p. 5163-5173.
70. Clay, M.R., et al., *Single-Marker Identification of Head and Neck Squamous Cell Carcinoma Cancer Stem Cells with Aldehyde Dehydrogenase.* Head and Neck-Journal for the Sciences and Specialties of the Head and Neck, 2010. **32**(9): p. 1195-1201.
71. Dontu, G., et al., *In vitro propagation and transcriptional profiling of human mammary stem/progenitor cells.* Genes Dev, 2003. **17**(10): p. 1253-70.
72. Ponti, D., et al., *Isolation and in vitro propagation of tumorigenic breast cancer cells with stem/progenitor cell properties.* Cancer Res, 2005. **65**(13): p. 5506-11.
73. Fan, X., et al., *Effective enrichment of prostate cancer stem cells from spheres in a suspension culture system.* Urol Oncol, 2012. **30**(3): p. 314-8.
74. Krishnamurthy, S. and J.E. Nor, *Head and neck cancer stem cells.* Journal of Dental Research, 2012. **91**(4): p. 334-40.
75. Chan, K.S., et al., *Identification, molecular characterization, clinical prognosis, and therapeutic targeting of human bladder tumor-initiating cells.* Proc Natl Acad Sci U S A, 2009. **106**(33): p. 14016-21.
76. Al-Hajj, M., et al., *Prospective identification of tumorigenic breast cancer cells.* Proc Natl Acad Sci U S A, 2003. **100**(7): p. 3983-8.
77. Singh, S.K., et al., *Identification of human brain tumour initiating cells.* Nature, 2004. **432**(7015): p. 396-401.
78. O'Brien, C.A., et al., *A human colon cancer cell capable of initiating tumour growth in immunodeficient mice.* Nature, 2007. **445**(7123): p. 106-10.
79. Ricci-Vitiani, L., et al., *Identification and expansion of human colon-cancer-initiating cells.* Nature, 2007. **445**(7123): p. 111-5.
80. Dalerba, P., et al., *Phenotypic characterization of human colorectal cancer stem cells.* Proc Natl Acad Sci U S A, 2007. **104**(24): p. 10158-63.
81. Suva, M.L., et al., *Identification of cancer stem cells in Ewing's sarcoma.* Cancer Res, 2009. **69**(5): p. 1776-81.
82. Prince, M.E., et al., *Identification of a subpopulation of cells with cancer stem cell properties in head and neck squamous cell carcinoma.* Proc Natl Acad Sci U S A, 2007. **104**(3): p. 973-8.
83. Yang, Z.F., et al., *Significance of CD90+ cancer stem cells in human liver cancer.* Cancer Cell, 2008. **13**(2): p. 153-66.
84. Schatton, T., et al., *Identification of cells initiating human melanomas.* Nature, 2008. **451**(7176): p. 345-9.
85. Zhang, S., et al., *Identification and characterization of ovarian cancer-initiating cells from primary human tumors.* Cancer Res, 2008. **68**(11): p. 4311-20.

86. Li, C., et al., *Identification of pancreatic cancer stem cells.* Cancer Res, 2007. **67**(3): p. 1030-7.
87. Hermann, P.C., et al., *Distinct populations of cancer stem cells determine tumor growth and metastatic activity in human pancreatic cancer.* Cell Stem Cell, 2007. **1**(3): p. 313-23.
88. Frank, N.Y., T. Schatton, and M.H. Frank, *The therapeutic promise of the cancer stem cell concept.* J Clin Invest, 2010. **120**(1): p. 41-50.
89. Li, X., et al., *Intrinsic resistance of tumorigenic breast cancer cells to chemotherapy.* J Natl Cancer Inst, 2008. **100**(9): p. 672-9.
90. Gupta, P.B., et al., *Identification of selective inhibitors of cancer stem cells by high-throughput screening.* Cell, 2009. **138**(4): p. 645-59.
91. Charafe-Jauffret, E., et al., *Aldehyde dehydrogenase 1-positive cancer stem cells mediate metastasis and poor clinical outcome in inflammatory breast cancer.* Clin Cancer Res, 2010. **16**(1): p. 45-55.
92. Schatton, T., N.Y. Frank, and M.H. Frank, *Identification and targeting of cancer stem cells.* Bioessays, 2009. **31**(10): p. 1038-49.
93. Bao, S., et al., *Glioma stem cells promote radioresistance by preferential activation of the DNA damage response.* Nature, 2006. **444**(7120): p. 756-60.
94. Phillips, T.M., W.H. McBride, and F. Pajonk, *The response of CD24(-/low)/CD44+ breast cancer-initiating cells to radiation.* J Natl Cancer Inst, 2006. **98**(24): p. 1777-85.
95. Harper LJ, C.D., Gammon L, Fazil B, Biddle A, Mackenzie IC., *Normal and malignant epithelial cells with stem-like properties have an extended G2 cell cycle phase that is associated with apoptotic resistance.* BMC Cancer., 2010 Apr **28**(10): p. 166.
96. Monzani, E., et al., *Melanoma contains CD133 and ABCG2 positive cells with enhanced tumourigenic potential.* Eur J Cancer, 2007. **43**(5): p. 935-46.
97. Bracken, A.P., et al., *Genome-wide mapping of Polycomb target genes unravels their roles in cell fate transitions.* Genes & Development, 2006. **20**(9): p. 1123-1136.
98. Molofsky, A.V., et al., *Bmi-1 dependence distinguishes neural stem cell self-renewal from progenitor proliferation.* Nature, 2003. **425**(6961): p. 962-7.
99. Liu, L., L.G. Andrews, and T.O. Tollefsbol, *Loss of the human polycomb group protein BMI1 promotes cancer-specific cell death.* Oncogene, 2006. **25**(31): p. 4370-5.
100. Baumann, M. and M. Krause, *CD44: A Cancer Stem Cell-Related Biomarker with Predictive Potential for Radiotherapy.* Clinical Cancer Research, 2010. **16**(21): p. 5091-5093.
101. Chikamatsu, K., et al., *Resistance to apoptosis-inducing stimuli in CD44+head and neck squamous cell carcinoma cells.* Head and Neck-Journal for the Sciences and Specialties of the Head and Neck, 2012. **34**(3): p. 336-343.
102. Krishnamurthy, S., et al., *Endothelial cell-initiated signaling promotes the survival and self-renewal of cancer stem cells.* Cancer Res, 2010. **70**(23): p. 9969-78.
103. Gadhoum, Z., et al., *CD44: a new means to inhibit acute myeloid leukemia cell proliferation via p27Kip1.* Blood, 2004. **103**(3): p. 1059-68.
104. Liu, J. and G. Jiang, *CD44 and hematologic malignancies.* Cell Mol Immunol, 2006. **3**(5): p. 359-65.
105. Krause, D.S., et al., *Requirement for CD44 in homing and engraftment of BCR-ABL-expressing leukemic stem cells.* Nat Med, 2006. **12**(10): p. 1175-80.
106. Takaishi, S., et al., *Identification of gastric cancer stem cells using the cell surface marker CD44.* Stem Cells, 2009. **27**(5): p. 1006-20.
107. Yang, Z.F., et al., *Identification of local and circulating cancer stem cells in human liver cancer.* Hepatology, 2008. **47**(3): p. 919-28.
108. Zhu, Z., et al., *Cancer stem/progenitor cells are highly enriched in CD133+CD44+ population in hepatocellular carcinoma.* Int J Cancer, 2010. **126**(9): p. 2067-78.

109. Shi, C., et al., *CD44+ CD133+ population exhibits cancer stem cell-like characteristics in human gallbladder carcinoma.* Cancer Biol Ther, 2010. **10**(11): p. 1182-90.
110. Ouhtit, A., et al., *In vivo evidence for the role of CD44s in promoting breast cancer metastasis to the liver.* American Journal of Pathology, 2007. **171**(6): p. 2033-9.
111. Petersen, O.W. and K. Polyak, *Stem cells in the human breast.* Cold Spring Harb Perspect Biol, 2010. **2**(5): p. a003160.
112. Feng, D., et al., *Identification and characterization of cancer stem-like cells from primary carcinoma of the cervix uteri.* Oncol Rep, 2009. **22**(5): p. 1129-34.
113. Collins, A.T., et al., *Prospective identification of tumorigenic prostate cancer stem cells.* Cancer Res, 2005. **65**(23): p. 10946-51.
114. Patrawala, L., et al., *Highly purified CD44+ prostate cancer cells from xenograft human tumors are enriched in tumorigenic and metastatic progenitor cells.* Oncogene, 2006. **25**(12): p. 1696-708.
115. Wei, C., et al., *Cancer stem-like cells in human prostate carcinoma cells DU145: the seeds of the cell line?* Cancer Biol Ther, 2007. **6**(5): p. 763-8.
116. Yang, Y.M. and J.W. Chang, *Bladder cancer initiating cells (BCICs) are among EMA-CD44v6+ subset: novel methods for isolating undetermined cancer stem (initiating) cells.* Cancer Invest, 2008. **26**(7): p. 725-33.
117. Reategui, E.P., et al., *Characterization of CD44v3-containing isoforms in head and neck cancer.* Cancer Biol Ther, 2006. **5**(9): p. 1163-8.
118. Wang, S.J. and L.Y. Bourguignon, *Hyaluronan and the interaction between CD44 and epidermal growth factor receptor in oncogenic signaling and chemotherapy resistance in head and neck cancer.* Arch Otolaryngol Head Neck Surg, 2006. **132**(7): p. 771-8.
119. de Jong, M.C., et al., *CD44 expression predicts local recurrence after radiotherapy in larynx cancer.* Clin Cancer Res, 2010. **16**(21): p. 5329-38.
120. Fang, S.H., et al., *Expansion of a cell population expressing stem cell markers in parathyroid glands from patients with hyperparathyroidism.* Ann Surg, 2010. **251**(1): p. 107-13.
121. Leung, E.L., et al., *Non-small cell lung cancer cells expressing CD44 are enriched for stem cell-like properties.* PLoS One, 2010. **5**(11): p. e14062.
122. Zhang, H.Z., et al., *The study of the tumor stem cell properties of CD133+CD44+ cells in the human lung adenocarcinoma cell line A549.* Cell Mol Biol (Noisy-le-grand), 2010. **56 Suppl**: p. OL1350-8.
123. Gibbs, C.P., et al., *Stem-like cells in bone sarcomas: implications for tumorigenesis.* Neoplasia, 2005. **7**(11): p. 967-76.
124. Xu, Y., I. Stamenkovic, and Q. Yu, *CD44 attenuates activation of the hippo signaling pathway and is a prime therapeutic target for glioblastoma.* Cancer Res, 2010. **70**(6): p. 2455-64.
125. Rath, P., et al., *Isolation and characterization of a population of stem-like progenitor cells from an atypical meningioma.* Exp Mol Pathol, 2011. **90**(2): p. 179-88.
126. Zoller, M., *CD44: can a cancer-initiating cell profit from an abundantly expressed molecule?* Nature Reviews Cancer, 2011. **11**(4): p. 254-267.
127. Goldstein, L.A., et al., *A Human-Lymphocyte Homing Receptor, the Hermes Antigen, Is Related to Cartilage Proteoglycan Core and Link Proteins.* Cell, 1989. **56**(6): p. 1063-1072.
128. Idzerda, R.L., et al., *Isolation and DNA-Sequence of a Cdna Clone Encoding a Lymphocyte Adhesion Receptor for High Endothelium.* Proceedings of the National Academy of Sciences of the United States of America, 1989. **86**(12): p. 4659-4663.
129. Naor, D., et al., *Involvement of CD44, a molecule with a thousand faces, in cancer dissemination.* Seminars in Cancer Biology, 2008. **18**(4): p. 260-267.

130. Ruiz, P., C. Schwarzler, and U. Gunthert, *Cd44 Isoforms during Differentiation and Development.* Bioessays, 1995. **17**(1): p. 17-24.
131. Almond, A., *Hyaluronan.* Cellular and Molecular Life Sciences, 2007. **64**(13): p. 1591-1596.
132. Aruffo, A., et al., *Cd44 Is the Principal Cell-Surface Receptor for Hyaluronate.* Cell, 1990. **61**(7): p. 1303-1313.
133. Toole, B.P. and V.C. Hascall, *Hyaluronan and tumor growth.* American Journal of Pathology, 2002. **161**(3): p. 745-747.
134. Ishii, S., et al., *Cd44 Participates in the Adhesion of Human Colorectal-Carcinoma Cells to Laminin and Type-Iv Collagen.* Surgical Oncology-Oxford, 1993. **2**(4): p. 255-264.
135. Jalkanen, S. and M. Jalkanen, *Lymphocyte Cd44 Binds the Cooh-Terminal Heparin-Binding Domain of Fibronectin.* Journal of Cell Biology, 1992. **116**(3): p. 817-825.
136. Toyamasorimachi, N. and M. Miyasaka, *A Novel Ligand for Cd44 Is Sulfated Proteoglycan.* International Immunology, 1994. **6**(4): p. 655-660.
137. Toole, B.P. and M.G. Slomiany, *Hyaluronan: a constitutive regulator of chemoresistance and malignancy in cancer cells.* Seminars in Cancer Biology, 2008. **18**(4): p. 244-50.
138. Bourguignon, L.Y., *Hyaluronan-mediated CD44 activation of RhoGTPase signaling and cytoskeleton function promotes tumor progression.* Seminars in Cancer Biology, 2008. **18**(4): p. 251-9.
139. Kalnina, Z., et al., *Alterations of pre-mRNA splicing in cancer.* Genes Chromosomes & Cancer, 2005. **42**(4): p. 342-357.
140. Okamoto, I., et al., *Proteolytic release of CD44 intracellular domain and its role in the CD44 signaling pathway.* Journal of Cell Biology, 2001. **155**(5): p. 755-762.
141. Tsukita, S., et al., *Erm Family Members as Molecular Linkers between the Cell-Surface Glycoprotein Cd44 and Actin-Based Cytoskeletons.* Journal of Cell Biology, 1994. **126**(2): p. 391-401.
142. Lokeshwar, V.B., N. Fregien, and L.Y.W. Bourguignon, *Ankyrin-Binding Domain of Cd44(Gp85) Is Required for the Expression of Hyaluronic Acid-Mediated Adhesion Function.* Journal of Cell Biology, 1994. **126**(4): p. 1099-1109.
143. Fehon, R.G., A.I. McClatchey, and A. Bretscher, *Organizing the cell cortex: the role of ERM proteins (vol 11, pg 276, 2010).* Nature Reviews Molecular Cell Biology, 2010. **11**(9): p. 675-675.
144. Mori, T., et al., *Structural Basis for CD44 Recognition by ERM Proteins.* Journal of Biological Chemistry, 2008. **283**(43): p. 29602-29612.
145. Ponta, H., L. Sherman, and P.A. Herrlich, *CD44: from adhesion molecules to signalling regulators.* Nat Rev Mol Cell Biol, 2003. **4**(1): p. 33-45.
146. Marhaba, R. and M. Zoller, *CD44 in cancer progression: adhesion, migration and growth regulation.* J Mol Histol, 2004. **35**(3): p. 211-31.
147. Kidwai, F., et al., *The effects of CD44 down-regulation on stem cell properties of head and neck cancer cell lines.* J Oral Pathol Med, 2013.
148. Shigeishi, H., et al., *Maintenance of Stem cell Self-renewal in Head and Neck Cancers Requires Actions of GSK3beta Influenced by CD44 and RHAMM.* Stem Cells, 2013.
149. Bourguignon, L.Y., et al., *Hyaluronan-CD44v3 interaction with Oct4-Sox2-Nanog promotes miR-302 expression leading to self-renewal, clonal formation, and cisplatin resistance in cancer stem cells from head and neck squamous cell carcinoma.* Journal of Biological Chemistry, 2012. **287**(39): p. 32800-24.
150. Zeisberg, M. and E.G. Neilson, *Biomarkers for epithelial-mesenchymal transitions.* J Clin Invest, 2009. **119**(6): p. 1429-37.

151. Kalluri, R. and R.A. Weinberg, *The basics of epithelial-mesenchymal transition.* J Clin Invest, 2009. **119**(6): p. 1420-8.
152. Bhat-Nakshatri, P., et al., *SLUG/SNAI2 and tumor necrosis factor generate breast cells with CD44+/CD24- phenotype.* BMC Cancer, 2010. **10**: p. 411.
153. Mani, S.A., et al., *The epithelial-mesenchymal transition generates cells with properties of stem cells.* Cell, 2008. **133**(4): p. 704-15.
154. Ahmed, N., et al., *Epithelial mesenchymal transition and cancer stem cell-like phenotypes facilitate chemoresistance in recurrent ovarian cancer.* Curr Cancer Drug Targets, 2010. **10**(3): p. 268-78.
155. Thiery, J.P., *Epithelial-mesenchymal transitions in development and pathologies.* Curr Opin Cell Biol, 2003. **15**(6): p. 740-746.
156. Shin, S.Y., et al., *Functional Roles of Multiple Feedback Loops in Extracellular Signal-Regulated Kinase and Wnt Signaling Pathways That Regulate Epithelial-Mesenchymal Transition.* Cancer Research, 2010. **70**(17): p. 6715-6724.
157. Wu, Y., et al., *Stabilization of Snail by NF-kappa B Is Required for Inflammation-Induced Cell Migration and Invasion.* Cancer Cell, 2009. **15**(5): p. 416-428.
158. Yang, M.H., et al., *Direct regulation of TWIST by HIF-1alpha promotes metastasis.* Nat Cell Biol, 2008. **10**(3): p. 295-305.
159. Gammon, L., et al., *Sub-sets of cancer stem cells differ intrinsically in their patterns of oxygen metabolism.* PLoS One, 2013. **8**(4): p. e62493.
160. Biddle, A., et al., *Cancer stem cells in squamous cell carcinoma switch between two distinct phenotypes that are preferentially migratory or proliferative.* Cancer Res, 2011. **71**(15): p. 5317-26.
161. Cheng, G.Z., et al., *Twist transcriptionally up-regulates AKT2 in breast cancer cells leading to increased migration, invasion, and resistance to paclitaxel.* Cancer Res, 2007. **67**(5): p. 1979-87.
162. Kallergi, G., et al., *Epithelial to mesenchymal transition markers expressed in circulating tumour cells of early and metastatic breast cancer patients.* Breast Cancer Res, 2011. **13**(3): p. R59.
163. Yang J, W.R., *Epithelial-mesenchymal transition: at the crossroads of development and tumor metastasis.* Dev Cell., 2008. **Jun**(14(6):): p. 818-29.
164. Skvortsova, I., et al., *Epithelial-to-mesenchymal transition and c-myc expression are the determinants of cetuximab-induced enhancement of squamous cell carcinoma radioresponse.* Radiother Oncol, 2010. **96**(1): p. 108-15.
165. Bandyopadhyay, A., et al., *Doxorubicin in combination with a small TGFbeta inhibitor: a potential novel therapy for metastatic breast cancer in mouse models.* PLoS One, 2010. **5**(4): p. e10365.
166. Blick, T., et al., *Epithelial Mesenchymal Transition Traits in Human Breast Cancer Cell Lines Parallel the CD44(hi/)CD24(lo/-) Stem Cell Phenotype in Human Breast Cancer.* Journal of Mammary Gland Biology and Neoplasia, 2010. **15**(2): p. 235-252.
167. Gjerdrum, C., et al., *Axl is an essential epithelial-to-mesenchymal transition-induced regulator of breast cancer metastasis and patient survival.* Proceedings of the National Academy of Sciences of the United States of America, 2010. **107**(3): p. 1124-1129.
168. Breuss, J.M., et al., *Expression of the beta 6 integrin subunit in development, neoplasia and tissue repair suggests a role in epithelial remodeling.* J Cell Sci, 1995. **108 (Pt 6)**: p. 2241-51.
169. Smythe, W.R., et al., *Integrin Expression in Non-Small-Cell Carcinoma of the Lung.* Cancer and Metastasis Reviews, 1995. **14**(3): p. 229-239.
170. Bates, R.C., et al., *Transcriptional activation of integrin beta6 during the epithelial-mesenchymal transition defines a novel prognostic indicator of aggressive colon carcinoma.* J Clin Invest, 2005. **115**(2): p. 339-47.

171. Thomas, G.J., M.L. Nystrom, and J.F. Marshall, *Alphavbeta6 integrin in wound healing and cancer of the oral cavity.* J Oral Pathol Med, 2006. **35**(1): p. 1-10.
172. Impola, U., et al., *Differential expression of matrilysin-1 (MMP-7), 92 kD gelatinase (MMP-9), and metalloelastase (MMP-12) in oral verrucous and squamous cell cancer.* Journal of Pathology, 2004. **202**(1): p. 14-22.
173. Thomas, G.J., et al., *Expression of the alpha v beta 6 integrin promotes migration and invasion in squamous carcinoma cells.* Journal of Investigative Dermatology, 2001. **117**(1): p. 67-73.
174. Thomas, G.J., et al., *alpha V beta 6 integrin promotes invasion of squamous carcinoma cells through up-regulation of matrix metalloproteinase-9.* International Journal of Cancer, 2001. **92**(5): p. 641-650.
175. Prime, S.S., et al., *The behaviour of human oral squamous cell carcinoma in cell culture.* J Pathol, 1990. **160**(3): p. 259-69.
176. Sugiyama, M., et al., *Comparison of integrin expression and terminal differentiation capacity in cell lines derived from oral squamous cell carcinomas.* Carcinogenesis, 1993. **14**(10): p. 2171-6.
177. Proby, C.M., et al., *Spontaneous keratinocyte cell lines representing early and advanced stages of malignant transformation of the epidermis.* Exp Dermatol, 2000. **9**(2): p. 104-17.
178. GEORGE J. TODARO and HOWARD GREEN, M.D., *Quantitative studies of the growth of mouse embryo cells in culture and their development into established lines.* Journal of Cell Bioligy, 1963, May(17): p. 299-313.
179. Mueller, M.M. and N.E. Fusenig, *Friends or foes - bipolar effects of the tumour stroma in cancer.* Nat Rev Cancer, 2004. **4**(11): p. 839-49.
180. Harper, L.J., et al., *Stem cell patterns in cell lines derived from head and neck squamous cell carcinoma.* J Oral Pathol Med, 2007. **36**(10): p. 594-603.
181. BriskeAnderson, M.J., J.W. Finley, and S.M. Newman, *The influence of culture time and passage number on the morphological and physiological development of Caco-2 cells.* Proceedings of the Society for Experimental Biology and Medicine, 1997. **214**(3): p. 248-257.
182. Xie, G.Z., et al., *Mammosphere cells from high-passage MCF7 cell line show variable loss of tumorigenicity and radioresistance.* Cancer Lett, 2012. **316**(1): p. 53-61.
183. Wang, S.J., et al., *CD44 variant isoforms in head and neck squamous cell carcinoma progression.* Laryngoscope, 2009. **119**(8): p. 1518-30.
184. Mostaan, L.V., et al., *Correlation between E-cadherin and CD44 adhesion molecules expression and cervical lymph node metastasis in oral tongue SCC: Predictive significance or not.* Pathology Research and Practice, 2011. **207**(7): p. 448-451.
185. Masuda, M., et al., *Decreased CD44H expression in early-stage tongue carcinoma associates with late nodal metastases following interstitial brachytherapy.* Head and Neck-Journal for the Sciences and Specialties of the Head and Neck, 2000. **22**(7): p. 662-665.
186. Hudson, D.L., P.M. Speight, and F.M. Watt, *Altered expression of CD44 isoforms in squamous-cell carcinomas and cell lines derived from them.* International Journal of Cancer, 1996. **66**(4): p. 457-463.
187. Bankfalvi, A., et al., *Gains and losses of adhesion molecules (CD44, E-cadherin, and beta-catenin) during oral carcinogenesis and tumour progression.* Journal of Pathology, 2002. **198**(3): p. 343-351.
188. Kokko, L.L., et al., *Significance of site-specific prognosis of cancer stem cell marker CD44 in head and neck squamous-cell carcinoma.* Oral Oncol, 2011. **47**(6): p. 510-6.
189. Biddle, A., et al., *CD44 Staining of Cancer Stem-Like Cells Is Influenced by Down-Regulation of CD44 Variant Isoforms and Up-Regulation of the Standard CD44*

Isoform in the Population of Cells That Have Undergone Epithelial-to-Mesenchymal Transition. PLoS One, 2013. **8**(2).
190. Joshua, B., et al., *Frequency of cells expressing CD44, a head and neck cancer stem cell marker: correlation with tumor aggressiveness.* Head Neck, 2012. **34**(1): p. 42-9.
191. Ledford, H., *Cancer theory faces doubts.* Nature, 2011. **472**(7343): p. 273-273.
192. Springer, G.F., *T and Tn, general carcinoma autoantigens.* Science, 1984. **224**(4654): p. 1198-206.
193. Mandel, U., et al., *Simple mucin-type carbohydrates in oral stratified squamous and salivary gland epithelia.* J Invest Dermatol, 1991. **97**(4): p. 713-21.
194. Barrandon, Y. and H. Green, *Three clonal types of keratinocyte with different capacities for multiplication.* Proc Natl Acad Sci U S A, 1987. **84**(8): p. 2302-6.
195. Barrandon, Y. and H. Green, *Cell size as a determinant of the clone-forming ability of human keratinocytes.* Proc Natl Acad Sci U S A, 1985. **82**(16): p. 5390-4.
196. Rochat, A., K. Kobayashi, and Y. Barrandon, *Location of stem cells of human hair follicles by clonal analysis.* Cell, 1994. **76**(6): p. 1063-73.
197. Pellegrini, G., et al., *Location and clonal analysis of stem cells and their differentiated progeny in the human ocular surface.* Investigative Ophthalmology & Visual Science, 1999. **40**(4): p. S323-S323.
198. Nakamura, T., K. Endo, and S. Kinoshita, *Identification of human oral keratinocyte stem/progenitor cells by neurotrophin receptor p75 and the role of neurotrophin/p75 signaling.* Stem Cells, 2007. **25**(3): p. 628-38.
199. Rheinwald, J.G. and H. Green, *Serial cultivation of strains of human epidermal keratinocytes: the formation of keratinizing colonies from single cells.* Cell, 1975. **6**(3): p. 331-43.
200. Tudor, D., et al., *The in vitro behaviour and patterns of colony formation of murine epithelial stem cells.* Cell Prolif, 2007. **40**(5): p. 706-20.
201. Hudson, D.L., et al., *Epithelial cell differentiation pathways in the human prostate: identification of intermediate phenotypes by keratin expression.* J Histochem Cytochem, 2001. **49**(2): p. 271-8.
202. Liu, Y., et al., *Keratin 15 promoter targets putative epithelial stem cells in the hair follicle bulge.* J Invest Dermatol, 2003. **121**(5): p. 963-8.
203. Waikel, R.L., et al., *Deregulated expression of c-Myc depletes epidermal stem cells.* Nat Genet, 2001. **28**(2): p. 165-8.
204. Saldanha, G., et al., *Nuclear beta-catenin in basal cell carcinoma correlates with increased proliferation.* Br J Dermatol, 2004. **151**(1): p. 157-64.
205. Tsuji, H., et al., *Nuclear localization of beta-catenin in the hair matrix cells and differentiated keratinocytes.* J Dermatol Sci, 2001. **27**(3): p. 170-7.
206. Jin, X., et al., *EGFR-AKT-Smad Signaling Promotes Formation of Glioma Stem-like Cells and Tumor Angiogenesis by ID3-Driven Cytokine Induction.* Cancer Res, 2011. **71**(22): p. 7125-34.
207. Park, S.M., et al., *The miR-200 family determines the epithelial phenotype of cancer cells by targeting the E-cadherin repressors ZEB1 and ZEB2.* Genes Dev, 2008. **22**(7): p. 894-907.
208. Tsuru, A., et al., *Regulation of the expression of vimentin gene during the differentiation of mouse myeloid leukemia cells.* J Cell Biol, 1990. **110**(5): p. 1655-64.
209. Jones, P.H. and F.M. Watt, *Separation of human epidermal stem cells from transit amplifying cells on the basis of differences in integrin function and expression.* Cell, 1993. **73**(4): p. 713-24.
210. Ghazizadeh, S. and L.B. Taichman, *Organization of stem cells and their progeny in human epidermis.* Journal of Investigative Dermatology, 2005. **124**(2): p. 367-372.
211. Kedjarune, U., et al., *Culturing primary human gingival epithelial cells: comparison of two isolation techniques.* J Craniomaxillofac Surg, 2001. **29**(4): p. 224-31.

212. Martin, T.A., et al., *The role of the CD44/ezrin complex in cancer metastasis.* Crit Rev Oncol Hematol, 2003. **46**(2): p. 165-86.
213. Lim, Y.C., et al., *Cancer stem cell traits in squamospheres derived from primary head and neck squamous cell carcinomas.* Oral Oncol, 2011. **47**(2): p. 83-91.
214. Nurmenniemi, S., et al., *A novel organotypic model mimics the tumor microenvironment.* American Journal of Pathology, 2009. **175**(3): p. 1281-91.
215. Tudor, D., et al., *Intrinsic patterns of behavior of epithelial stem cells.* J Investig Dermatol Symp Proc, 2004. **9**(3): p. 208-14.
216. Mackenzie, I.C., *Retroviral transduction of murine epidermal stem cells demonstrates clonal units of epidermal structure.* J Invest Dermatol, 1997. **109**(3): p. 377-83.
217. Ghazizadeh, S. and L.B. Taichman, *Multiple classes of stem cells in cutaneous epithelium: a lineage analysis of adult mouse skin.* EMBO J, 2001. **20**(6): p. 1215-22.
218. Costea, D.E., et al., *Epithelial stem cells and malignancy.* J Anat, 2008. **213**(1): p. 45-51.
219. Potten, C.S., *Cell replacement in epidermis (keratopoiesis) via discrete units of proliferation.* Int Rev Cytol, 1981. **69**: p. 271-318.
220. Mack, B. and O. Gires, *CD44s and CD44v6 expression in head and neck epithelia.* PLoS One, 2008. **3**(10): p. e3360.
221. Rajarajan, A., et al., *CD44 expression in oro-pharyngeal carcinoma tissues and cell lines.* PLoS One, 2012. **7**(1): p. e28776.
222. Trotta, B.M., et al., *Oral cavity and oropharyngeal squamous cell cancer: key imaging findings for staging and treatment planning.* Radiographics, 2011. **31**(2): p. 339-54.
223. Pietras, K. and A. Ostman, *Hallmarks of cancer: Interactions with the tumor stroma.* Experimental Cell Research, 2010. **316**(8): p. 1324-1331.
224. Calabrese, L., et al., *Role of sentinel lymph node biopsy in oral cancer.* Acta Otorhinolaryngol Ital, 2006. **26**(6): p. 345-9.
225. Fillmore, C.M. and C. Kuperwasser, *Human breast cancer cell lines contain stem-like cells that self-renew, give rise to phenotypically diverse progeny and survive chemotherapy.* Breast Cancer Research, 2008. **10**(2).
226. Charafe-Jauffret, E., et al., *Breast Cancer Cell Lines Contain Functional Cancer Stem Cells with Metastatic Capacity and a Distinct Molecular Signature.* Cancer Research, 2009. **69**(4): p. 1302-1313.
227. Gammon, L., et al., *Stem cell characteristics of cell sub-populations in cell lines derived from head and neck cancers of Fanconi anemia patients.* Journal of Oral Pathology & Medicine, 2011. **40**(2): p. 143-152.
228. Locke, M., et al., *Retention of intrinsic stem cell hierarchies in carcinoma-derived cell lines.* Cancer Research, 2005. **65**(19): p. 8944-8950.
229. Wang, L., et al., *Enrichment of prostate cancer stem-like cells from human prostate cancer cell lines by culture in serum-free medium and chemoradiotherapy.* Int J Biol Sci, 2013. **9**(5): p. 472-9.
230. Nichols, A.C., et al., *Frequent Mutations in TP53 and CDKN2A Found by Next-Generation Sequencing of Head and Neck Cancer Cell Lines.* Archives of Otolaryngology-Head & Neck Surgery, 2012. **138**(8): p. 732-739.
231. Pardal, R., M.F. Clarke, and S.J. Morrison, *Applying the principles of stem-cell biology to cancer.* Nature Reviews Cancer, 2003. **3**(12): p. 895-902.
232. Weiss, L., *Cancer cell heterogeneity.* Cancer and Metastasis Reviews, 2000. **19**(3): p. 345-350.
233. Burdall, S.E., et al., *Breast cancer cell lines: friend or foe?* Breast Cancer Research, 2003. **5**(2): p. 89-95.

234. Hijioka, H., et al., *Upregulation of Notch pathway molecules in oral squamous cell carcinoma.* Int J Oncol, 2010. **36**(4): p. 817-22.
235. Zhang, T., et al., *[The expression and significance of the Notch signaling pathway molecules in tongue squamous cell carcinoma].* Hua Xi Kou Qiang Yi Xue Za Zhi, 2013. **31**(3): p. 303-9.
236. Yoshida, R., et al., *The pathological significance of Notch1 in oral squamous cell carcinoma.* Lab Invest, 2013. **93**(10): p. 1068-81.
237. Pickering, C.R., et al., *Integrative genomic characterization of oral squamous cell carcinoma identifies frequent somatic drivers.* Cancer Discov, 2013. **3**(7): p. 770-81.
238. Agrawal, N., et al., *Exome sequencing of head and neck squamous cell carcinoma reveals inactivating mutations in NOTCH1.* Science, 2011. **333**(6046): p. 1154-7.
239. Stransky, N., et al., *The mutational landscape of head and neck squamous cell carcinoma.* Science, 2011. **333**(6046): p. 1157-60.
240. Clarke, R.B., et al., *Regulation of human breast epithelial stem cells.* Cell Prolif, 2003. **36 Suppl 1**: p. 45-58.
241. Wong, V.W., et al., *Lrig1 controls intestinal stem-cell homeostasis by negative regulation of ErbB signalling.* Nat Cell Biol, 2012. **14**(4): p. 401-8.

9. Appendix

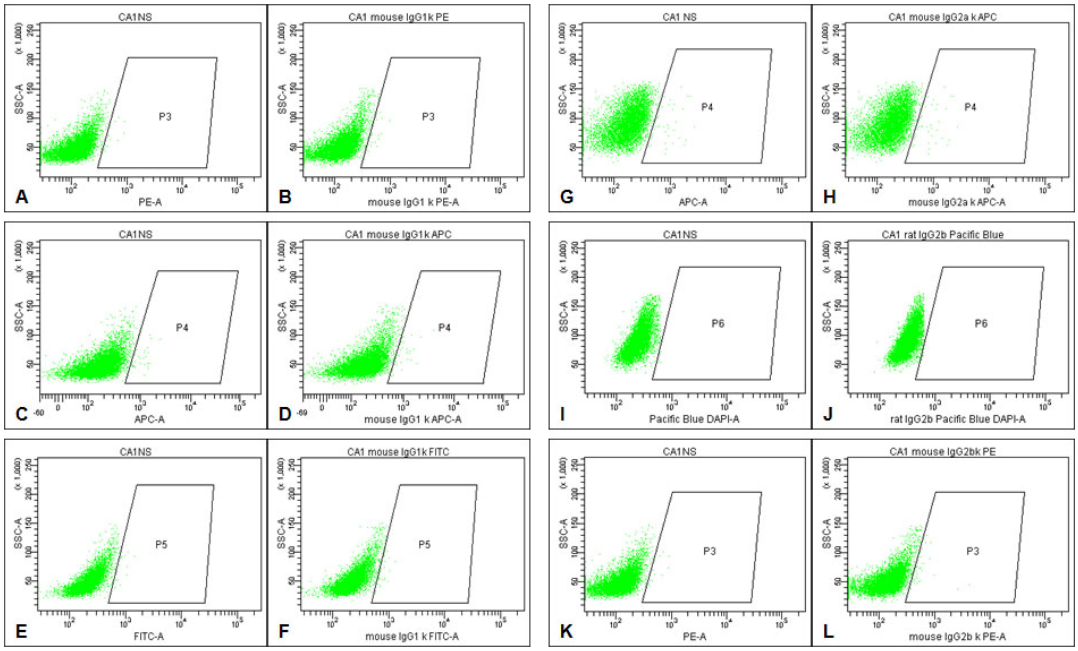

Figure 1: FACS isotype control antibodies tested on the HNSCC cell line CA1. CA1 cells were trypsinised and stained with isotype control antibodies conjugated to different fluorophors. Each stained sample (in B, D, F, H, J, L) was compared to a sample with no added antibody ("CA1 NS" in A, C, E, G, I, K) analysed at the same time. Three different mouse IgG1 κ isotype control antibodies conjugated to PE (B) APC (D) and FITC (F) were tested. There was no difference in signal intensity between these samples and the non-stained control samples (compare A and B, C and D, E and F). Similarly, immunolabelling with APC conjugated mouse IgG2a (H), pacific blue conjugated rat IgG2b (J) and PE conjugated mouse IgG2b (L) did not result in an increase in signal intensity (compare G and H, I and J, K and L).

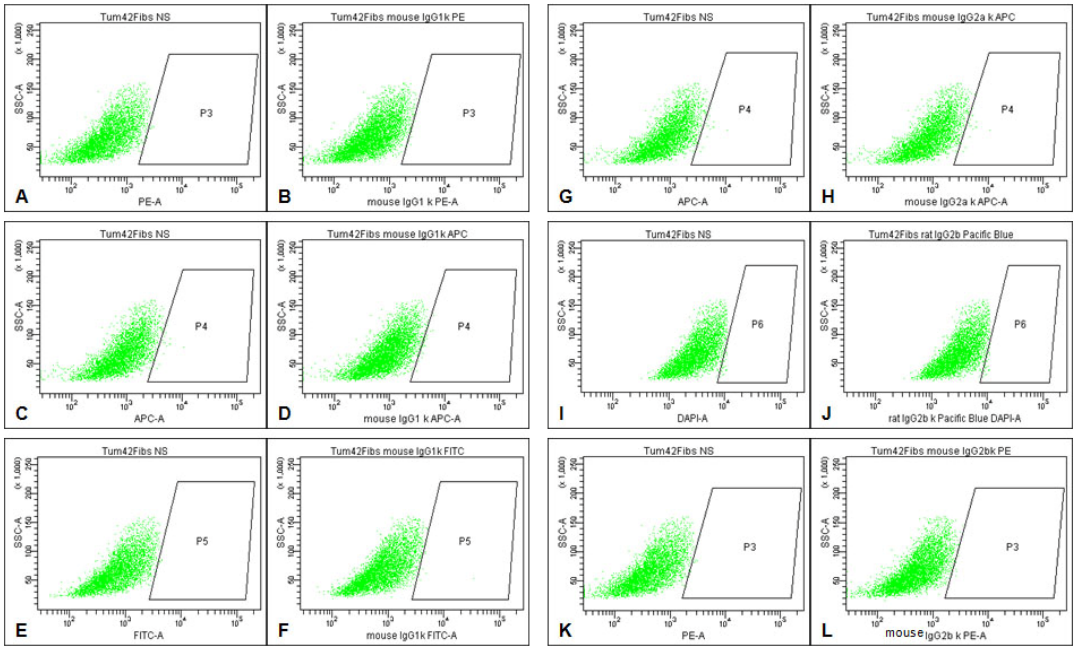

Figure 2: FACS isotype control antibodies tested on tumour-derived fibroblasts. Cultured tumour fibroblasts were trypsinised and stained with isotype control antibodies conjugated to different fluorophors. Each stained sample (in B, D, F, H, J, L) was compared to a sample with no added antibody ("CA1 NS" in A, C, E, G, I, K) analysed at the same time. Three different mouse IgG1 κ isotype control antibodies conjugated to PE (B) APC (D) and FITC (F) were tested. There was no difference in signal intensity between these samples and the non-stained control samples (compare A and B, C and D, E and F). Similarly, immunolabelling with APC conjugated mouse IgG2a (H), pacific blue conjugated rat IgG2b (J) and PE conjugated mouse IgG2b (L) did not result in an increase in signal intensity (compare G and H, I and J, K and L).

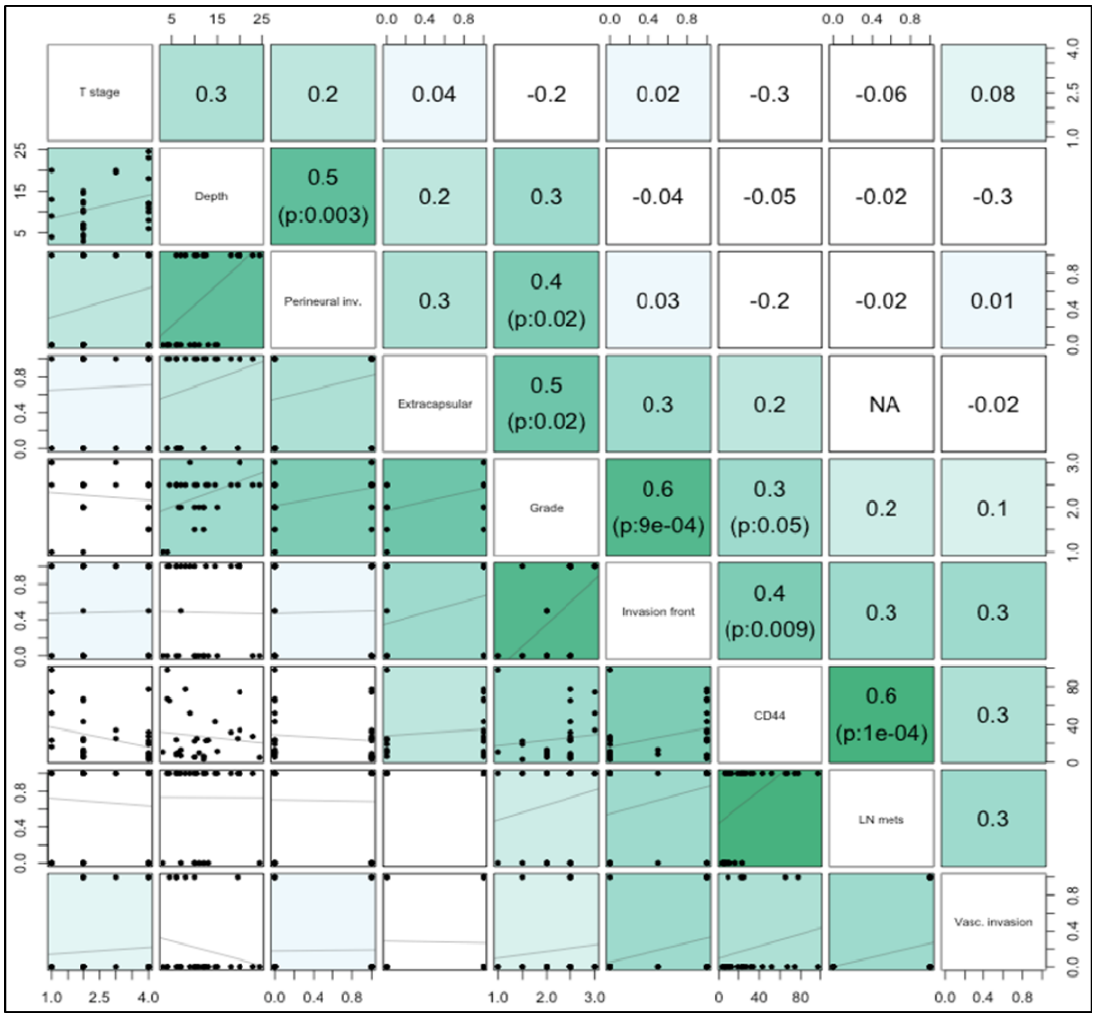

Figure 3: Spearman correlation matrix. Different shades of green represent different strengths of correlation between high frequency of CD44 expressing cells and the clinical parameter in question. The p-values for each correlation are given in brackets. The strongest correlation (dark green) was found with the presence of lymph node metastases. A weaker but significant correlation (lighter green) was found with the discohesive invasion front and high grade of the tumour. No correlation (white) was observed with T stage.

Table 1: Clinical and pathological parameters of OSCC samples that gave rise to epithelial cell lines*

Patient	TNM	Oral cavity site	Gender/ Age	Depth [mm]	Grade	Perineural invasion	Lymphovasc. invasion	Extracaps. spread	Invasion front	Excision
24	T2 N2b	floor of mouth, tongue	M 70	6,5	moderately diff.	N	N	N	largely cohesive	complete
24*n	T2 N2b	lymph node	M 72	NA	NA	NA	NA	N	NA	NA
25	T2 N2b	retromolar region	M 72	4,5	moderate to poorly diff.	N	Y	Y	discohesive, infiltrative	complete
30	T2 N1	floor of mouth	M 76	12,5	moderate to poorly diff.	Y	N	Y	discohesive	close
33	T2 N1	tongue	M 66	10.5	moderately diff	N	N	N	cohesive	complete
42	T4 N0	oral mucosa, maxilla	M 57	12	moderate to well diff	Y	N	NA	discohesive	complete
50	T2 Nx	mandible		8	moderately diff	N	N	NA	cohesive	close
57	T1 N2a	buccal mucosa, palate	F 83	20	poorly diff.	Y	N	Y	discohesive	close
57n	T1 N2a	lymph node	F 83	NA	NA	NA	NA	Y	NA	NA
AB	T4a N2c	floor of mouth	F 58	30	moderate to poorly diff	N	unknown	Y	discohesive	incomplete
EM	T3 N2b	retromolar region	M 55	6	poorly diff	Y	Y	Y	discohesive	close
GR	T2 N1	ventral tongue	M 48	4.5	moderate to poorly diff	N	Y	N	discohesive	close
LK	T2 N0	mandible, gingiva	M 56	10	moderately diff.	N	N	NA	discohesive	complete
LM	T2 N2b	mandible	F 65	20	moderately diff.	N	N	Y	cohesive	incomplete
Luc4	T3 N2b	Floor of mouth	M 78	23.5	moderate to poorly diff.	Y	N	Y	descohesive	incomplete
Luc11	T2 N0	buccal mucosa	M 38	9	moderate to poorly diff	N	N	NA	cohesive	complete

Table 1 (continued)

Patient	TNM	Oral cavity site	Gender/ Age	Depth [mm]	Grade	Perineural invasion	Lymphovasc. invasion	Extracaps. spread	Invasion front	Excision
MKn	T4a N2c	lymph node	M 61	NA	NA	NA	NA	Y	NA	NA
NA	T2 N0	tongue, (oral mucosa)	M 40	7	moderate to poorly diff.	Y	N	NA	discohesive, infiltrative	complete
NK	T3 N2a	tongue	M 56	20	poorly diff.	Y	N	Y	discohesive	incomplete
PB	T4a N0	oral mucosa, mandible	M 60	24,5	moderate to poorly diff.	Y	N	NA	discohesive	close

*diff.: differentiated; N: no; NA: not applicable; Y: yes

Table 2: Clinical and pathological parameters of OSCC samples that gave rise to fibroblastic cultures*

Patient	TNM	Oral cavity site	Gender/ Age	Depth [mm]	Grade	Perineural invasion	Lymphovasc. invasion	Extracaps. spread	Invasion front	Excision
17fibs	T4 T2	mandible	M59	4	moderately diff	N	N	Y	cohesive	close
20fibs	unknown	Soft palate	M 58	unknown	poorly diff	N	Y	unknown	discohesive	unknown
21fibs	T4 N2b	cheek and mandible	M 56	6	moderate to poorly diff.	N	N	Y	discohesive	complete
22*fibs	T4a N2b	palate, madible	M 74	15	moderate to poorly diff.	Y	N	Y	discohesive	close
23fibs	T4a N1	buccal mucosa	F 64	12	moderately diff.	Y	N	N	largely cohesive	incomplete
30fibs	T2 N1	floor of mouth	M 76	12,5	moderate to poorly diff.	Y	N	Y	discohesive	close
32fibs	T4a N1	floor of mouth, mandible	M 57	25	moderate to poorly diff.	Y	Y	N	cohesive	close
33fibs	T2 N1	tongue	M 66	10.5	moderately diff	N	N	N	cohesive	complete
37fibs	T4 N0	Maxilla, buccal mucosa	F 50	10	moderate to well	N	N	NA	discohesive	close
40fibs	T4a N2c	mandible	M 57	6.5	moderate to poorly diff.	N	N	Y	cohesive	close
41fibs	unknown	maxilla	F41	18	moderate to well diff.	Y	Y	unknown	discohesive	close
42fibs	T4 N0	oral mucosa, maxilla	M 57	12	moderate to well diff	Y	N	NA	discohesive	complete
55fibs	unknown	gingiva	M 65	unknown	moderately diff.	unknown	unknown	unknown	unknown	unknown
56fibs	T1 N0	floor of mouth	M 60	13	moderate to poorly diff.	N	N	NA	discohesive	complete
57fibs	T1 N2a	buccal mucosa, palate	F 83	20	poorly diff.	Y	N	Y	discohesive	close
Afibs	T4a N1	tongue, oropharynx	M 56	23	moderate to poorly diff.	Y	N	Y	largely cohesive	close

Table 2 (continued)

Patient	TNM	Oral cavity site	Gender/ Age	Depth [mm]	Grade	Perineural invasion	Lymphovasc. invasion	Extracaps. spread	Invasion front	Excision
Anfibs	T4a N1	lymph node	M 56	NA	NA	NA	NA	Y	NA	NA
ABfibs	T4a N2c	floor of mouth	F 58	30	moderate to poorly diff	N	unknown	Y	discohesive	incomplete
GRfibs	T2 N1	ventral tongue	M 48	4.5	moderate to poorly diff	N	Y	N	discohesive	close
JFfibs	T1 N0	floor of mouth	M 65	2.5	moderately diff	N	N	NA	discohesive	close
JNfibs	T2 N0	floor of mouth	M 54	8.5	moderate to poorly diff.	N	N	NA	discohesive	close
LMfibs	T2 N2b	mandible	F 65	20	moderately diff.	N	N	Y	cohesive	incomplete
NAfibs	T2 N0	tongue, (oral mucosa)	M 40	7	moderate to poorly diff.	Y	N	NA	discohesive, infiltrative	complete
NKfibs	T3 N2a	tongue	M 56	20	poorly diff.	Y	N	Y	discohesive	incomplete
PBfibs	T4a N0	oral mucosa, mandible	M 60	24,5	moderate to poorly diff.	Y	N	NA	discohesive	close

*diff.: differentiated; N: no; NA: not applicable; Y: yes

Table 3: Clinical and pathological parameters of tumour samples analysed by flow cytometry for expression of CD44.*

Patient	TNM	Oral cavity site	Gender/ Age	Depth [mm]	Grade	Perineural invasion	Lymphovasc. invasion	Extracaps. spread	Invasion front	Excision
18	T4 N0	mucosa of the mandible	F 56	11	moderately diff.	N	N	NA	cohesive	complete
21	T4 N2b	cheek and mandible	M 56	6	moderate to poorly diff.	N	N	Y	discohesive	complete
23	T4a N1	buccal mucosa	F 64	12	moderately diff.	Y	N	N	largely cohesive	incomplete
24	T2 N2b	floor of mouth, tongue	M 70	6,5	moderately diff.	N	N	N	largely cohesive	complete
25	T2 N2b	retromolar region	M 72	4,5	moderate to poorly diff.	N	Y	Y	discohesive, infiltrative	complete
27	T4 N0	oral mucosa, mandible	M 88	unknown	moderate to poorly diff.	Y	N	NA	discohesive, infiltrative	close
30	T2 N1	floor of mouth	M 76	12,5	moderate to poorly diff.	Y	N	Y	discohesive	close
42	T4 N0	oral mucosa, maxilla	M 57	12	moderate to well diff	Y	N	NA	discohesive	complete
44	T4 N2b	mandibular alveolus	F 76	8	poorly to moderately diff.	Y	Y	Y	discohesive	incomplete
46	T2 N0	buccal mucosa	M 62	3	well diff.	N	N	NA	cohesive	complete
46 (2)	T4 N2b	maxilla	M 85	unknown	moderate to well diff.	N	N	N	discohesive	complete
47	T2 N2b	lateral boarder of the tongue	F 81	12	moderately diff.	Y	N	Y	cohesive	close
48	T4 N2a	maxilla	F 61	10	moderate to well diff.	N	Y	Y	focally discohesive	complete
52	T2 N2b	floor of mouth, gingiva	M 86	6	moderate to poorly diff.	Y	Y	Y	cohesive	incomplete
54	T1 N1	tongue, oral mucosa	F 50	4	well diff.	N	N	N	cohesive	complete

Table 3 (continued)

Patient	TNM	Oral cavity site	Gender/ Age	Depth [mm]	Grade	Perineural invasion	Lymphovasc. invasion	Extracaps. spread	Invasion front	Excision
56	T2 N2c	tongue	F 47	15	moderately diff.	N	N	Y	discohesive	close
56 CM	pT1 N0	flour of mouth, ventral tongue	M 60	13	moderate to poorly diff.	N	N	NA	discohesive	complete
57JK	T1 N2a	buccal mucosa, palate	F 83	20	poorly diff.	Y	N	Y	discohesive	close
60	T2 N2b	buccal mucosa, mandibular alveolus	F 85	4	well to moderately diff.	N	N	Y	discohesive	incomplete
A	T4a N1	tongue, oropharynx	M 56	23	moderate to poorly diff.	Y	N	Y	largely cohesive	close
AB	T2 N1	tongue	M 64	14,5	moderate to poorly diff.	N	N	Y	discohesive	complete
CB	T2 N2b	tongue	F 63	10,5	moderate to poorly diff.	Y	N	Y	largely cohesive	close
EB	T4a N0	mandible	M 79	unknown	moderately diff.	N	N	NA	largely cohesive	close
IS	T2 N0	tongue	F 88	10	moderate to poorly diff.	Y	N	NA	discohesive	close
IV	T1 N1	tongue	F 69	9	poorly diff.	N	N	N	discohesive	complete
KR	T2 N1	tongue	F 57	7	moderately diff.	N	N	N	cohesive,	complete
PB	T4a N0	oral mucosa, mandible	M 60	24,5	moderate to poorly diff.	Y	N	NA	discohesive	close
LK	T2 N0	mandible, gingiva	M 56	10	moderately diff.	N	N	NA	discohesive	complete
MB	T1 N0	tongue	F 67	9,5	moderate to poorly diff.	N	N	NA	discohesive	complete
MK	T4a N2c	tongue, oral mucosa	M 61	18	moderate to poorly diff.	Y	N	Y	discohesive	close
MP	T3 N2b	tongue	M 54	19,5	moderate to poorly diff.	Y	Y	N	discohesive	close

Table 3 (continued)

Patient	TNM	Oral cavity site	Gender/ Age	Depth [mm]	Grade	Perineural invasion	Lymphovasc. invasion	Extracaps. spread	Invasion front	Excision
NA	T2 N0	tongue, (oral mucosa)	M 40	7	moderate to poorly diff.	Y	N	NA	discohesive, infiltrative	complete
NK	T3 N2a	tongue, slective neck diss	M 56	20	poorly diff.	Y	N	Y	discohesive	incomplete
RA	T2 N1	tongue	M 66	6	moderate to poorly diff.	N	Y	N	discohesive	close

*diff.: differentiated; N: no; NA: not applicable; Y: yes

Table 4: Quantification of the purity of epithelial and non-epithelial fractions of tumour cells separated by the negative or the positive selections (full sample list)*

	Negative selection		Positive selection	
	CK^- cells in negative (epi) fraction	CK^+ cells in positive (non-epi) fraction	CK^- cells in positive (epi) fraction	CK^+ cells in negative (non-epi) fraction
Tum AB	32/62 7/47 20/51 16/41 9/46 33/68 117/315 **(37.1%)** **epi 62.9%**	1/46 7/38 4/37 0/35 5/36 3/34 20/226 **(8.8%)** **epi 8.8%**	7/28 13/45 12/46 16/41 1/33 5/43 13/42 67/278 **(24.1%)** **epi 75.9%**	3/91 3/51 3/90 3/86 0/47 2/93 14/458 **(3.1%)** **epi 3.1%**
Tum LM	1/17 1/19 1/13 3/49 **(6.1%)** **epi 93.9%**	2/8 5/8 5/21 4/8 8/41 3/20 27/106 **(25.5%)** **epi 25.5%**	55/119 40/72 21/64 9/40 125/295 **(42.4%)** **epi 57.6%**	5/5 6/10 4/7 6/15 6/10 27/47 **(57.4%)** **epi 57.4%**
Tum GR	NA	NA	10/183 9/115 7/165 5/126 2/43 2/45 5/32 40/709 **(5.6%)** **epi 94.4%**	2/100 5/76 7/56 3/135 17/367 **(4.6%)** **epi 4.6%**
Tum ABn	34/86 32/102 28/104 38/105 27/97 9/38 9/30 177/562 **(31.5%)** **epi 68.5%**	2/105 1/109 1/124 3/58 2/70 1/104 1/28 0/29 11/627 **(1.8%)** **epi 1.8%**	NA	NA

Table 4 (continued):

	Negative selection		Positive selection	
	CK^- cells in negative (epi) fraction	CK^+ cells in positive (non-epi) fraction	CK^- cells in positive (epi) fraction	CK^+ cells in negative (non-epi) fraction
Tum RM	1/6 0/8 1/9 2/23 **(8.7%)** **epi 91.3%**	7/28 9/17 6/18 22/63 **(34.9%)** **epi 34.9%**	NA	NA

*Cells in up to 8 different fields of view were counted. Each line shows the number of contaminating cells per total number of cells counted in one field of view. The sum of all fields of view counted per sorted cell fraction is also shown and degree of contamination is given in brackets as a percentage. The percentage of epithelial cells (epi) in each sorted fraction is also shown and highlighted in yellow. NA: not analysed

Published OnlineFirst June 17, 2011; DOI: 10.1158/0008-5472.CAN-11-1059

Tumor and Stem Cell Biology

Cancer Research

Cancer Stem Cells in Squamous Cell Carcinoma Switch between Two Distinct Phenotypes That Are Preferentially Migratory or Proliferative

Adrian Biddle[1], Xiao Liang[2], Luke Gammon[2], Bilal Fazil[1], Lisa J. Harper[1], Helena Emich[1], Daniela Elena Costea[2], and Ian C. Mackenzie[1]

Abstract

Epithelial-to-mesenchymal transition (EMT) is an important driver of tumor invasion and metastasis, which causes many cancer deaths. Cancer stem cells (CSC) that maintain and initiate tumors have also been implicated in invasion and metastasis, but whether EMT is an important contributor to CSC function is unclear. In this study, we investigated whether a population of CSCs that have undergone EMT (EMT CSCs) exists in squamous cell carcinoma (SCC). We also determined whether a separate population of CSCs that retain epithelial characteristics (non-EMT CSCs) is also present. Our studies revealed that self-renewing CSCs in SCC include two biologically-distinct phenotypes. One phenotype, termed $CD44^{high}ESA^{high}$, was proliferative and retained epithelial characteristics (non-EMT CSCs), whereas the other phenotype, termed $CD44^{high}ESA^{low}$, was migratory and had mesenchymal traits characteristic of EMT CSCs. We found that non-EMT and EMT CSCs could switch their epithelial or mesenchymal traits to reconstitute the cellular heterogeneity which was characteristic of CSCs. However, the ability of EMT CSCs to switch to non-EMT character was restricted to cells that were also $ALDH1^+$, implying that only $ALDH1^+$ EMT cells had the ability to seed a new epithelial tumor. Taken together, our findings highlight the identification of two distinct CSC phenotypes and suggest a need to define therapeutic targets that can eradicate both of these variants to achieve effective SCC treatment. *Cancer Res; 71(15); 5317–26. ©2011 AACR.*

Introduction

Several studies have implicated cancer stem cells (CSC) in tumor invasion and metastasis (1, 2) and have related tumor recurrence after therapy to therapeutic resistance of CSCs (3, 4). Typically, CSCs are defined as a subpopulation of tumor cells having both tumour-initiating ability and the ability to reconstitute the cellular heterogeneity typical of the original tumor (5). For solid tumors, CSCs with these properties were first shown in breast cancers as cells with a $CD44^{high}CD24^{low}ESA^+$ staining pattern (6). As for several other malignancies, a subpopulation of $CD44^{high}$ cells with CSC properties has been identified within oral squamous cell carcinoma (OSCC; Ref. 7). In breast cancer and OSCC, subpopulations of cells with CSC properties have also been identified by positive activity of the detoxifying enzyme ALDH1 (8, 9).

Epithelial-to-mesenchymal transition (EMT) is a developmental process that creates mesoderm during gastrulation, in which epithelial cells acquire a migratory mesenchymal phenotype (10). In adult tissues, several stromal signals including TGF-β can induce EMT and lead to downregulation of epithelial products such as E-cadherin and upregulation of EMT-inducing transcription factors, such as Twist and Snail (11, 12). EMT has been proposed to play important roles in cancer and mutations in receptor tyrosine kinase or Wnt signaling pathways can predispose cells to undergo EMT (13). In cancer there is further promotion of EMT by both the inflammatory immune response (14) and by the hypoxic tumor environment (15). Breast-cancer cells with the $CD44^{high}CD24^{low}$ tumor-initiating phenotype express EMT markers, a finding that established a link between CSCs and EMT (16) and it is now increasingly recognized that EMT plays an important role in the metastasis of OSCC (15), breast cancer (17), and several other types of carcinoma. EMT has been implicated in therapeutic resistance and tumour recurrence (4, 18, 19) and is associated with resistance to EGFR inhibitors (20) and evasion of host immune responses to tumors (17, 21).

Authors' Affiliations: [1]Blizard Institute of Cell and Molecular Science, Barts and the London School of Medicine and Dentistry, Queen Mary University of London, 4 Newark Street, London; and [2]Gade Institute, University of Bergen, Haukeland University Hospital, Bergen, Norway

Note: Supplementary data for this article are available at Cancer Research Online (http://cancerres.aacrjournals.org/).

Corresponding Author: Adrian Biddle, Centre for Cutaneous Research, Blizard Institute of Cell and Molecular Science, 4 Newark Street, London, E1 2AT, UK. Phone: 44-20-7882-2342; Fax: 44-20-7882-7172; E-mail: a.biddle@qmul.ac.uk

doi: 10.1158/0008-5472.CAN-11-1059

Published OnlineFirst June 17, 2011; DOI: 10.1158/0008-5472.CAN-11-1059

Normal epithelial tissues are maintained by a proliferative stem-cell hierarchy and, when epithelial cells are seeded at low density *in vitro*, the stem cell fraction generates proliferating colonies termed holoclones that can be distinguished from the abortive colonies of differentiating cells, termed paraclones (22). Similar clonal patterns are present in cell lines generated from OSCC (23) and also from prostate cancers where holoclone cells, but not paraclone cells, are capable of forming tumors in mouse xenograft models (24). Here we show that, in addition to a holoclone-forming CSC population, cell lines derived from human oral and cutaneous SCC contain a novel CSC population that has undergone EMT and is migratory. The EMT and non-EMT CSC populations both show high expression of CD44 and the two populations coexist by switching between the two phenotypic states through EMT and the reverse process of mesenchymal-to-epithelial transition (MET). Both cell types are also present in cells freshly generated from OSCC tumors. We also show a further novel hierarchy within the EMT cell subpopulation itself that is related to the ability of cells to switch back to the non-EMT state.

Materials and Methods

Cell culture

The CA1 cell line was previously derived in our laboratory from a biopsy of OSCC of the floor of the mouth (25). The PM1, Met1, and Met2 cell lines were derived from matched premalignant and malignant cutaneous SCC tissues (26). All cell lines were grown in the highly supplemented epithelial growth medium (termed FAD) with 10% FBS (23). For suspension cultures, 0.75 cm^2 tissue culture wells were coated with polyhema (Sigma) (12mg/ml in 95% ethanol). Cells were then plated at a density of 1000 cells/ml with addition of 1% methylcellulose (Sigma) and incubated (37°C, 5% CO_2) and monitored for sphere growth. For TGF-β experiments, 20 ng/ml TGF-β (R&D systems) was added to the culture every 24 hours for 5 days. For inhibition, 10 μmol/L SB431542 (Sigma) was added either simultaneously with the TGF-β additions or for 5 days following 5 days of TGF-β treatment.

Fluorescence-activated cell sorting and immunofluorescence

For fluorescence-activated cell sorting (FACS), cells were detached using either trypsin-EDTA (PAA) or enzyme-free cell dissociation buffer (Invitrogen) at 37°C and then stained with antibodies at 1:100 dilution in PBS (PAA). The DAPI nuclear dye (Sigma) was used at 1 ug/ml to exclude dead cells. FACS sorted cells were collected into FAD medium for plating or into buffer RLT for RNA extraction. To test for ALDH1 activity, cells were stained with Aldefluor reagent (Aldagen) according to the manufacturers instructions prior to FACS. For immunofluorescence, cells were fixed in 4% paraformaldehyde, stained with antibodies at 1:100 dilution in PBS with 0.25% BSA, then permeabilized with 0.1% Triton-X prior to addition of DAPI at 1 ug/ml prior to imaging. The PE-CD44 (clone G44-26) and PE-Integrin β4 (clone 439-9B) antibodies were from BD biosciences; the APC-ESA (clone HEA-125) antibody was from Miltenyi Biotec.

RNA extraction, cDNA synthesis, and qPCR

RNA was extracted using the RNeasy micro kit (Qiagen). Reverse transcription into cDNA was conducted using the superscript III first strand synthesis supermix (Invitrogen), with inclusion of RT controls. QPCR was conducted in an ABI 7500 real-time PCR system (Applied Biosystems) using Power SYBR green mix (Applied Biosystems). GAPDH was used as a reference mRNA control. See supporting information for QPCR conditions and primer sequences.

Migration assays

10,000 cells were placed in FAD medium with 2% FBS in Transwell tissue culture inserts (8 μm membrane, Corning) in 24-well plates, with FAD medium containing 10% FBS in the bottom of the well. After 24 hours, the membranes were fixed in 4% paraformaldehyde, stained with crystal violet, the non-migrated cells on the top of the membrane removed with a cotton-wool bud, and the migrated cells on the underside of the membrane counted.

Generation of cells from primary human samples

Fresh OSCC tissue samples were collected following protocols approved by the local NHS Research Ethics Committee. They were minced into small pieces in tissue culture dishes, allowed to adhere, and FAD medium then added. Outgrowths of cells arising from the tumor pieces were dissociated and FACS sorted for the epithelial-specific marker Integrin β4 to collect fibroblast-free populations prior to examination.

Single-cell cloning

For single-cell cloning of the $CD44^{high}ESA^{high}$ and $CD44^{high}ESA^{low}$ populations, cells were sorted by FACS and then allowed to recover in culture before being resuspended, counted, and single-cell cloned in 48-well plates by limiting dilution. Wells were examined microscopically and those containing only a single clone were grown up for analysis. For single-cell cloning of the $CD44^{high}ESA^{low/+}$ and $CD44^{high}ESA^{low/-}$ populations, cells were sorted directly into 96-well plates using the single-cell plate sorting function of the FACSAria FACS sorter (BD biosciences). Clones were then checked and grown up as described above.

Tumourigenesis assays in mice

For these assays, which were performed at the Gade Institute in Bergen, nonobese diabetic/severe combined immunodeficiency (NOD/SCID) mice were used with all animal procedures approved by the Norwegian Animal Research Authority. Subpopulations of FACS-sorted $CD44^{high}ESA^{high}$ and $CD44^{high}ESA^{low}$ CA1 cells were suspended in 50 μL of Matrigel (BD Biosciences) and transplanted into the tongue. Immunohistochemical staining was carried out using the Autostainer universal staining system (DAKO-USA; Ref. 27). Five-μm formalin-fixed, paraffin-embedded sections from the tongues and neck lymph nodes of mice injected with different subpopulations of CA1 cells were stained with H&E or for p53 protein with a monoclonal specific antibody (DO-7 clone, titration 1:50; DAKO-Denmark).

Published OnlineFirst June 17, 2011; DOI: 10.1158/0008-5472.CAN-11-1059

Statistical analysis

All data are based on at least three experimental repeats unless otherwise stated, and are reported as mean ±SEM.

Results

A CD44^{high}ESA^{low} subpopulation exists in oral squamous cell carcinoma

Flow cytometric analysis of the CA1 cell line showed that a combination of staining for CD44 and ESA (epithelial-specific antigen, also known as EpCAM) consistently identified a CD44^{high}ESA^{low} subpopulation (Fig. 1A). The coexpression of high CD44, typical of a CSC, together with low expression of the epithelial marker, ESA, suggested the possible correspondence of this population to an EMT CSC subpopulation. Cells with CD44^{high}ESA^{high}, CD44^{high}ESA^{low}, and CD44^{low} expression patterns were therefore examined to establish their relationships respectively to (a) holoclone-forming, non-EMT CSCs, (b) CSCs that have undergone an EMT, and (c) paraclone-forming cells that lack the capacity to self-renew.

Morphological and behavioral differences between cell subpopulations in adherent and suspension cultures point to two distinct cancer stem cell phenotypes

As previously described, OSCC cells (including the CA1 cell line) plated at low density in adherent cultures form a range of colony morphologies, including self-renewing CD44^{high}ESA^{high} holoclone and differentiating CD44^{low} paraclone colonies (23, 28). However, when cultures were examined in more detail, individual elongated cells lying outside the compact holoclone colonies could be identified (Supplementary Fig. S1A) and were found to have a CD44^{high}ESA^{low} staining pattern (Supplementary Fig. S1B). When cell subpopulations were isolated by FACS and replated in culture, the CD44^{high}ESA^{low} cells displayed an elongated fibroblast-like appearance and dispersal as individual cells, characteristics of cells having undergone EMT (Fig. 1B, middle). CD44^{high}ESA^{high} cells grew as holoclones (Fig. 1B, left) and the CD44^{low} cells formed small abortive paraclone colonies (Fig. 1B, right). Counting the number of holoclones formed after plating the two non-EMT populations at clonal density

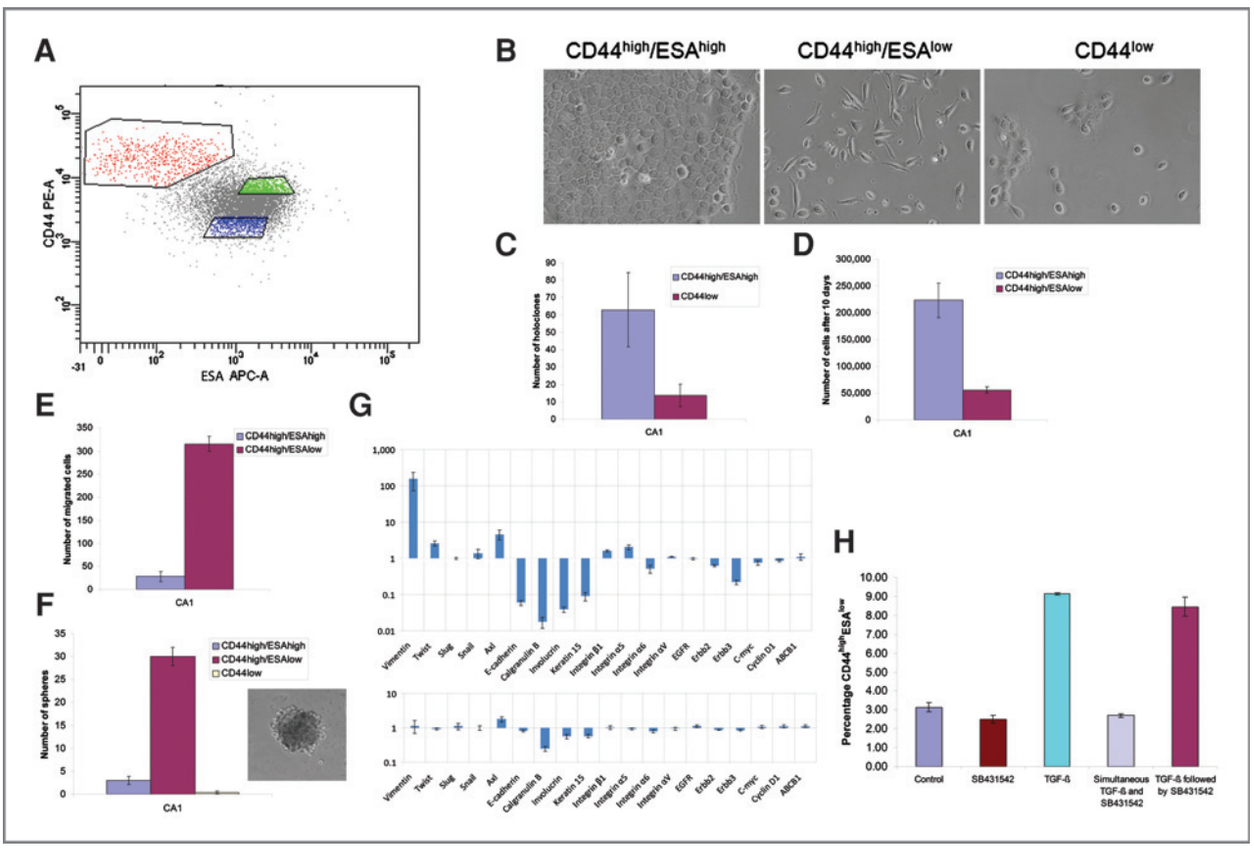

Figure 1. The CA1 OSCC cell line contains cancer stem cells that have undergone EMT. A, FACS sorting of CA1 cells by expression of CD44 and ESA. Sorted populations are gated. B, phase-contrast images of the populations shown in (A), after being plated at clonal density (1,000 cells/ml) and allowed to grow for 7 days. C, holoclone counts for the CD44^{high}ESA^{high} and CD44^{low} populations, after plating at clonal density. D, cell counts (cells/ml) for the CD44^{high}ESA^{high} and CD44^{high}ESA^{low} populations, 10 days after plating at clonal density. E, the number of migrated cells from the CD44^{high}ESA^{high} and CD44^{high}ESA^{low} populations in Transwell migration assays. F, Left, sphere counts for the populations shown in (A). Right, a typical CA1 sphere. G, QPCR analysis of the populations shown in (A). Top, gene expression in CD44^{high}ESA^{low} cells relative to that in CD44^{low} cells. Bottom, gene expression in CD44^{high}ESA^{high} cells relative to that in CD44^{low} cells. H, the size of the CD44^{high}ESA^{low} population (as % of total cell number) after 5 days of treatment with TGF-β or the TGF-β inhibitor SB431542.

Published OnlineFirst June 17, 2011; DOI: 10.1158/0008-5472.CAN-11-1059

confirmed that the $CD44^{high}ESA^{high}$ cells represent the holoclone-forming CSC type (Fig. 1C).

Sorted populations of $CD44^{high}ESA^{low}$ cells grew slower in adherent culture conditions than the $CD44^{high}ESA^{high}$ cells (Fig. 1D). Time-lapse video showed the high motility of these cells (Supplementary Movies S1A and S1B) and also suggested the generation and escape of motile cells at the periphery of holoclone colonies. $CD44^{high}ESA^{low}$ cells showed a much higher rate of migration in 3-dimensional *in vitro* transwell migration assays (Fig. 1E and Supplementary Fig. S1C).

As ability to grow as floating spheres is a characteristic of CSCs in breast (29) and brain tumors (30), we counted the number of spheres formed when the three populations were seeded in suspension culture using nonadherent plates (Fig. 1F). The $CD44^{high}ESA^{low}$ cells formed 10 times more spheres than the $CD44^{high}ESA^{high}$ cells, and 80 times more than the $CD44^{low}$ cells. The $CD44^{high}ESA^{low}$ cells therefore represent a subpopulation of CSCs greatly enriched for sphere-forming ability. Laser capture of central and peripheral cell areas of epithelial colonies, followed by their transfer to suspension culture, indicated that the cells around colony peripheries form spheres (Supplementary Fig. S1D), whereas those in the center of colonies yield no spheres, a further confirmation of the presence of $CD44^{high}ESA^{low}$ EMT CSCs at the colony peripheries.

An epithelial-to-mesenchymal transition–related gene expression pattern in the $CD44^{high}ESA^{low}$ cells

To investigate the expression of EMT-related genes, we undertook quantitative RT-PCR of the $CD44^{high}ESA^{low}$, $CD44^{high}ESA^{high}$, and $CD44^{low}$ populations. This showed (Fig. 1G) that the $CD44^{high}ESA^{low}$ cells have greater expression of Vimentin, Twist, Snail, and Axl, all markers of EMT, and lower expression of the epithelial-specific genes E-cadherin, Calgranulin B, Involucrin, and Keratin 15. Expression of Integrins α5 and β1 was moderately greater and expression of Integrin α6, C-myc, and the Erbb2 and Erbb3 receptors was lower. Far smaller differences were seen between the $CD44^{high}ESA^{high}$ and $CD44^{low}$ populations although $CD44^{high}ESA^{high}$ cells showed moderately greater expression of Axl, and lower expression of Calgranulin B and Involucrin indicating less expression of epithelial-differentiation markers. Antibody staining for Vimentin (Supplementary Fig. S1E) showed that the elongated cells around colony peripheries express Vimentin, whereas those inside the colonies do not.

TGF-β is a known inducer of EMT and, for further confirmation that the $CD44^{high}ESA^{low}$ population represents cells having undergone EMT, we added TGF-β to cell cultures and examined the CD44 and ESA cell surface-staining pattern (Fig. 1H). After TGF-β addition the $CD44^{high}ESA^{low}$ population approximately tripled in size, indicating that enhanced induction of EMT causes cells to acquire the $CD44^{high}ESA^{low}$ staining pattern. Addition of SB431542, a potent and selective TGF-β inhibitor, completely reversed the ability of TGF-β to drive an enlargement of the $CD44^{high}ESA^{low}$ population. Interestingly, however, SB431542 did not cause the size of the $CD44^{high}ESA^{low}$ population to drop below that seen in the control cells, nor did it reverse the TGF-β induced EMT once established, indicating that TGF-β is not required for the maintenance of the EMT phenotype.

Epithelial-to-mesenchymal transition cancer stem cells are present in cell lines generated from progressive stages of cutaneous squamous cell carcinoma

We next investigated whether the $CD44^{high}ESA^{low}$ EMT CSC population identified in OSCC is also present in cell lines derived from cutaneous SCC. Such cells were present in 3 matched specimens derived from the same patient (26) and measurement of the size of the $CD44^{high}ESA^{low}$ populations in each of these three cell lines revealed stark differences between different stages of malignancy (Fig. 2A). PM1, a cell line derived from premalignant dysplastic skin, did not contain a detectable $CD44^{high}ESA^{low}$ population. Met1, a line derived from a primary SCC, contained a $CD44^{high}ESA^{low}$ population representing 2.2 ± 0.25% of the total population (Fig. 2B). Met2, a line derived from a recurrent SCC arising at the same site, contained a $CD44^{high}ESA^{low}$ population representing 29.7 ± 5.73% of the total (Fig. 2C).

Quantitative RT-PCR of FACS sorted populations from Met1 and Met2 (Fig. 2D) showed patterns similar to those for OSCC. In both cell lines, the $CD44^{high}ESA^{low}$ cells show greater expression of Vimentin than the $CD44^{high}ESA^{high}$ and $CD44^{low}$ cells, and have lower expression of E-cadherin, Calgranulin B, Involucrin, Keratin 15, Integrin α6, C-myc, Erbb2, and Erbb3. In Met2, the $CD44^{high}ESA^{low}$ cells also have greater expression for Twist, Snail, and Axl, perhaps suggesting that they have undergone a more complete EMT than the corresponding population in Met1. As with the CA1 OSCC line, only small differences were seen between the $CD44^{high}ESA^{high}$ and $CD44^{low}$ populations in Met1 and Met2 (Fig. 2D, bottom).

Adherent cultures of $CD44^{high}ESA^{low}$ cells of both cell lines showed an elongated, fibroblast-like appearance (Fig. 2E, middle), whereas $CD44^{high}ESA^{high}$ cells grew as holoclones (Fig. 2E, left), and $CD44^{low}$ cells formed small paraclone colonies (Fig. 2E, right). As with OSCC, holoclone counts confirmed that the $CD44^{high}ESA^{high}$ population represents the non-EMT CSC type (Fig. 2F) and sphere formation in suspension culture indicated that in both lines the $CD44^{high}ESA^{low}$ cells represent a subpopulation of CSCs greatly enriched for sphere forming ability (Fig. 2G). In comparison to $CD44^{high}ESA^{high}$ cells, $CD44^{high}ESA^{low}$ cells proliferated at a slower rate in adherent culture (Fig. 2H) and had a greater ability to migrate in a 3D *in vitro* Transwell migration assay (Fig. 2I and Supplementary Fig. S2), with the latter ability considerably more pronounced in Met2. The FACS sorted $CD44^{high}ESA^{high}$ and $CD44^{high}ESA^{low}$ cells could be passaged indefinitely, further indicating their ability to self-renew.

Epithelial-to-mesenchymal transition cancer stem cells are present in cell populations freshly isolated from oral squamous cell carcinoma tumors

To determine whether an EMT CSC population exists in OSCC tumors *in vivo*, populations of cells were generated as explants from fresh samples of OSCC. After removal of

Published OnlineFirst June 17, 2011; DOI: 10.1158/0008-5472.CAN-11-1059

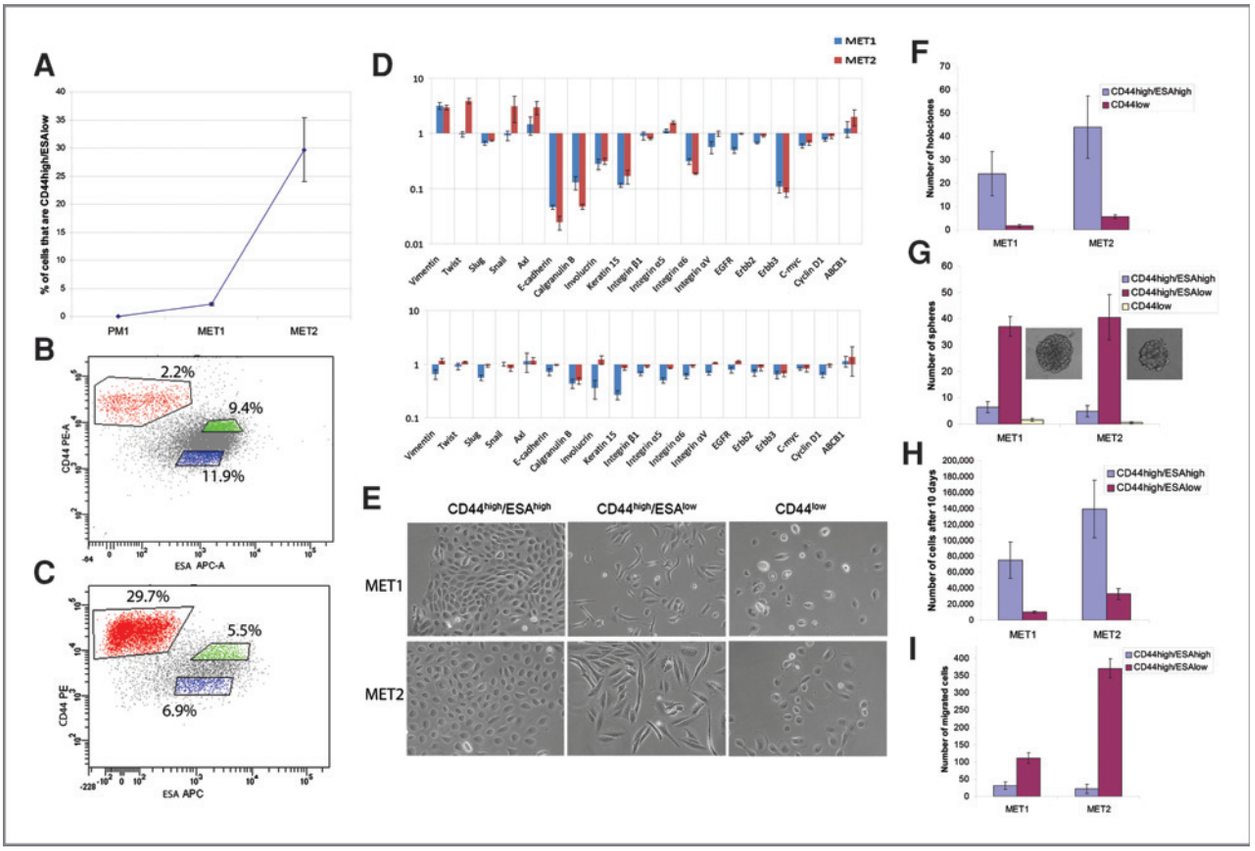

Figure 2. Cell lines from progressive stages of cutaneous SCC contain cancer stem cells that have undergone EMT. A, graph showing the % of cells in the $CD44^{high}ESA^{low}$ population of three cell lines representing progression of cutaneous SCC. B and C, FACS sorting of MET1 (B) and MET2 (C) cells by expression of CD44 and ESA. Sorted populations are gated and shown as% of total cells. D, QPCR analysis of the populations shown in (B) and (C). Top, gene expression in $CD44^{high}ESA^{low}$ cells relative to that in $CD44^{low}$ cells. Bottom, gene expression in $CD44^{high}ESA^{high}$ cells relative to that in $CD44^{low}$ cells. E, phase-contrast images of the populations shown in (B) and (C), after being plated at clonal density (1000 cells/ml) and allowed to grow for 7 days. F, holoclone counts for the $CD44^{high}ESA^{high}$ and $CD44^{low}$ populations, after plating at clonal density. G, sphere counts for the populations shown in (B) and (C). Representative MET1 and MET2 spheres are shown. H, cell counts (cells/ml) for the $CD44^{high}ESA^{high}$ and $CD44^{high}ESA^{low}$ populations, 10 days after plating at clonal density. I, the number of migrated cells from the $CD44^{high}ESA^{high}$ and $CD44^{high}ESA^{low}$ populations in transwell-migration assays.

fibroblasts, cells were FACS sorted on the basis of expression of CD44 and ESA, and were analyzed by RT-PCR. Cells explanted from each of three tumors were found to contain a $CD44^{high}ESA^{low}$ population that represented 28.0%, 8.2%, and 5.1% of the total population (Fig. 3A–C). The $CD44^{high}ESA^{low}$ cells of all three tumors showed greater expression of Vimentin and Twist and less expression of E-cadherin (Fig. 3D).

The two cancer stem cell phenotypes exhibit distinct *in vivo* behaviors that reflect their *in vitro* properties

Upon orthotopic injection into NOD/SCID mice, both CSC phenotypes show tumor initiating ability (Fig. 4A). However, only the EMT CSCs exhibited any lymph node infiltration after 26 days (Fig. 4A and Supplementary Fig. S3A). Conversely, the non-EMT CSCs exhibited faster tumor growth at early time points (Fig. 4B). Examination of tumors produced by both CSC phenotypes after 26 days by FACS (Supplementary Fig. S3B) and H&E staining (Supplementary Fig. S3C) showed a return to a heterogenous cell population and no apparent difference in tumor histology, indicating that each CSC phenotype can repopulate the other *in vivo*.

There is switching between the two cancer stem cells phenotypes, and single-cell cloning identifies a hierarchy of bipotent and unipotent epithelial-to-mesenchymal transition cells

$CD44^{high}ESA^{high}$ and $CD44^{high}ESA^{low}$ populations from CA1 and Met1 were FACS sorted and single-cell cloned to determine whether such clones give rise to both EMT and non-EMT cells, thus indicating bipotency of the clonal cell of origin. Clones were grown up, stained for CD44 and ESA, and analyzed. The results (Fig. 5) indicated that 100% of $CD44^{high}ESA^{high}$ clones were bipotent as indicated by the production of both non-EMT and EMT cell populations. Conversely, not all $CD44^{high}ESA^{low}$ clones were bipotent; only a fraction of the $CD44^{high}ESA^{low}$ clones (50% in CA1 and 29% in Met1) produced mixed populations. The rest were unipotent and, despite several subsequent rounds of passaging, gave rise only to EMT cells.

Published OnlineFirst June 17, 2011; DOI: 10.1158/0008-5472.CAN-11-1059

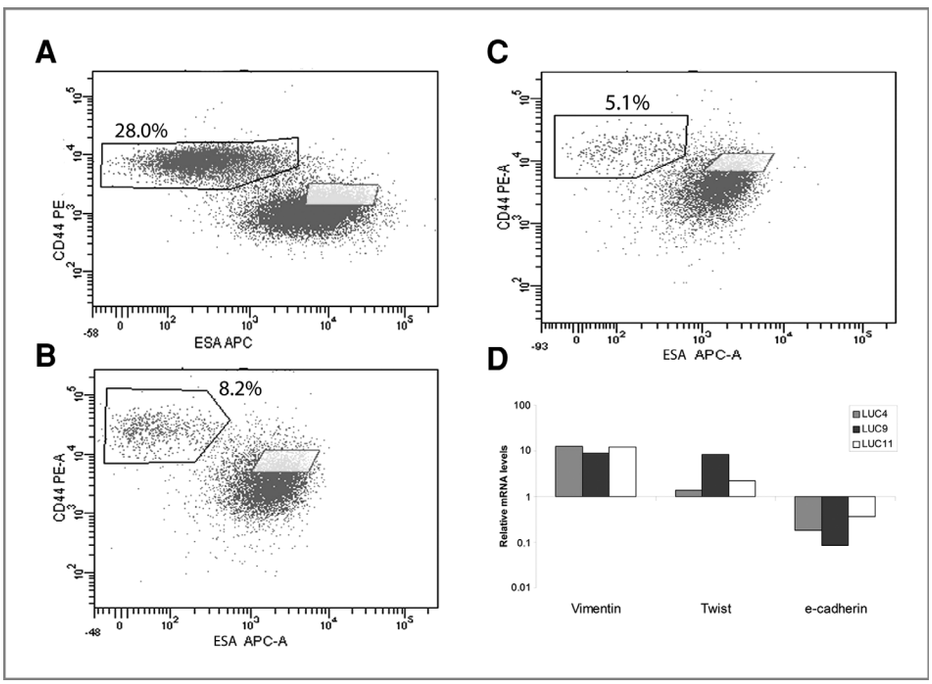

Figure 3. EMT CSCs in fresh OSCC tumors. A, B, and C, FACS sorting by expression of CD44 and ESA for cells generated from 3 OSCC tumors, termed (A) LUC4, (B) LUC9, and (C) LUC11. The $CD44^{high}ESA^{low}$ population is gated and shown as % of total cells. D, QPCR analysis of the cells generated from the 3 tumors; gene expression in the gated $CD44^{high}ESA^{low}$ population relative to that in the rest of the cells.

$CD44^{high}ESA^{low/+}$ marker expression identifies the bipotent epithelial-to-mesenchymal transition cancer stem cells

We investigated whether differences in levels of ESA expression might distinguish bipotent from unipotent EMT cells present in SCC. We FACS sorted $CD44^{high}ESA^{low/+}$ and $CD44^{high}ESA^{low/-}$ cell populations from CA1 for single-cell cloning (illustrated in Fig. 6A). Clones were grown up and assessed by FACS for the presence of both non-EMT and EMT cell populations. The results indicated that none of the $CD44^{high}ESA^{low/-}$ clones were bipotent but that heterogeneity was regenerated by 44% of the $CD44^{high}ESA^{low/+}$ clones (Fig. 6B), showing that the EMT CSCs capable of undergoing MET lie at the ESA^{high} end of the $CD44^{high}ESA^{low}$ population. Analysis of sphere forming abilities for each of the CA1, Met1, and Met2 cell lines indicated similar numbers of spheres produced by $CD44^{high}ESA^{low/+}$ and $CD44^{high}ESA^{low/-}$ populations (Fig. 6C). Therefore, despite differences in plasticity these populations have similar abilities to grow as floating spheres. A single-cell clone created from a CA1 bipotent EMT CSC was FACS sorted for single cell cloning of the $CD44^{high}ESA^{low/+}$ and $CD44^{high}ESA^{low/-}$ cell populations (Supplementary Fig. S4A). 92% of the $CD44^{high}ESA^{low/+}$ clones were bipotent whereas only 17% of the $CD44^{high}ESA^{low/-}$ clones were bipotent. The presence of a proportion of clones that were unipotent shows that the cloned bipotent EMT CSC gave rise directly to unipotent EMT cells.

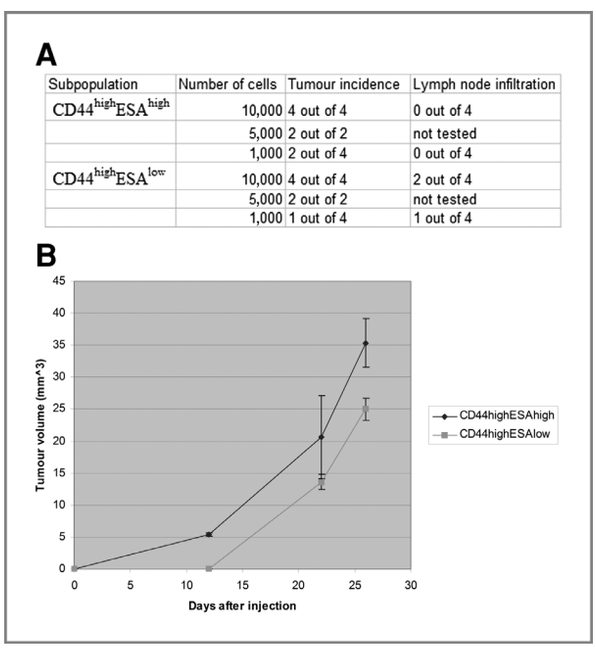

Subpopulation	Number of cells	Tumour incidence	Lymph node infiltration
$CD44^{high}ESA^{high}$	10,000	4 out of 4	0 out of 4
	5,000	2 out of 2	not tested
	1,000	2 out of 4	0 out of 4
$CD44^{high}ESA^{low}$	10,000	4 out of 4	2 out of 4
	5,000	2 out of 2	not tested
	1,000	1 out of 4	1 out of 4

Figure 4. EMT CSCs drive metastatic dissemination and non-EMT CSCs drive tumor growth *in vivo*. A, tumor incidence and rate of lymph node infiltration from orthotopic tongue injections of CA1 cells. B, tumor growth rate after orthotopic tongue injection of 5000 CA1 cells. $n = 2$.

The $CD44^{high}ESA^{low/+}$ bipotent epithelial-to-mesenchymal transition cancer stem cells are $ALDH1^{+}$

Interestingly, we found that $CD44^{high}ESA^{low/+}$ cells show considerably higher activity than $CD44^{high}ESA^{low/-}$ cells for the CSC marker ALDH1 (Fig. 6D). We therefore investigated a possible link between the bipotency of EMT CSCs and their ALDH1 activity. For each cell line, $CD44^{high}ESA^{low}$ cells were fractionated on the basis of ALDH1 activity (Fig. 6E) and then assayed for the number of non-EMT cells they produce in culture. The results

Published OnlineFirst June 17, 2011; DOI: 10.1158/0008-5472.CAN-11-1059

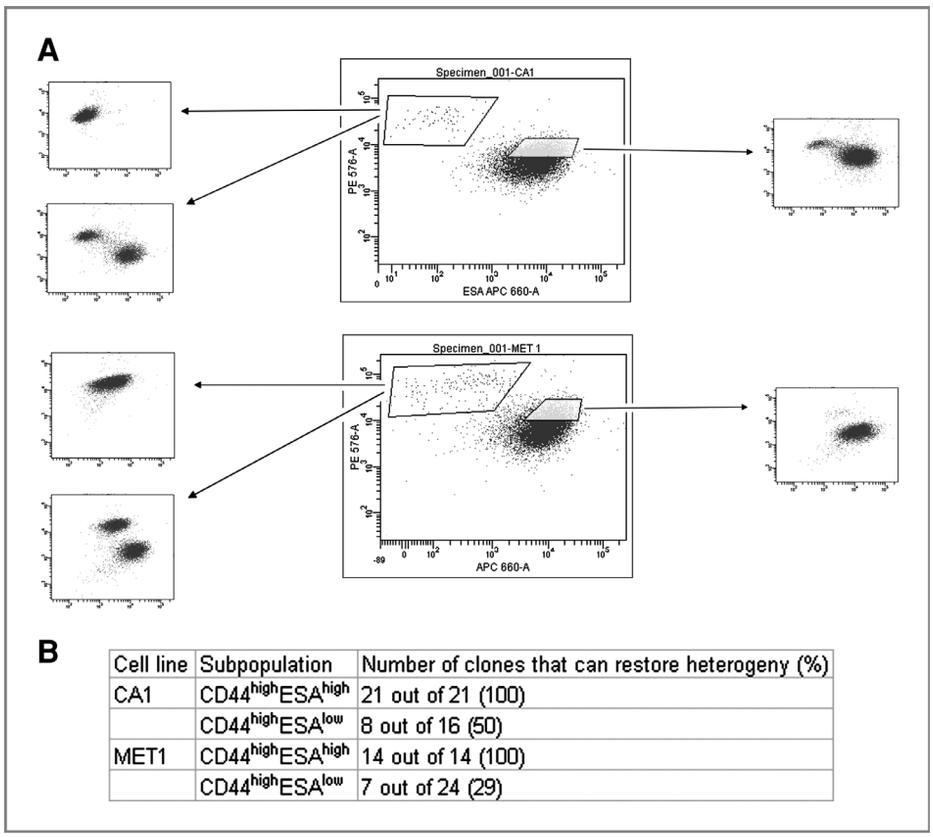

Cell line	Subpopulation	Number of clones that can restore heterogeny (%)
CA1	$CD44^{high}ESA^{high}$	21 out of 21 (100)
	$CD44^{high}ESA^{low}$	8 out of 16 (50)
MET1	$CD44^{high}ESA^{high}$	14 out of 14 (100)
	$CD44^{high}ESA^{low}$	7 out of 24 (29)

Figure 5. Single cell cloning of the CSC populations. A, FACS sorting of CA1 (top) and MET1 (bottom) cells by expression of CD44 (*y*-axis) and ESA (*x*-axis), for single cell cloning of the gated populations. To the sides are representative FACS plots of populations produced by the single cell clones. B, table showing the number of single cell clones from the two FACS sorted populations which were able to give rise to both non-EMT and EMT cells.

(Fig. 6F) show that after growing up from clonal density the percentage of non-EMT cells was consistently greater for the $CD44^{high}ESA^{low}ALDH1^{+}$ cells than for the $CD44^{high}ESA^{low}ALDH^{-}$ cells; 6.9 times, 27.4 times, and 5.9 times greater in CA1, Met1, and Met2, respectively. Therefore, high ALDH1 expression marks bipotent EMT CSCs. As for $CD44^{high}ESA^{low/+}$ and $CD44^{high}ESA^{low/-}$ cells, both bipotent $CD44^{high}ESA^{low}ALDH^{+}$ cells and unipotent $CD44^{high}ESA^{low}ALDH^{-}$ cells formed similar numbers of spheres in suspension culture (Fig. 6G). Suspension culture did not enable the unipotent $CD44^{high}ESA^{low}ALDH^{-}$ cells to change their phenotype (Supplementary Fig. S4B), indicating that their unipotent state is not an artefact of adherent culture. Assessment of 4 bipotent and four unipotent single cell clones formed from $CD44^{high}ESA^{low}$ Met1 cells indicated that the $CD44^{high}ESA^{low}$ cells in the bipotent clones had consistently greater ALDH1 activity than those in the unipotent clones (Supplementary Fig. S4C), further confirming a link between bipotent EMT CSCs and ALDH1 positivity.

Discussion

Our investigations show that cultures of malignant cell populations consistently contain motile cells with a fibroblast-like morphology and that such cells stain strongly for CD44 but only weakly for ESA. Cells with a $CD44^{high}ESA^{low}$ phenotype isolated from OSCC cell lines, from fresh samples of OSCC tumor, and from primary and recurrent cutaneous SCC, express Vimentin, Twist and Axl, genes that act as markers of EMT, and show reduced expression of epithelial markers such as e-cadherin, Involucrin and CK15. These cells proliferate slowly, are more migratory, and when grown in suspension culture they display the sphere forming ability that has previously been associated with stem cells (31). We also show a separate $CD44^{high}ESA^{high}$ cell population that, when isolated by FACS, is highly proliferative and forms holoclone colonies in adherent culture that are indefinitely self-renewing and typical of epithelial stem cells. Injection into NOD/SCID mice indicates that the attributes showed by these cells *in vitro* are maintained *in vivo*. Taken together, these findings indicate that SCCs contain CSCs with two distinct phenotypes, one similar to normal epithelial stem cells, and another similar to the EMT CSCs described by Mani and colleagues (16). These findings fit well with the "migrating cancer stem cell" concept of Brabletz (32) which requires malignant stem cells to acquire two phenotypes; one that is associated with growth and another that is migratory and characterized by "transient expression of epithelial to mesenchymal transition-associated genes, which can be reversed by a mesenchymal to epithelial transition (MET), leading to epithelial redifferentiation," and thus enables secondary tumor formation at a metastatic site.

We propose a malignant stem cell model that defines the hierarchical cellular relationships within the tumor. In this

Published OnlineFirst June 17, 2011; DOI: 10.1158/0008-5472.CAN-11-1059

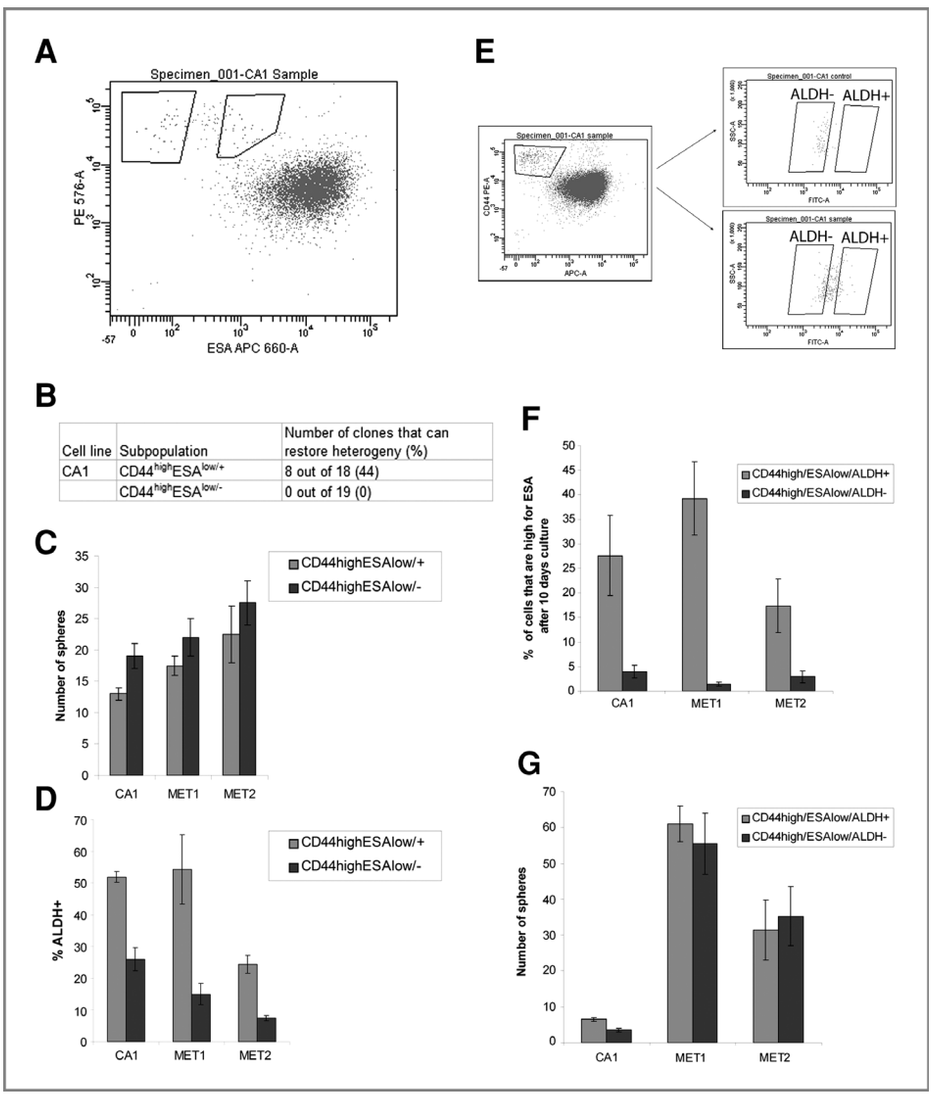

Figure 6. $CD44^{high}ESA^{low/+}ALDH1^{+}$ marker expression identifies the EMT CSCs that are capable of reconstituting tumour heterogeneity. A, FACS sorting of CA1 cells by expression of CD44 (*y*-axis) and ESA (*x*-axis), for single-cell cloning of the gated $CD44^{high}ESA^{low/+}$ and $CD44^{high}ESA^{low/-}$ populations. B, table showing the number of single cell clones from the two FACS sorted populations described in (A) which were able to give rise to both non-EMT and EMT cells. C, sphere counts for the $CD44^{high}ESA^{low/+}$ and $CD44^{high}ESA^{low/-}$ populations from CA1, MET1 and MET2. D, the percentage of the $CD44^{high}ESA^{low/+}$ and $CD44^{high}ESA^{low/-}$ cells that are $ALDH1^{+}$ (using the method described in Fig. 6E) in the CA1, MET1, and MET2 lines. E, representative FACS sort for the CA1 line, showing how the $CD44^{high}ESA^{low}$ population was selected and then fractionated on the basis of ALDH1 expression (ALDH1-FITC on the *x*-axis of the right-hand plots). The Aldefluor assay inhibitor DEAB was used to enable negative control staining for the setting of gates (top right), and then $ALDH1^{+}$ and $ALDH1^{-}$ cells were selected in the absence of the inhibitor (bottom right). F, the ability to reconstitute the heterogeneous population, as shown by the production of non-EMT cells 10 days after the FACS sorted populations described in (E) were plated at clonal density. G, sphere counts for the populations described in (E).

model (Fig. 7), $CD44^{high}ESA^{high}$ holoclone-forming non-EMT CSCs have division patterns directed largely to self-renewal but they also generate cells entering two distinct pathways of differentiation. One type loses CD44 expression, lacks self-renewal ability and forms paraclones, a change interpreted as entry into an abortive epithelial terminal differentiation pathway. The other cell type is $CD44^{high}ESA^{low}$, is migratory, and has expression patterns and behavior indicative of EMT. FACS isolation of populations of non-EMT and EMT cells indicates that the cells of one population regenerate cells of the other through reciprocal processes of EMT and MET, and this phenotypic plasticity is maintained *in vivo*; therefore, it seems that CSCs have the ability to take on an EMT phenotype for migration to a secondary site, before reverting back to the proliferative non-EMT phenotype to enable formation of a metastatic tumor at that secondary site. Single-cell cloning indicates that ability to undergo MET is restricted to a subpopulation of the EMT cells that is marked by the $CD44^{high}ESA^{low/+}ALDH^{+}$ expression pattern. Thus, whereas the non-EMT population shows a differentiation hierarchy that can be assayed as loss of self-renewal capacity, the EMT population has a secondary differentiation hierarchy that can be assayed in terms of the plasticity required to reconstitute tumor heterogeneity. As migrating EMT cells undergo an MET to establish a new epithelial metastasis, it seems that it is the $CD44^{high}ESA^{low/+}ALDH^{+}$ EMT cells that are endowed with the greatest metastatic potency. These results may explain the observation that metastatic ability of breast cancer cells is restricted to $ALDH1^{+}$ cells (1).

Analyses of the properties of CSCs are largely dependent on the ability to accurately identify and assay them. We show that clonogenic assays under adherent conditions report the content of $CD44^{high}ESA^{high}$ cells but that tumor sphere formation represents the $CD44^{high}ESA^{low}$ population. As $CD44^{high}ESA^{low}$ cells usually represent only a minor fraction of the total CSC population, sphere-forming

Published OnlineFirst June 17, 2011; DOI: 10.1158/0008-5472.CAN-11-1059

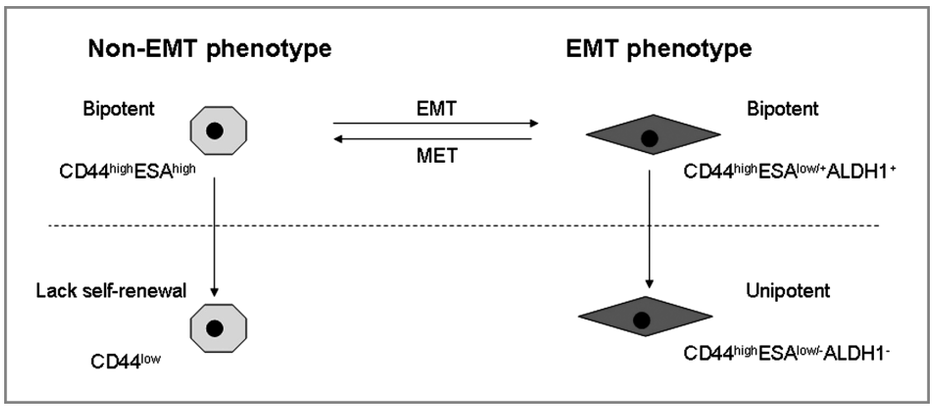

Figure 7. A model showing the different cell types present in SCC, their marker expression, and their relationships to one another.

assays will significantly underestimate the total number of self-renewing CSCs present. Conversely, assays of clonogenicity may exclude the EMT population. These results highlight the importance of using multiple methods for assaying the CSC content within a heterogenous tumor-cell population.

The demonstration that EMT and non-EMT CSCs co-exist in pathologic tissues identifies potentially important new targets for therapeutic interventions intended to halt tumor recurrence and metastatic spread. EMT cells show resistance to conventional chemotherapy in breast cancer (4, 19) and SCC (18), but drug screening has disclosed the existence of agents that are selectively toxic to EMT cells and suggests that such resistance can be overcome (4). Differential properties of EMT and non-EMT cells, such as downregulation of Erbb2 and Erbb3 in EMT cells, suggests they may also vary in their resistance to inhibitors of EGFR and other receptor families. Direct analyses of the responses of EMT and non-EMT CSCs are required and the ability to assess these *in vitro* may enable more rapid development of combinational therapies that act effectively on the entire CSC population.

Disclosure of Potential Conflicts of Interest

No potential conflicts of interest were disclosed.

Acknowledgments

We thank Gary Warnes, Sandra Martins, and Cleo Bishop for technical assistance, and Iain Hutchison and Kim Piper for supplying tumors.

Grant Support

This work was funded by the NC3Rs, Fanconi Anaemia Research Fund, and the Norwegian Research Council.

The costs of publication of this article were defrayed in part by the payment of page charges. This article must therefore be hereby marked *advertisement* in accordance with 18 U.S.C. Section 1734 solely to indicate this fact.

Received April 4, 2011; revised June 7, 2011; accepted June 13, 2011; published OnlineFirst June 17, 2011.

References

1. Charafe-Jauffret E, Ginestier C, Iovino F, Tarpin C, Diebel M, Esterni B, et al. Aldehyde dehydrogenase 1-positive cancer stem cells mediate metastasis and poor clinical outcome in inflammatory breast cancer. Clin Cancer Res 2010;16:45–55. PMCID: 2874875.
2. Hermann PC, Huber SL, Herrler T, Aicher A, Ellwart JW, Guba M, et al. Distinct populations of cancer stem cells determine tumor growth and metastatic activity in human pancreatic cancer. Cell Stem Cell 2007;1:313–23.
3. Li X, Lewis MT, Huang J, Gutierrez C, Osborne CK, Wu MF, et al. Intrinsic resistance of tumorigenic breast cancer cells to chemotherapy. J Natl Cancer Inst 2008;100:672–9.
4. Gupta PB, Onder TT, Jiang G, Tao K, Kuperwasser C, Weinberg RA, et al. Identification of selective inhibitors of cancer stem cells by high-throughput screening. Cell 2009;138:645–59.
5. Clarke MF, Dick JE, Dirks PB, Eaves CJ, Jamieson CH, Jones DL, et al. Cancer stem cells–perspectives on current status and future directions: AACR Workshop on cancer stem cells. Cancer Res 2006;66:9339–44.
6. Al-Hajj M, Wicha MS, Benito-Hernandez A, Morrison SJ, Clarke MF. Prospective identification of tumorigenic breast cancer cells. Proc Natl Acad Sci U S A 2003;100:3983–8. PMCID: 153034.
7. Prince ME, Sivanandan R, Kaczorowski A, Wolf GT, Kaplan MJ, Dalerba P, et al. Identification of a subpopulation of cells with cancer stem cell properties in head and neck squamous cell carcinoma. Proc Natl Acad Sci U S A 2007;104:973–8. PMCID: 1783424.
8. Ginestier C, Hur MH, Charafe-Jauffret E, Monville F, Dutcher J, Brown M, et al. ALDH1 is a marker of normal and malignant human mammary stem cells and a predictor of poor clinical outcome. Cell Stem Cell 2007;1:555–67. PMCID: 2423808.
9. Clay MR, Tabor M, Owen JH, Carey TE, Bradford CR, Wolf GT, et al. Single-marker identification of head and neck squamous cell carcinoma cancer stem cells with aldehyde dehydrogenase. Head Neck 2010;32:1195–201.
10. Hay ED. The mesenchymal cell, its role in the embryo, and the remarkable signaling mechanisms that create it. Dev Dyn 2005;233:706–20.
11. Thiery JP. Epithelial-mesenchymal transitions in development and pathologies. Curr Opin Cell Biol 2003;15:740–6.
12. Yang J, Mani SA, Donaher JL, Ramaswamy S, Itzykson RA, Come C, et al. Twist, a master regulator of morphogenesis, plays an essential role in tumor metastasis. Cell 2004;117:927–39.
13. Shin SY, Rath O, Zebisch A, Choo SM, Kolch W, Cho KH. Functional roles of multiple feedback loops in extracellular signal-regulated kinase and wnt signaling pathways that regulate epithelial-mesenchymal transition. Cancer Res 2010;70:6715–24.

Published OnlineFirst June 17, 2011; DOI: 10.1158/0008-5472.CAN-11-1059

14. Wu Y, Deng J, Rychahou PG, Qiu S, Evers BM, Zhou BP. Stabilization of snail by NF-kappaB is required for inflammation-induced cell migration and invasion. Cancer Cell 2009;15:416–28. PMCID: 2881229.
15. Yang MH, Wu MZ, Chiou SH, Chen PM, Chang SY, Liu CJ, et al. Direct regulation of TWIST by HIF-1alpha promotes metastasis. Nat Cell Biol 2008;10:295–305.
16. Mani SA, Guo W, Liao MJ, Eaton EN, Ayyanan A, Zhou AY, et al. The epithelial-mesenchymal transition generates cells with properties of stem cells. Cell 2008;133:704–15. PMCID: 2728032.
17. Gjerdrum C, Tiron C, Hoiby T, Stefansson I, Haugen H, Sandal T, et al. Axl is an essential epithelial-to-mesenchymal transition-induced regulator of breast cancer metastasis and patient survival. Proc Natl Acad Sci U S A 2010;107:1124–9. PMCID: 2824310.
18. Skvortsova I, Skvortsov S, Raju U, Stasyk T, Riesterer O, Schottdorf EM, et al. Epithelial-to-mesenchymal transition and c-myc expression are the determinants of cetuximab-induced enhancement of squamous cell carcinoma radioresponse. Radiother Oncol 2010; 96:108–15.
19. Bandyopadhyay A, Wang L, Agyin J, Tang Y, Lin S, Yeh IT, et al. Doxorubicin in combination with a small TGFbeta inhibitor: a potential novel therapy for metastatic breast cancer in mouse models. PLoS One 2010;5:e10365. PMCID: 2860989.
20. Fuchs BC, Fujii T, Dorfman JD, Goodwin JM, Zhu AX, Lanuti M, et al. Epithelial-to-mesenchymal transition and integrin-linked kinase mediate sensitivity to epidermal growth factor receptor inhibition in human hepatoma cells. Cancer Res 2008;68:2391–9.
21. Kudo-Saito C, Shirako H, Takeuchi T, Kawakami Y. Cancer metastasis is accelerated through immunosuppression during Snail-induced EMT of cancer cells. Cancer Cell 2009;15: 195–206.
22. Barrandon Y, Green H. Three clonal types of keratinocyte with different capacities for multiplication. Proc Natl Acad Sci U S A 1987;84:2302–6. PMCID: 304638.
23. Locke M, Heywood M, Fawell S, Mackenzie IC. Retention of intrinsic stem cell hierarchies in carcinoma-derived cell lines. Cancer Res 2005;65:8944–50.
24. Li H, Chen X, Calhoun-Davis T, Claypool K, Tang DG. PC3 human prostate carcinoma cell holoclones contain self-renewing tumor-initiating cells. Cancer Res 2008;68:1820–5.
25. Mackenzie IC. Growth of malignant oral epithelial stem cells after seeding into organotypical cultures of normal mucosa. J Oral Pathol Med 2004;33:71–8.
26. Proby CM, Purdie KJ, Sexton CJ, Purkis P, Navsaria HA, Stables JN, et al. Spontaneous keratinocyte cell lines representing early and advanced stages of malignant transformation of the epidermis. Exp Dermatol 2000;9:104–17.
27. Costea DE, Loro LL, Dimba EA, Vintermyr OK, Johannessen AC. Crucial effects of fibroblasts and keratinocyte growth factor on morphogenesis of reconstituted human oral epithelium. J Invest Dermatol 2003;121:1479–86.
28. Harper LJ, Piper K, Common J, Fortune F, Mackenzie IC. Stem cell patterns in cell lines derived from head and neck squamous cell carcinoma. J Oral Pathol Med 2007;36:594–603.
29. Ponti D, Costa A, Zaffaroni N, Pratesi G, Petrangolini G, Coradini D, et al. Isolation and in vitro propagation of tumorigenic breast cancer cells with stem/progenitor cell properties. Cancer Res 2005;65: 5506–11.
30. Singh SK, Clarke ID, Terasaki M, Bonn VE, Hawkins C, Squire J, et al. Identification of a cancer stem cell in human brain tumors. Cancer Res 2003;63:5821–8.
31. Dontu G, Abdallah WM, Foley JM, Jackson KW, Clarke MF, Kawamura MJ, et al. In vitro propagation and transcriptional profiling of human mammary stem/progenitor cells. Genes Dev 2003;17:1253–70. PMCID: 196056.
32. Brabletz T, Jung A, Spaderna S, Hlubek F, Kirchner T. Opinion: migrating cancer stem cells - an integrated concept of malignant tumour progression. Nat Rev Cancer 2005;5:744–9.

STEM CELLS®

CANCER STEM CELLS

Maintenance of Stem cell Self-renewal in Head and Neck Cancers Requires Actions of GSK3β Influenced by CD44 and RHAMM.

Hideo Shigeishi[1,2], Adrian Biddle[1], Luke Gammon[1], Helena Emich[1], Camila.O. Rodini[1], Emilios Gemenetzidis[1], Bilal Fazil[1], Masaru Sugiyama[3], Nobuyuki Kamata[2], Ian C. Mackenzie[1]

[1] Blizard Institute, Barts and the London School of Medicine and Dentistry, Queen Mary University of London, 4 Newark Street, London, E1 2AT.; [2] Department of Oral and Maxillofacial Surgery, Division of Cervico-Gnathostomatology, Graduate School of Biomedical Sciences, Hiroshima University, 1-2-3 Kasumi, Minami-ku, Hiroshima 734-8553, Japan.; [3] Department of Public Oral Health, Division of Oral Health Science, Graduate School of Biomedical Sciences, Hiroshima University, 1-2-3 Kasumi, Minami-ku, Hiroshima 734-8553, Japan.

Key Words. Cancer stem cells • CD44 • GSK3β • head and neck squamous cell carcinoma • RHAMM

ABSTRACT

Cells sorted from head and neck cancers on the basis of their high expression of CD44 have high potency for tumor initiation. These cells are also involved in epithelial to mesenchymal transition (EMT) and we have previously reported that cancer stem cells (CSCs) exist as two biologically distinct phenotypes. Both phenotypes are $CD44^{high}$ but whereas one is also ESA^{high} and maintains epithelial characteristics, the other is ESA^{low}, has mesenchymal characteristics and is migratory. Examining CD44-regulated signal pathways in these cells we show that CD44, and also RHAMM, act to inhibit phosphorylation of glycogen synthase kinase 3β (GSK3β) and that such inhibition reduces the formation of both "tumour spheres" and "holoclone" colonies, functional indicators of stemness. GSK3β inhibition also reduces the expression of stem cell markers such as Oct4, Sox2 and Nanog and up-regulates expression of the differentiation markers Calgranulin B and Involucrin in the $CD44^{high}/ESA^{high}$ cell fraction. Transition of CSCs out of EMT and back to the epithelial CSC phenotype is induced by GSK3β knockdown. These results indicate that GSK3β plays a central role in determining and maintaining the phenotypes and behavior of CSCs *in vitro* and are likely to be involved in controlling the growth and spread of tumours *in vivo.*

INTRODUCTION

Various reports indicate that many cancers contain a subpopulation of cells that is endowed with the stem cell properties of self-renewal and tumor-initiating capacity [1, 2]. Based on their high levels of expression of CD44, enriched populations of these cancer stem cells (CSCs) have been isolated and enriched from a range of solid tumors, including head and neck squamous cell carcinomas (HNSCC) [3-7]. Cells that have

Author contributions: H.S.: Conception and design, financial support, administrative support, collection and/or assembly of data, data analysis and interpretation, manuscript writing, final approval of manuscript. A.B.: Conception and design, data analysis and interpretation, manuscript writing, final approval of manuscript. L.G.: Conception and design, data analysis and interpretation, manuscript writing, final approval of manuscript. H.E.: data analysis and interpretation, final approval of manuscript. C.O.R.: data analysis and interpretation, final approval of manuscript. E.G.: data analysis and interpretation, final approval of manuscript. B.F.: data analysis and interpretation, final approval of manuscript. M.S.: Conception and design, financial support, administrative support, final approval of manuscript. N.K.: Conception and design, financial support, administrative support, final approval of manuscript. I.C.M.: Conception and design, financial support, data analysis and interpretation, manuscript writing, final approval of manuscript.

Address correspondence to: Ian C. Mackenzie, Blizard Institute, Barts and The London School of Medicine and Dentistry, Queen Mary University of London, 4 Newark Street, London E1 2AT, UK. Tel: 020 7882 7159, Fax: 020 7882 7172, E-mail: i.c.mackenzie@qmul.ac.uk; *Abbreviations*: CSC; cancer stem cell, GSK3β; glycogen synthase kinase 3β, RHAMM; Receptor for hyaluronan-mediated motility, ERK; extracellular regulated kinase ; (In all figures, error bars represent Mean ± SD for 3-8 independent experiments with statistical significances of P <0.05, P <0.01, and P <0.001 indicated by *, **, and *** respectively); Received October 18, 2012; accepted for publication April 02, 2013; 1066-5099/2013/$30.00/0 doi: 10.1002/stem.1418

This article has been accepted for publication and undergone full peer review but has not been through the copyediting, typesetting, pagination and proofreading process which may lead to differences between this version and the Version of Record. Please cite this article doi: 10.1002/stem.1418

high expression of CD44 and show stem cell properties are also present in cell lines derived from HNSCC and other malignancies [8-10]. CD44 is a multifunctional and ubiquitously expressed glycoprotein adhesion molecule derived from a gene with 18 exons, 9 of which are expressed in the standard form (CD44s) with alternative splicing of the remainder generating a great many variant (CD44v) isoforms [11]. CD44 expression potentially influences stem cell behavior by a wide range of mechanisms and interactions with hyaluronan, its principal ligand, activate several signaling pathways influencing tumour growth, motility and metastasis [12, 13]. Although CD44 provides a consistent marker for some CSCs, the functional significance of its expression, and particularly of its roles in CSC self-renewal and differentiation, remain uncertain. Like CD44, RHAMM (receptor for hyaluronic acid-mediated motility) binds hyaluronan [14, 15]. Oncogenic expression of RHAMM has been reported for HNSCC and it has also been implicated in promoting proliferation of tumor cells [16]. One of the actions of RHAMM is to co-operate with CD44 in forming complexes that coordinately activate the MAP/ERK1,2 pathway [17]. Such complexes sustain high motility of breast cancer cells but, while RHAMM acts partly as a non-integral cell surface hyaluronan receptor, it is also found as an intracellular protein that binds to mitotic spindles and has less certain functions [18].

Several reports have indicated a role for epithelial to mesenchymal transition (EMT) in metastasis [19, 20] and in generating cells that express marker patterns characterizing breast CSCs [21] and show enhanced resistance to therapeutic killing [22]. We have reported that these phenomena are related to the presence of two biologically distinct CSC phenotypes both of which have high levels of expression of CD44 but differ in their levels of expression of Epithelial Specific Antigen (ESA) [23]. One phenotype has a $CD44^{high}/ESA^{high}$ marker pattern, is proliferative, forms cohesive colonies in vitro, and has epithelial characteristics. The other has a $CD44^{high}/ESA^{low}$ marker pattern, is migratory, has mesenchymal characteristics, and a pattern of gene expression indicative of EMT. Brabletz [19] has suggested a role for EMT in metastasis during which CSCs undergo EMT to escape from the parent tumour, invade locally and then migrate to distant sites where they undergo mesenchymal to epithelial transition (MET) to generate secondary tumours [24]. Although CSCs switch both in and out of the EMT phenotype, only $CD44^{high}/ESA^{low}$ cells that also express ALDH1 are able to switch back to the $CD44^{high}/ESA^{high}$ phenotype to reconstitute the cellular-heterogeneity typical of the original tumour [23]. Interestingly, in head and neck cancers, only $CD44^{high}$ cells that also express aldehyde dehydrogenase (ALDH) are involved in EMT and show high potency for tumor initiation [23, 24].

HNSCC cell lines plated at low density form a range of heterogeneous colony morphologies that corresponded to the holoclone, meroclone and paraclone colonies that result from the presence of hierarchies of cells at different stage of maturation [10, 25]. After single cell cloning, the small, tightly packed cells of holoclones have a persistently high proliferative potential, corresponding to stem cell self-renewal [25]. It has also been reported that self-renewing stem cells have the ability to form tumour spheres under suspension culture conditions [26] but we previously reported that, in HNSCC, the ability to form tumour spheres in suspension cultures is associated with EMT CSC whereas the ability to form holoclones under adherent condition is mainly a property of epithelial CSC [23].

Glycogen synthase kinase 3β (GSK3β) is known to regulate cell cycle progression and cell proliferation [27]. Several oncogenic signalling pathways, e.g., Wnt/AKT, MAP kinase and phosphoinositide 3-kinase (PI3-K) pathways, act to inhibit the activity of GSK3β [28-29]. AKT-mediated inactivation of GSK3β leads to nuclear translocation of β-catenin [29] and inactivation of GSK3β is thought to drive oncogenic progression in oral SCC through an accelerated cell cycle progression and enhanced

tumour invasion and metastasis [30]. However, β-catenin becomes vulnerable to destruction if E-cadherin is lost via EMT [31] and degradation of membranous β-catenin is necessary for the invasion and metastasis of oral SCC [32]. These recent observations suggest that GSK3β remains active in CSCs that have undergone EMT and imply an oncogenic role of GSK3 acting through the EMT CSC phenotype. In this study, we investigated the influences of GSK3β on the self-renewal, switching and differentiation of CSCs and report a GSK3β-based mechanism that influences these events.

MATERIALS AND METHODS

Cell Culture

The CA1 and LUC4 cell lines were established from oral SCCs [23] and the MET2 line was established from a cutaneous SCC [33]. All cell lines were grown in a highly supplemented epithelial growth medium (termed FAD) with 10% FBS under 5% CO_2 in air at 37°C. For re-plating and for assays, cells were released from flasks using Accutase (PAA Laboratories, Austria).

Colony and sphere formation assays.

To test the ability of cells to form holoclone colonies [25], 5 $X10^2$ cells in 0.5 ml of medium were added to each well of 24 well plates and the number of holoclones counted 7 days after cell plating. For growth as tumour spheres in suspension cultures, 0.75 cm^2 wells were coated with 12 mg/ml PolyHEMA (2-hydroxyethyl methacrylate, SIGMA) in 95% ethanol prior to seeding cells at a density of 2 $X10^3$ cells/ well in 0.5 ml medium with addition of 1% methylcellulose (Sigma) to prevent cell aggregation. After two weeks, plates were assayed visually for the formation of floating tumour spheres and the number of spheres counted. Results were expressed as the mean ± SD for more than 3 independent cultures.

In vitro scratch assay

To assess cell motility, scratch assays were performed as described previously [34]. A scratch was made on the confluent cell layers using 200µl micropipette tip and the wound monolayer was washed to remove the dislodged cells. The images of the wounded area were captured at 0h and 24h by phase contrast microscopy and a digital camera. Adobe Photoshop Elements version 4.0 software was used to quantify migration of cells by subtracting the area of the scratch remaining at 24h from the original scratch area which provided the percentage of scratch occupied by newly migrated cells as an index of migration.

Fluorescence-activated cell sorting

FACS analyses used an anti-CD44-PE-conjugated antibody, an anti-ESA-APC-conjugated antibody (both from BD Biosciences), and an anti-human RHAMM (CD168) rabbit monoclonal antibody (OriGene Technologies, 1:150). An anti-human phosphorylated-GSK3β rabbit polyclonal, which detects inactivating phosphorylation at ser9, was used to detect inactivated GSK3β (1:200, Cell Signaling Technology). An anti-rabbit FITC-conjugated antibody (1:1000, BD Biosciences) was used as a secondary antibody at dilution. DAPI was used at a concentration of 1 µg/ml to exclude dead cells. Samples were assayed on a Becton Dickenson LSRII FACS (Oxford, UK) and sorted using Becton Dickenson FACSAria equipment. FACS Diva version 6.1.1. (BD Biosciences) software was used to analyze the data. Intensities of FITC fluorescent signals for RHAMM and phosphorylated- GSK3β were measured using FACS Diva version 6.1.1 software (BD Biosciences) and shown as Mean ±SEM. For multiple staining procedures, cells were fixed with 4% formaldehyde in PBS, stained for CD168 (RHAMM) for 1h, washed and then stained with an anti-rabbit secondary antibody (Alexafluor 488) at 1:1000 for 30 min. Anti-CD44 and ESA antibodies were then added. For CD44v staining, cells were detached using enzyme-free cell dissociation buffer (Invitrogen). They were then stained with antibodies at 1:100 dilution in PBS (PAA). The DAPI nuclear dye (Sigma) was used at 1 ug/ml to exclude dead cells. The antibodies used were as follows;

PE-CD44 (clone G44-26) was from BD biosciences; APC-ESA (clone HEA-125) was from Miltenyi Biotec; PE-CD44v3 (clone 3G5) was from R&D systems; FITC-CD44v6 (clone VFF7) was from Bender Medsystems; CD44v5 (clone VFF8) was from AbD Serotec; the FITC rabbit-anti-mouse secondary antibody was from Invitrogen. The FITC- and PE- conjugated mouse IgG isotype control antibodies were from BD Biosciences.

Quantitative RT-PCR Analysis

RNA was extracted by the RNAeasy micro kit (Qiagen) and reverse transcription into cDNA was conducted using the superscript III first strand synthesis supermix (Invitrogen). For QPCR of Sox2, Nanog, Oct4, Calgranulin B, Involucrin, and G3PDH, the quantification of mRNA levels was carried out using the ABI 7500 real-time PCR system (Applied Biosystems, Warrington, UK) and Power SYBR green mix (Applied Biosystems). The reaction mixture contained 1.0 µg of cDNA, 12.5 µl of SYBR Green Mix, and 10 µmol of each pair of oligonucleotide primers. GAPDH was used as a reference mRNA control. The PCR program was as follows: initial melting at 95˚C for 10 min followed by 40 cycles at 95˚C for 15 sec, 60˚C for 30 sec and 72˚C for 40 sec. Reverse transcribed Human Total Reference RNA (Stratagene, Cheshire, UK) was used to make a standard curve. PCR for the standard and variant forms of CD44 was performed essentially according to Rajarajan et al. [35] combining a CD44 standard sense primer with an appropriate exon-specific antisense primer. The reaction mixture contained 1.0 µg of cDNA, 2.0 µl of 10X Buffer (TOYOBO, Japan), 2 mM of dNTPs, 10µM of each primer and 2.5 units/µl of Taq DNA polymerase (TOYOBO, Japan). The PCR program was as follows: initial melting at 95˚C for 2 min followed by 35 cycles at 95˚C for 1 min, 57˚C for 1 min and 72˚C for 2 min. PCR products were separated by 1.5% agarose gel electrophoresis. DNA ladder (100bp DNA Ladder, TOYOBO, Japan) was used for the PCR marker. Primer details are provided in the Supplemental material and the results are expressed as the Mean ± SD for 3 independent experiments.

Western Blotting

The cells were lysed in RIPA buffer [2.5 mM Tris pH 7.3, 152 mM NaCl, 0.0005% SDS, 1% NP-40, CompleteMini protease inhibitor (Roche Diagnostic Ltd, Burgess Hill, UK)]. Protein concentrations were measured using a protein assay reagent (BIO-RAD). Protein samples (15 µg) were solubilized in sample buffer by boiling, and then run in a 10% polyacrylamide gel and blotted onto a nitrocellulose. The bands on western blotting were detected using an enhanced chemiluminescence western blotting reagent (GE Healthcare). The antibodies, all used at 1:1000 dilution, were an anti-human CD44 mouse monoclonal anti-body, an anti-human GSK3β mouse monoclonal antibody, and an anti-human phosphorylated- GSK3β (Ser9) rabbit polyclonal antibody (all from Cell Signaling Technology), an anti-human RHAMM (CD168) rabbit monoclonal anti-body (OriGene Technologies), an anti-human ERK1/2 rabbit polyclonal antibody, an anti-human phosphorylated-ERK1/2 mouse monoclonal antibody, and anti-human GAPDH mouse monoclonal antibody (all from Abcam). Also used were an anti-human Vimentin mouse monoclonal antibody (BD Pharmingen) and an anti-human E-cadherin rabbit polyclonal antibody (Santa Cruz Biotechnology). GAPDH was used as a loading control in all blots.

Inhibition of GSK3β CD44 and RHAMM functions

To inhibit GSK3β cells were sorted as needed into sub-populations and were re-plated in culture medium containing the inhibitor N-(4-Methoxybenzyl)-N'-(5-nitro-1,3-thiazol-2-yl) urea (Calbiochem 361549) at a concentration of 200nM. Stealth™ siRNAs were used for RHAMM and GSK3β knockdown (Invitrogen). siGLO RISC-Free Control siRNA (Thermo Fisher Scientific Inc) was used as control. CD44 proteins were knocked down using siRNA ON-TARGET-plus SMARTpool siRNA for human CD44 (Thermo Fisher Scientific Inc).

Cells were transiently transfected with the indicated combinations of the siRNAs using HiPerFect transfection reagent (Qiagen), according to the manufacturer's recommendations.

Immunofluorescence Microscopy

Immunofluorescence was performed as described previously (16, 25). Cells were seeded onto glass Lab-Tek II Chamber Slides (Thermo Fisher Scientific Inc) and incubated for a day. The growth medium was then removed, and cell monolayers were washed three times with a 1% PBS solution and fixed with 3.5% paraformaldehyde for 10 min at room temperature. Cells were washed three times with PBS and permeabilized by Triton X-100 (0.2%, 10 min at room temperature). Nonspecific binding sites were blocked by treatment at room temperature for 30 min with PBS containing 1% BSA. The cells were washed three times with PBS before incubating with the following antibodies: 1) anti-RHAMM rabbit monoclonal antibody (1:200, OriGene Technologies); 2) anti-GSK3β mouse monoclonal antibody (1:200, Cell Signaling Technology), 3) anti-phosphorylated-GSK3β rabbit polyclonal antibody (1:200, Cell Signaling Technology). Staining for RHAMM and phosphorylated-GSK3β used an Alexa-Fluor-labeled goat anti-rabbit or anti-mouse secondary antibodies (Invitrogen). Cells were counter-stained with DAPI for visualization of nuclear morphology.

Statistical Methods

At least three independent samples were available for all data points and statistical analyses were performed using a paired Student's t-test or a Welch's t-test for samples with unequal variance. *P* values less than 0.05 were regarded as statistically significant.

RESULTS

$CD44^{high}/ESA^{high}$ and $CD44^{high}/ESA^{low}$ phenotypes are present in SCC cell lines.

SCC cells were fractionated by fluorescence-activated cell sorting (FACS) using antibodies against CD44 and ESA (Fig 1A; Supplementary Fig S1A) and, as previously reported, CSCs include two biologically-distinct phenotypes [23]. Each of the cell lines examined contained cells with high expression of CD44 that were either a) ESA^{low} and exhibited a spindle-like appearance had high expression of Snail, Vimentin and Axl and low expression of E-cadherin (Fig 1B-D; Supporting Information Fig S1B and C) or, b) ESA^{high} and formed holoclones, had high expression of E-cadherin, low expression of Snail and Vimentin and grew faster in adherent culture conditions than $CD44^{high}/ESA^{low}$ cells, (Fig 1C, D, F; Supporting Information Fig S1C). The $CD44^{high}/ESA^{low}$ cell type had mesenchymal features, generated more motile cells in "scratch" assays (Fig 1E; Supplementary Fig S1D) and was designated as "EMT CSC". The $CD44^{high}/ESA^{high}$ phenotype preserved epithelial characteristics, and was designated as "EPI CSC". The $CD44^{low}$ cells formed only paraclone-like cells and were unable to form self-renewing holoclones or grow extensively (Fig 1B; Supplementary Fig S1B).

GSK3β is necessary for the self-renewal of CSCs.

Examining the number of tumour spheres and holoclones formed by the EMT and EPI CSCs of the CA1, MET2 and LUC4 cell lines we found that significantly greater numbers of tumour spheres were formed by EMT CSCs, and of holoclones by EPI CSCs. The number of tumour spheres formed by the EMT CSCs (Fig 2A) appeared to correlate with the size of the fraction of EMT CSCs present in the unsorted parental population (7.5%, 16.5% and 21.0% in CA1, MET2 and LUC4, respectively).

Western blotting to assess total GSK3β and phosphorylated-GSK3β indicated a relationship between the self-renewal ability of CSCs and

GSK3β activity. In the high sphere-forming MET2 and LUC4 lines, the $CD44^{high}/ESA^{low}$ cells had low levels of phosphorylated-GSK3β whereas in the low sphere-forming CA1 line the $CD44^{high}/ESA^{low}$ cells exhibited higher expression of phosphorylated-GSK3β (Fig 2B). FACS analyses of EMT CSCs, EPI CSCs and $CD44^{low}$ cells for their levels of phosphorylated-GSK3β used a triple combination of antibodies against CD44, ESA and phosphorylated-GSK3β. These showed that within each line, the EMT CSCs had the lowest expression of phosphorylated-GSK3β and $CD44^{low}$ cells the highest (Supplementary Fig 2A). Western blots showed high levels of CD44 and low levels of phosphorylated-GSK3β in EMT cells (Figure 2B). Quantitative analyses indicated that these differences were significant and that sphere forming ability correlated negatively with levels of phosphorylated-GSK3β (Supplementary Fig S2 B, C). Given that GSK3β is inactivated by phosphorylation at ser9, it appears that tumour sphere formation in suspension culture, a property indicative of maintenance of a stem cell state, is correlated with highly active GSK3β.

To clarify potential roles of GSK3β in the self-renewal of CSCs, the formation of tumour spheres and of holoclones was examined after GSK3β inactivation using either chemical inhibition or siRNA knockdown. After GSK3β inactivation, no significant changes in the overall growth rates of $CD44^{high}/ESA^{low}$ or $CD44^{high}/ESA^{high}$ cells were observed after 7 days of adherent culture (Supplementary Fig S3A). However, inactivation of GSK3β clearly decreased tumour sphere formation by $CD44^{high}/ESA^{low}$ cell fractions (Fig 2C and D; Supporting Information Fig S3B-D). After inhibition of GSK3β the number of holoclones formed by $CD44^{high}/ESA^{high}$ cells decreased for each of the LUC4, MET2 and CA1 cell lines indicating their loss of self-renewal abilities (Fig 2E; Supplementary Fig S3E and F). Collectively, these results indicate that active GSK3β is necessary for the self-renewal of both EMT and EPI CSCs.

Self-renewing $CD44^{high}/ESA^{low}$ cells show less GSK3β phosphorylation.

Immunofluorescence indicated the uniform cytoplasmic presence of GSK3β in nearly all $CD44^{high}/ESA^{low}$ and $CD44^{high}/ESA^{high}$ cells (Fig 2F). However, staining for phosphorylated GSK3β showed the lowest expression in $CD44^{high}/ESA^{low}$ cells, higher expression in $CD44^{high}/ESA^{high}$ cells, and the highest expression in $CD44^{low}$ cells (Fig 2F). Nuclear staining for GSK3β was high in ESA^{low} cells, intermediate in ESA^{high} cells, and lowest in $CD44^{low}$ cells but nuclear staining for phosphorylated GSK3β was generally absent (Fig 2G). Very few of the cells present in tumour spheres showed expression of phosphorylated-GSK3β (Fig 2G). These observations are consistent with the results of western blotting for phosphorylated-GSK3β (Fig 2B) and provide further support for the notion that non-phosphorylated GSK3β (i.e., active GSK3β) plays a central role in maintaining the self-renewing state of EMT and EPI CSCs.

CSC expression of stem cell markers is reduced in by GSK3β inhibition.

To further clarify the role played by GSK3β in the maintenance of CSCs, mRNA expression of the stem cell markers Sox2, Oct4 and Nanog was evaluated by RT-PCR. Except for Sox2 in $CD44^{high}/ESA^{high}$ cells, inactivation of GSK3β significantly reduced each of these markers in both $CD44^{high}/ESA^{low}$ and $CD44^{high}/ESA^{high}$ cells (Fig 3A and B). These findings further indicate a critical role played by GSK3β in the maintenance of the stem cell state of CSCs.

Inactivation of GSK3β induces cell differentiation.

To examine roles of GSK3β in maintaining the EMT and EPI CSC phenotypes, changes in the proportions of $CD44^{high}/ESA^{low}$, $CD44^{high}/ESA^{high}$ and $CD44^{low}$ cells were examined after GSK3β inhibition or knockdown. For all cell lines, the percentage of both $CD44^{high}/ESA^{low}$ and $CD44^{high}/ESA^{high}$ cells decreased, but the percentage of $CD44^{low}$ cells

consistently increased (Fig 3C; Supplementary Fig S4A). The increase in $CD44^{low}$ cells suggested a shift of CSCs into differentiation, a change that would be expected to increase expression of epithelial differentiation markers such as Involucrin and Calgranulin B. Inactivation of GSK3β produced significantly increased levels of expression of these genes in $CD44^{high}/ESA^{high}$ cells (Fig 3D and E) indicating that GSK3β acts to suppress entry of CSC into differentiation.

To examine more closely how knockdown of GSK3β influences the differentiation of EPI CSCs, $CD44^{high}/ESA^{high}$ cells were sorted for single cell cloning and clones derived from individual $CD44^{high}/ESA^{high}$ cells were examined after 4 weeks of growth in culture. All clones produced $CD44^{low}$ populations (Supplementary Fig S5A). For all $CD44^{high}/ESA^{high}$ clones, knock down of GSK3β reduced the formation of holoclones (Supplementary Fig S5A S5A). It also increased the size of the $CD44^{low}$ population identified by FACS analysis (Supplementary Fig S5B), supporting the concept that inhibition of GSK3β attenuates self-renewal and induces differentiation of EPI CSCs.

Inactivation of GSK3β promotes MET of $CD44^{high}/ESA^{low}$ cells.

Lack of induction of differentiation markers in $CD44^{high}/ESA^{low}$ cells after GSK3β inhibition suggested that EMT CSCs do not directly enter terminal differentiation. However, GSK3β inhibition was found to lead to a reduced percentage of EMT CSCs (Fig 3C; Supplementary Fig S4A), less expression of Snail and Vimentin, and increased expression of E-cadherin (Supplementary Fig S4B). This indicated a shift of EMT CSCs into the $CD44^{high}/ESA^{high}$ phenotype, suggesting maintenance of cells in the $CD44^{high}/ESA^{low}$ cell compartment requires active GSK3β.

To examine the phenotypic plasticity of EMT CSCs in terms of their ability to switch back to the EPI CSC phenotype, $CD44^{high}/ESA^{low}$ cells were sorted for single cell cloning. Initially all developing clones formed cells with a spindle-like appearance. After 8 weeks of culture the clonal populations were examined by FACS and this showed that of the 17 single cell clones examined, 8 maintained an entirely $CD44^{high}/ESA^{low}$ identity without any cells switching into the EPI CSC phenotype (Fig 4A). These were termed Type 1 clones. The formation of tumour spheres by Type 1 clones was significantly suppressed by knockdown of GSK3β. However, FACS analyses indicated that this was not associated with a switch into the EPI CSC phenotype (Fig 4A and B). Nine of the 17 single cell clones derived from $CD44^{high}/ESA^{low}$ cells were able to switch and gave rise to both $CD44^{high}/ESA^{low}$ and $CD44^{high}/ESA^{high}$ cell populations. These clones initially displayed a spindle-like appearance (Fig 4C, left) but by 8 weeks of culture had visibly generated a mixture of both EMT and epithelial cells (Fig 4C, right). Interestingly, for all of these clones, termed Type 2 clones, inactivation of GSK3β greatly accelerated the transition into $CD44^{high}/ESA^{high}$ cells and produced a marked shift towards the EPI CSC phenotype within 5 days (Fig 4D). Inactivation of GSK3β in Type 2 clones significantly decreased expression of Snail and Vimentin and up-regulated expression of E-cadherin (Fig 4E), findings consistent with loss of GSK3β activity promoting a switch of EMT CSCs back towards the EPI CSC phenotype.

CD44 and RHAMM are required for self-renewal of CSCs and regulate GSK3β.

$CD44^{high}/ESA^{high}$ cells showed considerably higher expression of RHAMM than $CD44^{high}/ESA^{low}$ cells (Fig 5A, Supplementary Fig S4A) and FACS analysis, using triple staining for CD44, ESA and FITC-labeled RHAMM, confirmed that RHAMM was most highly expressed on $CD44^{high}/ESA^{high}$ cells (Fig 5A). Immunofluorescent staining confirmed expression of both RHAMM and CD44 in $CD44^{high}/ESA^{high}$ holoclone cells (Fig 5B). Both RHAMM and CD44 knockdown resulted in phosphorylation (inactivation) of GSK3β and phosphorylation (activation) of ERK1/2 (Fig 5C). Holoclone formation by $CD44^{high}/ESA^{high}$

cells was significantly inhibited by both RHAMM and CD44 knockdown (Fig 5D). Knockdown of CD44 caused a significant decrease in the number of tumour spheres formed by $CD44^{high}/ESA^{low}$ cells but, in contrast, knockdown of RHAMM did not (Fig 5E). CD44 and RHAMM knockdown also significantly decreased expression of Sox2, Nanog and Oct4 in $CD44^{high}/ESA^{high}$ cells (Fig 5F) and it also up-regulated expression of the differentiation markers Involucrin and Calgranulin B (Fig 5G). These results support the notion that CD44 is required for self-renewal of both EPI and EMT CSCs, whereas RHAMM is required for self-renewal only of EPI CSCs. Both CD44 and RHAMM contribute towards maintenance of active GSK3, potentially through blocking the activation of ERK1/2, which is a known inhibitor of GSK3β [36].

Due to alternatively spliced exon products, CD44 exists as a standard form and as range of variant isoforms whose differential expression has been linked to the behavior of head and neck cancers and to EMT [11, 13, 37]. For the Ca1 and Met 2 cell lines, Epi CSCs have higher expression of variant isoforms than EMT CSCs [37]. Therefore, to assess the expression pattern for the LUC4 cell line used in the present study, cell subpopulations were examined for the expression of standard and variant isoforms by flow cytometry and by QPCR. Cytometry of cells stained with antibodies against total CD44 and ESA showed similar levels of CD44 surface expression on both ESA^{high} and ESA^{low} cells. However, staining for the CD44v3, v5 and v6 isoforms indicated markedly less expression of these isoforms on the ESA^{low} EMT cell fraction. QPCR for the v3, v4, v5, v6 and v7 isoforms similarly indicated their low expression in the $CD44^{high}/ESA^{low}$ EMT cell fraction compared with the Epi CSC, parental or $CD44^{low}$ cell fractions, whereas the standard CD44 isoform was more highly expressed in the EMT and Epi CSC fractions than in the parental and $CD44^{low}$ fractions (Figure S6).

DISCUSSION

The use of CD44 to identify a population of highly tumorigenic cells has been described for HNSCC as well as for breast, colon, prostate and other cancers [3-5, 7]. However, the mechanisms maintaining the balance between self-renewal and differentiation of $CD44^{high}$ CSCs have been uncertain and recently this problem has been further complicated by work indicating the presence of two biologically-distinct phenotypes of CSCs in HNSCC and breast cancers [23, 38]. In HNSCC, both CSC phenotypes are relatively $CD44^{high}$ but one is ESA^{high} and the other ESA^{low}. Consequently, three distinct cell sub-populations can be identified: CSCs with an EMT phenotype, CSCs with an epithelial phenotype, and $CD44^{low}$ cells that have entered the differentiation pathway and lost self-renewal ability [23]. In this study, we have begun to examine transitions occurring between these cell types and have focused on potential roles of GSK3β in mediating the choice between their self-renewal and differentiation. Assessment of sphere formation and clonogenicity after GSK3β inhibition demonstrated that GSK3β is required to maintain both $CD44^{high}/ESA^{low}$ and $CD44^{high}/ESA^{high}$ cells in a self-renewing state. This finding is strengthened by the lack of significant levels of inactive (phosphorylated) GSK3β in either of the self-renewing sphere-forming or holoclone-forming populations. The few holoclones that continued to grow in the presence of GSK3β inhibitor showed lack of phosphorylation (Figure 5B) and inactivation of GSK3β reduced the population of $CD44^{high}/ESA^{high}$ cells and shifted cells into the $CD44^{low}$ compartment with loss of self-renewal ability.

Under various pathological conditions, upstream signal pathways such as PI3K/AKT, Raf/MEK/ERK and Wnt induce phosphorylation and inactivation of GSK3β [29, 30, 39]. Our observations indicate that the preservation of functionally active GSK3β is required for CSC self-renewal and that this is promoted by signalling pathways initiated by CD44 and

RHAMM. One action of CD44 is to inhibit phosphorylation of AKT, thus preventing AKT from phosphorylating GSK3β at Ser9 and inhibiting its activity [40, 41]. In oral SCC, RHAMM has an important role in promoting tumor proliferation [42] and, like CD44, RHAMM have been shown to act together in a hyaluronan-dependent autocrine mechanism to co-ordinate signaling that sustains cancer cell motility [18]. Knockdown of CD44 induced phosphorylation of GSK3β and reduced the holoclone forming ability of EPI CSCs and the sphere forming ability of EMT CSCs. Phosphorylation of GSK3β induced by knockdown of RHAMM similarly reduced holoclone forming ability but had less effect on sphere formation. These results indicate that CD44 and RHAMM act upstream to prevent GSK3β phosphorylation and maintain activities necessary to promote CSC self-renewal. High levels of expression of CD44 are associated with stem cell properties such as self-renewal [12] and also commonly mark CSCs isolated both from fresh tumours and from malignant cell lines [3-10]. A switch from variant CD44 isoforms to the standard isoform appears necessary for EMT in breast cancer cells where the epithelial phenotype is maintained by the expression of ESRP1 (epithelial splicing regulatory protein-1) which promotes alternative splicing [43]. The low expression levels of variant CD44 isoforms by EMT CSCs of our oral cancer cell lines suggests that the standard CD44 isoform, which is expressed by both CSC phenotypes, may be required for the self-renewal of stem cell compartments while the variant isoforms are associated with maintenance the epithelial phenotype.

Brabletz [19] has proposed that invasion and metastasis are dependent both on EMT and on the reverse process of mesenchymal to epithelial transition (MET): whereas EMT initially provides cells with the ability to escape from a tumour and migrate to distant sites, MET is subsequently required to restore the epithelial nature of developing secondary tumours. A great deal is now known about EMT and about the cytokines and growth factors in the tumour environment that induce EMT [20, 44, 45]. However, much less is known about factors that induce MET [46, 47]. Some EMT CSCs have the ability to switch spontaneously into the EPI CSC phenotype [23] and GSK3β , in addition to its roles in self-renewal, also appears to influence this transition. When the high levels of active GSK3β normally present in $CD44^{high}/ESA^{low}$ cells are knocked down, cells that are capable of shifting into the $CD44^{high}/ESA^{high}$ phenotype do so more rapidly. Signalling through GSK3β may thus be a key regulator of the MET shift that enables metastatic tumour cells to produce new tumours at secondary sites.

Figure 6 illustrates the proposed roles of active GSK3β in promoting the self-renewal of both EMT and EPI CSCs and the effects of loss of its activity on the MET of EMT CSCs and the differentiation of EPI CSCs. Typically, the bulk of tumour cells, both *in vivo* and in cell lines, is not self-renewing and consists of $CD44^{low}$ differentiating cells [23]. In the presence of active GSK3β, the EPI CSC fraction is self-renewing but with loss of GSK3β activity this fraction generates differentiating $CD44^{low}$ cells. The EPI CSC fraction is also able to undergo EMT to generate the EMT CSC fraction, a transition influenced by autocrine and paracrine actions of cytokines such as TGFβ [20, 44]. EMT CSCs are also able to self-renew and to switch back to the EPI CSC phenotype and, although the mechanism inducing this change is unclear, it is associated with loss of GSK3β activity. GSK3β is thus key to the regulation of the choice between CSC self-renewal and differentiation. Inducing loss of GSK3β activity might therefore be used therapeutically to enhance differentiative loss of the EPI CSC phenotype. However, blocking GSK3β activity may have conflicting results in terms of tumour behavior. Its loss, by reducing the self-renewal ability of CSCs, should reduce the CSC population, but the promotion of MET by inactivation of GSK3β may aid development of secondary metastatic tumours. However, it now seems apparent that tumour growth depends on self-renewal of CSCs, and that tumour

invasion and metastasis is related to EMT and the reverse process of MET. A better understanding of how these processes are controlled and sustained seems necessary to enable future therapies to successfully manipulate loss of both EMT CSC and EPI CSC, an effect apparently required for eradication of an entire tumour.

ACKNOWLEDGMENTS

This work was supported by grants to Dr. Shigeishi from the Scientific Research Fund of Sugiyama Chemical Industrial Laboratory (2011), the Satake Fund for Scientific Research from Hiroshima University Supporters' Association (2011) and a Grant-in-aid for Scientific Research (C) (No.11008667) from the Japanese Ministry of Education, Culture, Sports, and Technology. It was also supported by grants from the NC3Rs, the Fanconi Anemia Research Fund, Bart's and The London Charitable Foundation, and the Saving Faces Research Foundation.

Conflict of Interest

The authors declare that there is no conflict of interest.

REFERENCES

1. Clarke MF, Dick JE, Dirks PB et al. Cancer stem cells--perspectives on current status and future directions: AACR Workshop on cancer stem cells. Cancer Res 2006;66:9339-9344.
2. Reya T, Morrison SJ, Clarke MF et al. Stem cells, cancer, and cancer stem cells. Nature 2001; 414:105-111.
3. Al-Hajj M, Wicha MS, Benito-Hernandez A et al. Prospective identification of tumorigenic breast cancer cells. Proc Natl Acad Sci U S A 2003;100:3983-3988.
4. Collins AT, Berry PA, Hyde C et al. Prospective identification of tumorigenic prostate cancer stem cells. Cancer Res 2005; 65:10946-10951.
5. Dalerba P, Dylla SJ, Park IK et al. Phenotypic characterization of human colorectal cancer stem cells. Proc Natl Acad Sci U S A 2007;104:10158-10163.
6. Li C, Heidt DG, Dalerba P et al. Identification of pancreatic cancer stem cells. Cancer Res 2007; 67:1030-1037.
7. Prince ME, Sivanandan R, Kaczorowski A et al. Identification of a subpopulation of cells with cancer stem cell properties in head and neck squamous cell carcinoma. Proc Natl Acad Sci U S A 2007;104:973-978.
8. Fillmore CM, Kuperwasser C. Human breast cancer cell lines contain stem-like cells that self-renew, give rise to phenotypically diverse progeny and survive chemotherapy. Breast Cancer Res 2008 10:R25.
9. Harper LJ, Piper K, Common J et al. Stem cell patterns in cell lines derived from head and neck squamous cell carcinoma. J Oral Pathol Med 2007;36:594-603.
10. Patrawala L, Calhoun T, Schneider-Broussard R et al. Highly purified CD44+ prostate cancer cells from xenograft human tumors are enriched in tumorigenic and metastatic progenitor cells. Oncogene 2006; 25:1696-1708.
11. Wang SJ, Wong G, de Heer AM et al. CD44 variant isoforms in head and neck squamous cell carcinoma progression. Laryngoscope 2009;119:1518-1530.
12. Bourguignon LY, Wong G, Earle C et al. Hyaluronan-CD44v3 interaction with Oct4/Sox2/Nanog promotes miR-302 expression leading to self-renewal, clonal formation and cisplatin resistance in cancer stem cells from head and neck squamous cell carcinoma. J Biol Chem 2012 DOI: 10.1074/jbc.M111.308528
13. Zoller M. CD44: can a cancer-initiating cell profit from an abundantly expressed molecule? Nat Rev Cancer 2011;211:254-267.
14. Turley EA, Noble PW, Bourguignon LY. Signaling properties of hyaluronan receptors. J Biol Chem 2002; 277:4589-4592.
15. Wang C, Entwistle J, Hou G et al. The characterization of a human RHAMM cDNA: conservation of the hyaluronan-binding domains. Gene 1996;174:299-306.
16. Shigeishi H, Fujimoto S, Hiraoka M et al. Overexpression of the receptor for hyaluronan-mediated motility, correlates with expression of microtubule-associated protein in human oral squamous cell carcinomas. Int J Oncol 2009;34:1565-1571.
17. Telmer PG, Tolg C, McCarthy JB et al. How does a protein with dual mitotic spindle and extracellular matrix receptor functions affect tumor susceptibility and progression? Commun Integr Biol 2011;4:182-185.
18. Hamilton SR, Fard SF, Paiwand FF et al. The hyaluronan receptors CD44 and Rhamm(CD168) form complexes with ERK1,2 that sustain high basal motility in breastcancer cells. J Biol Chem 2007; 282:16667-16680.
19. Brabletz T, Jung A, Spaderna S et al. Opinion: migrating cancer stem cells - an integrated concept of malignant tumour progression. Nat Rev Cancer;2005:5:744-749.

20. Thiery JP. Epithelial-mesenchymal transitions in tumour progression. Nature Reviews Cancer 2002; 2:442-454.
21. Mani SA, Guo W, Liao MJ et al. The epithelial-mesenchymal transition generates cells with properties of stem cells. Cell 2008;133:704-715.
22. Gupta PB, Onder TT, Jiang G et al. Identification of selective inhibitors of cancer stem cells by high-throughput screening. Cell 2009;138:645-659.
23. Biddle A, Liang X, Gammon L et al. Cancer stem cells in squamous cell carcinoma switch between two distinct phenotypes that are preferentially migratory or proliferative. Cancer Res 2011;71:5317-5326.
24. Chen YC, Chen YW, Hsu HS et al. Aldehyde dehydrogenase 1 is a putative marker for cancer stem cells in head and neck squamous cancer. Biochem Biophys Res Commun 2009;385:307-313.
25. Locke M, Heywood M, Fawell S et al. Retention of intrinsic stem cell hierarchies in carcinoma-derived cell lines. Cancer Res 2005;65:8944-8950.
26. Dontu G, Wicha MS. Survival of mammary stem cells in suspension culture: implications for stem cell biology and neoplasia. J Mammary Gland Biol Neoplasia 2005;10:75-86.
27. Cohen P, Frame S. The renaissance of GSK3. Nat Rev Mol Cell Biol 2001;2:769-776.
28. Dale TC. Signal transduction by the Wnt family of ligands. Biochem J 1998;329:209-223.
29. Pap M, Cooper GM. Role of glycogen synthase kinase-3 in the phosphatidylinositol 3-Kinase/Akt cell survival pathway. J Biol Chem 1998;273:19929-19932.
30. Mishra R. Glycogen synthase kinase 3 beta: can it be a target for oral cancer. Mol Cancer2010;9:14
31. Higashikawa K, Yoneda S, Tobiume K et al. Snail-induced down-regulation of DeltaNp63alpha acquires invasive phenotype of human squamous cell carcinoma. Cancer Res 2007;67:9207-9213.
32. Kudo Y, Kitajima S, Ogawa I et al. Invasion and metastasis of oral cancer cells require methylation of E-cadherin and/or degradation of membranous beta-catenin. Clin Cancer Res 2004;10:5455-5463.
33. Proby CM, Purdie KJ, Sexton CJ et al. Spontaneous keratinocyte cell lines representing early and advanced stages of malignant transformation of the epidermis. Exp Dermatol 2000;9:104-117.
34. Liang CC, Park AY, Guan JL. In vitro scratch assay: a convenient and inexpensive method for analysis of cell migration in vitro. Nat Protoc 2007;2:329-333.
35. Rajarajan A, Stokes A, Bloor BK, et al. CD44 expression in oro-pharyngeal carcinoma tissues and cell lines. PLoS One 2012;7:e28776.
36. Ding Q, Xia W, Liu JC et al. Erk associates with and primes GSK-3beta for its inactivation resulting in upregulation of beta-catenin. Mol Cell 2005;19:159-170.
37. Biddle A, Gammon L, Fazil B et al. CD44 staining of cancer stem-like cells is influenced by down regulation of CD44 variant isoforms in the population of cells that has undergone epithelial-to-mesenchymal transition. PlosOne 2013;8:e57314.
38. Liu S, Clouthier SG, Wicha MS. Role of microRNAs in the regulation of breast cancer stem cells. J Mammary Gland Biol Neoplasia 2012;17:15-21.
39. Yan D, Avtanski D, Saxena NK et al. Leptin-induced Epithelial-Mesenchymal Transition in Breast Cancer Cells Requires β-Catenin Activation via Akt/GSK3- and MTA1/Wnt1 Protein-dependent Pathways. J Biol Chem 2012;287:8598-8612.
40. Cross DA, Alessi DR, Cohen P et al. Inhibition of glycogen synthase kinase-3 by insulin mediated by protein kinase B. Nature 1995;378:785-759.
41. Subramaniam V, Vincent IR, Gardner H et al. CD44 regulates cell migration in human colon cancer cells via Lyn kinase and AKT phosphorylation. Exp Mol Pathol 2007;83:207-215.
42. Hardwick C, Hoare K, Owens R et al. Molecular cloning of a novel hyaluronan receptor that mediates tumor cell motility. J Cell Biol 1992;117:1343-1350.
43. Brown RL, Reinke LM, Damerow MS, et al. CD44 splice isoform switching in human and mouse epithelium is essential for epithelial-mesenchymal transition and breast cancer progression. J Clin Invest 2011; 121:1064-1074.
44. Brabletz T. To differentiate or not--routes towards metastasis. Nat Rev Cancer 2012;12:425-436.
45. López-Novoa JM, Nieto MA. Inflammation and EMT: an alliance towards organ fibrosis and cancer progression. EMBO Mol Med 2009;1:303-314.
46. Buijs JT, Henriquez NV, van Overveld PG et al. Bone morphogenetic protein 7 in the development and treatment of bone metastases from breast cancer. Cancer Res 2007;67:8742-8751.
47. Yee DS, Tang Y, Li X et al. The Wnt inhibitory factor 1 restoration in prostate cancer cells was associated with reduced tumor growth, decreased capacity of cell migration and invasion and a reversal of epithelial to mesenchymal transition. Mol Cancer;2010:9:162.

See www.StemCells.com for supporting information available online.

Figure 1. SCC cell lines contain distinct CSC phenotypes. (A) LUC4 cells show the CD44^{high}/ESA^{low}, CD44^{high}/ESA^{high} and CD44^{low} populations. (B) Phase contrast appearance of re-plated parent and sorted populations. (C) EMT markers assessed by PCR analyses and (D) western blotting. (E) Assay indicating greater migration of CD44^{high}/ESA^{low} cells. (F) Cell counts indicating lower rate of growth of CD44^{high} /ESA^{low} cells.

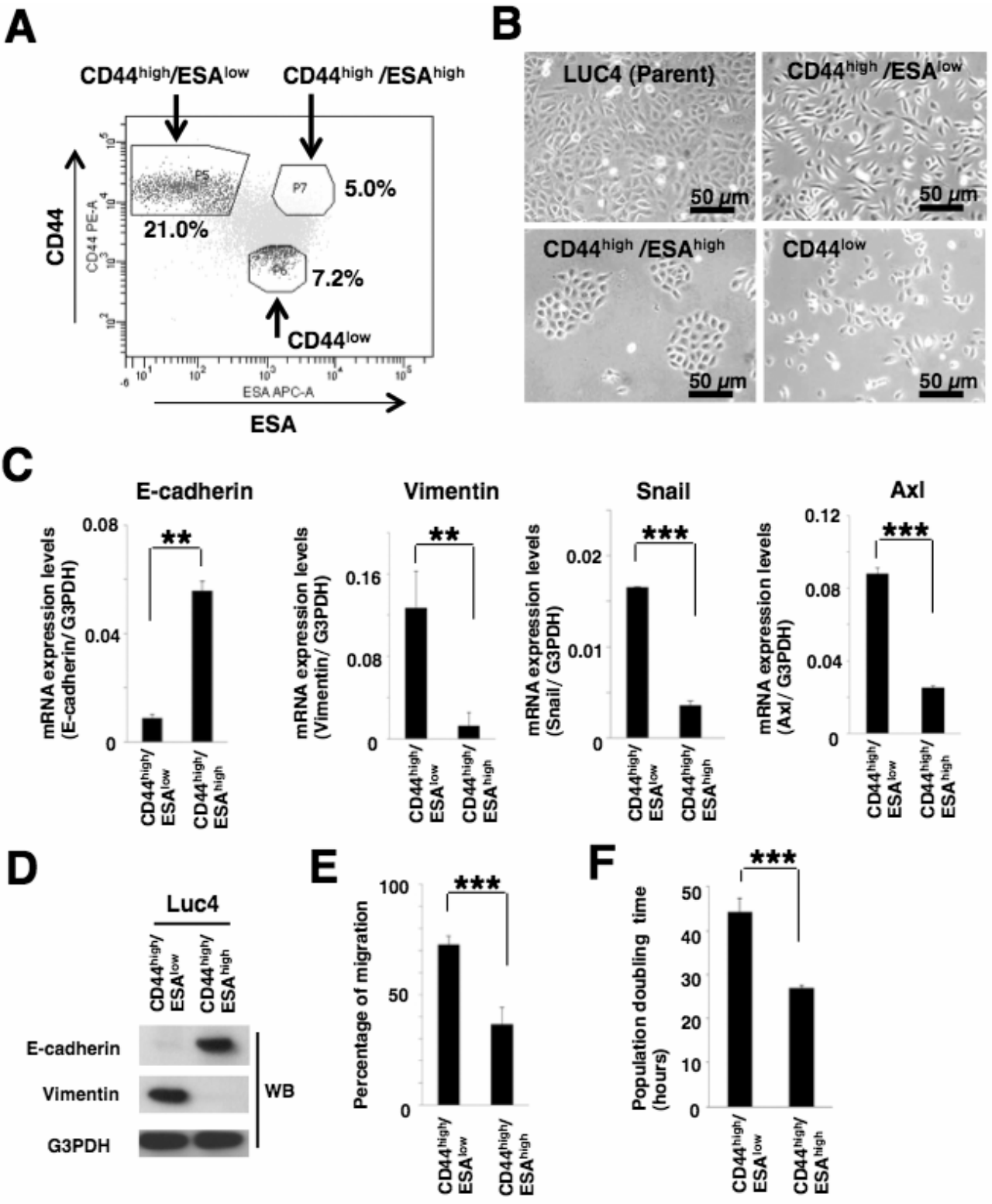

Figure 2. GSK3β is essential for tumour sphere and holoclone colony formation. (A) Tumour sphere formation by $CD44^{high}/ESA^{low}$ and $CD44^{high}/ESA^{high}$ cells. (B) Total and phosphorylated GSK3 asessed by western blotting. (C,D,E) Tumour sphere and holoclone formation reduced by GSK3β inhibition or knockdown. IF staining for total (left) and phosphorylated (right) GSK3β in adherent cultures (F). Cell sub-populations stained for total (left) and phosphorylated (right) GSK3β to show presence or absence of nuclear staining (G, upper 3 sets of panels) (G). Lower panels, tumour spheres stained for total and phosphorylated GSK3β, and also DAPI to show nuclei.

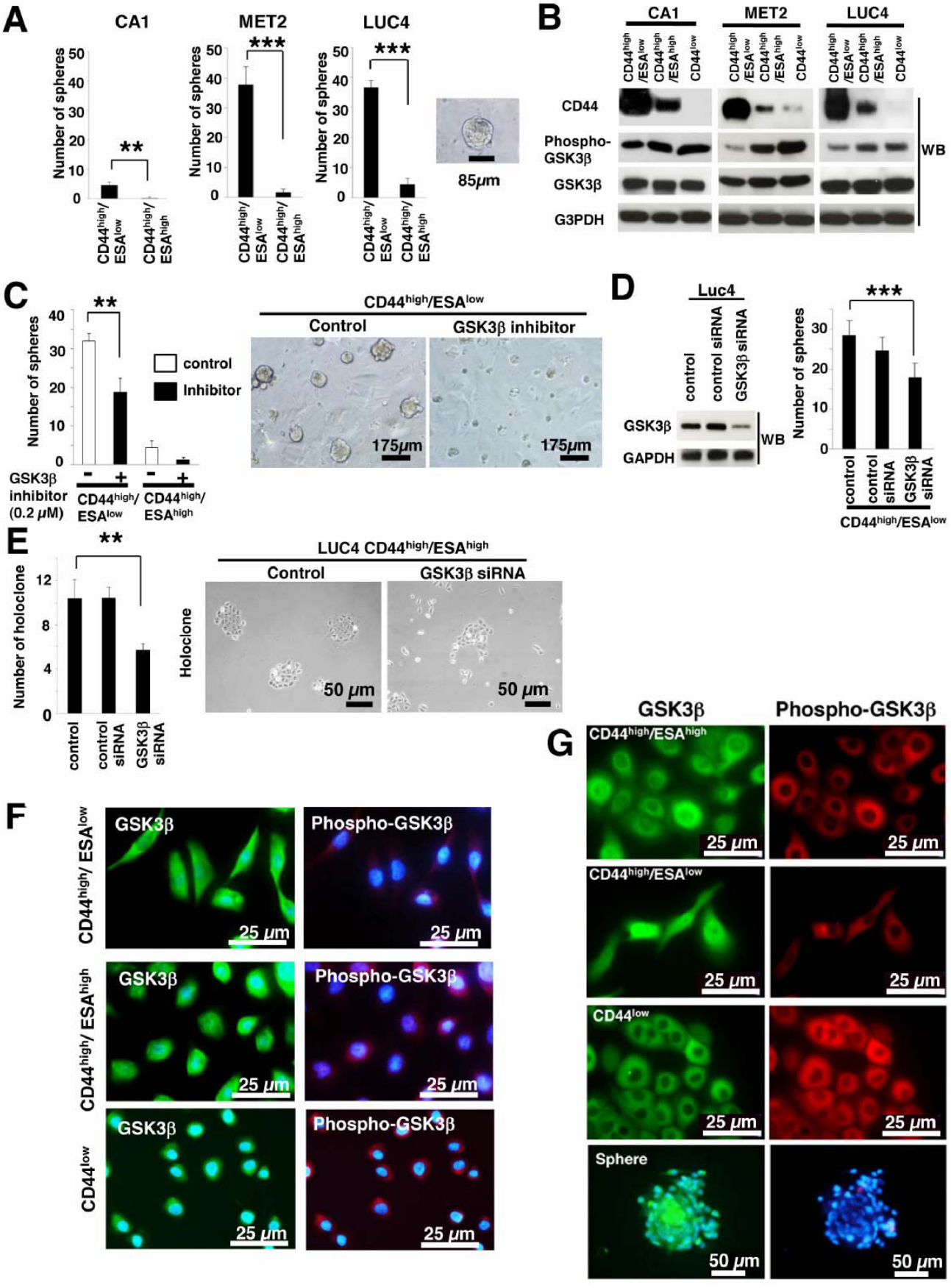
A
CA1
MET2
LUC4
Number of spheres
**
***
CD44high/ESAlow
CD44high/ESAhigh
85μm
B
CD44high/ESAlow
CD44high/ESAhigh
CD44low
CD44
Phospho-GSK3β
GSK3β
G3PDH
WB
C
CD44high/ESAlow
Control
GSK3β inhibitor
control
Inhibitor
GSK3β inhibitor (0.2 μM)
175μm
D
Luc4
control
control siRNA
GSK3β siRNA
GAPDH
E
LUC4 CD44high/ESAhigh
Number of holoclone
Holoclone
50 μm
F
CD44high/ ESAlow
CD44high/ ESAhigh
CD44low
25 μm
G
GSK3β
Phospho-GSK3β
CD44high/ESAhigh
CD44high/ESAlow
CD44low
Sphere
25 μm
50 μm

Figure 3. GSK3β inhibition reduces expression of stem cell markers and increases differentiation markers. GSK3β inhibition and knockdown lead to lower expression of Sox2, Oct4, and Nanog (A, B), to significant changes in the proportions of $CD44^{high}/ESA^{low}$, $CD44^{high}/ESA^{high}$ and $CD44^{low}$ cell indicated by FACS analyses (C), and altered patterns of expression of Involucrin and Calgranulin B (D,E).

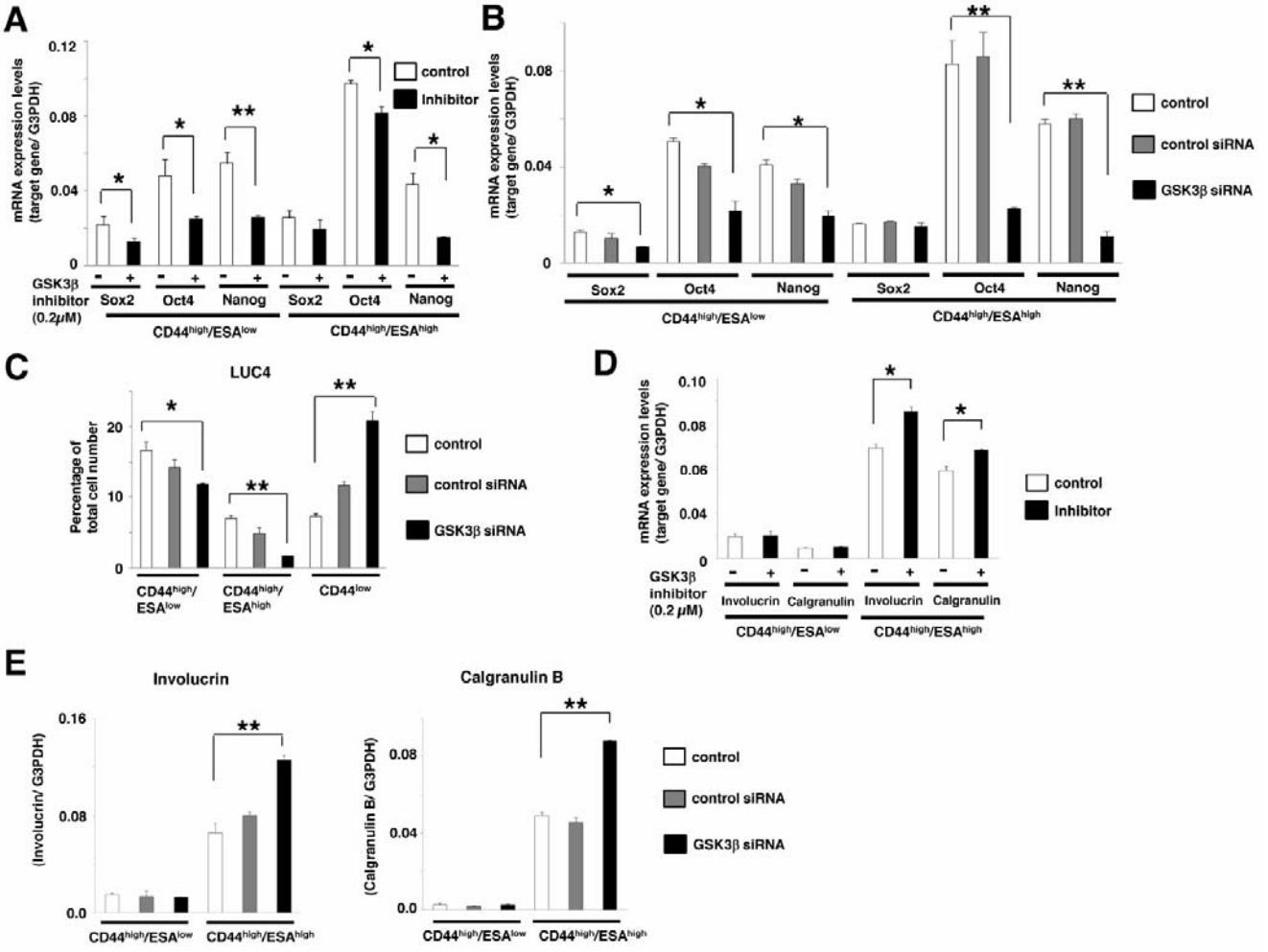

Figure 4. Single cell cloning of $CD44^{high}/ESA^{low}$ CSCs. Some clones produced only $CD44^{high}/ESA^{low}$ spindle-like populations (A) and for these clones GSK3β knockdown (B) did not induce a shift towards an EPI CSC population. Other clones generated mixed EMT and EPI CSC populations (C). GSK3β knockdown accelerated their shift towards the $CD44^{high}/ESA^{high}$ phenotype (C) and down-regulated Snail and Vimentin and up-regulated E-cadherin (E).

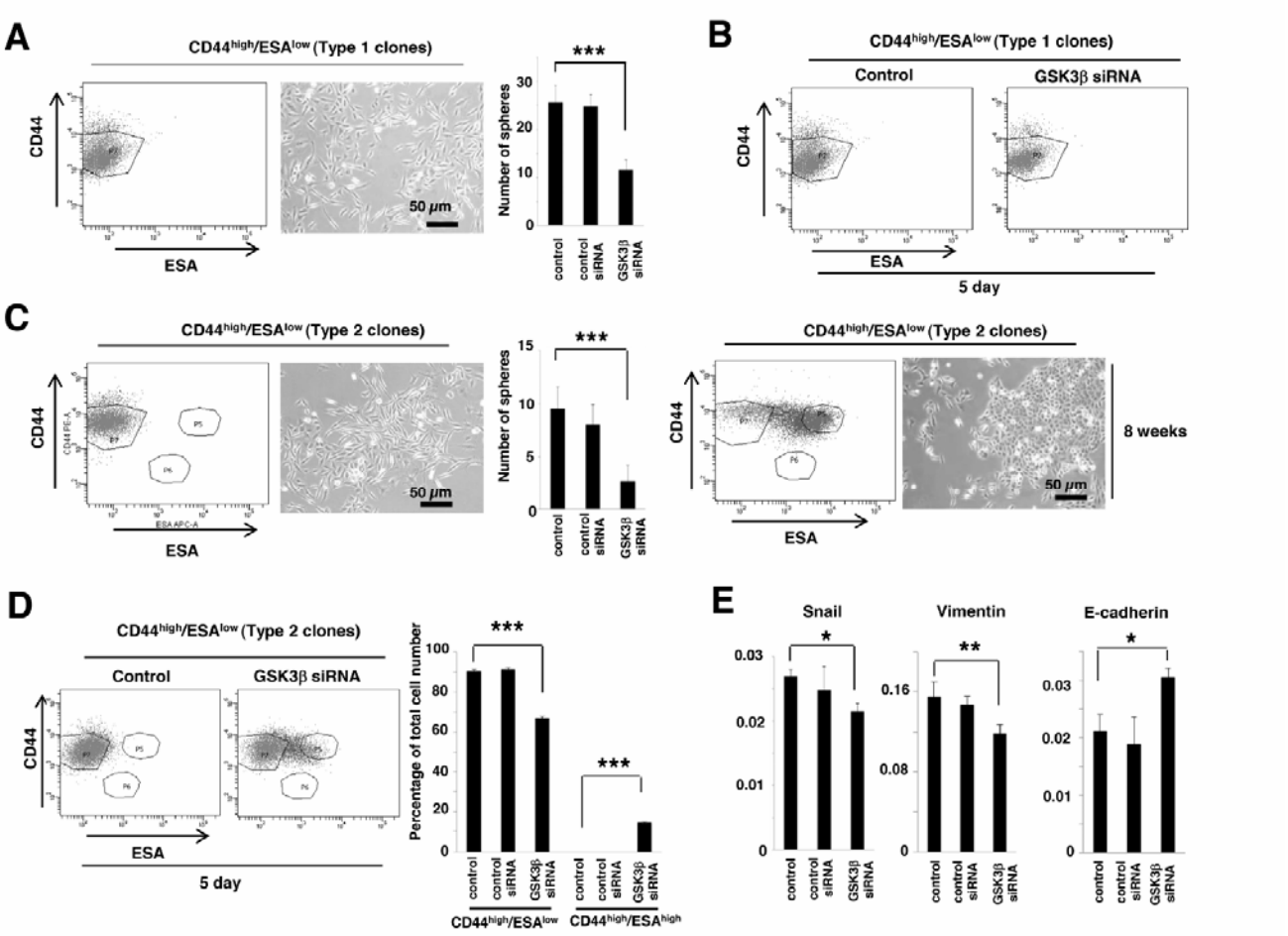

Figure 5. CSC self-renewal requires CD44 and RHAMM. RHAMM expression was higher in $CD44^{high}/ESA^{high}$ cells (A). Holoclone cells showed staining for both RHAMM and CD44, and cells of the few holoclones continuing to grow in the presence of inhibitor had escaped GSK3β phosphorylation (B). Knockdown of RHAMM or CD44 in $CD44^{high}/ESA^{low}$ cells increased phospho-GSK3β and phospho-Erk (C). In $CD44^{high}/ESA^{high}$ cells it suppressed holoclone and sphere formation (D,E), reduced stem cell markers (F), and increased Calgranulin B and Involucrin (G).

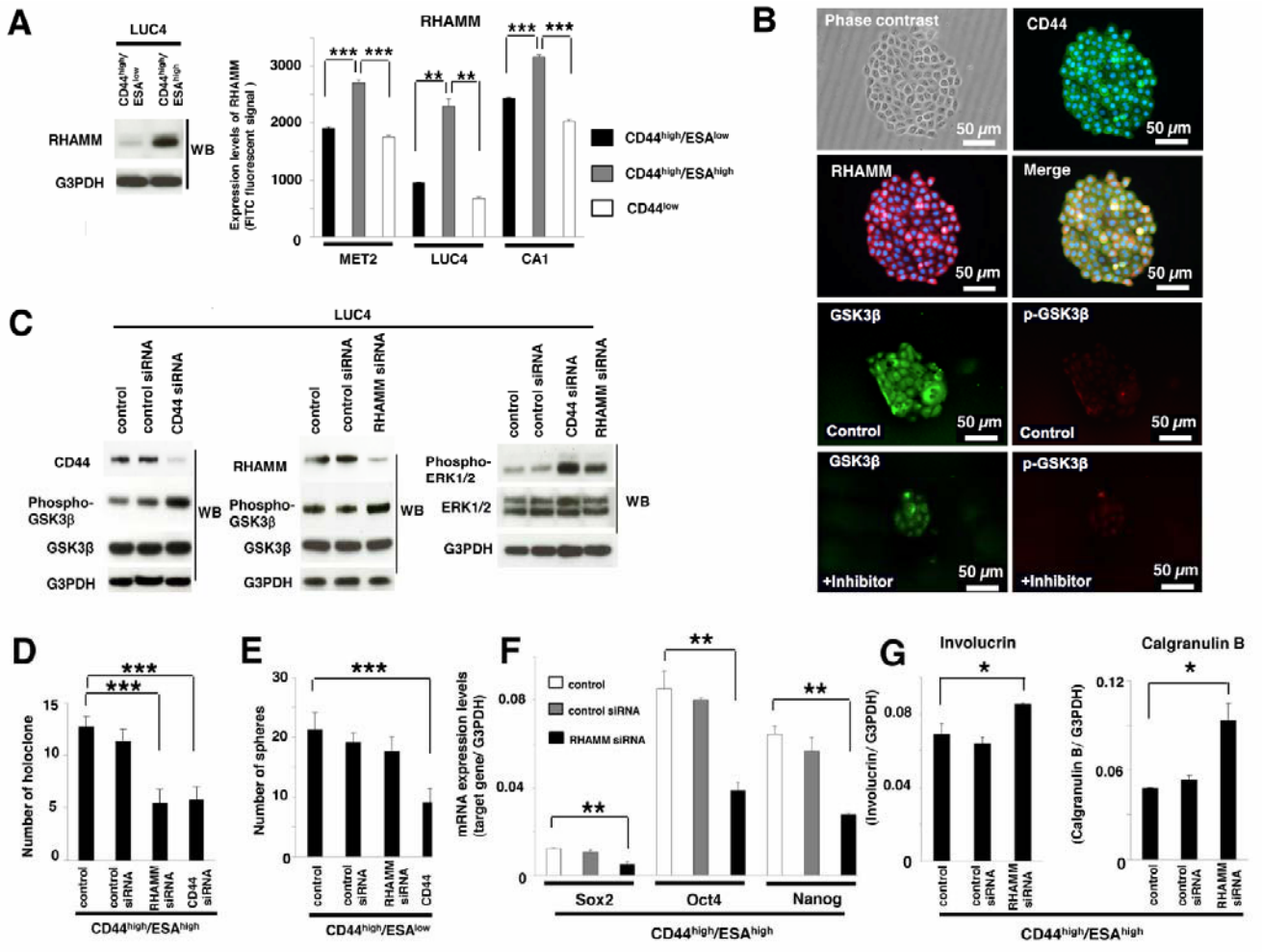

Figure 6. GSK3β maintains CSCs in a self-renewing state and its inhibition induces MET or differentiation of CSCs. This diagram summarizes changes in CSC populations associated with GSK3β activity. For description see text.